January 2012

Water Level Quantiles Of Devils Lake Under Down-Scaled Gcm Predictions Using A Coupled Hydro-Climatic Model

Hasin Shahad Munna

WATER LEVEL QUANTILES OF DEVILS LAKE UNDER DOWN-SCALED GCM PREDICTIONS USING A COUPLED HYDRO-CLIMATIC MODEL

by

Hasin Shahad Munna

Bachelor of Science, Bangladesh University of Engineering and Technology, 2009

A Thesis

Submitted to the Graduate Faculty

of the

University of North Dakota

in partial fulfillment of the requirements

for the degree of

Master of Science

Grand Forks, North Dakota

August

2012

This thesis, submitted by Hasin Shahad Munna in partial fulfillment of the requirements for the Degree of Master of Science from the University of North Dakota, has been read by the Faculty Advisory Committee under whom the work has been done and is hereby approved.

Dr. Yeo Howe Lim, Chair
Associate Professor of Department of Civil Engineering

Dr. Xiaodong Zhang
Associate Professor of Department Earth System Science and Policy

Dr. Harvey Gullicks
Chair and Associate Professor of Department of Civil Engineering

This thesis meets the standards for appearance, conforms to the style and format requirements of the Graduate School of the University of North Dakota, and is hereby approved.

Dr. Wayne Swisher
Dean of the Graduate School
Date: July 26th, 2012

PERMISSION

Title	Water Level Quantiles Of Devils Lake Under Down-Scaled GCM Predictions Using A Coupled Hydro-Climatic Model
Department	Civil Engineering
Degree	Master of Science

In presenting this thesis in partial fulfillment of the requirements for a graduate degree from the University of North Dakota, I agree that the library of this University shall make it freely available for inspection. I further agree that permission for extensive copying for scholarly purposes may be granted by the professor who supervised my thesis work or, in his absence, by the chairperson of the department or the dean of the Graduate School. It is understood that any copying or publication or other use of this thesis or part thereof for financial gain shall not be allowed without my written permission. It is also understood that due recognition shall be given to me and to the University of North Dakota in any scholarly use which may be made of any material in my thesis.

Signature _____

Hasin Shahad Munna

Date July 26th, 2012

TABLE OF CONTENTS

LIST OF FIGURES xi

LIST OF TABLES xviii

ACKNOWLEDGEMENTS xxi

ABSTRACT xxii

CHAPTER

1. INTRODUCTION 1

2. PREVIOUS STUDIES 6

3. METHODOLOGY AND MODEL 11

3.1 Scope of the Study 11

3.2 Description of Watersheds 15

3.3 Rainfall-Runoff Model (HEC-HMS) 19

3.3.1 Basin Model 19

3.3.2 Meteorological Model 22

3.3.2.1 Base Temperature 23

3.3.2.2 PX Temperature 23

3.3.2.3 Wet Melt-rate 23

3.3.2.4 Rain Rate Limit 23

3.3.2.5 ATI Melt-Rate Coefficient 24
3.3.2.6 Cold Limit 24
3.3.2.7 Cold Content 24
3.3.2.8 Water Capacity 24
3.3.2.9 ATI Melt-Rate Function 24
3.3.2.10 Initial and Constant Loss 25
3.3.3 Time Series and Paired Data Manager 26
3.3.4 Control Specifications Manager 26
3.4 Reservoir Model (HEC-ResSim) Description 26
3.4.1 Watershed Setup Module 27
3.4.2 Reservoir Network Module 27
3.4.3 Simulation Module 27
4. CALIBRATION OF THE COUPLED HYDRO-CLIMATIC MODEL 30
4.1 Overview and Data Sources 30
4.2 Calibration Parameters of HEC-HMS and HEC-ResSim Model 30
4.3 Calibration Steps 31
4.3.1 Gage Stations and Climate Data 32
4.3.2 Sensitivity of the Loss Parameters 35
4.3.3 Calibration of HMS-Model A and HMS-Model B 36

4.3.4 Combined Approach in Calibration 39
4.4 Reasons of Deviations in Coupled ResSim and HMS-Model B 44
4.5 Selected Parameters for Future Simulation (2021-2050) 47
4.6 Calibration of Lake Evaporation Model 48
4.6.1 Methods Analyzed 48
4.6.1.1 Penman Equation Method 49
4.6.1.2 Makkink Method 49
4.6.1.3 Doorenbos and Pruitt Method 50
4.6.1.4 Hargreaves Method 51
4.6.1.5 Abtew Method 51
4.6.1.6 Jensen and Haise Method 52
4.6.1.7 Priestley and Taylor Method 52
4.6.1.8 McGuinness and Bordne Method 53
4.6.1.9 Turc Method 53
4.6.2 Selected Method 54
4.6.3 Future Evaporation Estimates 57
5. SIMULATION OF THE COUPLED HYDRO-CLIMATIC MODEL 59
5.1 Steps Followed in Simulating Future Water Level 59
5.2 General Circulation Model (GCM): Climate Data 60

5.3 HEC-DSSVue 61

5.3.1 Data Interoperability Issues 62

5.4 Importing the Climate Data in DSSVue 64

5.5 Simulation of Reservoir Model 64

5.6 Sensitivity Analysis 75

6. FREQUENCY ANALYSIS OF LAKE-LEVELS 79

6.1 Specific Lake Conditions 79

6.2 Probability Distribution Functions (PDFs) 80

6.2.1 Normal/Gaussian Distribution 82

6.2.2 Lognormal Distribution 83

6.2.3 Pearson type 3 (Gamma) Distribution 84

6.2.4 Log Pearson type 3 Distribution 84

6.3 Frequency Analysis: HEC-SSP 85

6.3.1 Frequency Analysis of Observed Lake-Stages 85

6.3.2 Frequency Analysis of Simulated Lake-Stages 85

6.3.3 Frequency Analysis using Lake-Volumes 87

6.3.4 Frequency Analysis of Observed Lake-Volumes 88

6.3.5 Frequency Analysis of Simulated Lake-Volumes 89

6.3.6 Conditional Frequency Analysis 90

6.3.7 Conditional Probabilities of Lake-Stages 92

6.3.8 Conditional Probabilities of Lake-Volumes 93

7. DISCUSSION 94

7.1 Discussion on Steps Followed to Obtain the Future Lake-Level Traces 94

7.2 Discussion on Basin Delineation 95

7.3 Discussion on Data, Modeling and Calibration 95

7.4 Discussion on Lake Evaporation Model 97

7.5 Discussion on HEC-DSSVue 98

7.6 Discussion on Previous Studies and Comparison with Research Outcomes 99

8. CONCLUSION 105

APPENDICES 107

A. Area Calculation from Geo-pdf Maps 108

B. Unique IDs of Sub-Areas in the Basin Model of HEC-HMS 112

B.1 Naming of the Sub-Areas of the Basin Model in HEC-HMS 112

B.2 Numbers to Identify Sub-Areas, Reaches and Junctions 112

C. Calibration Steps 114

C.1 Step 1: Loss Calibration of Mauvais Coulee: HMS-Model A 115

C.2 Step 2: Application of the Calibrated Parameters in HMS-Model B 121

C.3 Step 3: Snow-Melt Calibration 123

C.4 Step 4: Sensitivity of Loss Parameters 125

C.5 Step 5: Calibration of Mauvais Basin for Multiple Years 126

C.6 Step 6: Combined Approach in Calibration 129

D. Calibration Plots of Loss Calibration of Mauvais Coulee 130

D.1 Calibration using Precipitation Gage at Minnewaukan 130

D.2 Calibration using Precipitation Gage at Towner 135

E. Calibration Plots of Snow-Melt Calibration of Mauvais Coulee 146

F. Plots of the Combined Approach in Calibration 156

F.1 Calibration Plots of HMS-Model A Coupled with ResSim Model 156

F.2 Calibration Plots of HMS-Model B Coupled with ResSim Model 158

G. HEC-DSSVue 160

G.1 File Format in HEC-DSSVue 160

G.2 Individual Cell Number, ID, Latitude and Longitude 162

H. Frequency Analysis 164

H.1 General Skew Coefficient in USA 164

H.2 Table of Frequency Factor, k 165

H.3 Observed Lake-Levels Fitted using Different PDFs 168

H.4 Simulated Lake-Levels Fitted using Different PDFs 169

H.5 Observed Lake-Volumes Fitted using Different PDFs 171

H.6 Simulated Lake-Volumes Fitted using Different PDFs 172

REFERENCES 174

LIST OF FIGURES

Figure Page

1. Historic lake levels (annual peak) of Devils Lake 2

2. Lands, houses and roadways affected by floodwater (Source: USGS, FEMA) 2

3. Contour map of Devils Lake, Stump Lake and Sheyenne River at 1458 ft 4

4. Change in annual mean of precipitation from 1950-2006 (Source: USGS) 9

5. Plot of the water level of Devils Lake along with 10 year running average of annual precipitation estimates using PRISM data 10

6. Sub-basins of the Devils Lake (Source: USGS) 13

7. Combined sub-basins delineated using ArcGIS and ArcHydro 16

8. Geo-pdf map of Devils Lake used for sub-basin delineation (Source: USGS) 17

9. Geo-pdf map of New Rockford used for sub-basin delineation (Source: USGS) 17

10. Layout of Combined Watershed in HEC-HMS 20

11. Grid layout for the HEC-HMS model 21

12. ResSim module concept (Source: USACE HEC-ResSim Manual) 28

13. Schematic layout of the HEC-ResSim model 28

14. Gauge locations in the watershed of Devils Lake 34

15. Sensitivity of initial loss in the HEC-HMS model 35

16. Sensitivity of constant loss in the HEC-HMS model 36

17. Runoff plot and summary results in calibrating the loss parameters of the Mauvais Coulee 37

18. Comparison between precipitation observations in Towner station and NASA (TMPA) Satellite (Jun 6, 2001 to Jul 15, 2001) 38

19. Simulated water level from the HMS-Model A + ResSim 42

20. Water balance from the HMS-Model A + ResSim 42

21. Increase in Water Level from the HMS-Model A + ResSim 42

22. Simulated water level from the HMS-Model B + ResSim 43

23. Water Balance from the HMS-Model B + ResSim 43

24. Increase in Water Level from the HMS-Model B + ResSim 43

25. Simulated water level using coupled ResSim and HMS-Model B 46

26. Experiment 1: Replacing the high precipitation events by zero 46

27. Experiment 2: Replacing the high precipitation events by Langdon values 46

28. Experiment 3: Distributing the high precipitation event 46

29. Calibration plot of the modeled evaporation vs. values obtained from Crary station (2000-2010) 55

30. Results of the regression analysis in an annual basis 56

31. Flowchart explaining the sequence of tasks in simulating the future water level 60

32. Example plot of future precipitation (A1B_CSMK3) 63

33. Example plot of future temperature (A1B_CSMK3) 63

34. Simulated water level in Case 1: A1B_CSMK3_2021-2050 65

35. Simulated water level in Case 2: A1B_GFCM21_2021-2050 66

36. Simulated water level in Case 3: A1B_GIAOM_2021-2050 67

37. Simulated water level in Case 4: A1B_HADCM3_2021-2050 68

38. Simulated water level in Case 5: A2_GFCM21_2021-2050 69

39. Simulated water level in Case 6: A2_HADCM3_2021-2050 70

40. Simulated water level in Case 7: B1_CSMK3_2021-2050 71

41. Simulated water level in Case 8: B1_GFCM21_2021-2050 72

42. Simulated water level in Case 9: B1_GIAOM_2021-2050 73

43. Simulated water level in Case 10: B1_HADCM3_2021-2050 74

44. Experimental simulation of water level considering average lake evaporation of 27 in/year 76

45. Experimental simulation of water level considering average lake evaporation of 30 in/year 77

46. Shift in mean water level due to change in average lake evaporation by 3 in/year 78

47. Observed lake-levels fitted using normal distribution 86

48. Observed lake-levels fitted using log-normal distribution 87

49. Trend line and equation of the stage-volume function 88

50. Observed lake-volumes fitted using Lognormal probability distribution 89

51. Observed lake-volumes fitted using Pearson type 3 probability distribution 90

52. Historic record of precipitation in Devils Lake, 1950-1999 (Source: USGS) 100

53. Mean precipitation (in) - January to June (Scenario: A1B) 101

54. Mean precipitation (in) - January to June (Scenario: A2) 101

55. Mean precipitation (in) - January to June (Scenario: B1) 102

56. Mean precipitation (in) - July to December (Scenario: A1B) 102

57. Mean precipitation (in) - July to December (Scenario: A2) 102

58. Mean precipitation (in) - July to December (Scenario: B1) 103

59. Area calculation of Devils Lake (North) using geo-pdf maps 108

60. Area calculation of Devils Lake (South 1) using geo-pdf maps 108

61. Area calculation of Devils Lake (South 2) using geo-pdf maps 109

62. Area calculation of Devils Lake (South 3) using geo-pdf maps 109

63. Area calculation of Devils Lake North Slope (Down) using geo-pdf maps 110

64. Area calculation of Devils Lake North Slope (Up) using geo-pdf maps 110

65. Area calculation of Devils Lake South Slope (Down) using geo-pdf maps 111

66. Area calculation of Devils Lake South Slope (Up) using geo-pdf maps 111

67. Precipitation at Minnewaukan and Runoff at Cando (Observed) 117

68. Runoff plot and summary results of Trial 21 in calibrating the loss parameters of the Mauvais coulee 120

69. Runoff plot and summary results of HMS-Model B using calibration parameters obtained from HMS-Model A 121

70. Comparison between precipitation observations in Towner station and NASA satellite (Jun 6, 2001 to Jul 15, 2001) 122

71. Sensitivity of initial loss on the model. 125

72. Sensitivity of constant loss on the model. 126

73. Runoff plot and summary results for multiple year calibration using HMS-Model A 127

74. Runoff plot and summary results for multiple year calibration using HMS-Model B 128

75. Calibration plot of Trial 1 (Loss calibration: storm-based) 130

76. Calibration plot of Trial 2 (Loss calibration: storm-based) 131

77. Calibration plot of Trial 3 (Loss calibration: storm-based) 131

78. Calibration plot of Trial 4 (Loss calibration: storm-based) 132

79. Calibration plot of Trial 5 (Loss calibration: storm-based) 132

80. Calibration plot of Trial 6 (Loss calibration: storm-based) 133

81. Calibration plot of Trial 7 (Loss calibration: storm-based) 133

82. Calibration plot of Trial 8 (Loss calibration: storm-based) 134

83. Calibration plot of Trial 9 (Loss calibration: storm-based) 134

84. Loss calibration of Mauvais coulee (Precipitation: Towner) - Trial 1..... 135

85. Loss calibration of Mauvais coulee (Precipitation: Towner) - Trial 2..... 136

86. Loss calibration of Mauvais coulee (Precipitation: Towner) - Trial 3..... 136

87. Loss calibration of Mauvais coulee (Precipitation: Towner) - Trial 4..... 137

88. Loss calibration of Mauvais coulee (Precipitation: Towner) - Trial 5..... 137

89. Loss calibration of Mauvais coulee (Precipitation. Towner) - Trial 6..... 138

90. Loss calibration of Mauvais coulee (Precipitation. Towner) - Trial 7..... 138

91. Loss calibration of Mauvais coulee (Precipitation: Towner) - Trial 8..... 139

92. Loss calibration of Mauvais coulee (Precipitation: Towner) - Trial 9..... 139

93. Loss calibration of Mauvais coulee (Precipitation: Towner) - Trial 10..... 140

94. Loss calibration of Mauvais coulee (Precipitation: Towner) - Trial 11..... 140

95. Loss calibration of Mauvais coulee (Precipitation: Towner) - Trial 12..... 141

96. Loss calibration of Mauvais coulee (Precipitation: Towner) - Trial 13..... 141

97. Loss calibration of Mauvais coulee (Precipitation: Towner) - Trial 14..... 142

98. Loss calibration of Mauvais coulee (Precipitation: Towner) - Trial 15..... 142

99. Loss calibration of Mauvais coulee (Precipitation: Towner) - Trial 16..... 143

100. Loss calibration of Mauvais coulee (Precipitation: Towner) - Trial 17..... 143

101. Loss calibration of Mauvais coulee (Precipitation: Towner) - Trial 18..... 144

102. Loss calibration of Mauvais coulee (Precipitation: Towner) - Trial 19..... 144

103. Loss calibration of Mauvais coulee (Precipitation: Towner) - Trial 20..... 145

104. Loss calibration of Mauvais coulee (Precipitation: Towner) - Trial 21..... 145

105. Snowmelt calibration of Mauvais coulee - Trial 1..... 146

106: Snowmelt calibration of Mauvais coulee - Trial 2 147

107. Snowmelt calibration of Mauvais coulee - Trial 3..... 147

108. Snowmelt calibration of Mauvais coulee - Trial 4..... 148

109. Snowmelt calibration of Mauvais coulee - Trial 5..... 148

110. Snowmelt calibration of Mauvais coulee - Trial 6..... 149

111. Snowmelt calibration of Mauvais coulee – Trial 7 149

112. Snowmelt calibration of Mauvais coulee – Trial 8 150

113. Snowmelt calibration of Mauvais coulee – Trial 9 150

114. Snowmelt calibration of Mauvais coulee – Trial 10 151

115. Snowmelt calibration of Mauvais coulee – Trial 11 151

116. Snowmelt calibration of Mauvais coulee – Trial 12 152

117. Snowmelt calibration of Mauvais coulee – Trial 13 152

118. Snowmelt calibration of Mauvais coulee – Trial 14 153

119. Snowmelt calibration of Mauvais coulee – Trial 15 153

120. Snowmelt calibration of Mauvais coulee – Trial 16 154

121. Snowmelt calibration of Mauvais coulee – Trial 17 154

122. Snowmelt calibration of Mauvais coulee – Trial 18 155

123. Snowmelt calibration of Mauvais coulee – Trial 19 155

124. Calibration of HMS-Model A + ResSim (Combined approach) - Initial loss: 0.0 in; Constant loss: 0.085 in/hr; Seepage: 0 cfs 156

125. Calibration of HMS-Model A + ResSim (Combined approach) - Initial loss: 0.1 in; Constant loss: 0.085 in/hr; Seepage: 20 cfs 157

126. Calibration of HMS-Model A + ResSim (Combined approach) - Initial loss: 0.1 in; Constant loss: 0.085 in/hr; Seepage: 0 cfs 157

127. Calibration of HMS-Model A + ResSim (Combined approach) - Initial loss: 0.1 in; Constant loss: 0.085 in/hr; Seepage: 10 cfs 157

128. Calibration of HMS-Model B + ResSim (Combined approach) - Initial loss: 0.0 in; Constant loss: 0.085 in/hr; Seepage: 0 cfs 158

129. Calibration of HMS-Model B + ResSim (Combined approach) - Initial loss: 0.1 in; Constant loss: 0.085 in/hr; Seepage: 0 cfs 158

130. Calibration of HMS-Model B + ResSim (Combined approach) - Initial loss: 0.1 in; Constant loss: 0.085 in/hr; Seepage: 50 cfs 159

131. Calibration of HMS-Model B + ResSim (Combined approach) - Initial loss: 0.1 in; Constant loss: 0.085 in/hr; Seepage: 20 cfs 159

132. Map of general skew coefficient in USA (Source: IACWD, 1982) 164

133. Observed lake-levels fitted using Pearson type 3 distribution..... 168

134. Observed lake-levels fitted using Log Pearson type 3 distribution 168

135. Simulated lake-levels fitted using Normal distribution 169

136. Simulated lake-levels fitted using Log-Normal distribution 169

137. Simulated lake-levels fitted using Pearson type 3 distribution..... 170

138. Simulated lake-levels fitted using LP type 3 distribution..... 170

139. Observed lake-volumes fitted using Normal distribution..... 171

140. Observed lake-volumes fitted using LP type 3 distribution..... 171

141. Simulated lake-volumes fitted using Normal distribution..... 172

142. Simulated lake-volumes fitted using Pearson type 3 distribution..... 172

143. Simulated lake-volumes fitted using Log-Normal distribution 173

144. Simulated lake-volumes fitted using LP type 3 distribution..... 173

LIST OF TABLES

Table Page

1. Calculated areas (sq. miles) of the sub-areas in the HEC-HMS model 18

2. Unique IDs used in the HEC-HMS model 22

3. Calibration parameters in HEC-HMS 31

4. Data products and parameters obtained from NASA 33

5. Calibration Results (2003-10) using HMS-Model A + ResSim model 40

6. Calibration Results (2003-2010) using HMS-Model B + ResSim model 40

7. Calibrated values of melt-rate coefficient and continuous loss for both HMS-Model A and HMS-Model B 41

8. Snow-melt parameters (Temperature Index) for both HMS-Model A and B coupled with ResSim model 41

9. Comparison of TMPA by NASA's satellite with observed value in Langdon Gage Station 45

10. Selected HEC HMS model parameters for future simulation (2021-2050) 47

11. Equations evaluated for the calibration of the lake evaporation model 52

12. Original and recalibrated coefficients in evaporation modeling 54

13. The three lake evaporation methods showing better R^2 values 55

14. Summary of the calibration and regression analysis of the lake evaporation model .. 57

15. Annual average of the simulated future (2021-2050) lake evaporation 58

16. Description of the Parts in a .dss file used in simulation of future water levels 62

17. Data types in a .dss file 62

18. Simulation Case 1: A1B_CSMK3_2021-2050 65
19. Simulation Case 2: A1B_GFCM21_2021-2050 66
20. Simulation Case 3: A1B_GIAOM_2021-2050 67
21. Simulation Case 4: A1B_HADCM3_2021-2050 68
22. Simulation Case 5: A2_GFCM21_2021-2050 69
23. Simulation Case 6: A2_HADCM3_2021-2050 70
24. Simulation Case 7: B1_CSMK3_2021-2050 71
25. Simulation Case 8: B1_GFCM21_2021-2050 72
26. Simulation Case 9: B1_GIAOM_2021-2050 73
27. Simulation Case 10: B1_HADCM3_2021-2050 74
28. Probabilities and return periods of current lake-level using different PDFs 86
29. Probabilities and return periods of current lake-volume using different PDFs 89
30. Probability of synthetic lake-level series, P(A/B) in % 92
31. Conditional probability (of synthetic lake-level series, P(A and B), in % 92
32. Probability of synthetic lake-volume series, P(A/B) in % 93
33. Conditional probability of synthetic lake-volume series, P(A and B), in % 93
34. Description of gage locations for storm-based loss calibration 116
35. Trial results of loss calibration of Mauvais coulee 118
36. Description of gage location at Cando (stream flow) and Towner (precipitation) ... 118
37. Trial results of loss calibration of Mauvais coulee 119
38. Initial trial results of the snow-melt calibration 124
39. Trial results of loss calibration of Mauvais Coulee 124
40. Table of all cell numbers, ID, latitude and longitude 162

41. Frequency factor *k* for gamma and LP3 distributions (Haan, 1977, Table 7.7) 165

ACKNOWLEDGEMENTS

First and foremost, I would like to thank my advisor Dr. Yeo Howe Lim, for guiding me throughout my graduate studies. The effort and hours he spent on a daily basis to explain my questions and to help me solve numerous research problems is truly inspiring. The research would not have been possible without the guidance of Dr. Xiaodong Zhang and Dr. Andrei Kirilenko. I am also in debt to Dr. Harvey Gullicks, my co-supervisor and to Josh Hassell, my colleague.

I would not have come this far if it was not for my mother, Talat Ara Begum and father, Saleh Md. Hasib for always motivating me to go the extra mile. I am blessed to have my younger brother Hasin Fahad Jinna who took care of the family when it needed the most. I cannot thank enough my better half Rumana Rashid without whom I would have been totally lost. I am also extremely thankful to my uncle Dr. Saleh Faruque and Aunt Yasmin Faruque for all their support and affection.

I have to thank Ramy and Dipesh, for enduring all my irregularities and making our apartment our home. I am grateful to my relatives for supporting my family during my absence. Thanks to all my cousins and friends for their best wishes.

I would also like to acknowledge the support of the National Aeronautics and Space Administration (NASA) and North Dakota Water Resource Research Institute (NDWRRI) for funding my research.

Finally, I thank ALLAH, the Almighty for everything.

To My Loving Mother

Talat Ara Begum

ABSTRACT

The research focuses in calibrating a coupled rainfall-runoff model and a reservoir model for the Devils Lake using data from both ground gage stations and NASA satellite observations. The purpose is to determine the feasibility of using spatially distributed GCM data with a well calibrated hydro-climatic model to predict the probable flood severities. A temperature-based evaporation prediction model is also developed to simulate the outflow from the terminal lake. Future hydrology of the basin and lake levels of Devils Lake are simulated using the weather samples obtained from several downscaled GCM runs under varying scenarios due to anthropogenic modifications and the resulting composition of the atmosphere. 100 traces of future water levels of the Devils Lake have been generated using the predicted temperature and precipitation by the GCMs. The synthetic traces show a downward trend in water levels for a 30 year simulation period. The annual peak series of the synthetic traces (both stage and volume) are sorted and analyzed to obtain the probabilities and return periods of extreme flood events. The Bulletin 17B recommended LP3 method along with Gaussian/Normal, Lognormal and Gamma/Pearson type 3 distributions are applied for comparison purposes. The Log-Normal probability distribution, in both cases (stage and volume) provided with better fits. Water levels of closed-basin lakes are usually characterized by high serial dependence. The lake is already in its highest peak of the recorded history (1454 ft, spring, 2011), which is set as the base condition for the simulation of future water levels. These circumstances require the probability to be calculated both in a

conditional and unconditional basis. Moreover, the probability is calculated both in terms of stage and volume and probabilities of water levels being 1456, 1458 and 1460 ft have been reported. Considering the stage of the lake, the conditional probabilities are 0.008, 0.003 and .001 percent and the unconditional probabilities are 1.12, 0.44 and 0.189 percent respectively. By converting the stages into volumes, the conditional probabilities are 0.004, 0.002 and 0.0009 percent and the unconditional probabilities are 1.5, 0.68 and 0.31 percent respectively. These lower probability values indicate a lower chance of spilling into the Sheyenne river in the near future based on GCM predictions.

CHAPTER 1

INTRODUCTION

Devils Lake, located in Ramsey County and Benson County in northeastern North Dakota is the largest natural lake in North Dakota and is a sub-basin of the Red River of the North. Although it lies entirely within the Red River Basin, it has no natural outlet at current water levels. Geologic evidence shows that the water level in Devils Lake has fluctuated widely from completely dry (about 1400 feet above mean sea level) to overflowing into the Sheyenne River (about 1458 feet amsl) since its inception during the glacier period. After the historical low of about 1402 feet (only 2 feet deep) in 1940 during the great drought of 1930's, the lake has been rising continuously. The lake has more than quadrupled in size since the early 1990s, which is assumed to be occurring due to a series of wet years. The Devils Lake started spilling into the adjacent Stump Lake in 1999, and by 2007 the two lakes completely merged together. Figure 1 shows the water level of Devils Lake, from which it is evident that the Devils Lake basin is experiencing significant flooding problems since the early 1990s. Recently the combined lake level has touched 1454.30 ft (June 27, 2011, Figure 1), which is the highest in the recorded history of the past century.

The continued flooding of Devils Lake has caused tremendous sufferings for the people of the affected region. It has destroyed hundreds of homes, inundated thousands of acres of productive farmland and disrupted transportation system (Figure 2). Flooding forced the raising of roads, bridges, levees and other infrastructures. Since 1992, more

than $1 billion have been spent by federal, state, and local agencies to address the effects of the rising lake (U.S. Army Corps of Engineers, 2010).

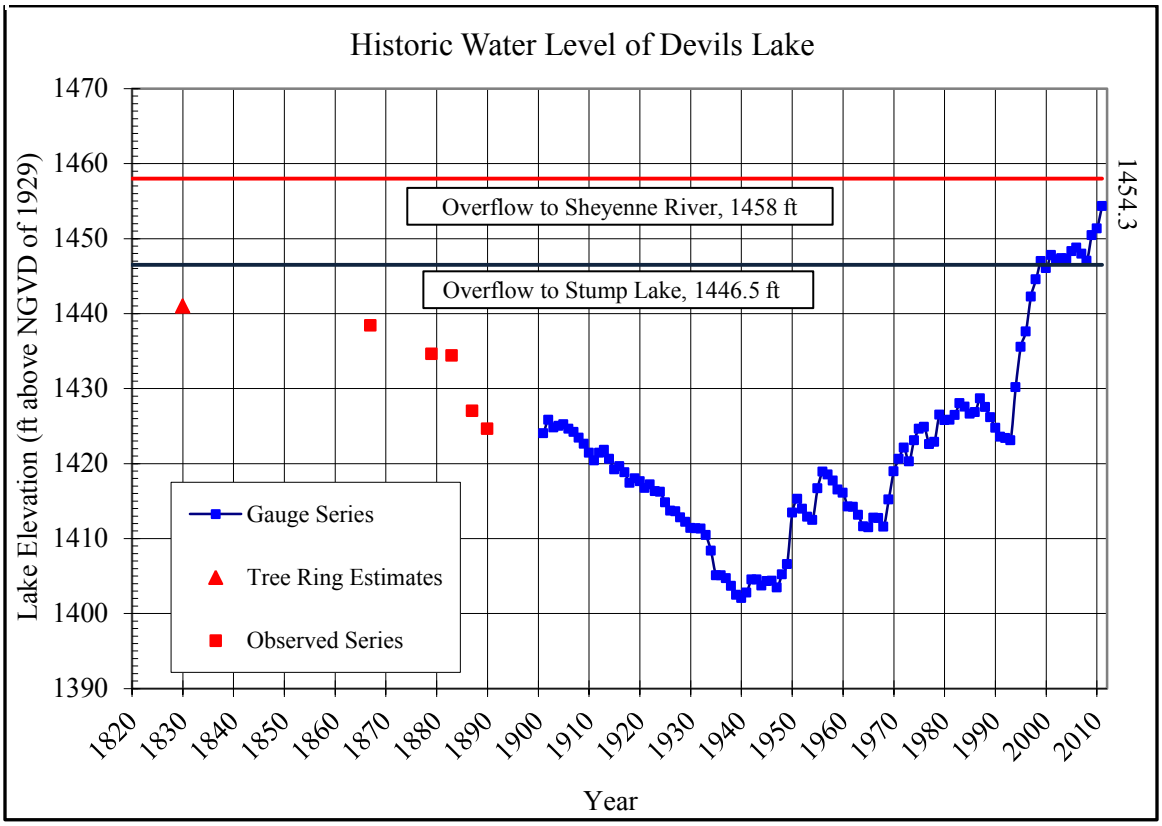

Figure 1: Historic lake levels (annual peak) of Devils Lake

Figure 2: Lands, houses and roadways affected by floodwater (Source: USGS, FEMA)

The basin of Devils Lake consists of approximately 3,810 square miles out of which runoff from about 3,320 square miles flows to Devils Lake and runoff from the remainder of about 490 square miles contributes to Stump Lake (Vecchia, 2008; Nustad *et al*, 2011). The elevation of Devils Lake rose more than 30 ft from 1992 to 2011, and through the process of merging with Stump Lake, it inundated thousands of acres of surrounding lands. With the continued trend of rising, the combined lake is on the eve of spilling to the Sheyenne River (spills at 1458 ft). The probable spilling can create devastating flooding in the downstream locations. The impact of flooding and probable spill warrant a very good understanding of the hydrology of the region and prediction of future climate pattern to forecast the growth of the combined lakes in future years.

It is important to study the historical rise of the Devils Lake and Stump Lake, leading to the formation of a combined lake and reaching the potential spill elevation, to calibrate and simulate a hydro-climatic model for future time steps. Geologic and other records suggest that Devils Lake has been a dry lake in the past, but also has spilled to the Sheyenne River at least twice during the last 4,000 years (Bluemle, 1991; Murphy *et al*, 1997). In May 1992, the water level of Devils Lake was 1423.65 ft and the water level of Stump Lake was below 1400 ft. Combined volume of Devils Lake and Stump Lake was about 590,000 acre-ft and the combined surface area was about 49,000 acres (Vecchia, 2008). Since then the Devils Lake started to rise continuously. The Devils Lake starts to spill into Stump Lake at water levels greater than 1446.5 ft and at water levels more than 1458.0 ft, the combined lakes begin to spill to the Sheyenne River through Tolna Coulee (Figure 1 and Figure 3). Water began spilling from Devils Lake to Stump Lake in May 1999, and by September 2007 Devils Lake and Stump Lake became a single and

continuous water body with an elevation of 1,447.1 ft, a combined volume of about 2.9 million acre-ft, and a combined surface area of about 140,000 acres. Therefore, from 1992 to 2007 the combined volume increased by about 2.3 million acre-ft and the combined area increased by about 91,000 acres (Vecchia, 2008). Without any erosion, the initial spill elevation from the combined Devils and Stump Lake to Sheyenne River was 1459 ft. In 2009, after removing a berm from the outlet channel by the City of Devils Lake, the spill elevation is reduced to 1458 ft (Vecchia, 2011). A contour map of the basin at 1458 ft amsl can be seen in Figure 3, which portrays the extent of the combined lakes at that elevation. It can be seen from the figure that the combined lakes will start

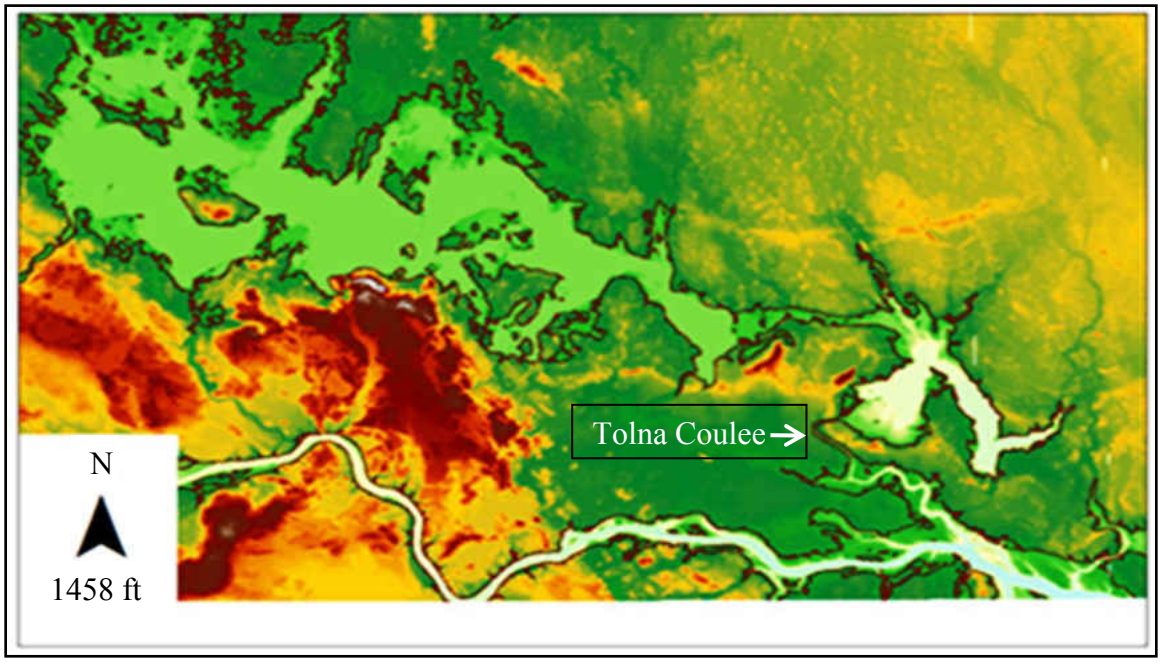

Figure 3: Contour map of Devils Lake, Stump Lake and Sheyenne River at 1458 ft

Note: The dark red color represents higher elevations and light green color represents lower elevations.

spilling into the Sheyenne River through Tolna Coulee from the south east end if the water level rises more than 1458 feet. At this elevation the City of Devils Lake will be under serious threat inundating more than 50,000 acres of new land, thousands of structures, millions of trees and destroying transportation routes into and out of Devils Lake city. From 1991 to 2009, the rising water has caused a loss of $130 million in land and commodity by inundating the surroundings of Devils Lake and the smaller lakes in the upper drainage basin (Zhang, 2010).

The unprecedented crisis was influential in pursuing continued research on the hydrology of the affected area. The thesis is focused in devising the mechanism of implementing the GCM-derived climate forecasts into a calibrated hydro-climatic model to inform the potential future water level of the lake system and investigate the probabilities of extreme flood events in future years.

CHAPTER 2

PREVIOUS STUDIES

Numerous studies have been conducted describing the hydrology and climatology of the Devils Lake region to assess the growth of the lake and determine the probability of flooding in future years. Murphy *et al* (1997) analyzed the long-term geologic record of Devils Lake and found the water levels to be consistent with a two-state climate model, in which the climatic conditions randomly shifted between normal (1950-79) and wet (1980-99) periods. The average duration of the normal and wet periods were estimated to be 120 years and 20 years respectively. Wiche *et al* (2000) pointed out that the atmospheric weather patterns from 1977 to 1999 were wetter than before 1977, and predicted that the wet conditions in 2000 are expected to continue beyond the first decade of the 21st century. The general climatic conditions have continued to be wet since 2000. Recent research on climate dynamics and paleo-climatic evidences predicted that the conditions that began around 2007 are not likely to end anytime soon (Vecchia, 2008). There is about a 72% chance that the wet conditions will last at least 10 more years and about a 37% chance that the wet conditions will last at least 30 more years (Vecchia, 2008).

In previous studies water-balance, statistical and 2D hydro-dynamic models have been used to simulate the future probable water levels for Devils Lake. A monthly water-balance model was developed by Ryan *et al* (1988) to simulate the elevation of Devils Lake for both low and high runoff conditions. An annual lake-volume model and a

statistical water mass-balance model were used by Wiche *et al* (1996), to estimate probable future water levels. Vecchia (2002) also developed a monthly water-balance and stochastic regression model to determine the potential effects of emergency outlet alternatives on future water levels and the water quality of Devils Lake. Their results estimated 0.02 % chance of Devils Lake rising above the spill elevation to Stump Lake. Conversely, considering a 20 year wet climatic period, the results estimated more than 50 % chance of Devils Lake spilling to Stump Lake and more than 0.05 % chance of Devils Lake spilling to the Sheyenne River.

Vecchia (2008) updated and recalibrated the 2002 stochastic regression model to analyze flood risks for the residents near Devils Lake. Inputs of various hydrologic and climatic parameters for 1950-99 were extended to include data for 2000-06. It was assumed that the lake evaporation for 2000–2006 would be similar to the lake evaporation for 1980–99. A monthly time series model, used to generate future sequences of monthly precipitation and evaporation, was simulated and traces of future lake levels were obtained for 2008-40. For the simulations, with the wet period lasting until 2010, 90 % of the simulated lake levels in 2010 were between about 1444 and 1452 ft. However, after that the lake levels progressively declined and most of the traces were between about 1420 and 1440 ft with the median being about 1428 ft in 2040. For the simulations with the wet period lasting until 2040, the simulated lake levels were highly variable and most of the traces were between about 1434 and 1456 ft and the median being 1444 ft in 2040. The report concluded that there is about a 1 % chance of Devils Lake exceeding 1459.9 ft (1.9 foot above the natural spill elevation), a 5 % chance of exceeding 1455.7 ft,

and a 10 % chance of exceeding 1453.8 ft sometime between 2008 and 2015 (Vecchia, 2008).

Vecchia (2011) modified the 2008 model and combined it with a downstream stochastic routing model to simulate future Devils Lake level for 2011-30 considering three outlet alternatives. A baseline simulation result with no outlets was also shown for comparison with the outlet simulations. The model used randomly generated future monthly sequences of precipitation, evaporation and inflow for Devils Lake where the sequences depend on initial conditions for 2010 and forecasted information for 2011 from the National Weather Service (NWS). The annual chance of Devils Lake exceeding 1454.0 for the baseline condition was reported to be 98.9 % in 2011, 57 % in 2015, and 10.8 % in 2030. The cumulative % chance of Devils Lake exceeding 1458.0 ft (the spill elevation) was reported to be 0.6 % in 2011, 27.8 % by 2015, and 44.7 % by 2030 (Vecchia, 2011). In this thesis, conditional probabilities of reaching high stages (i.e. 1456, 1458 and 1460 ft) are calculated using GCM predicted precipitation and temperature values. The base water level is set as 1454 ft, which is estimated as a 1 in 140 year event. The calculated conditional probabilities are lower than the values reported by USGS (Vecchia, 2011) whereas the unconditional probability is 1.1% using both normal and log normal distributions.

Nustad *et al* (2011) developed a numerical model using UnTRIM and calibrated it from April 1 through September 30, 2006 to simulate and evaluate the effects of an extreme flood event on the water levels of Devils Lake. Ground water contribution was not included in the model and precipitation and evapotranspiration were combined as one term called net evaporation. An extreme flood scenario based on an inflow of one-half

the probable maximum flood (1.44 million acre-ft) was simulated, which produced a maximum water level of around 1461.9 ft, which is well above the spilling elevation.

The study by USGS (Vecchia, 2008) reported that the annual precipitation from 1950-79 averaged about 18.3 inches per year, compared to about 22.4 inches per year for 1980-2006. The increase in mean precipitation of about 4.1 inches per year is a 6 in 10,000 chance, which is yielded by a two-sample t-test.

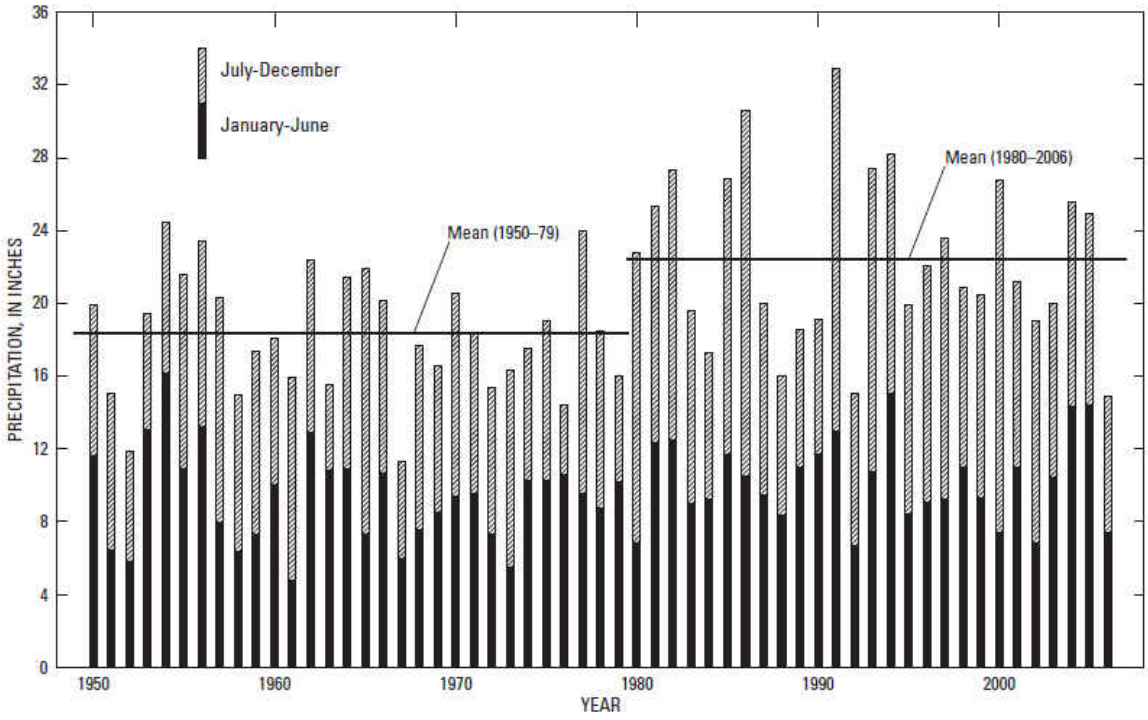

Figure 4: Change in annual mean of precipitation from 1950-2006 (Source: USGS)

Another study from NOAA (NOAA, 2010) explained the changing precipitation patterns at Devils Lake. The precipitation estimates obtained from PRISM datasets are plotted as a 10 year running average, which can be seen in Figure 5. The plot shows a significant increase in annual precipitation starting from the mid 90's. Using the century-

long record over the area, a positive correlation of +0.71 is found that confirms the strong temporal coherence between climate and hydrology of the region.

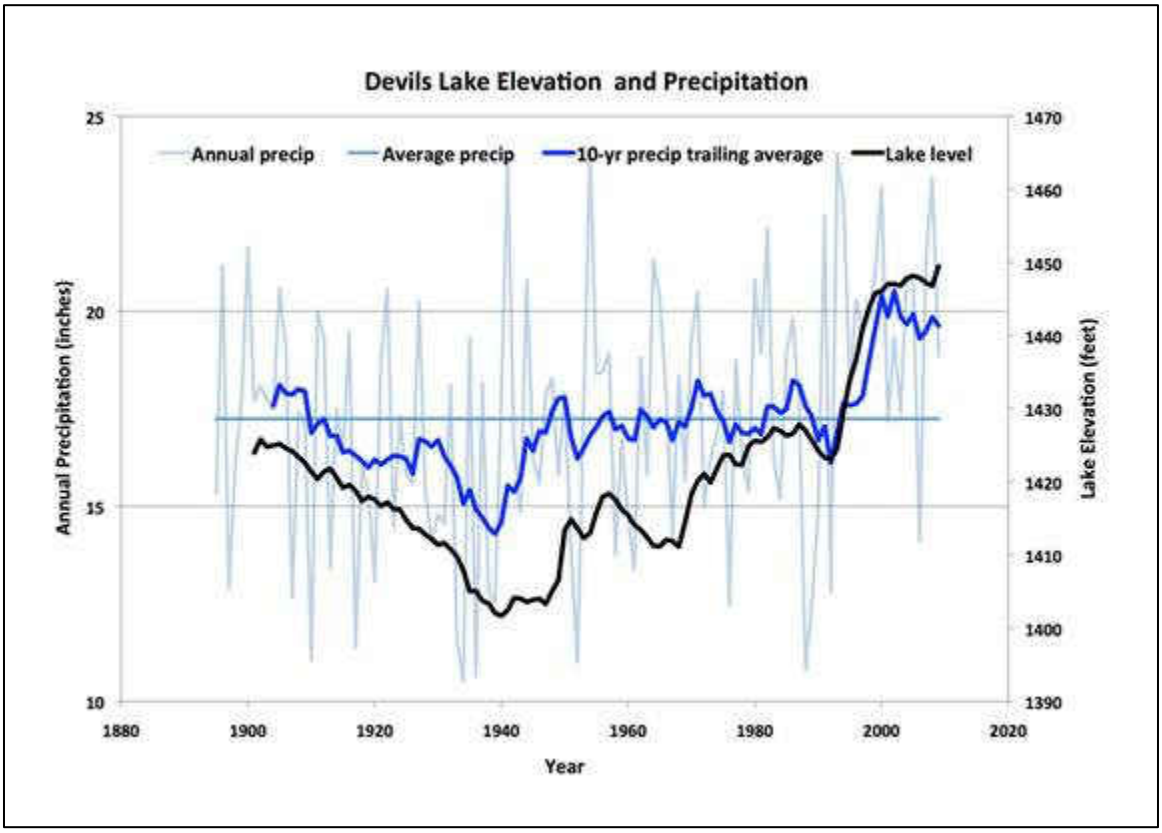

Figure 5: Plot of the water level of Devils Lake along with 10 year running average of annual precipitation estimates using PRISM data

CHAPTER 3

METHODOLOGY AND MODEL

3.1 Scope of the Study

The previous studies on the lake are based on monthly water-balance, hydro-dynamic and statistical probabilities. General Circulation Models (GCM) downscaled for specific study regions have never been used in conjunction with HEC models to understand the fluctuation of the lake levels in a daily basis for future years. In this research, a coupled hydro-climatic model has been developed, which is driven by downscaled GCM-generated climate inputs under various scenarios, which are dependent on changing anthropogenic factors. The purpose is to determine the feasibility of using spatially distributed GCM data with a well calibrated hydro-climatic model to inform the probable flood severities for the simulation period of 30 years (2021-2050). To run the simulation, base condition is assumed to be the peak water level of 2011, which is 1454 ft above National Geodetic Vertical Datum of 1929 (NGVD 29). Unless stated otherwise, this datum will be used as the reference for elevations throughout the thesis.

Several softwares developed by the Hydrologic Engineering Center (HEC) of US Army Corps of Engineers (USACE) have been implemented in achieving the research goal, e.g., HEC-HMS, HEC-DSSVue, HEC-ResSim and HEC-SSP. Moreover, ArcGIS and ArcHydro have been used to process the Digital Elevation Models (DEMs) of the study area to delineate the watershed and to calculate the required physical properties. Modeling the lake consists of four parts:

1) Watershed delineation using geo-processing tools, e.g., ArcGIS and ArcHydro
2) Watershed modeling using HEC-HMS
3) Reservoir modeling using HEC-ResSim
4) Evaporation modeling, which is done by developing a temperature-based method

Eight sub-basins of the Devils lake basin are identified and the contributing areas are calculated. A plot of the sub-basins from USGS is showed in Figure 6. In this project, the Comstock and Little Coulee sub-basin are considered as a single sub-basin. Six of the sub-basins are delineated using ArcGIS and ArcHydro tools (Figure 7), which is done by Joshua Hassell (Hassell, 2010). The delineation is done using available Digital Elevation Models (DEMs) from USGS. Numerous short streams feeding the Devils Lake make the delineation of the North and South sub-basins more complex in ArcGIS. Hence, the two remaining sub-basins are delineated using geo-pdf maps (Figure 8 and Figure 9).

The purpose of the watershed model is to calculate the runoff to the Devils Lake from its sub-basins. Proper distribution and representation of daily precipitation and temperature data are important factors in modeling a watershed. So in addition to ground gage data, spatially distributed daily climate data obtained from TRMM Multi-satellite Precipitation Analysis (TMPA) by NASA's satellite observations are also used to analyze the effects on the model. The runoff output is imported in a reservoir simulation model called HEC-ResSim to estimate the daily water level. The watershed model is calibrated using climate data from both ground gage and NASA TMPA, whereas the reservoir model is calibrated based on historical values of lake levels.

Figure 6: Sub-basins of the Devils Lake (Source: USGS)

Fluctuations in the water level of the Devils Lake happen on a relatively short time scale in response to seasonal variability and on a long time scale in response to climate variability. Because of seasonal variability, water levels in any given year start rising in the spring in response to snow melt and rain, reaching a peak water level sometime between April and July and decline through the summer months in response to evaporation, reaching a minimum in late fall or early winter (Wiche, 1994). Because of

climate variability, Devils Lake is extremely sensitive to long-terms shifts in global circulation patterns. So the water level depends on many years of antecedent precipitation, runoff, and evaporation (Wiche *et al*, 2000). If either precipitation and runoff, or evaporation dominates, a corresponding response occurs in the water level. Being a terminal lake the only natural mechanism for removal of water from Devils Lake is evaporation. So it is very important to devise a mechanism to estimate the evaporation for future years. A temperature-based model has been calibrated to predict the future evaporation pattern by analyzing eight radiation-based methods and a simplified Penman type method. The one with the best calibration fit has been chosen to simulate future evaporation with seasonal effects.

To estimate the growth of the lake throughout the simulation period (2021-2050), data obtained from different GCMs under three different scenarios are used. These data present an ensemble of precipitation and temperature estimation that represent the future climate and are not the exact prediction of the future climate at a specific point of time. To account for the uncertainty of the distribution of wet and dry years, ten reshuffled groups of temperature and precipitation values for each set of climate data have been used. HEC-DSSVue, a data storage system has also been analyzed to check its data interoperability between the watershed (HMS) and reservoir (ResSim) model.

Properly calibrated hydro-climatic model driven by reshuffled GCM climate data series is expected to predict the severity of flood in Devils Lake basin, which will be a great aided tool in planning and materializing future flood mitigation measures for this flood affected area.

3.2 Description of Watersheds

Figure 7 shows a schematic of the sub-basins of the Devils Lake. The Basin, sub-basins and their sub-areas are delineated by processing the DEMs using ArcGIS and ArcHydro. Comstock Coulee sub-basin is relatively smaller in size and adjacent to the Little Coulee sub-basin. These two sub-basins have been considered as a combined sub-basin and the eight sub-basins have been delineated to be used in the coupled hydro-climatic model. Six of the eight sub-basins were delineated using ArcGIS and ArcHydro by Joshua Hassell (Hassell, 2010). Many short streams flowing towards the lake shore area makes ArcGIS and ArcHydro not very efficient in delineating the North and South slope sub-basins. To overcome the obstacle these two sub-basins are delineated using Geo-PDF maps (Figure 8 and Figure 9) and TerraGo tools (Appendix A).

To delineate the sub-basins using ArcGIS software, DEMs of 1 arc second (30 meter) resolution are downloaded from USGS and the tools listed below are used in a sequential manner (Lim *et al*, 2010) to obtain the final product. The complete procedure of delineating the sub-basins can also be found in the design report of Joshua Hassell (Hassell, 2010). Figure 7 shows the combined schematic of the six sub-basins delineated using ArcGIS and ArcHydro tools. Table 1 lists all the individual sub-areas in square miles, calculated using both GIS and TerraGo tools. Area of the combined lake is also determined.

The contributing sub-basins to the Devils Lake are Mauvais coulee, Calio coulee, Edmore coulee, Starkweather coulee, Little and Comstock coulee, Stump Lake, Devils Lake North and Devils Lake South. To model the watershed several geo-processing tools are used, which are Fill (Hydrology), Flow Direction (Hydrology), Flow Accumulation

(Hydrology), Stream Definition (Arc-Hydro), Stream Link (Hydrology), Catchment Grid Delineation (Arc-Hydro), Catchment Polygon Processing (Arc-Hydro) and Calculate Areas (Spatial Statistics).

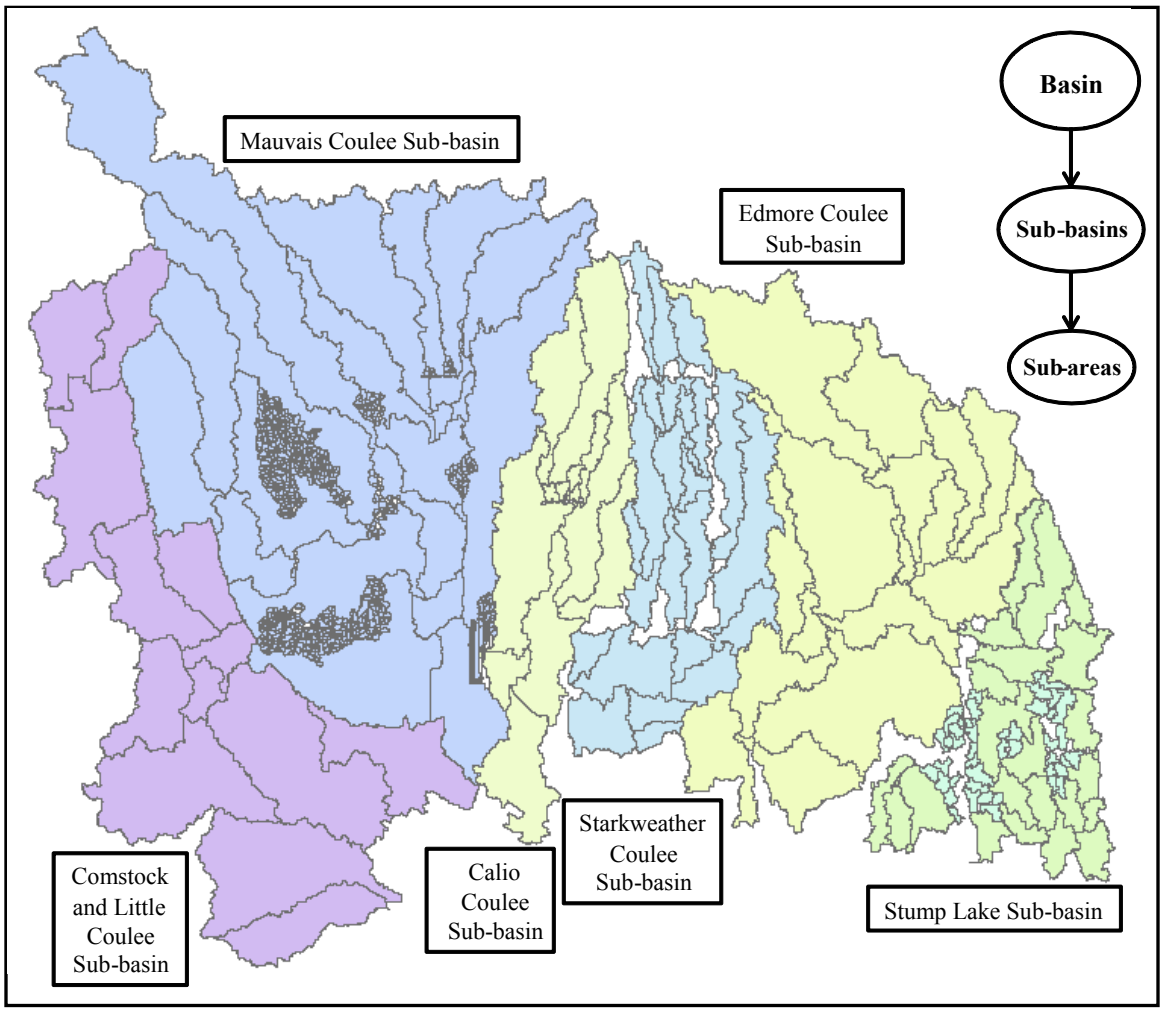

Figure 7: Combined sub-basins delineated using ArcGIS and ArcHydro

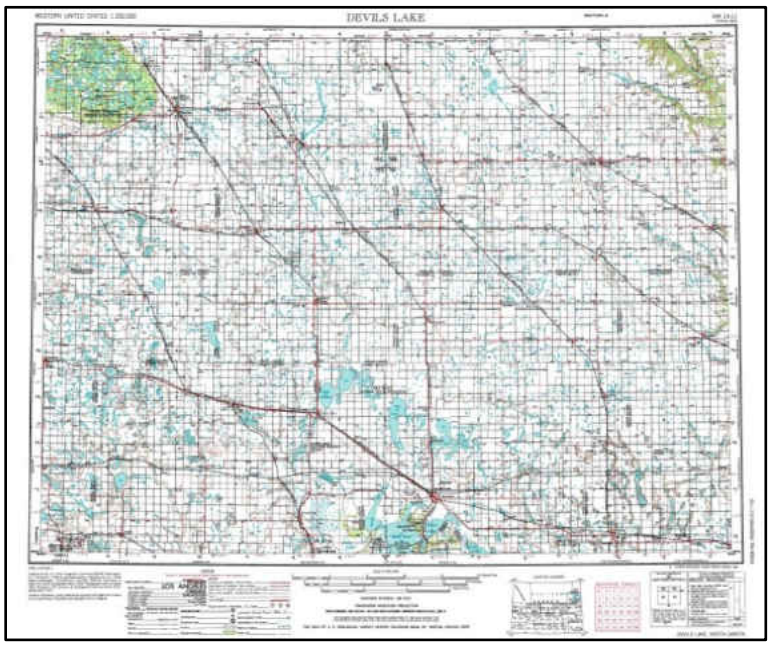

Figure 8: Geo-pdf map of Devils Lake used for sub-basin delineation (Source: USGS)

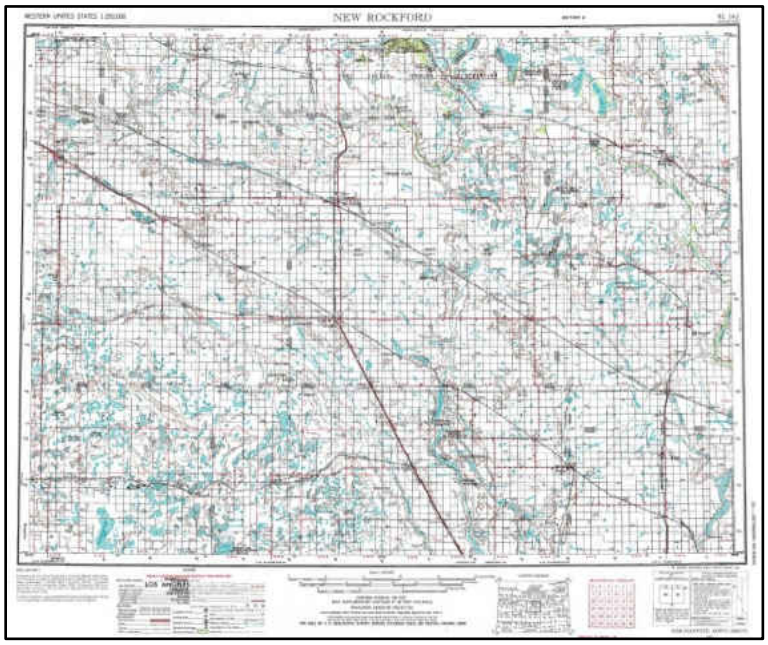

Figure 9: Geo-pdf map of New Rockford used for sub-basin delineation (Source: USGS)

Table 1: Calculated areas (sq. miles) of the sub-areas in the HEC-HMS model

Mauvais basin

Name	1_M-1	2_M-2	3_M-3	4_M-4	5_M-5	6_M-6	7_M-7
Area	38.6	46.3	30.8	42.4	50.2	57.9	30.8
Name	8_M-8	9_M-9	10_M-10	11_M-11	12_M-12	13_M-13	14_M-14
Area	38.6	50.1	54.1	34.7	30.8	38.6	57.9
Name	15_M-15	16_M-16	17_M-17	18_M-18	19_M-19	20_M-20	
Area	65.06	54.05	42.4	34.75	50.19	30.88	

Calio basin

Name	21_C-1	22_C-2	23_C-3	24_C-4	25_C-5	26_C-6	27_C-7	28_C-8	29_C-9
Area	38.11	25.76	30.07	7.86	21	45.92	27.58	8.57	30.09

Starkweather basin

Name	30_W-1	31_W-2	32_W-3	33_W-4	34_W-5	35_W-6	36_W-7	37_W-8
Area	13.9	20.49	13.26	25.03	34.58	16.92	19.17	15.44
Name	38_W-9	39_W-10	40_W-11	41_W-12	42_W-13	43_W-14	44_W-15	45_W-16
Area	10.84	21.5	12.82	30.82	11.4	7.52	3.98	16.14

Edmore basin

Name	46_E-1	47_E-2	48_E-3	49_E-4	50_E-5	51_E-6	52_E-7	53_E-8
Area	24.04	83.39	39.75	19.62	72.72	18.6	12.47	36.64
Name	54_E-9	55_E-10	56_E-11	57_E-12	58_E-13	59_E-14	60_E-15	
Area	22.92	83.36	20.66	7.56	25.12	26.71	25.91	

Little Coulee basin

Name	61_L-1	62_L-2	63_L-3	64_L-4	65_L-5	66_L-6	67_L-7
Area	22.77	29.08	66.12	25.55	36.67	28.77	10.84
Name	68_L-8	69_L-9	70_L-10	71_L-11	72_L-12	73_L-13	
Area	7.75	62.8	65.15	28.97	80.91	40.77	

Stump Lake basin

Name	74_S-1	75_S-2	76_S-3	77_S-4	78_S-5	79_S-6	80_S-7	81_S-8
Area	19.73	25.31	12.87	17.04	19.01	15.63	10.71	19.04
Name	82_S-9	83_S-10	84_S-11	85_S-12	86_S-13	87_S-14	88_S-15	89_S-16
Area	19.45	23.94	36.72	13.98	7.91	10.66	9.03	11.29
Name	90_S-17	91_S-18	92_S-19	93_S-20	94_S-21	95_S-22		
Area	12.99	13.24	11.61	15.22	12.66	10.68		

Total Area

Name	Mauvais	Calio	Stark weather	Edmore	Little and Comstock	Stump Lake	D.L. North	D.L. South	Lake Area
Area	879.13	234.96	273.81	519.47	506.15	348.72	445.33	350.42	206.46

3.3 Rainfall-Runoff Model (HEC-HMS)

The Hydrologic Modeling System (HEC-HMS) is designed to simulate the rainfall-runoff processes of dendritic watershed systems and is applicable in a wide range of geographic areas. The program is a generalized modeling system capable of representing many different watersheds. A model of the watershed is constructed by separating the hydrologic cycle into manageable pieces and constructing boundaries around the watershed of interest. The program features a completely integrated work environment including a database, data entry utilities, computation engine, and results reporting tools. A graphical user interface allows the seamless movement between the different parts of the program. The fundamental components of a HMS model are:

1. Basin Model,
2. Meteorological Model,
3. Time Series Data Manager,
4. Paired Data Manager and
5. Control specification manager.

The layout of the combined model and the grid pattern set for the model are shown in Figure 10 and Figure 11. Grid lines along both latitude and longitude are $0^0 15' 0''$ apart and a set of temperature and precipitation values are available for each grid cell.

3.3.1 Basin Model

The basin model consists of several sub-basins, sub-areas, reaches, junctions and a sink, which represents the lake body. Different loss method, transform method and base flow method can be set for each sub-basin and sub-area. In the combined HMS model

initial and constant method has been selected as the loss method. SCS Unit Hydrograph is set as the transform method and base flow is considered negligible. The initial loss specifies the amount of incoming precipitation that will be infiltrated or stored in the watershed before surface runoff begins. There is no recovery of the initial loss during periods without precipitation. The constant rate determines the rate of infiltration that will occur after the initial loss is satisfied. The same rate is applied regardless of the length of the simulation. Determination of the appropriate values for these two variables varies from place to place and need calibration.

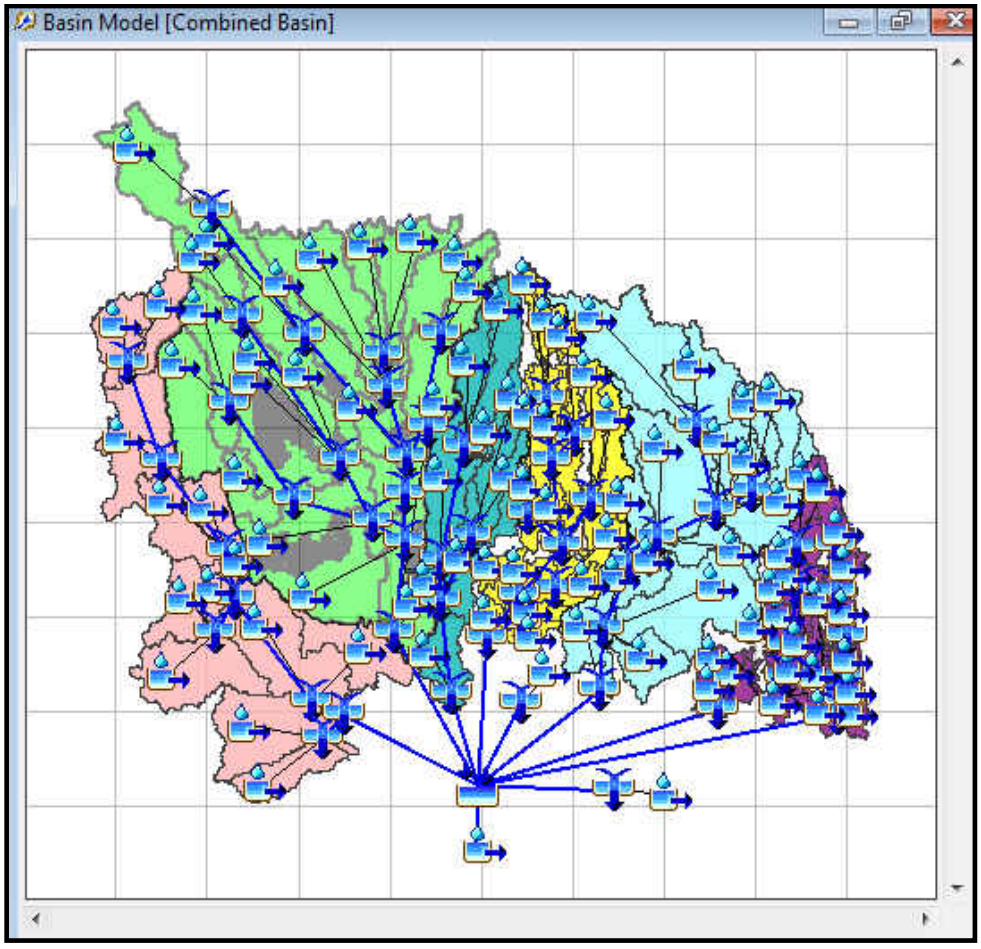

Figure 10: Layout of Combined Watershed in HEC-HMS

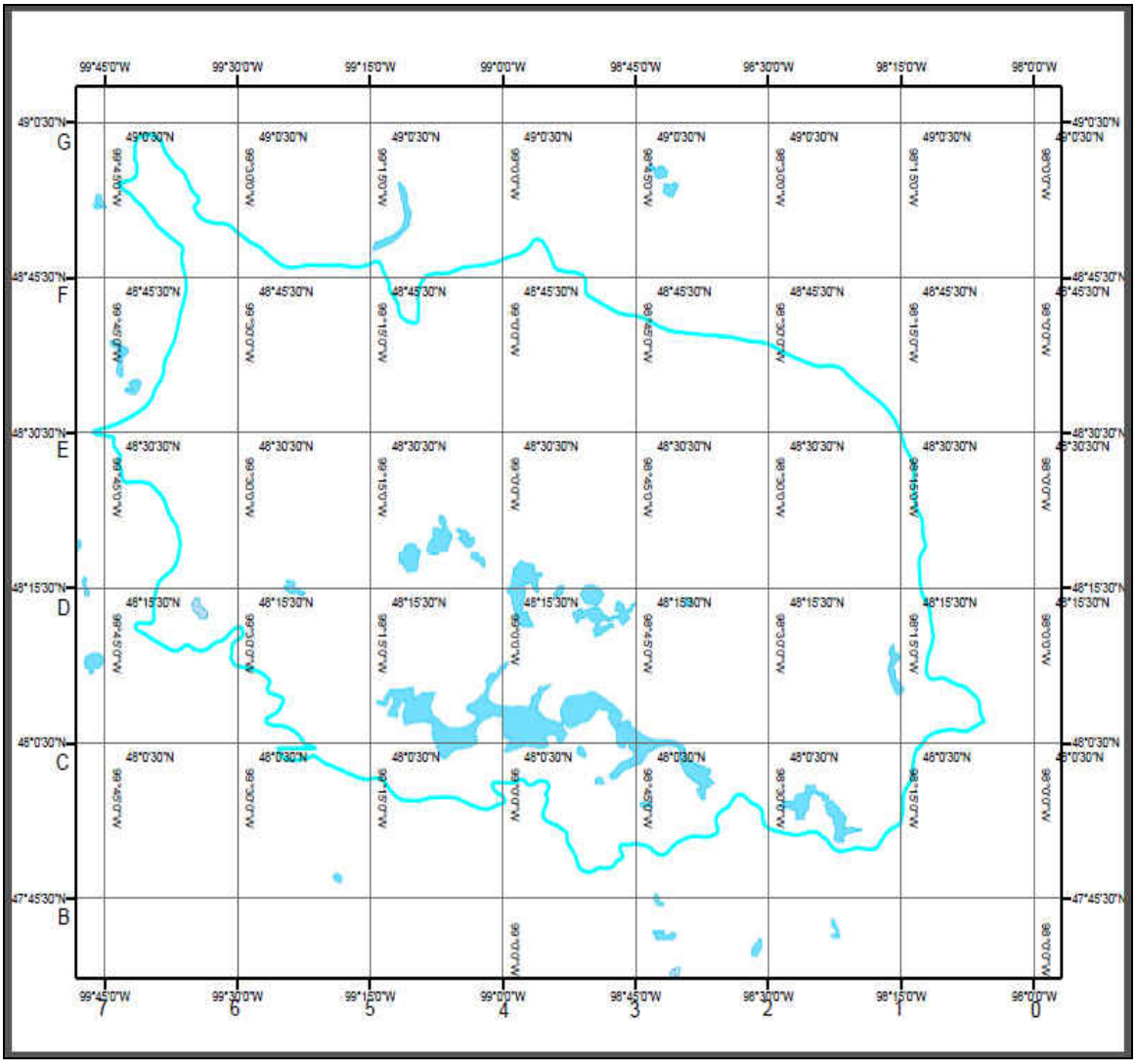

Figure 11: Grid layout for the HEC-HMS model

Percentage of impervious area has been specified for each sub-area. The approximation on impervious area has been carried out based on observations and simple calculations from google maps. It is found that the percentage of impervious area is very low (less than 1%) in most of the areas. No loss calculations are carried out on the impervious area; all precipitation on that portion of the sub-area becomes excess precipitation and subject to direct runoff. Downstream junction of each reach has been specified and routing is set as Lag method. Each sub-area is connected to the next

downstream junction where the flow accumulates and finally reaches the sink, which represents the Devils Lake. The combined model contains 97 sub-areas, 58 reaches and 59 junctions, which are named in an orderly manner, which is described in Table 2. Another sub-area called Devils Lake is created to generate the runoff due to rain on the lake itself and its area is set as the area of the lake. Very small losses have been considered for this sub-area as all the water in the form of precipitation falls directly on the lake. Details on naming the sub-basins and their components in HEC-HMS can be found in Appendix B.1.

Table 2: Unique IDs used in the HEC-HMS model

Name	Code	Sub-area	Reach	Junction
Mauvais	M	1 to 20	1 to 14	1 to 15
Calio	C	21 to 29	15 to 19	16 to 20
Starkweather	W	30 to 45	20 to 29	21 to 30
Edmore	E	46 to 60	30 to 36	31 to 37
Little & Comstock Coulee	L	61 to 73	37 to 44	38 to 45
Stump Lake	S	74 to 95	45 to 56	46 to 57
Devils Lake North	DL	96	57	58
Devils Lake South	DS	97	58	59

3.3.2 Meteorological Model

The meteorological model contains information on gage weights, snow-melt and unit system. The total watershed is divided into 48 grid cells of equal size. Climatic data are obtained from NASA satellite for each of those grid cells. Precipitation gage weights are set for contributing gages. Temperature Index method is selected for the snow-melt

model. Defining the snowmelt model requires the knowledge of several parameters (Source: HEC-HMS User Manual), which are described below.

3.3.2.1 Base Temperature

The difference between the base temperature and the air temperature defines the temperature index used in calculating snowmelt. If the air temperature is less than the base temperature, then the amount of melt is assumed to be zero. Typically, the base temperature should be 0°C (32°F) or close to it.

3.3.2.2 PX Temperature

The PX temperature is used to differentiate between precipitation falling as rain or snow. When the air temperature is less than the specified temperature, any precipitation is assumed to be snow. When the air temperature is above the specified temperature, any precipitation is assumed to be rain. This temperature is usually one to two degrees above freezing.

3.3.2.3 Wet Melt-rate

The wet melt-rate is used during time periods of precipitation when the precipitation is falling as rain, at rates greater than the rain rate limit. It represents the rate at which the snowpack melts when it is raining on the pack.

3.3.2.4 Rain Rate Limit

The rain rate limit differentiates the dry melt rate and wet melt rate. The wet melt-rate is applied as the melt-rate when it is raining at rates greater than the rain rate limit. If the rain rate is less than the rain rate limit, the melt-rate is computed as if there were no precipitation.

3.3.2.5 ATI Melt-Rate Coefficient

A melt-rate must be calculated for time intervals when the precipitation rate is less than the rain rate limit. A typical value for the coefficient is 0.98.

3.3.2.6 Cold Limit

The cold limit accounts for the rapid changes in temperature that the snowpack undergoes during high precipitation rates. When the precipitation rate exceeds the specified cold limit, the antecedent cold content index is set to the temperature of the precipitation. If the temperature is above the base temperature, the cold content index is set to the base temperature. If the temperature is below the base temperature, the cold content index is set to the actual temperature. If the precipitation rate is less than the cold limit, cold content index is computed as an antecedent index. A typical value is 20 mm/day (0.8 in/day).

3.3.2.7 Cold Content

This is a separate index from the one used to update the melt-rate index. A typical value for the coefficient is 0.84.

3.3.2.8 Water Capacity

The maximum liquid water capacity specifies the amount of melted water that must accumulate in the snowpack before liquid water becomes available at the soil surface for infiltration or runoff. Typically, the maximum liquid water held in the snowpack is on the order of 3%-5% of the snow water equivalent.

3.3.2.9 ATI Melt-Rate Function

An antecedent temperature index melt-rate function is used to calculate a melt-rate from the current melt-rate index. The function must be specified separately in the

Paired Data Manager before it can be used in the snow melt method. The function defines appropriate melt-rates to use over the range of melt-rate index values that will be encountered during a simulation.

Using the difference between the air temperature and the melt temperature of the snowpack, the temperature index method calculates snow-melt. A linear relationship is assumed between this temperature difference and the snow melt rate (Vuyovich *et al, 2010*). This is often a reasonable assumption as the air temperature is physically associated with the predominant energy fluxes associated with melt (Ohmura, 2001). Snowmelt is estimated as

$$M = (T_a - T_b)\, C_m \qquad (1)$$

where,

C_m = the melt rate coefficient (in/°F-day) (usual values from 0.04-0.08 in/°F-day);

T_a = the air temperature (°F); and

T_b = the melt temperature of the snow pack (generally 32°F).

The melt coefficient, C_m, can represent a dry melt rate or a rain melt rate. The rain melt rate is applied when the snowpack is melting and rain is falling at a rate greater than the rain rate limit. The dry melt is applied when the precipitation rate is lower than the rain rate limit.

3.3.2.10 Initial and Constant Loss

The initial loss specifies the amount of incoming precipitation that will be infiltrated or stored in the watershed before surface runoff begins. There is no recovery of the initial loss during periods without precipitation.

The constant loss rate determines the rate of infiltration that will occur after the initial loss is satisfied. The same rate can be applied regardless of the length of the simulation. Usual value ranges from 0.05-0.15 in/hr for clay loams, shallow sandy loam, soils low in organic content and soils usually high in clay, which is more applicable for the Devils Lake study area.

3.3.3 Time Series and Paired Data Manager

The time series data manager contains the precipitation and temperature data location. The data are stored in HEC-DSSVue, which is a data storage tool developed by the Army Corps of Engineers. HEC-DSSVue performed as an extremely handy data bridge tool between the watershed model and the reservoir model. The paired data manager stores paired data that can be plugged into the model manually. In this model the ATI melt-rate functions were stored in the paired data manager.

3.3.4 Control Specifications Manager

The control specification manager stores the information about duration of the simulation. The time interval of the simulation run is set as '1 Day' and start date and end date is set according to requirement.

3.4 Reservoir Model (HEC-ResSim) Description

The HEC-ResSim model is developed to represent the lake. The model stores the physical dimensions of the lake. Using HEC-DSSVue the model also stores the Runoff to the lake and evaporation from the lake. No losses in the reaches have been considered here as those parameters are previously taken care of in the watershed model. Seepage is assumed to be negligible and set to zero for simulation purposes. The model is able to

simulate the lake water level in a daily basis using the runoff amount into the lake and evaporation out of the lake. Water spills through Tolna Coulee at an elevation of 1458 ft. To model the event, a dam is considered at 1458 ft. The model consists of three steps: Watershed Setup**,** Reservoir Network and Simulation. The module concept and layout are presented in Figure 12 and Figure 13.

3.4.1 Watershed Setup Module

In the watershed setup module, a schematic layout of the network is developed, which is shown in Figure 13. Using the stream alignment tool, all the streams are delineated.

3.4.2 Reservoir Network Module

In the reservoir network module, reaches are created on the streams by using the reach tool. The reservoirs are placed and junctions are defined. The reservoir network module allows the editing of the reservoir, junction and reach properties. The top elevation of the dam is set to the natural spilling elevation, which is 1458 ft and the length at the top of the dam is set to 650 ft.

Evaporation from lake, which is the primary source of water loss, is modeled in HEC-ResSim. The operation set is defined and observed water level of the lake is used for benchmarking with computed water levels.

3.4.3 Simulation Module

The final step in this modeling is the simulation, which is performed in daily basis from January 2003 to December 2010. The climate data obtained from TMPA is available from 2002-2010 (Table 4). That is why this time period has been selected for

the simulation. The simulation provides us with the water level of the lake at daily time intervals.

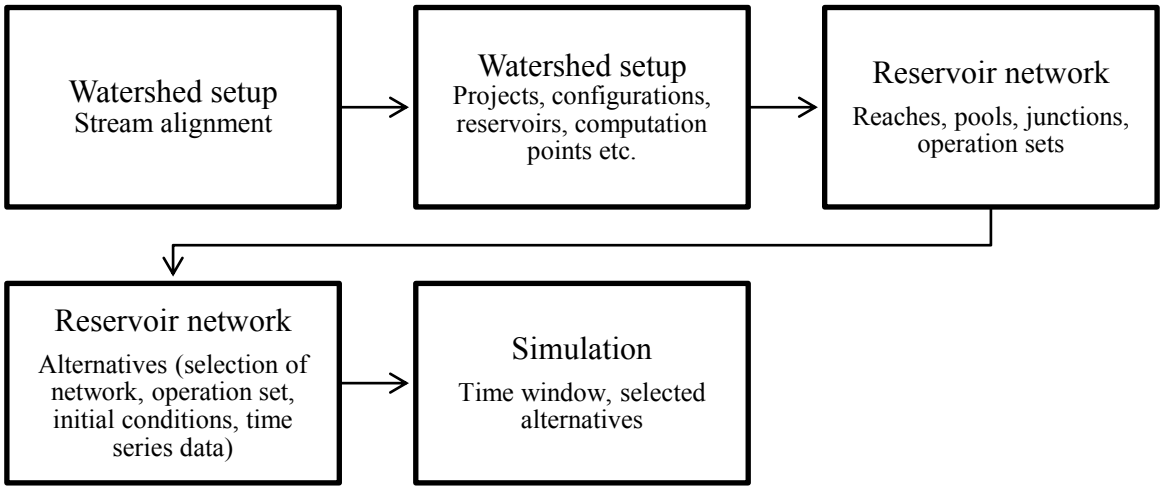

Figure 12: ResSim module concept (Source: USACE HEC-ResSim Manual)

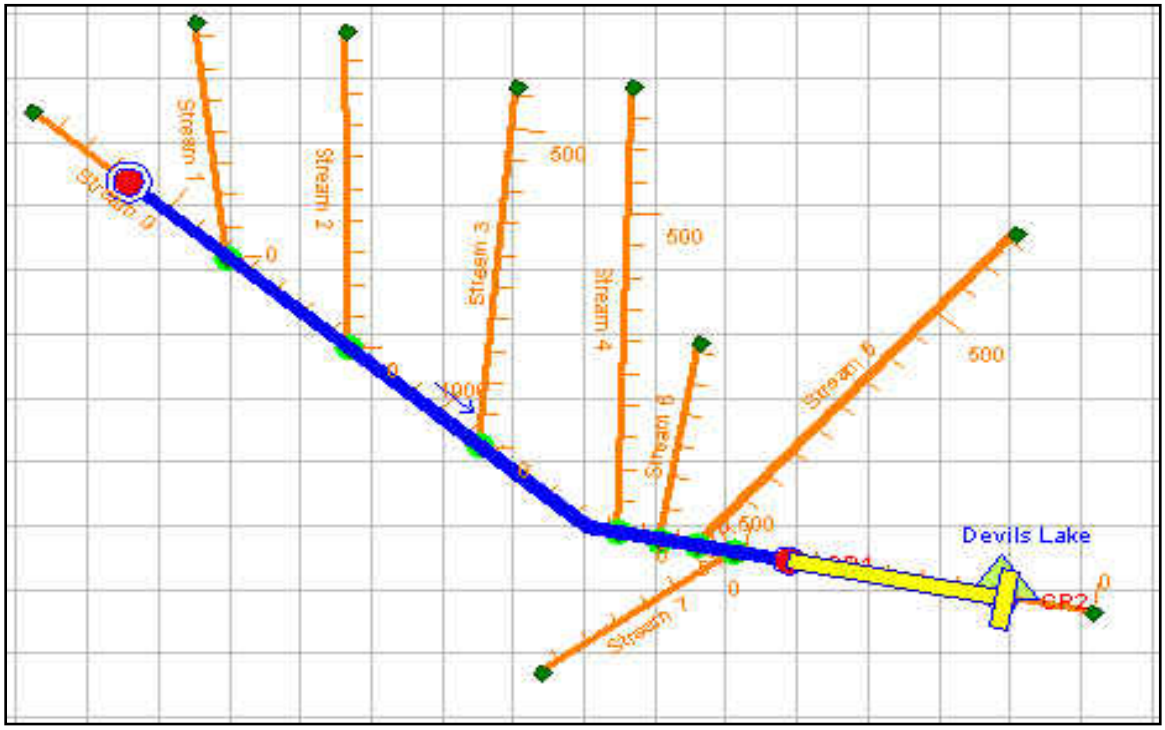

Figure 13: Schematic layout of the HEC-ResSim model

The dark yellow lines represent the inputs from each sub-basin that flows into the Devils Lake. The Devils Lake is represented by the light yellow portion on the bottom right corner of Figure 13. The blue line represents the reach connection that takes the flow to the reservoir. The green circles represent the junction.

CHAPTER 4

CALIBRATION OF THE COUPLED HYDRO-CLIMATIC MODEL

4.1 Overview and Data Sources

Calibration is done based on the Mauvais Coulee basin by generating the runoff and comparing it with the observed values from USGS stream flow gage station at Cando, ND. Ideally calibration is required for each of the sub-basins to accurately represent the run off volumes in the model. But due to limited data availability, the calibration is limited to Mauvais coulee, assuming similar conditions throughout the basin. Two different sets of climate data (precipitation and temperature) have been used in modeling the watershed which are:

a) Ground gage climate observations and

b) TRMM Multi-satellite Precipitation Analysis (TMPA) by NASA.

To facilitate the understanding of the calibration process, throughout the report, the watershed model in HEC-HMS will be referred as **HMS-Model A** to indicate the use climate data from a single ground gage and as **HMS-Model B** to indicate the use of spatially distributed climate inputs from TMPA by NASA.

4.2 Calibration Parameters of HEC-HMS and HEC-ResSim Model

There are several factors in calibrating the HEC-HMS model and the HEC-ResSim model. In HEC-ResSim the calibration factors are evaporation and seepage. The calibration factors in HMS are listed in Table 3.

Table 3: Calibration parameters in HEC-HMS

Initial Loss (in)	ATI melt-rate coefficient
Constant Loss (in/hr)	ATI melt-rate function
PX and Base Temperature (^{0}F)	Cold limit (in/day)
Wet melt-rate (in/^{0}F-day)	ATI cold-rate coefficient
Melt rate, C_m	Rain rate Limit (in/day)

The value of constant loss varies from 0.05-0.15 (in/hr) as suggested in the HMS user's manual. The manual also provides usual values of some of the snow melt parameters. Typically, the PX temperature is one to two degrees above freezing and the base temperature is 0^0C (32^0F) or close to it. These values are set to 33.5^0F and 32^0F respectively. Cold limit is set as 0.8 in/day. ATI melt rate and cold rate coefficients are set as 0.98 and 0.84 as suggested in the user's manual.

4.3 Calibration Steps

In this section the important steps and outcomes of the calibration process are explained. Water starts freezing during the end of fall and the beginning of winter. Snow accumulates throughout the winter and starts melting during the spring. The spring melt is one of the key factors in calibrating the model. During summer, the lake receives runoff mainly due to precipitation. The model is calibrated both for snow melt and summer runoffs details of which can be found in Appendix C. The HEC-HMS model uses the temperature index method to model the snow melt, which requires a significant amount of model inputs, which are listed in Table 3. The user's manual provides a general guideline on the usual values of some of the parameters, but to obtain a better fit

with observed flows, calibration is required. Calibration of the snow melt is done in a trial and error basis by varying the values of the parameters within the suggested range and comparing the results with observed runoff estimates. On the other hand, for the calibration of summer runoff, the fundamental calibration parameters are the loss coefficients. The initial and constant loss method is chosen for modeling the loss. A sensitivity analysis of the snow melt and loss parameters is also performed to check their effects on the model.

4.3.1 Gage Stations and Climate Data

At the initial stage of calibration, the goal is to obtain the runoff at a station by running the model and compare the flow with the observed values. The biggest sub-basin in the Devils Lake basin is the Mauvais Basin. Gage station on Mauvais Coulee (Figure 14) at Cando (USGS: 05056100) is selected for the calibration as it has continuously observed stream flow data from June 1956.

The climate data required to drive the model includes precipitation, temperature and evaporation. For HMS-Model A, several ground gage stations are available for historic precipitation and temperature series, but a few of them have continuous observations for longer periods. Some of the stations are active only during the summer months and remain close during the winter periods.

As a first step, short term calibration is done for both snow melt and summer storms. For this purpose climate series containing multiple years are not necessary. Instead it is more important to select a station that can represent the Mauvais sub-basin for climate inputs. Gage station at Towner (Figure 14) is selected for this purpose as the station better represents the Mauvais sub-basin.

During the last steps of calibration, a different approach is followed, which includes calibrating the HMS model with the ResSim model for 2003-2010. This necessitates the availability of continuous climate data for 2003-2010. So a new ground gage station at Langdon (Figure 14) is selected for continuous precipitation and temperature data.

As evaporation is one of the key forms of outflow from the lake, it is very important to have accurate evaporation estimates. Penman evaporation estimates at Crary (Figure 14) are downloaded from North Dakota Agricultural Weather Network (NDAWN) and is used in the model to represent the evaporation from the lake. The report from USGS (Vecchia, 2008) suggested the annual evaporation values from the lake. A multiplier is used with the values from Crary to match the average annual evaporation values reported by the USGS study.

The feasibility of implementing spatially varied precipitation data from TRMM Multi-satellite Precipitation Analysis (TMPA) and temperature data from Atmospheric Infrared Sounder (AIRS) provided by NASA are also investigated in this research project. The details on source, resolution and coverage (Zhang, 2010) are listed in Table 4. To be used in the model, daily data with a spatial resolution of $\frac{1}{4}$ degree are used.

Table 4: Data products and parameters obtained from NASA

Instrument/Model/Parameter	Spatial Resolution	Spatial Coverage	Temporal Resolution	Temporal Coverage
TMPA Precipitation (TMI, SSM/I, AMSR-E, AMSU-B)	$\frac{1}{4}$ deg	Global 50N-50S	3-hourly, Daily	1998-Present
Aqua AIRS Surface Air Temperature	1.0 deg	Global	Gridded	2002-Present

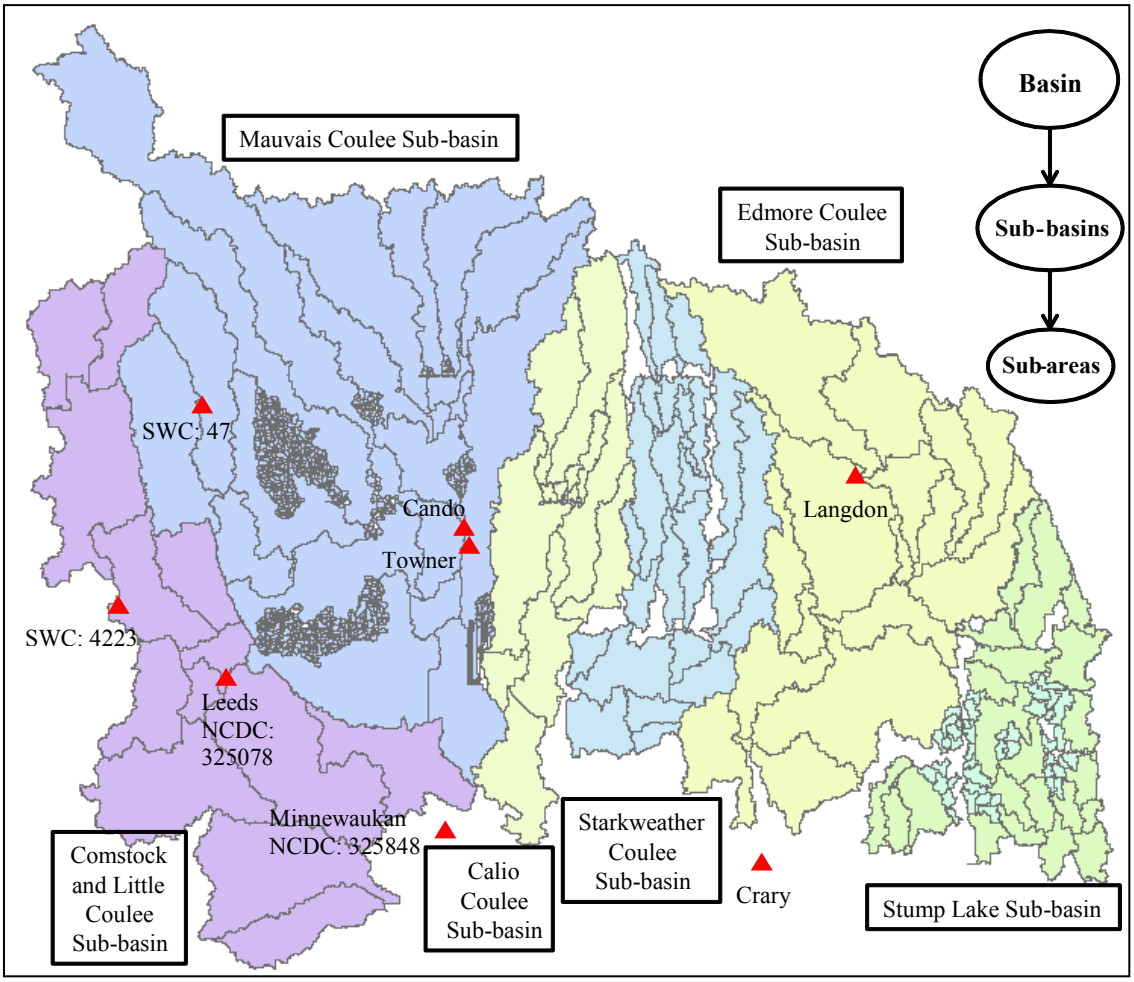

Figure 14: Gauge locations in the watershed of Devils Lake

For the simulation of future years, 30 year precipitation and temperature data from General Circulation Models are obtained. As the GCM projections at a temporal scale below one month are not considered reliable (Kilsby *et al*, 1999), further modifications are needed, which are done by Professor Dr. Andrei Kirilenko (Kirilenko, 2010). The obtained products are the ensembles of precipitation and temperature estimates with daily temporal resolution and a spatial resolution of $\frac{1}{4}$ deg. To treat the uncertainty of climate variables, the data sets for both precipitation and temperature are reshuffled by Dr. Andrei Kirilenko and 10 more series are generated from each series of

climate ensembles. The final products are 100 sets of temperature and precipitation data series generated by 4 GCM models (CSMK3, GFCM21, GIAOM and HADCM3) under 3 SRES scenarios (A1B, A2 and B1).

Future estimates of evaporation are also required to simulate the outflow from the model. To generate future evaporation series, a model is developed by selecting one from the nine calibrated models having the best fit with the evaporation series obtained from Crary weather station. The model is primarily dependent on temperature for which the AIRS generated temperature series are used.

4.3.2 Sensitivity of the Loss Parameters

The loss parameters play a key role in generating the runoff from the sub-basins. So a sensitivity analysis of the loss parameters is performed. It is found that the constant loss (in/hr) has greater effect on generating total runoff than initial loss (in). On the other hand the peak outflow is primarily sensitive to constant loss. The constant loss parameter affects the runoff throughout the simulation period whereas the initial loss is the amount that is abstracted before surface runoff begins. The plots of the sensitivity analysis can be seen in Figure 15 and Figure 16.

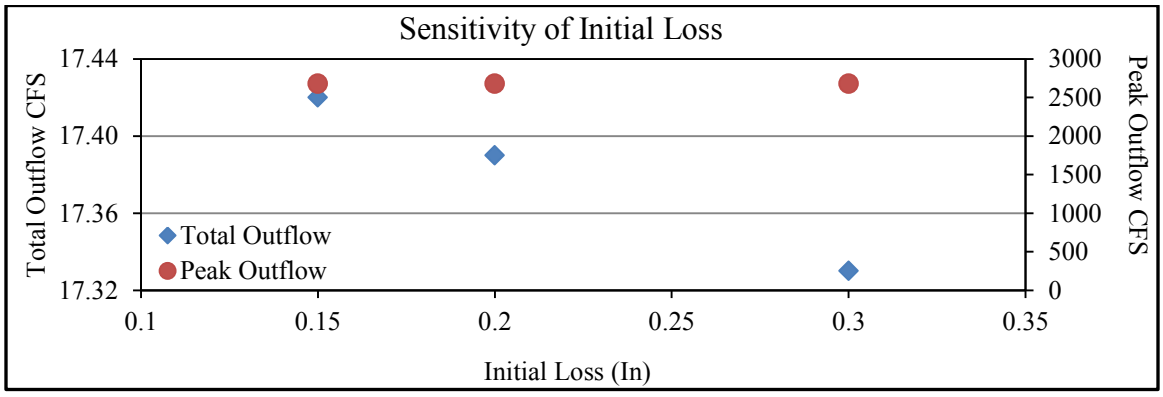

Figure 15: Sensitivity of initial loss in the HEC-HMS model

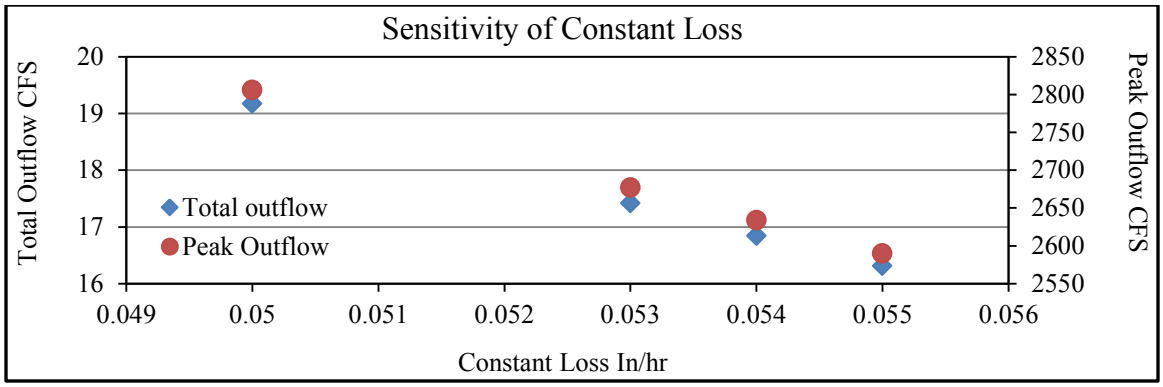

Figure 16: Sensitivity of constant loss in the HEC-HMS model

4.3.3 Calibration of HMS-Model A and HMS-Model B

The HMS-Model A is calibrated for both loss and snow melt parameters and the obtained values are used in the HMS-Model B. As a first step, the HMS-Model A is calibrated for individual summer storms. The best fit is observed using 0.235 in as the initial loss and 0.115 in/hr as the constant loss. The calibration is done from June 6 to July 15, 2001. Precipitation data is used from gage station at Towner and the runoffs are compared with the values from stream flow gage station at Cando. The observed runoff is 0.22 inch. The plot showing the fit can be seen in Figure 17. The calibrated parameters for HMS-Model A are used in HMS-Model B and a total deviation of about 0.18 inch in total outflow is observed. The deviation is significantly large and the potential reason for this deviation is the difference in precipitation estimates in the TMPA data. The cumulative rainfall (TMPA) amount is 35% lower (6.27 inch in Towner vs. 4.06 inch in TMPA data) than gage observations in Towner station. The time series from both sources are plotted to investigate the difference in precipitation estimates in terms of magnitude. It is very important to capture the big storm events accurately as that generates considerable amount of runoffs. The smaller rainfall events are usually trapped in the

vegetation and returns back to the environment. Figure 18 shows a comparative picture of the difference in precipitation data from Towner and TMPA. It is evident from the figure that several high precipitation events are not recorded in the observations from TMPA. The high precipitation events are distributed rather than concentrated in the first part of the calibration time period as observed in Towner gage data. Consecutive days of higher precipitation events create greater runoffs whereas the same amount of total precipitation distributed temporally in smaller magnitudes may generate considerably lower volumes.

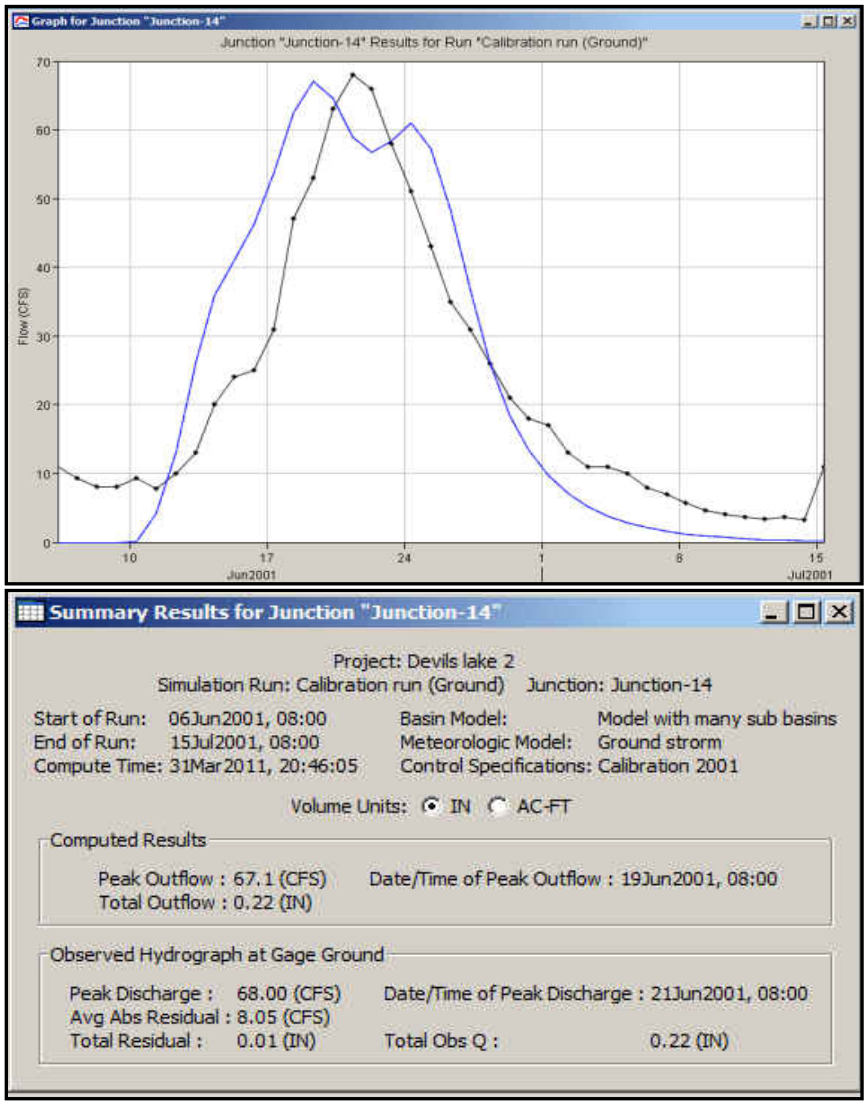

Figure 17: Runoff plot and summary results in calibrating the loss parameters of the Mauvais Coulee

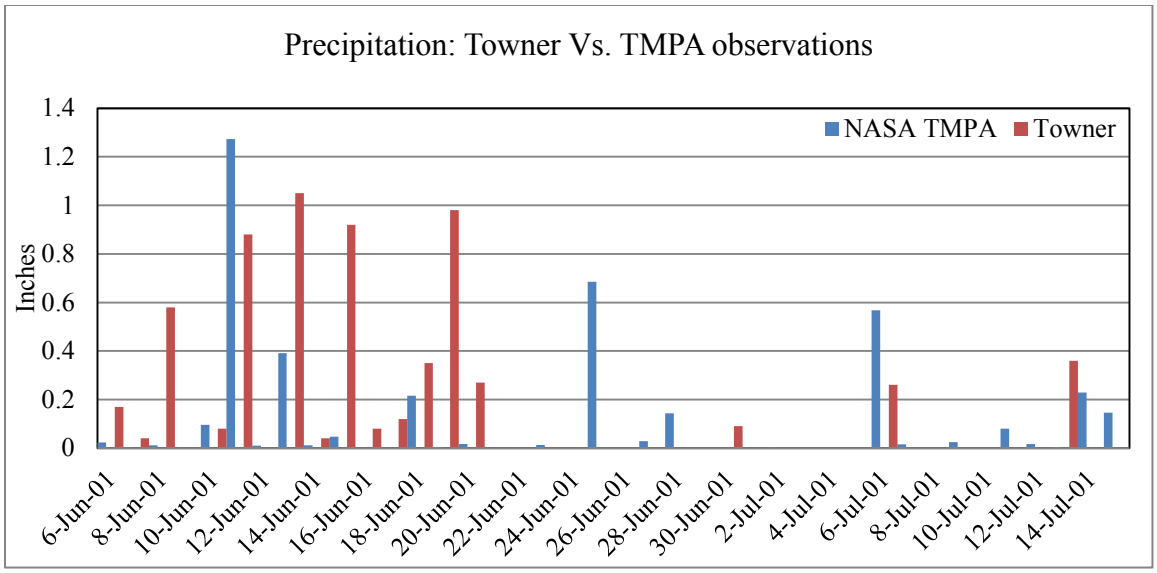

Figure 18: Comparison between precipitation observations in Towner station and NASA (TMPA) Satellite (Jun 6, 2001 to Jul 15, 2001)

At the next stage, calibration trials are also performed for snow melt and deviations are observed when the same values of parameters are used in both models. These findings illustrate the shortcomings of calibrating the models for smaller time periods. A new approach is selected to calibrate the models for multiple years. The calibration period is chosen from 2003 to 2010 based on the availability of data for both models. The ground observation gage for precipitation is changed to Langdon experimental farm (Figure 14) due to gaps in continuous data in Towner gage station. After performing several simulation runs the constant loss is found to be 0.0979 in/hr for HMS-Model A and 0.0955 in/hr for HMS-Model B. In both cases initial loss is set as 0.1 inch and the total outflow from Mauvais basin is modeled accurately, which is 13.89 inches. At this stage the models are ready to be coupled with the HEC-ResSim model to generate the water levels of the lake. Hence all the sub-basins are merged together in a single setup for both HMS-Model A and HMS-Model B. The calibrated parameters for

Mauvais sub-basin are applied for all the sub-basins. As the previous values of loss parameters are based on the Mauvais Coulee and do not represent the whole basin, a modification in the constant loss through calibration is required.

4.3.4 Combined Approach in Calibration

The calibrated model is coupled with HEC-ResSim, and simulations are performed to obtain daily water levels from 2003 to 2010. To represent the precipitation over the lake itself, an extra sub-area is created in both HMS-Model A and B. The runoff generated from this sub-area represents the amount of water that directly contributes to the lake in the form of precipitation. The physical properties of the lake are made available in the HEC-ResSim model. Evaporation is the major source of outflow from the water body. To obtain a proper fit with observed water levels in Devils Lake, calibration of the evaporation is required. Time series values of penman evaporation are obtained from Crary gage station from North Dakota Agricultural Weather Network (NDAWN). Multiplier coefficients for evaporation series ranging from 0.6 to 0.8 are analyzed to calibrate the HEC-ResSim model with observed water levels. At this stage a combined approach is followed where both the HEC-HMS and HEC-ResSim models are calibrated simultaneously. With varying loss parameters, the runoff is generated from both HMS-Model A and B and used in the HEC-ResSim model separately to simulate the water level. Adjustment of the melt rate coefficient, C_m is also made. Calibration results for HMS-Model A and B, both coupled with the HEC-ResSim model separately, are summarized in Table 5 and Table 6. The deviations from the observed lake levels have been calculated as RMS errors, which are 1.49 ft using HMS-Model A and 1.73 ft using HMS-Model B. The final obtained calibration parameters are listed in Table 7 and Table

8. Plots of the fit of the final calibrated models are given in Figure 19 through Figure 21 for coupled HMS-Model A & ResSim and in Figure 22 through Figure 24 for coupled HMS-Model B & ResSim.

Table 5: Calibration Results (2003-10) using HMS-Model A + ResSim model

Meltrate, C_m	Constant Loss in sub-areas	Multiplier Coefficient for evaporation	RMS Error, ft
0.08	0.085	0.7	2.19
0.06	0.085	0.7	3.44
0.06	0.085	0.7	2.81
0.06	0.085	0.7	1.67
0.06	0.085	0.7	2.05
0.06	**0.085**	**0.7**	**1.49**
0.05	0.085	0.7	1.61
0.05	0.085	0.6	1.86
0.05	0.12	0.7	2.95
0.04	0.085	0.6	1.83
0.04	0.085	0.7	1.86

Table 6: Calibration Results (2003-2010) using HMS-Model B + ResSim model

Meltrate, C_m	Constant Loss in sub-areas	Multiplier Coefficient for evaporation	RMS Error, ft
0.08	0.085	0.7	4.89
0.07	0.085	0.7	4.77
0.06	0.085	0.7	4.54
0.06	0.1	0.7	3.22
0.06	0.12	0.7	1.99
0.05	0.085	0.7	4.26
0.05	0.085	0.7	3.34
0.05	0.1	0.7	2.89
0.05	**0.12**	**0.7**	**1.73**

Table 7: Calibrated values of melt-rate coefficient and continuous loss for both HMS-Model A and HMS-Model B

Parameter	HMS-Model A	HMS-Model B
Melt rate Coefficient., C_m	0.06	0.05
Constant Loss (in/hr)	0.085	0.12

Table 8: Snow-melt parameters (Temperature Index) for both HMS-Model A and B coupled with ResSim model

Parameter	Unit	Value
PX Temperature	Deg F	33.5
Base Temperature	Deg F	32
Wet Melt-rate	In/Deg F-Day	0.06
Rain Rate Limit	In/Day	0.01
ATI Melt-rate Coefficient		0.98
Cold Limit	In/Day	0.8
ATI Cold-rate Coefficient		0.84
Water Capacity	%	5
Ground-melt	In/Day	0

Calibration plots of the ResSim model coupled with the HMS-Model A

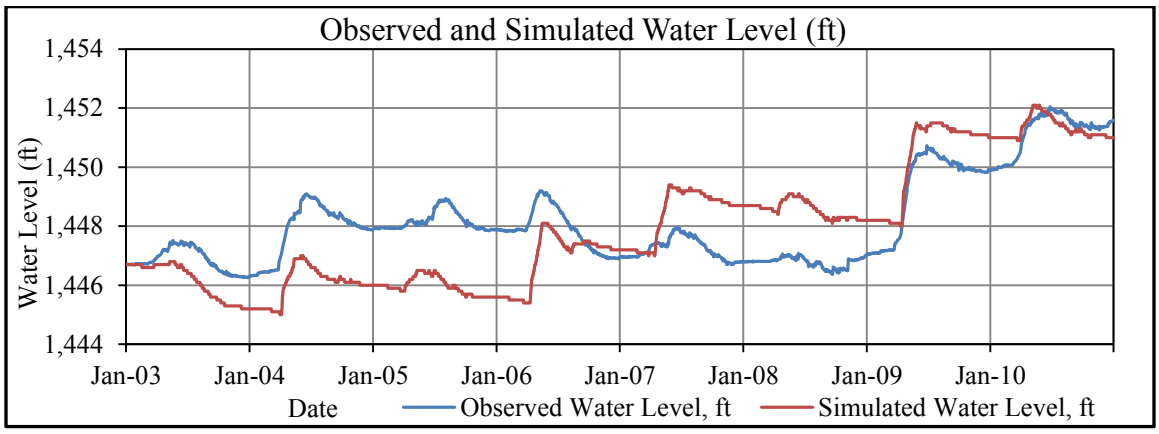

Figure 19: Simulated water level from the HMS-Model A + ResSim

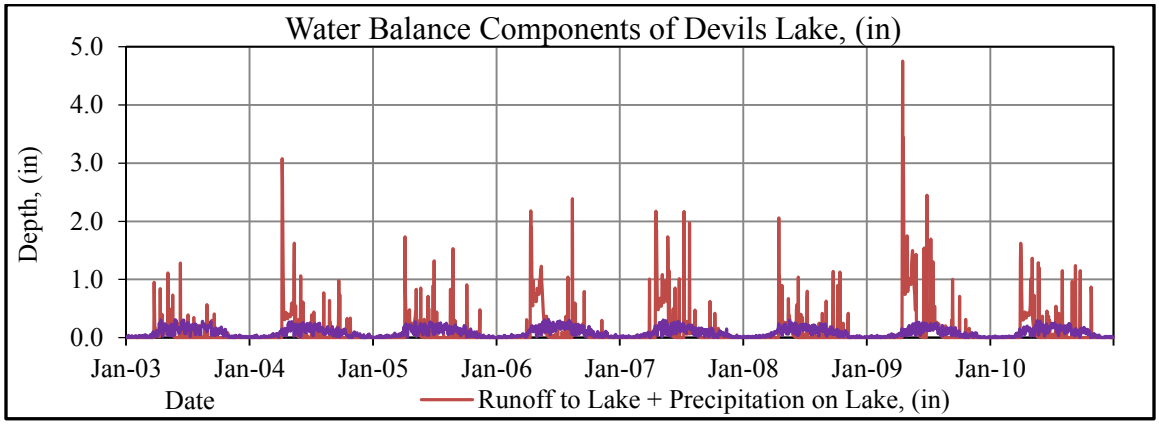

Figure 20: Water balance from the HMS-Model A + ResSim

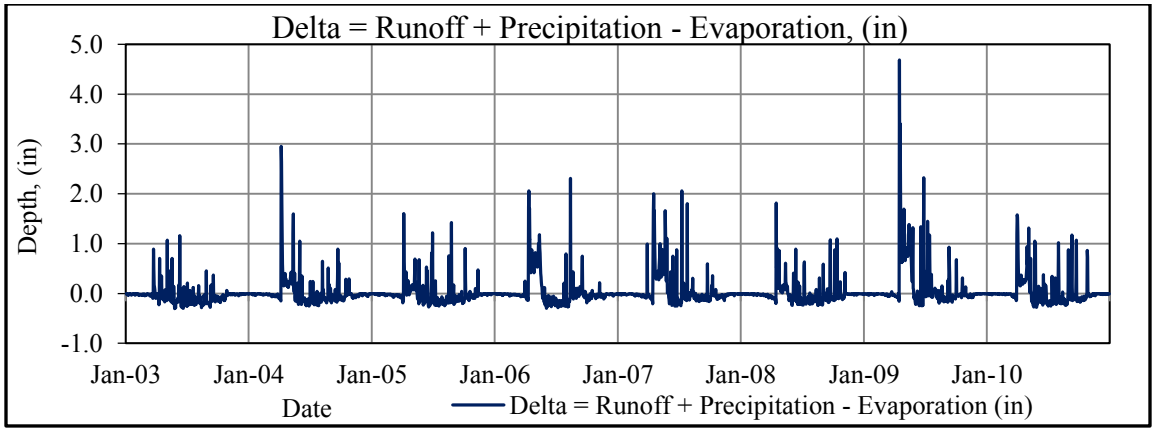

Figure 21: Increase in Water Level from the HMS-Model A + ResSim

Calibration plots of the ResSim model coupled with the HMS-Model B

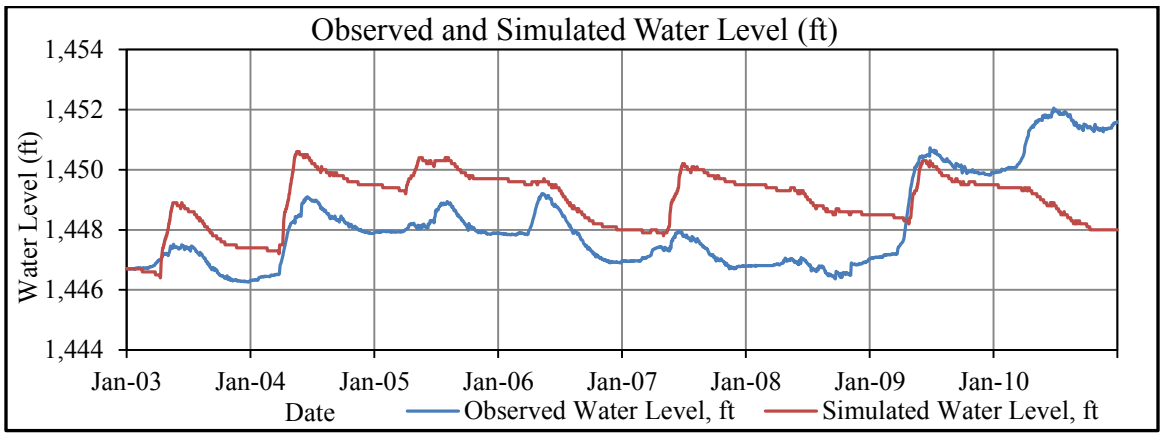

Figure 22: Simulated water level from the HMS-Model B + ResSim

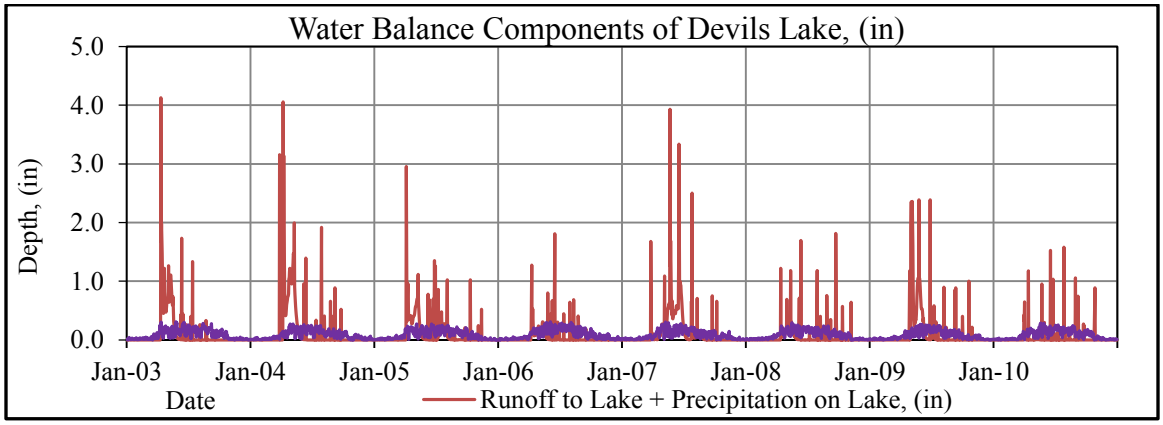

Figure 23: Water Balance from the HMS-Model B + ResSim

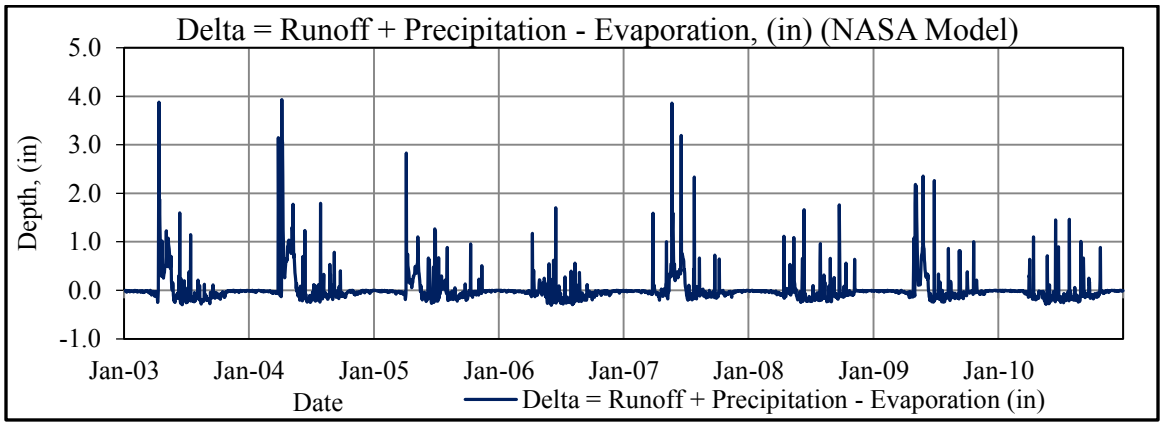

Figure 24: Increase in Water Level from the HMS-Model B + ResSim

4.4 Reasons of Deviations in Coupled ResSim and HMS-Model B

In Figure 22, it is found that there are few unusual peaks and troughs in the simulated water levels, which are not observed in the ground. Specially, in the water balance plot (Figure 23), several peaks are observed in 2007, which causes the simulated water level to rise unexpectedly. An investigation of the precipitation data reveals some interesting facts. In the observations from TMPA by NASA's satellite, unexpectedly high precipitation amounts have been recorded at least three times, which are not observed in the Langdon ground gage station. However, in quantifying precipitation depths, it is not unreasonable to rely more on ground observations. These erroneous extreme events have helped the simulated water level to rise unexpectedly. Again in year 2010 the model simulates unexpectedly lower water levels. Different experiments and tests applied on these models conclude that proper representation of bigger precipitation events play a very important role in generating runoff and hence simulating water level with a better fit. The lack of accurate precipitation distribution is hence considered to be the key reason for the mismatch in water level during 2007 and 2010. Mismatch in 2008 is nothing but the after effect of the significant jump in 2007. Due to storage effects, the water level remained continuously up in 2008, which finally came closer in 2009. Effects of the unexpected magnitude of precipitation in 2007 are summarized below.

In summer, the precipitation generates runoff immediately after the storm event. So the magnitude of each storm event affects more in simulating the summer runoff and subsequent water level. In winter, the precipitation accumulates in the form of snow and starts generating runoff as soon as the temperature goes above freezing point (32^0 F). So

in this case the total accumulated depth of snow rather than individual events affects more in simulating the spring runoff and corresponding water level.

The unexpectedly high precipitation events in NASA TMPA observations are recorded on 22 May, 18 June and 26 July of 2007. All Grid location does not affect the model the same way. It depends on the weight of the grid in the model. Values in grid 3E, 4E, 5E, 6E, 2D, 3D, 4D, 5D and 3C affect the model most. Table 9 lists the magnitude of high precipitation records affecting the model.

Table 9: Comparison of TMPA by NASA's satellite with observed value in Langdon Gage Station

Date (2007)	Max in a grid, (in)	Avg. of 48 grids, (in)	Avg. of 9 grids with higher impact on the model, (in)	Obs. value in Langdon Gage Station, (in)	Deviation in precipitation estimation by TMPA
May 22	5.21	3.55	4.42	1.33	+3.09
June 18	3.14	1.45	1.98	0.29	+1.69
July 26	3.37	2.02	2.79	2.03	+0.76

Three experiments are performed to study the effects of these deviations on simulated water levels. The experiments are carried out under the hypothesis that, if these high precipitation events are responsible for the abrupt jump in water level in 2007, then by redistributing these events, it is possible to achieve a better match with observed values. Each experiment shows significant improvement and proves the assumed reasons behind the deviations in the stated years as shown in Figure 25 through Figure 28.

Experiment 1 : These three precipitation events are replaced by no precipitation.

Experiment 2 : These events are replaced by Langdon ground gage observations.

Experiment 3 : These precipitation events are distributed in two weeks.

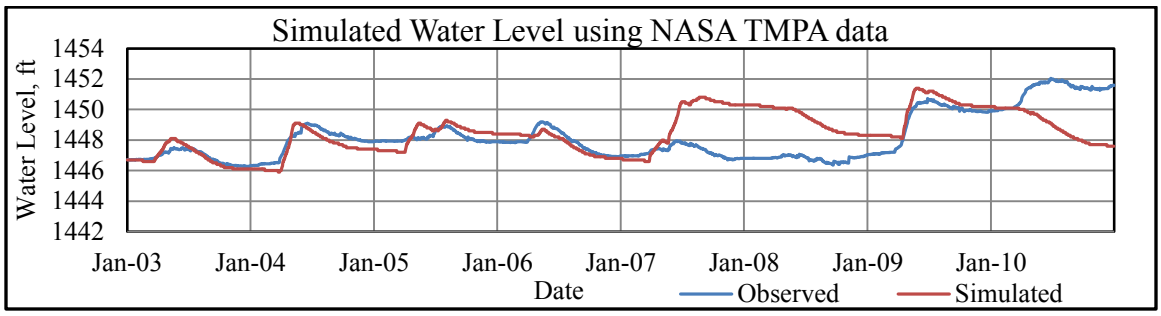

Figure 25: Simulated water level using coupled ResSim and HMS-Model B

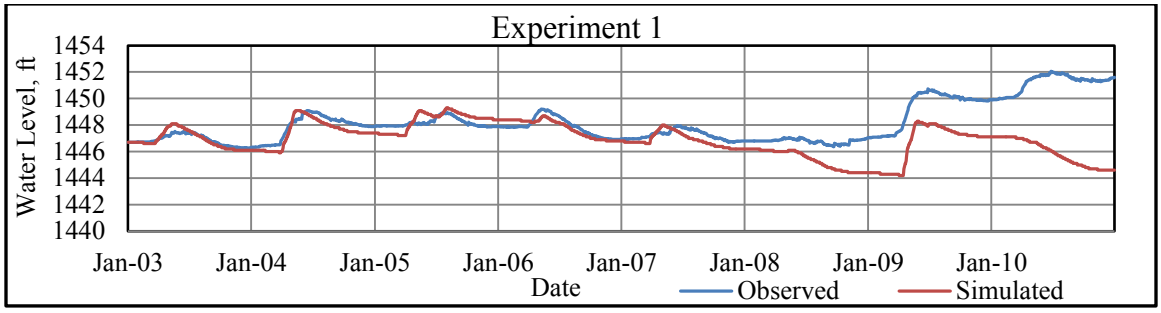

Figure 26: Experiment 1: Replacing the high precipitation events by zero

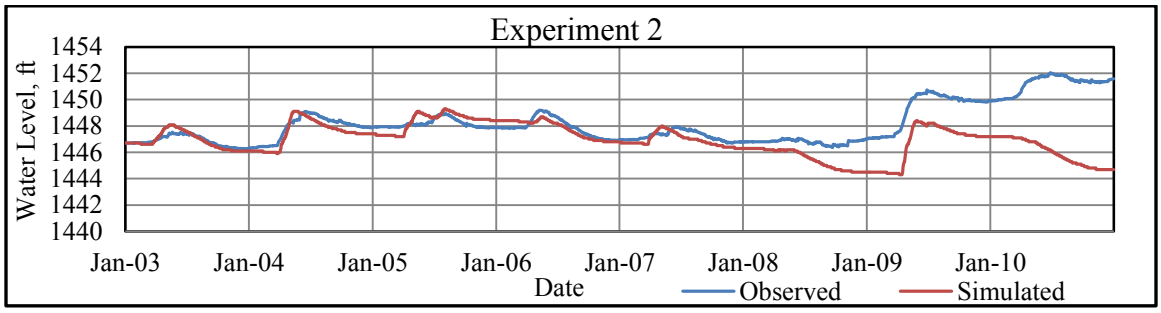

Figure 27: Experiment 2: Replacing the high precipitation events by Langdon values

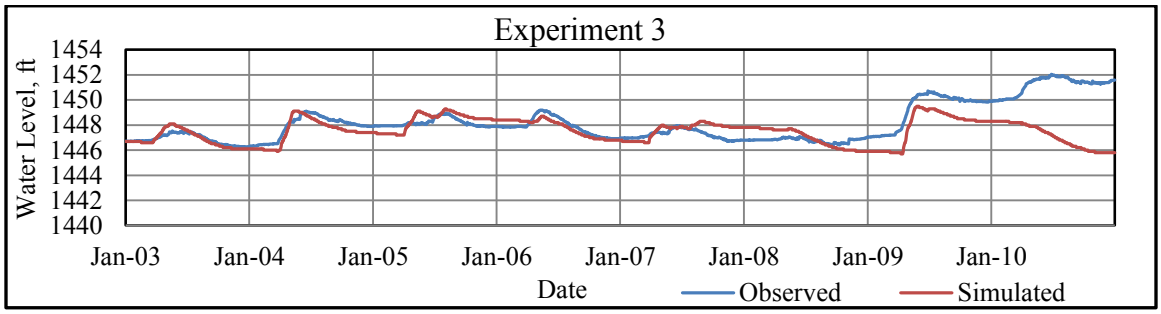

Figure 28: Experiment 3: Distributing the high precipitation event

4.5 Selected Parameters for Future Simulation (2021-2050)

The main objective of the calibration is to use the model for future lake level prediction using downscaled GCM generated climate data, which is spatially distributed in a grid format, similar to the climate data from TMPA by NASA's satellite. So, to run the model for future years, the calibration parameters obtained from coupled ResSim and HMS-Model B are selected, which are presented in Table 10.

Table 10: Selected HEC HMS model parameters for future simulation (2021-2050)

Parameter	Unit	Value
PX Temperature	Deg F	33.5
Base Temperature	Deg F	32
Wet Melt-Rate	In/Deg F-Day	0.06
Rain Rate Limit	In/Day	0.01
ATI Melt-Rate Coefficient		0.98
Cold Limit	In/Day	0.8
ATI Cold-Rate Coefficient		0.84
Water Capacity	%	5
Ground-Melt	In/Day	0
Melt-Rate Coefficient, Cm		0.05
Initial Loss for sub-areas	in	0.1
Continuous Loss for sub-areas	in/hr	0.12
Seepage	cfs	0.0
Multiplier Coefficient for evaporation		0.7

4.6 Calibration of Lake Evaporation Model

Modeling of the water resources of a lake or reservoir system requires a good knowledge of the magnitude and variation of evaporative losses. For future water level a well calibrated model is required that can simulate the evaporation based on temperature. Evaporation, being a complex process, is governed by temperature, humidity, wind speed, radiation, etc., and is rarely measured directly above water surfaces. The objective is to analyze the methods listed in Table 11 and develop the best method through calibration that can generate evaporation estimates with significant level of accuracy (Shahad, 2012). Then the method will be applied to produce future evaporation estimates using projected temperature time series from several down-scaled GCMs. Penman evaporation values obtained from the weather station at Crary, ND have been selected for calibration. The data station is about 3.72 miles from the nearest water body of Devils Lake.

4.6.1 Methods Analyzed

A simplified version of the Penman equation and eight other radiation-based equations (Table 11) are analyzed in a case study on Devils Lake, North Dakota, USA. The calculated data is compared with Penman evaporation estimates generated from the weather station data observed at Crary in North Dakota. The achieved values show unacceptable deviation from the data obtained from Crary . Then these evaporation equations are calibrated for the study area and compared with observed data. Regression analyses are performed that produce linear equations following the format of

$$Y = m.X + c \qquad (2)$$

where, *m* is the slope and *c* is the *y* intercept. The desired values of *m* and *c* are 1 and 0 respectively.

Required time series data are obtained from US Geological Survey (USGS, 2010), National Climatic Data Center (NCDC, 2010) and North Dakota Agricultural Weather Network (NDAWN, 2010). The equations listed in Table 11 are used with original coefficients to estimate evaporation and compared with the obtained values from Crary. Large errors are observed by using original coefficients. Then these equations are recalibrated for the study area. The recalibrated values for these equations are given in Table 12. After recalibration, the "Doorenbos and Pruitt", "Jensen and Haise" and "Hargreaves" method produced significantly improved results (Table 13).

4.6.1.1 Penman Equation Method

The classical form for the Penman (Penman, 1948) equation to estimate potential evaporation:

$$E_{PEN} = \frac{\Delta}{\Delta+\gamma}.\frac{R_n}{\lambda} + \frac{\gamma}{\Delta+\gamma}.\frac{6.43(f_u)D}{\lambda} \quad (3)$$

where, E_{PEN} is potential open water evaporation (mm/d); R_n is net radiation at the surface (MJ/m^2/d), Δ is the slope of the saturation vapor pressure curve (kPa/^{0}C), γ is psychrometric coefficient (kPa/ ^{0}C), λ is latent heat of vaporization (MJ/kg); f_u is wind function and

$$f_u = a_u + b_u u \quad (4)$$

where, a_u and b_u are wind function coefficients, and u is wind speed at 2 m height (m/s).

4.6.1.2 Makkink Method

Makkink (1957) estimated *E* as:

$$E = 0.61\frac{\Delta}{\Delta+\gamma}\frac{R_S}{58.5} - 0.012 \quad (5)$$

where, R_s is solar radiation in equivalent millimeters of evaporation per day. Δ is the slope of the saturation vapor pressure curve (in mbar/ ^{0}C), γ (in mbar/ ^{0}C) is the psychometric constant.

4.6.1.3 Doorenbos and Pruitt Method

According to Doorenbos and Pruitt method,

$$E = a\left(\frac{\Delta}{\Delta+\gamma}R_s\right) + b \quad (6)$$

where,

a = an adjustment factor that varies with mean relative humidity and daytime wind speed and

$$a = 1.066 - 0.13 \times 10^{-2}RH + 0.045U_d - 0.20 \times 10^{-3}RH \times U_d - 0.315 \times 10^{-4}RH^2 - 0.11 \times 10^{-2}U_d^2 \quad (7)$$

RH = Mean relative humidity in %

U_d = Mean daytime wind speed in meters per second

Δ = Slope of the saturation vapor pressure curve (in mbar/ ^{0}C) and

$$\Delta = 33.8639[0.05904(0.00738T + 0.8072)^7 - 0.0000342] \quad (8)$$

T = Temperature in ^{0}C

γ = Psychometric constant (in mbar/ ^{0}C) and

$$\gamma\left(\frac{mbar}{℃}\right) = \frac{C_pP}{0.622\lambda} \quad (9)$$

C_p = Specific heat of air (in cal/g/ ^{0}C), ranging from 0.2397 to 0.260.

P = Atmospheric pressure (in mbar) and

$$P = 1013 - 0.1055EL \quad (10)$$

EL = Elevation (m).

λ = Latent heat (in calories per gram) and

$$\lambda \left(\frac{cal}{g}\right) = 595 - 0.51T \quad (11)$$

R_s = Solar radiation in mm/day

b = Adjustment factor

The Doorenbos and Pruitt (Doorenbos *et al,* 1977) method is an adaptation of the Makkink (Makkink, 1957) method and was recommended over the Penman method when measured wind and humidity data were not available or could not be estimated with reasonable confidence.

4.6.1.4 Hargreaves Method

Hargreaves (Hargreaves, 1975) and Hargreaves and Samni (Hargreaves *et al*, 1982) proposed several equations for calculating potential evaporation, E (in mm/day). One of the equations is written as:

$$\lambda E = 0.0135(T + 17.8)\, R_s \quad (12)$$

where, R_s is solar radiation in equivalent millimeters of evaporation per day, λ (in calories per gram) is latent heat and T is the air temperature in ^{0}C. The Hargreaves method was derived from 8 years of cool season Alta Fescue grass lysimeter data from Davis, California.

4.6.1.5 Abtew Method

Abtew (Abtew, 1996) used a simple model that estimates E from solar radiation as:

$$E = a(R_s/\lambda) \quad (13)$$

where, E is in millimeters per day, R_s is in MJ/m^2/day, λ is in MJ/kg, and a is a dimensionless coefficient.

Table 11: Equations evaluated for the calibration of the lake evaporation model

Name of Method	Generalized Equations
1. A simplified version of Penman Method	$E \approx 0.047R_S\sqrt{T+9.5} - 2.4\left(\frac{R_S}{R_A}\right)^2 + 0.09(T+20)(1-\frac{RH}{100})$
2. Makkink Method	$E = 0.61\frac{\Delta}{\Delta+\gamma}\frac{R_s}{58.5} - 0.012$
3. Doorenbos and Pruitt Method	$E = a\left(\frac{\Delta}{\Delta+\gamma}R_s\right) + b$
4. Hargreaves Method	$\lambda E = 0.0135(T+17.8)R_s$
5. Abtew Method	$E = a\left(\frac{R_s}{\lambda}\right)$
6. Jensen and Haise Method	$\lambda E = C_t(T-T_x)R_s$
7. Priestley and Taylor Method	$E = a\left(\frac{\Delta}{\Delta+\gamma}\right)\left(\frac{R_n}{\lambda}\right)$
8. McGuinness and Bordne Method	$E = \left\{(0.0082T - 0.19)\left(\frac{R_s}{1500}\right)\right\}2.54$
9. Turc Method	$E = 0.013\frac{T}{T+15}(R_s+50);\ for\ RH \geq 50$ $E = 0.013\frac{T}{T+15}(R_s+50)\left(1+\frac{50-RH}{70}\right);\ for\ RH < 50$

4.6.1.6 Jensen and Haise Method

Jensen and Haise (Jensen *et al*, 1963) developed the following relation:

$$\lambda E = C_t(T - T_x)R_s \tag{14}$$

where, R_s have the same meaning and units as before, E is in millimeters per day, C_t (temperature constant) = 0.025, and T_x = -3 when T is in degrees Celsius. These coefficients were considered to be constant for a given area.

4.6.1.7 Priestley and Taylor Method

Priestley and Taylor (Priestley *et al*, 1972) proposed a simplified version of the combination equation (Penman, 1948) for use when surface areas generally were wet, which is a condition required for potential evaporation, *E*. The aerodynamic component

was deleted and the energy component was multiplied by a coefficient, $\alpha = 1.26$, when the general surrounding areas were wet or under humid conditions,

$$E = \alpha\left(\frac{\Delta}{\Delta+\gamma}\right)\left(\frac{R_n}{\lambda}\right) \quad (15)$$

where, R_n is the net radiation (cal/cm^2 day), and other notations have the same meaning as before. In this study, owing to a lack of observation data, R_n is estimated using an equation proposed by Linsley (Linsley *et al*, 1982).

$$R_n = (7.14 \times 10^{-3} R_s) + \{5.26 \times 10^{-6} R_s\,(T + 17.8)^{1.87}\} - \left(3.94 \times 10^{-6} {R_s}^2\right) - \left\{2.39 \times 10^{-9} {R_s}^2 (T - 7.2)^2\right\} - 1.02 \quad (16)$$

where, R_n is in equivalent millimeters of evaporation per day.

4.6.1.8 McGuinness and Bordne Method

McGuinness and Bordne (McGuinness *et al*, 1972) proposed,

$$E = \left\{(0.0082T - 0.19)\left(\frac{R_s}{1500}\right)\right\} 2.54 \quad (17)$$

where, E is in centimeters per day for a monthly period, T is in degrees Fahrenheit, and R_s is in cal/cm^2/day. This method is based on an analysis of a lysimeter data in Florida.

4.6.1.9 Turc Method

Under general climatic conditions of Western Europe, Turc (Turc, 1961) computed E in millimeters per day for 10-day periods as

$$E = 0.013\frac{T}{T+15}(R_s + 50); \qquad for\ RH\ \geq 50 \quad (18)$$

$$E = 0.013\frac{T}{T+15}(R_s + 50)\left(1 + \frac{50-RH}{70}\right);\ for\ RH < 50 \quad (19)$$

where, T is the air temperature in ^{0}C, R_s is the total solar radiation in cal/cm^2/day, and RH is the relative humidity in percent.

Table 12: Original and recalibrated coefficients in evaporation modeling

Name of Method	Generalized Form	Parameter	
		Original Value	Recalibrated Value
1. Doorenbos and Pruitt	$E = a\left(\frac{\Delta}{\Delta+\gamma}R_s\right) + b$	a, b = - 0.3	$a' = a$ / 26.5, b = 0.05
2. Jensen and Haise	$E = C_t(T - T_x)\,{}^{R_s}/_{\lambda}$	C_t = 0.025, T_x = - 3	C_t = 0.345, T_x = - 20.5
3. McGuinness and Bordne	$E = (aT - b)\frac{R_s}{c}$	a = 0.020828, b = 0.4826, c = 1500	a = 0.018, b = 0.562, c = 15000
4. Priestly and Taylor	$E = a\left(\frac{\Delta}{\Delta+\gamma}\right)\frac{R_n}{\lambda} + b$	a = 1.26, b = 0	a = 8, b = 0.15
5. Abtew	$E = a\frac{R_s}{\lambda}$	a = 0.53	a = 0.024
6. Hargreaves	$E = a(T + b)\,{}^{R_s}/_{\lambda}$	a = 0.0135, b = 17.8	a = 0.35, b = 20
7. Turc	$E = a\left(\frac{T}{T+15}\right)(R_s + b)$	a = 0.013, b = 50	a = 0.00077, b = - 0.28
8. Makkink	$E = a\frac{\Delta}{\Delta+\gamma}\frac{R_s}{58.5} + b$	a = 0.61, b = - 0.012	a = 2.125, b = - 0.12

4.6.2 Selected Method

Through calibration, "Doorenbos and Pruitt" method shows the best results and is selected to be used as a temperature-based model for estimating future evaporation estimates. The plot of the modeled values versus obtained evaporation time series from Crary is given in Figure 29. Plots of the regression analysis are shown in Figure 30. Values of R^2, m and c of regression analysis performed on data from years 2000-10 are listed in Table 14.

Table 13: The three lake evaporation methods showing better R^2 values

No.	Method	Best value of R^2	Year
1	Doorenbos and Pruitt	0.9404	2009
2	Hargreaves	0.9239	2009
3	Jensen and Haise	0.9196	2009

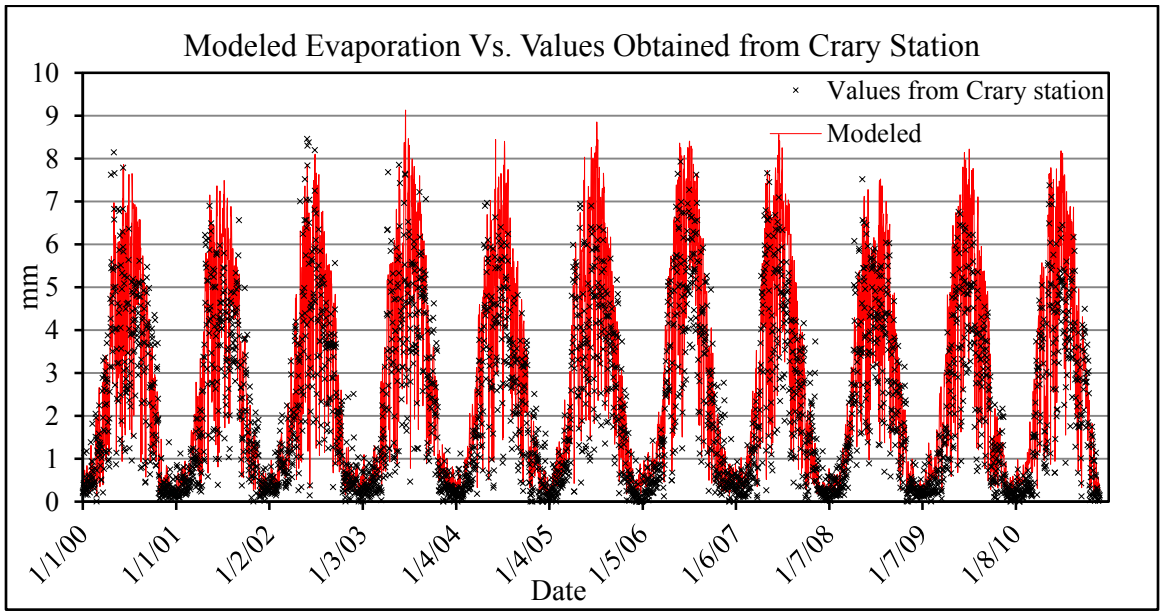

Figure 29: Calibration plot of the modeled evaporation vs. values obtained from Crary station (2000-2010)

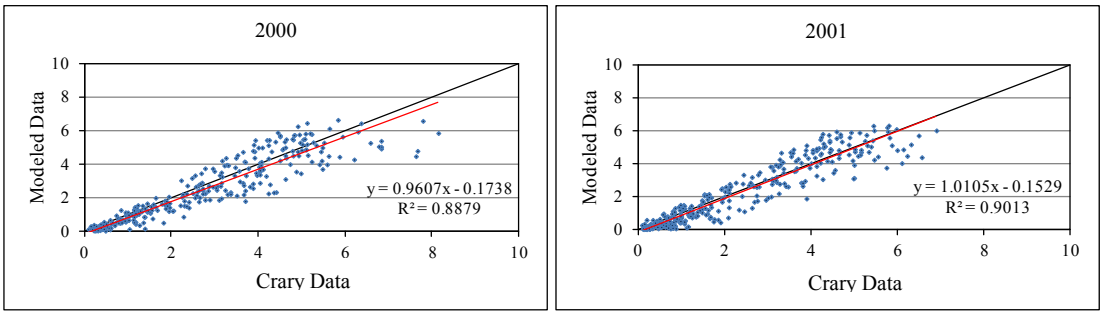

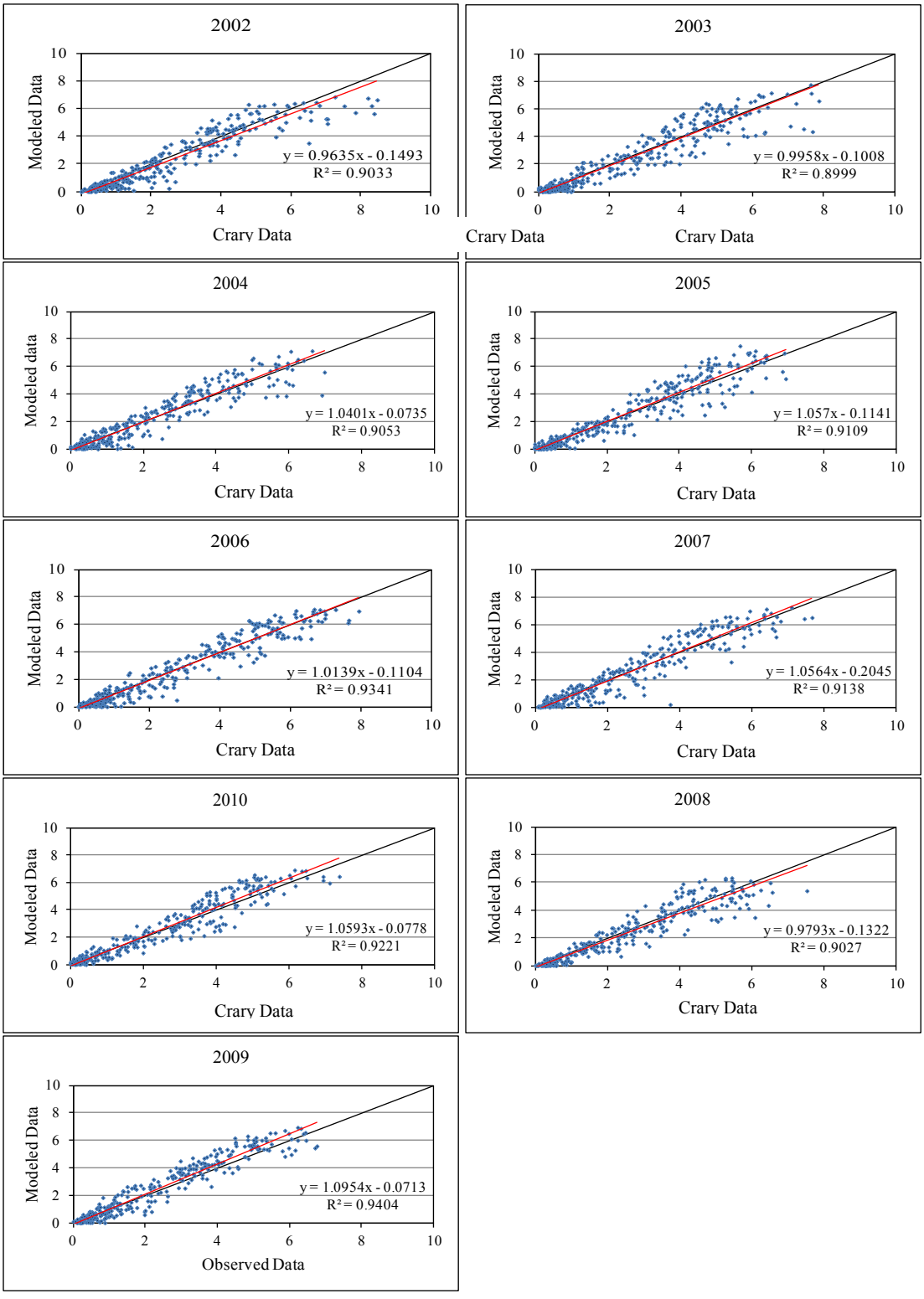

Figure 30: Results of the regression analysis in an annual basis

4.6.3 Future Evaporation Estimates

Historical evidence shows that average annual evaporation of DL has increased slightly from 1950-79 (29.6 in) to 1980-2006 (30.9 in) (Vecchia, 2008). Future temperature series are projected by four GCMs (CSMK3, GFCM21, GIAOM, and HADCM3), and run under three SRES scenarios (A1B, A2, and B1). The GCM projections are further downscaled by LARS-WG stochastic weather generator to produce 10 samples (0-9) of daily temperature under the changed climate conditions for each GCM/scenario pair. The details on the downscaling for the Devils Lake region are found in Kirilenko et al. (2010). The projected temperature series are used in the developed evaporation model to estimate the future evaporation patterns. Historic data have been used to represent the other variables in model. The summary of the simulated evaporation series is given in Table 15, where the annual average is calculated to be 30.38 inches.

Table 14: Summary of the calibration and regression analysis of the lake evaporation model

Yr	2000	2001	2002	2003	2004	2005	2006	2007	2008	2009	2010
R^2	0.89	0.9	0.9	0.9	0.91	0.91	0.93	0.91	0.9	0.94	0.92
m	0.96	1.01	0.96	1	1.04	1.06	1.01	1.06	0.98	1.1	1.06
c	-0.17	-0.15	-0.15	-0.1	-0.07	-0.11	-0.11	-0.21	-0.13	-0.07	-0.08

Table 15: Annual average of the simulated future (2021-2050) lake evaporation

Shuffle No.		0	1	2	3	4	5	6	7	8	9
A1B	CSMK3	30.2	30.2	30.23	30.21	30.2	30.22	30.22	30.21	30.19	30.22
	GFCM21	30.42	30.41	30.42	30.4	30.48	30.4	30.41	30.4	30.45	30.4
	GIAOM	30.48	30.47	30.51	30.47	30.48	30.49	30.48	30.5	30.5	30.48
	HADCM3	30.7	30.71	30.74	30.69	30.69	30.7	30.69	30.69	30.7	30.68
A2	GFCM21	30.47	30.45	30.48	30.47	30.46	30.47	30.47	30.47	30.48	30.48
	HADCM3	30.4	30.36	30.35	30.37	30.38	30.38	30.34	30.4	30.38	30.36
B1	CSMK3	30.01	30	30.02	30.01	30.01	30.02	30.01	30.02	30.01	30.01
	GFCM21	30.29	30.27	30.3	30.29	30.3	30.31	30.29	30.29	30.27	30.3
	GIAOM	30.55	30.53	30.56	30.57	30.56	30.58	30.56	30.55	30.58	30.55
	HADCM3	30.33	30.33	30.33	30.32	30.3	30.33	30.33	30.33	30.32	30.34

CHAPTER 5

SIMULATION OF THE COUPLED HYDRO-CLIMATIC MODEL

5.1 Steps Followed in Simulating Future Water Level

This section illustrates the procedures of driving the watershed (HEC-HMS) and reservoir model (HEC-ResSim) using the climate data (precipitation and temperature) of different General Circulation Models (GCMs) under varying scenarios for selected time periods (2021-2050). Running the simulation consists of several steps, which are listed below and also shown as a flow chart in Figure 31.

a) Importing the precipitation series into HEC-DSSVue.

b) Importing the temperature series into HEC-DSSVue.

c) Editing the precipitation.dss files in the usable format.

d) Editing the temperature.dss files in the usable format.

e) Generating future evaporation series using the model spreadsheet.

f) Importing evaporation series into HEC-DSSVue in the usable format.

g) Plugging the precipitation and temperature series into the watershed model.

h) Running the watershed model to generate runoff into the lake.

i) Exporting the runoff output in a .dss file.

j) Plugging the evaporation and runoff series into the reservoir model.

k) Driving the reservoir model to generate the water level.

l) Exporting the output in a spreadsheet.

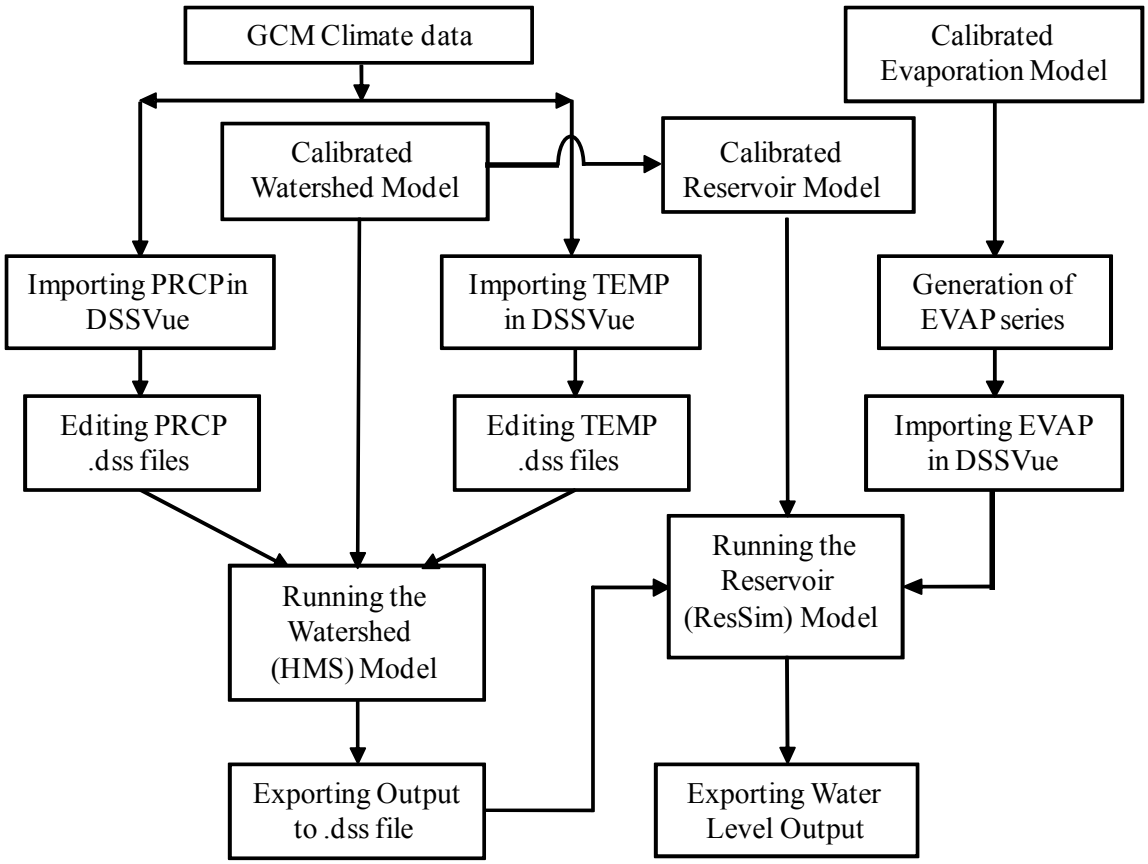

Figure 31: Flowchart explaining the sequence of tasks in simulating the future water level

5.2 General Circulation Model (GCM): Climate Data

Four GCMs with three different scenarios (A1B, A2 and B1) are selected for the assessment of future climate, which are CSMK3, GFCM21, GIAOM and HADCM3. For A2 scenario, data from CSMK3 and GIAOM are not available. So a total of ten cases are used to drive the coupled hydro-climatic model for future time periods. Here one thing should be noted that the GCM climate data are only ensembles of future climate pattern and not exact predictions of the climate. As the hydro-climatic model is dependent on storage of water in the lake body, ten sets of reshuffled data for each case are used. This is also an important step in capturing the uncertainty of future climate. So a total of 100

sets of climatic series are used for the final simulations. In this thesis, data are obtained and processed for years 2021-2050 and used for future simulations.

5.3 HEC-DSSVue

The U.S. Army Corps of Engineers' Hydrologic Engineering Center Data Storage System, or HEC-DSS, is a database system designed to efficiently store and retrieve scientific data that is typically sequential. Such data types include, but are not limited to, time series data, curve data, spatial-oriented gridded data etc. The system was designed to make it easy for users and application programs to retrieve and store data. HEC-DSS is incorporated into most of HEC's major application programs.

Data is stored in blocks, or records, within a file and each record is identified by a unique name called a "Pathname." Each time data is stored or retrieved from the file using other HEC software, its pathname must be given. The pathname is the key to the data's location in the database. They are separated into six parts (delimited by slashes "/") labeled "A" through "F," as follows: /A/B/C/D/E/F/

A typical regular-interval time series might be:

//1B2020/PRECIP-INC/01JAN2021 - 31DEC2050/1DAY/PRCP_2021-2050/

For regular-interval time series data, the part naming convention in the model is explained Table 16. There are four data "Types" recognized by the DSS, which are listed in Table 17.

Table 16: Description of the Parts in a .dss file used in simulation of future water levels

Part	Type	Value	Description
A	Optional	User Defined	Project, watershed, or basin name
B	Optional	User Defined	Location, Grid Name etc.
C	Mandatory	Fixed	Data parameter, e.g., Temp., Precip-Inc etc.
D	Mandatory	Fixed	Starting and ending date of data series
E	Mandatory	Fixed	Time interval
F	Mandatory	User Defined	Additional user-defined descriptive information

Table 17: Data types in a .dss file

Data Type	Example
PER-AVER	Temperature
PER-CUM	Incremental Precipitation
INST-VAL	Stages
INST-CUM	Precipitation Mass Curve

5.3.1 Data Interoperability Issues

To import simulated synthetic precipitation and temperature series DSSVue is used, which can import properly oriented ASCII files. The ASCII files are arranged following the NCDC text data format. The NCDC plug-in comes as a default package with HEC-DSSVue 2.0.1. Few incompatibilities are observed when data is imported using this plug-in. First, the C Part in the .dss file needs to be automatically read as 'TEMPERATURE', but after importing it shows 'TEMP'. Second, the unit of temperature needs to be read as 'DEG F' where it is found as 'DEG-F' after importing. These problems can be solved manually by renaming those portions. But for hundreds of

files, a solution is needed. After consulting with the HEC-DSSVue help center, a new and modified NCDC.jar file is obtained, which worked without any error. Sample plots of the precipitation and temperature time series after importing from the ASCII files of A1B.CGMR.2011-2030 are shown in Figure 32 and Figure 33. Description about the data format can be found in Appendix G.

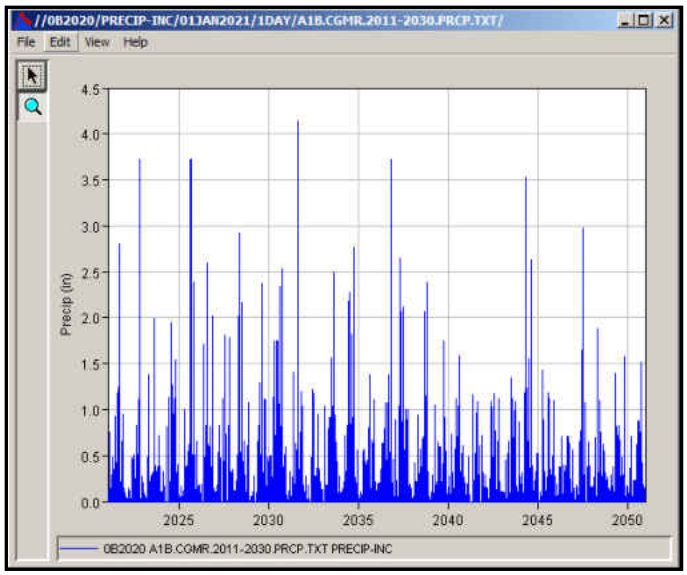

Figure 32: Example plot of future precipitation (A1B_CSMK3)

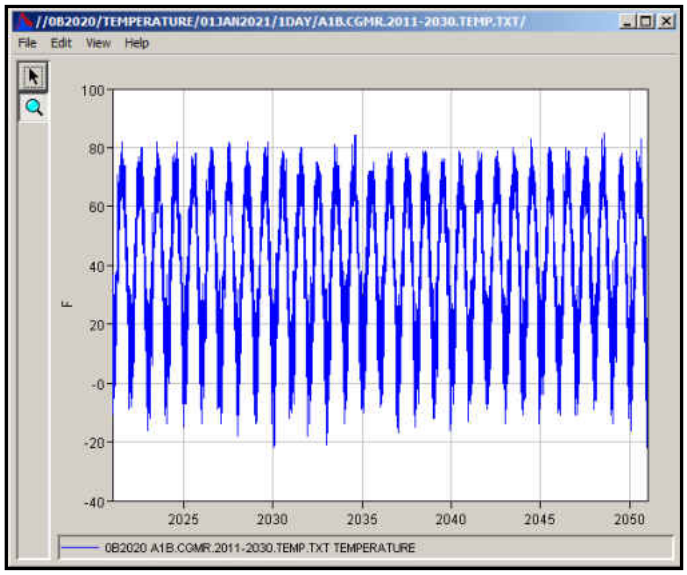

Figure 33: Example plot of future temperature (A1B_CSMK3)

5.4 Importing the Climate Data in DSSVue

The GCM climate data are obtained as properly formatted ASCII files. For this, the digital file format of daily data (3200-3210/CDO) from NCDC is followed. The models (both watershed and reservoir) are set to import data in .dss format. To import and convert the ASCII files into .dss files, NCDC plug-in of HEC-DSSVue is used. After importing as .dss files, each file contains six parts: Part A through Part F. The HMS model was set in such a way that it can read data from a particular folder provided the name of the input file is same.

5.5 Simulation of Reservoir Model

The reservoir model for estimating future lake levels follows the calibration parameters discussed in Table 10. The 'Lookback' value is set to the water level during the simulation time (June, 2011), which is 1454 ft above National Geodetic Vertical Datum of 1929 (NGVD 29). Simulations are performed for 100 sets (10 cases) of data series. The output is summarized below from Table 18 to Table 27 and Figure 34 to Figure 43 for each of the 10 cases.

Table 18: Simulation Case 1: A1B_CSMK3_2021-2050

Shuffle	0	1	2	3	4	5	6	7	8	9	All
Max	1454.9	1454	1454.2	1454	1454.2	1454	1454.7	1454.2	1454	1454.9	1454.9
Min	1438.7	1434.6	1437.8	1439.2	1434.5	1438.4	1436.7	1436.4	1437.7	1437.3	1434.5
Mean	1443.626	1444.016	1444.071	1444.227	1443.865	1443.549	1444.195	1443.2	1443.811	1443.384	1443.794

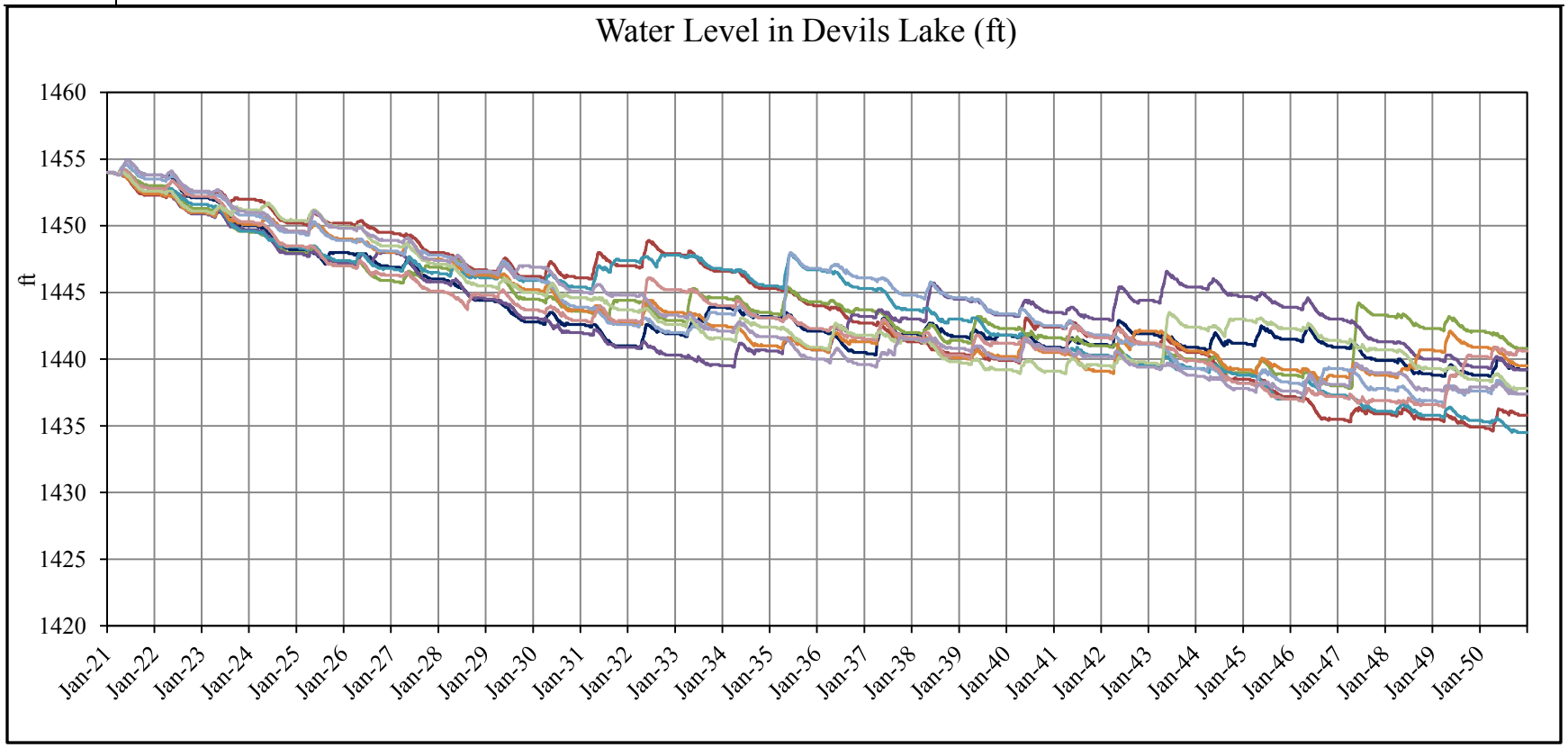

Figure 34: Simulated water level in Case 1: A1B_CSMK3_2021-2050

Table 19 : Simulation Case 2: A1B_GFCM21_2021-2050

Shuffle	0	1	2	3	4	5	6	7	8	9	All
Max	1454.1	1454	1454.2	1454	1454	1454	1454	1454.2	1454.2	1454.1	1454.2
Min	1435.6	1433.5	1437.6	1436.2	1434.5	1435.8	1435.2	1436.2	1436.6	1436.6	1433.5
Mean	1442.6	1441.59	1442.15	1442.4	1442.68	1442.84	1441.69	1442.04	1442.3	1442.38	1442.27

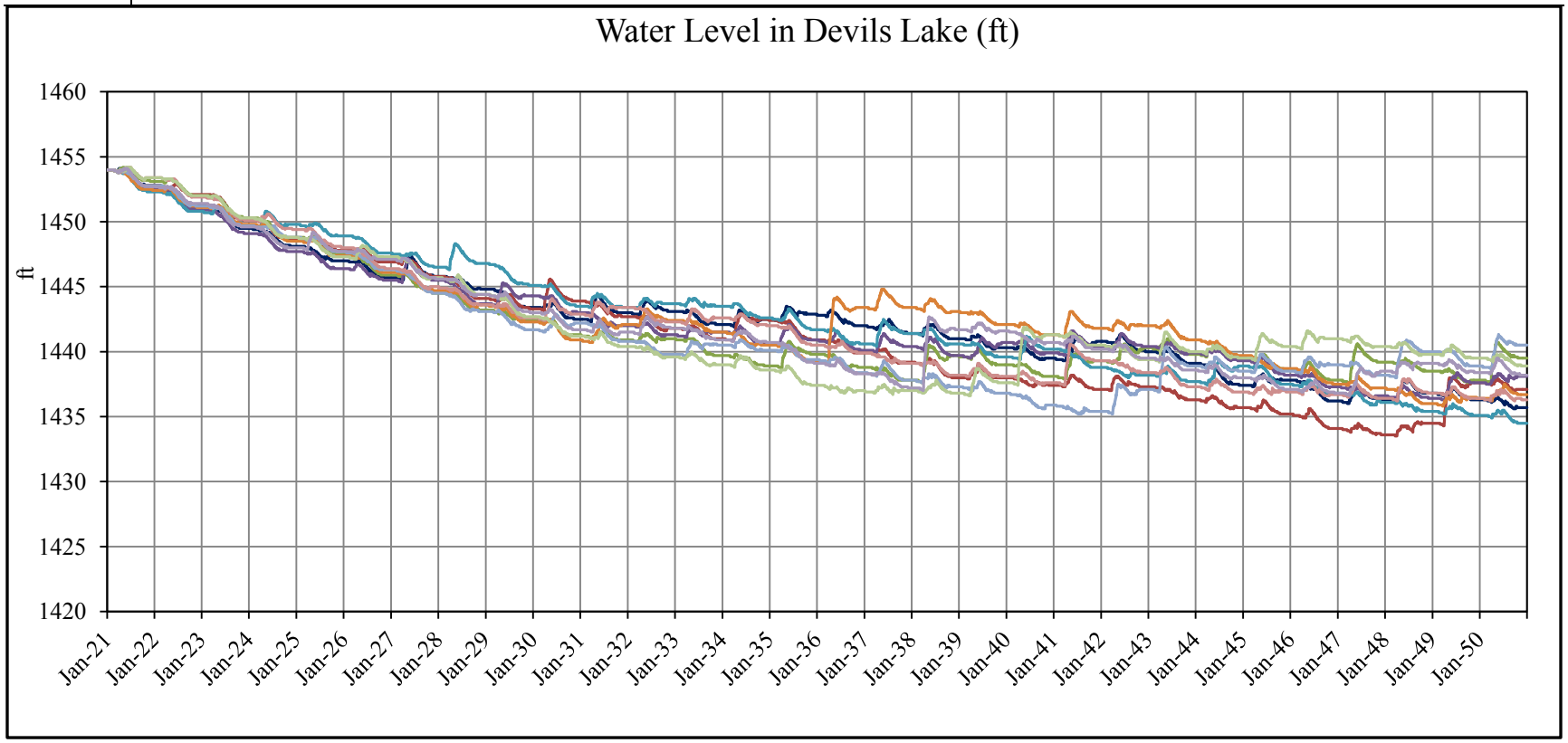

Figure 35: Simulated water level in Case 2: A1B_GFCM21_2021-2050

Table 20: Simulation Case 3: A1B_GIAOM_2021-2050

Shuffle	0	1	2	3	4	5	6	7	8	9	All
Max	1454	1454	1454.1	1454.6	1454.1	1454	1454	1454	1454	1454	1454.6
Min	1434.8	1436.1	1434.1	1435.8	1433.5	1437.3	1436.5	1435.2	1434.9	1433.8	1433.5
Mean	1442.06	1442.34	1442.44	1441.97	1442.98	1443.44	1441.89	1443.63	1442.36	1442.79	1442.59

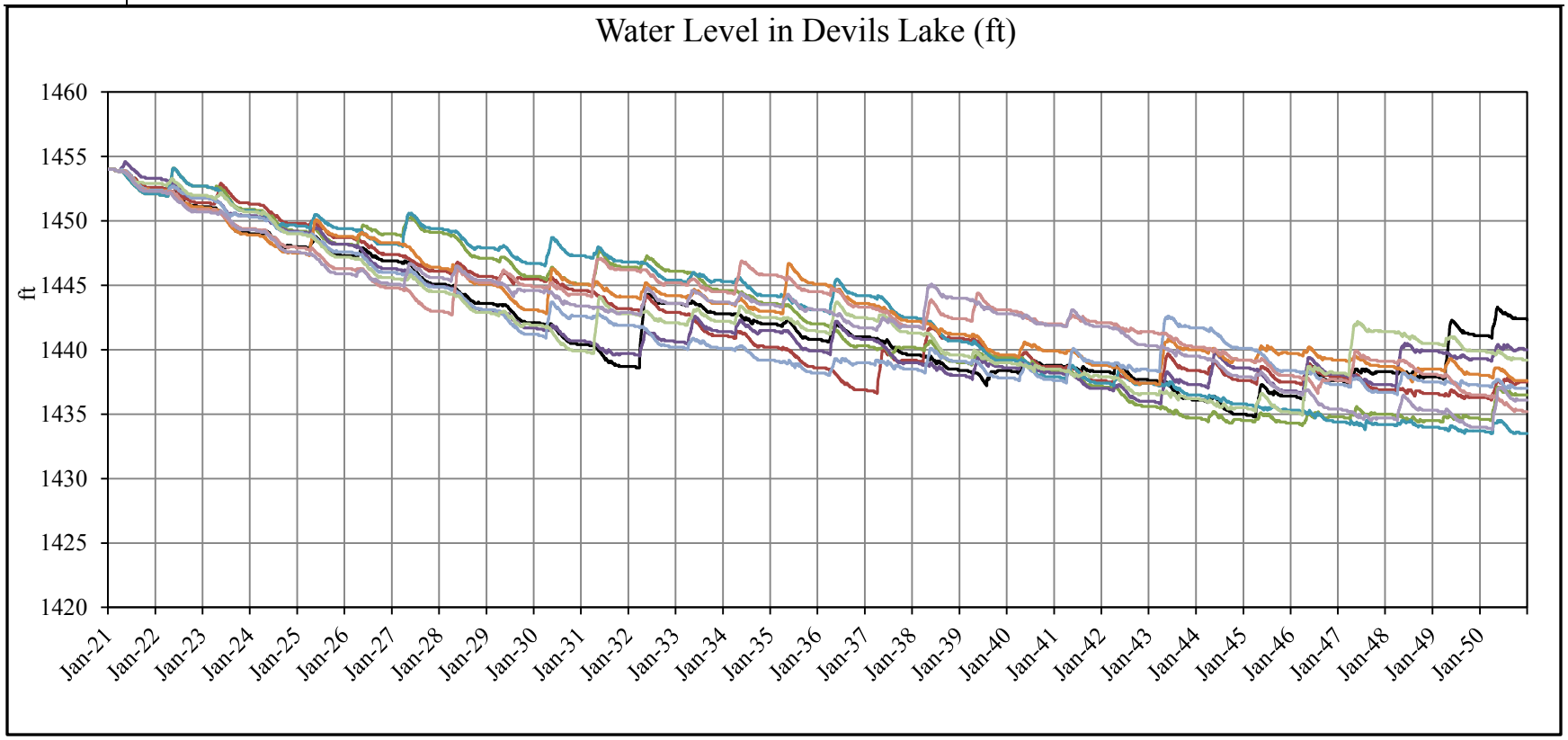

Figure 36: Simulated water level in Case 3: A1B_GIAOM_2021-2050

Table 21: Simulation Case 4: A1B_HADCM3_2021-2050

Shuffle	0	1	2	3	4	5	6	7	8	9	All
Max	1454	1454	1454	1454.4	1454	1454	1454	1455.2	1454	1454	1455.2
Min	1436.7	1438.1	1434.5	1436.6	1438.5	1434	1434.3	1436.6	1436.5	1437.5	1434
Mean	1442.87	1443.51	1444.09	1443.77	1442.61	1442.07	1442.06	1444.12	1443.39	1443.02	1443.15

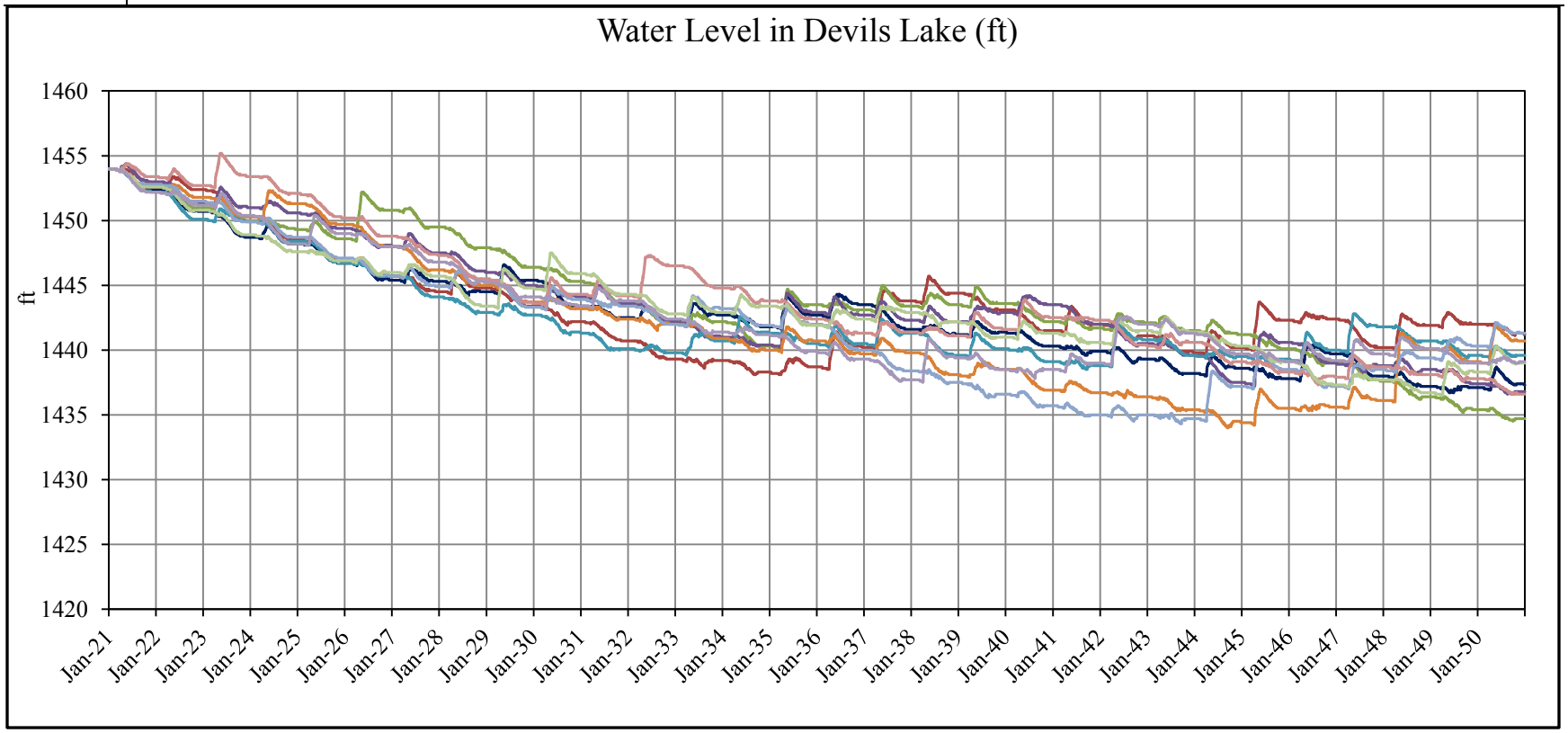

Figure 37: Simulated water level in Case 4: A1B_HADCM3_2021-2050

Table 22: Simulation Case 5: A2_GFCM21_2021-2050

Shuffle	0	1	2	3	4	5	6	7	8	9	All
Max	1454.7	1454.3	1454	1454.1	1454.1	1454.3	1454	1454.3	1454.1	1454	1454.7
Min	1433.3	1436	1435.6	1423.3	1425.8	1424.2	1425.6	1425.6	1424.7	1425.5	1423.3
Mean	1442.02	1442.15	1442.29	1434.96	1436.67	1436.09	1436.29	1436.36	1436.37	1436.41	1437.96

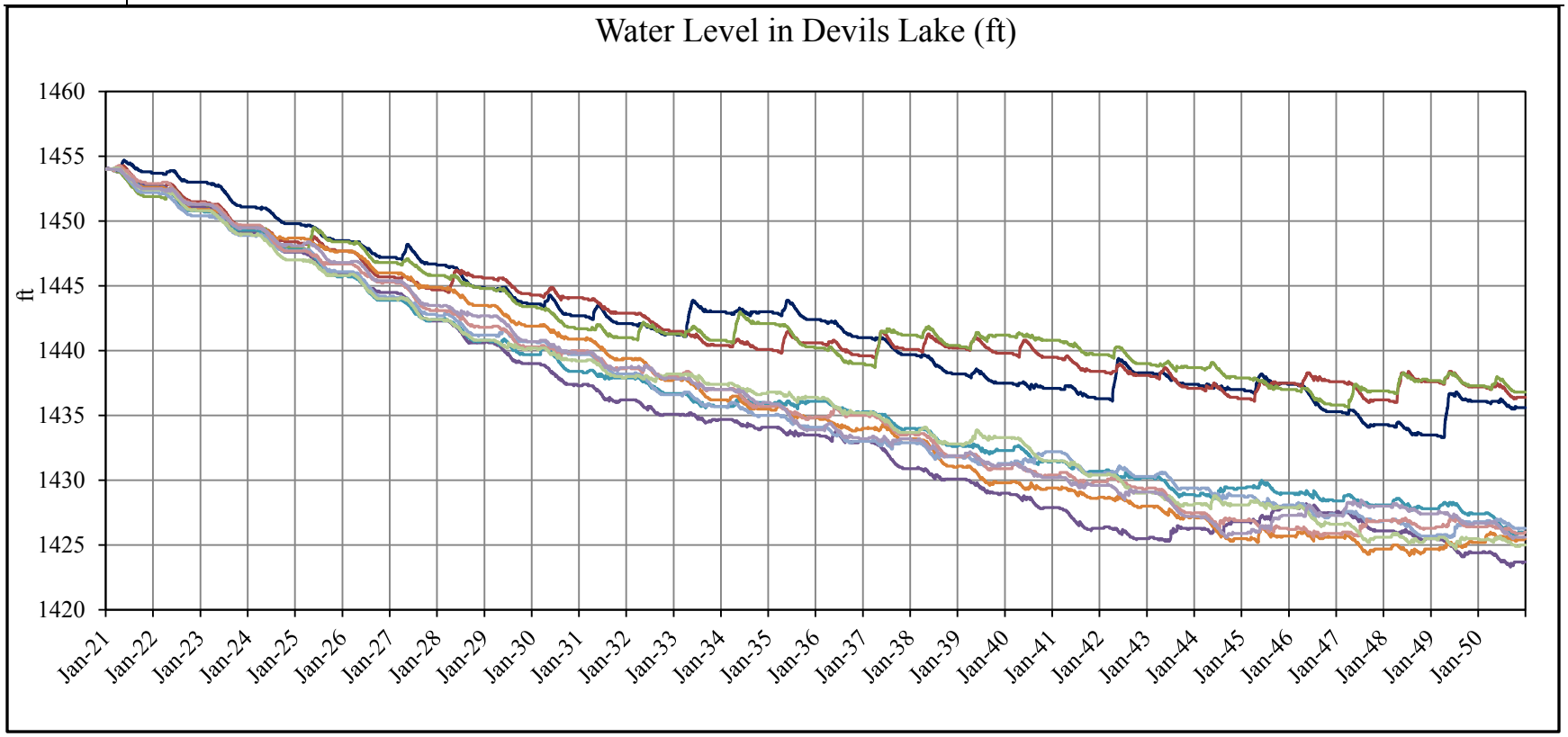

Figure 38: Simulated water level in Case 5: A2_GFCM21_2021-2050

Table 23: Simulation Case 6: A2_HADCM3_2021-2050

Shuffle	0	1	2	3	4	5	6	7	8	9	All
Max	1454.1	1454	1454	1454	1454	1454	1454	1454	1454.1	1454	1454.1
Min	1428.8	1429	1427.6	1428.1	1428.1	1427.6	1428.4	1427.4	1427.1	1427.8	1427.1
Mean	1437.94	1438.11	1438.03	1438	1438.55	1438.64	1438.59	1438.18	1437.7	1438.96	1438.27

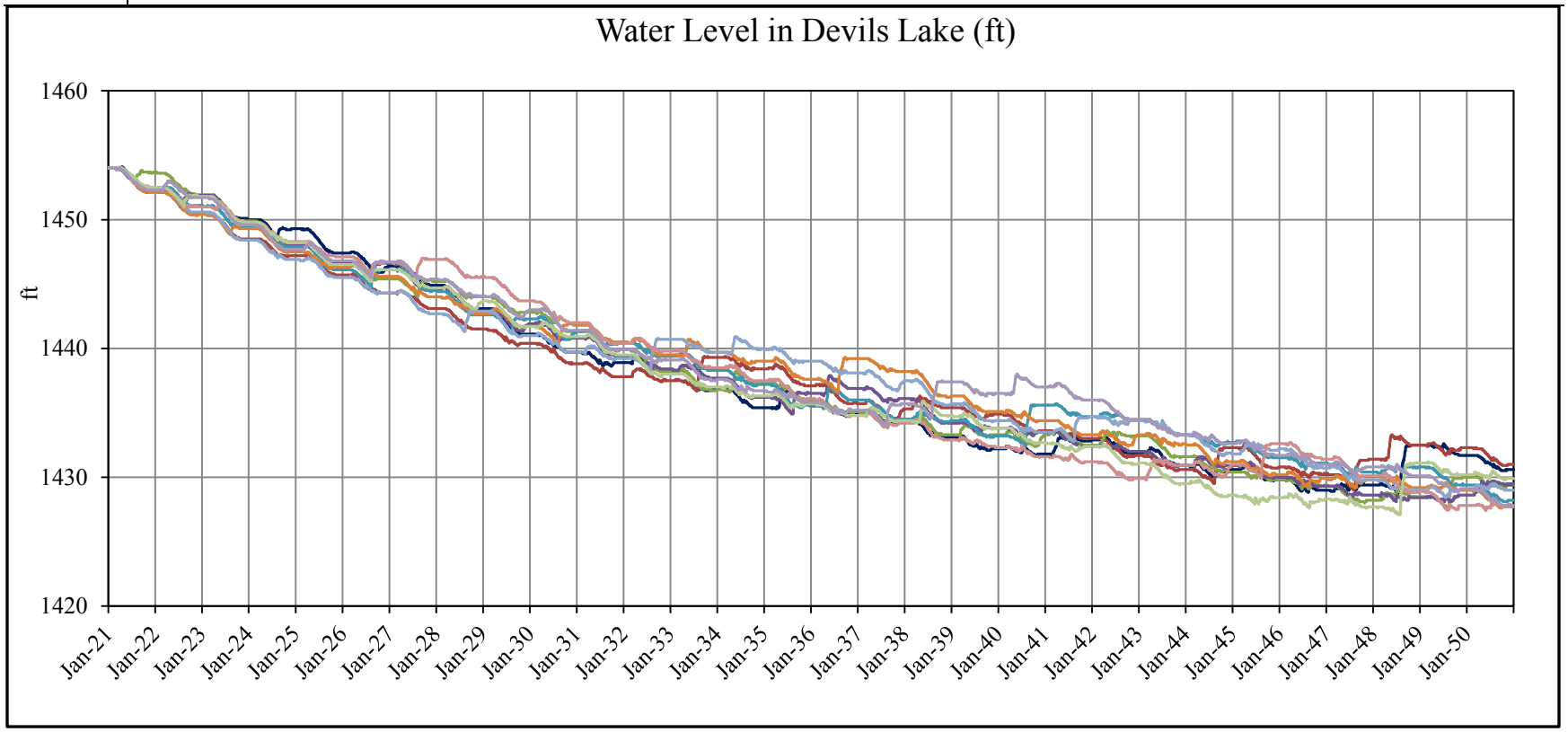

Figure 39: Simulated water level in Case 6: A2_HADCM3_2021-2050

Table 24: Simulation Case 7: B1_CSMK3_2021-2050

Shuffle	0	1	2	3	4	5	6	7	8	9	All
Max	1454	1454.1	1454	1454.5	1454.2	1454	1454	1454	1454	1454	1454.5
Min	1432	1430.1	1429.5	1430.4	1431.8	1431.8	1430	1430.6	1430.6	1429.6	1429.5
Mean	1439.08	1438.47	1439.08	1439.29	1439.4	1438.68	1438.81	1439.53	1438.71	1439.59	1439.06

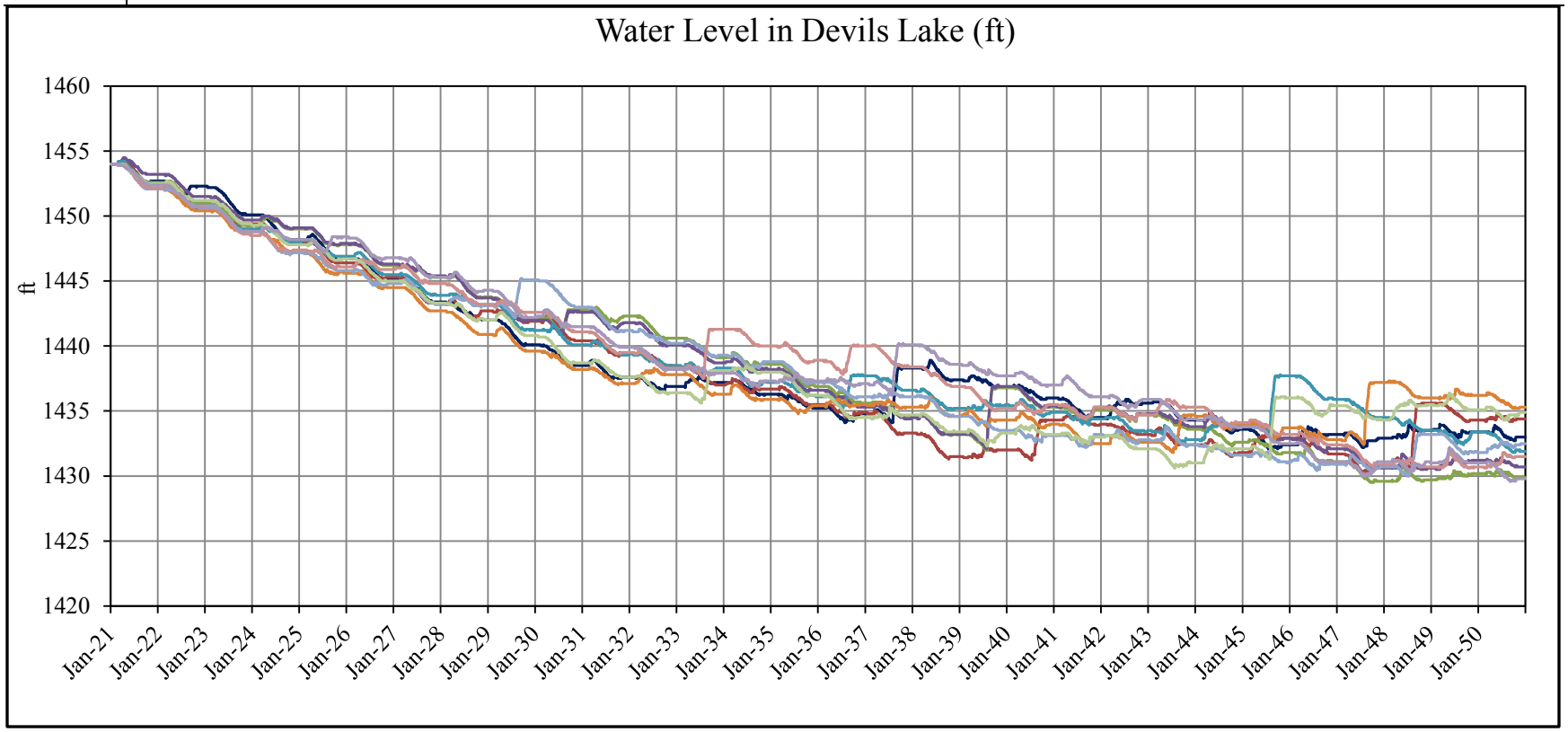

Figure 40: Simulated water level in Case 7: B1_CSMK3_2021-2050

Table 25: Simulation Case 8: B1_GFCM21_2021-2050

Shuffle	0	1	2	3	4	5	6	7	8	9	All
Max	1454.1	1454.3	1454.1	1454	1454	1454	1454	1454.7	1454.1	1454.1	1454.7
Min	1425.6	1428.9	1429.3	1427.2	1427.5	1429.1	1426.7	1427.1	1425.6	1426.1	1425.6
Mean	1437.29	1437.21	1437.27	1436.87	1437.43	1437.39	1437.24	1437.18	1437.65	1437.05	1437.26

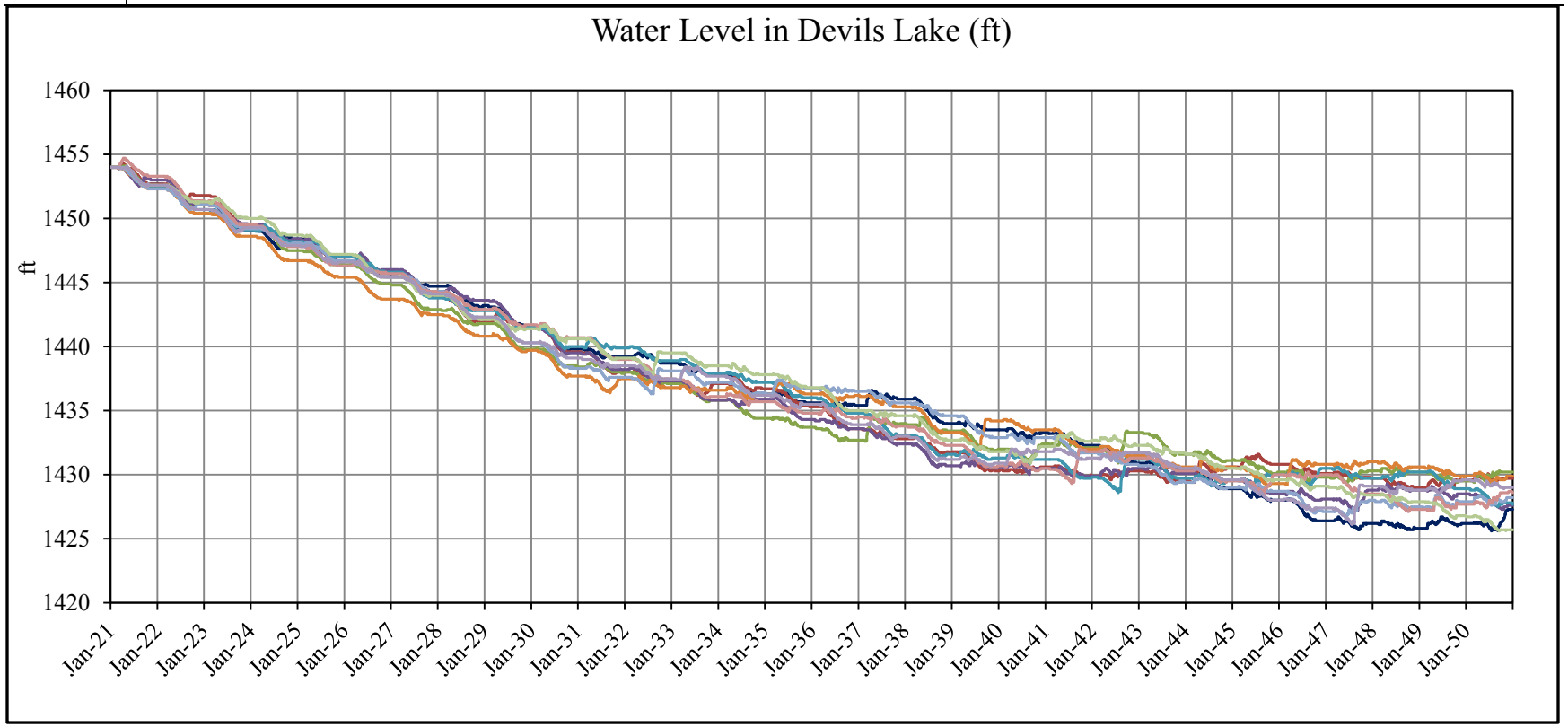

Figure 41: Simulated water level in Case 8: B1_GFCM21_2021-2050

Table 26: Simulation Case 9: B1_GIAOM_2021-2050

Shuffle	0	1	2	3	4	5	6	7	8	9	All
Max	1454.1	1454	1454.1	1454	1454.1	1454	1454.1	1454	1454	1454.1	1454.1
Min	1427.1	1424.6	1427.5	1425.8	1424.8	1427.6	1427	1423	1427.6	1426	1423
Mean	1436.37	1436.56	1436.62	1436.83	1437.01	1436.67	1436.57	1435.75	1436.63	1436.4	1436.54

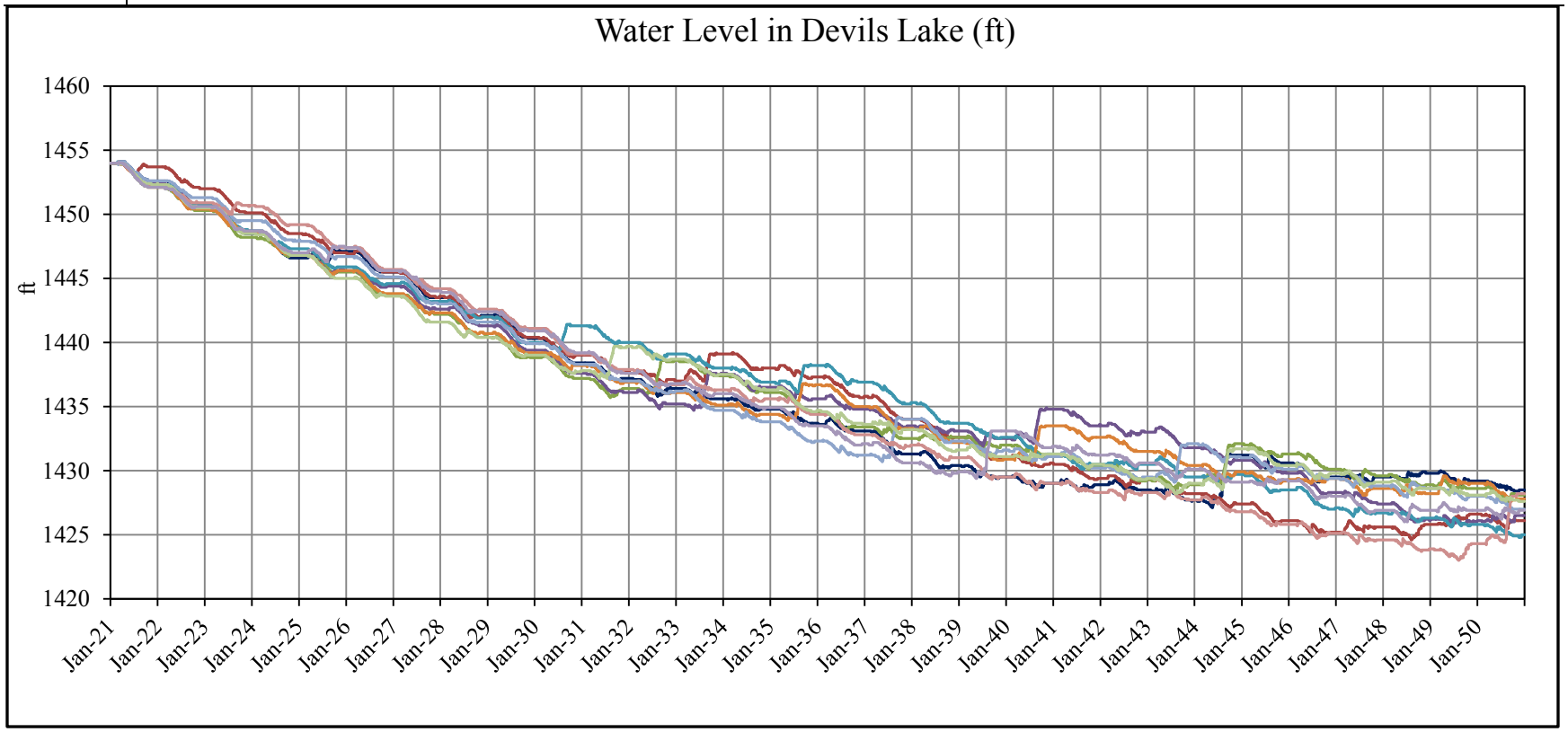

Figure 42: Simulated water level in Case 9: B1_GIAOM_2021-2050

Table 27: Simulation Case 10: B1_HADCM3_2021-2050

Shuffle	0	1	2	3	4	5	6	7	8	9	All
Max	1454.4	1454.4	1454.3	1454	1454	1454.2	1454.4	1454.2	1454.2	1454	1454.4
Min	1431.2	1429.6	1427.9	1429.7	1426.4	1429.2	1427.3	1430.7	1429.7	1428.7	1426.4
Mean	1438.67	1438.56	1439.3	1438.66	1438.24	1437.98	1438.9	1439.02	1437.91	1437.88	1438.51

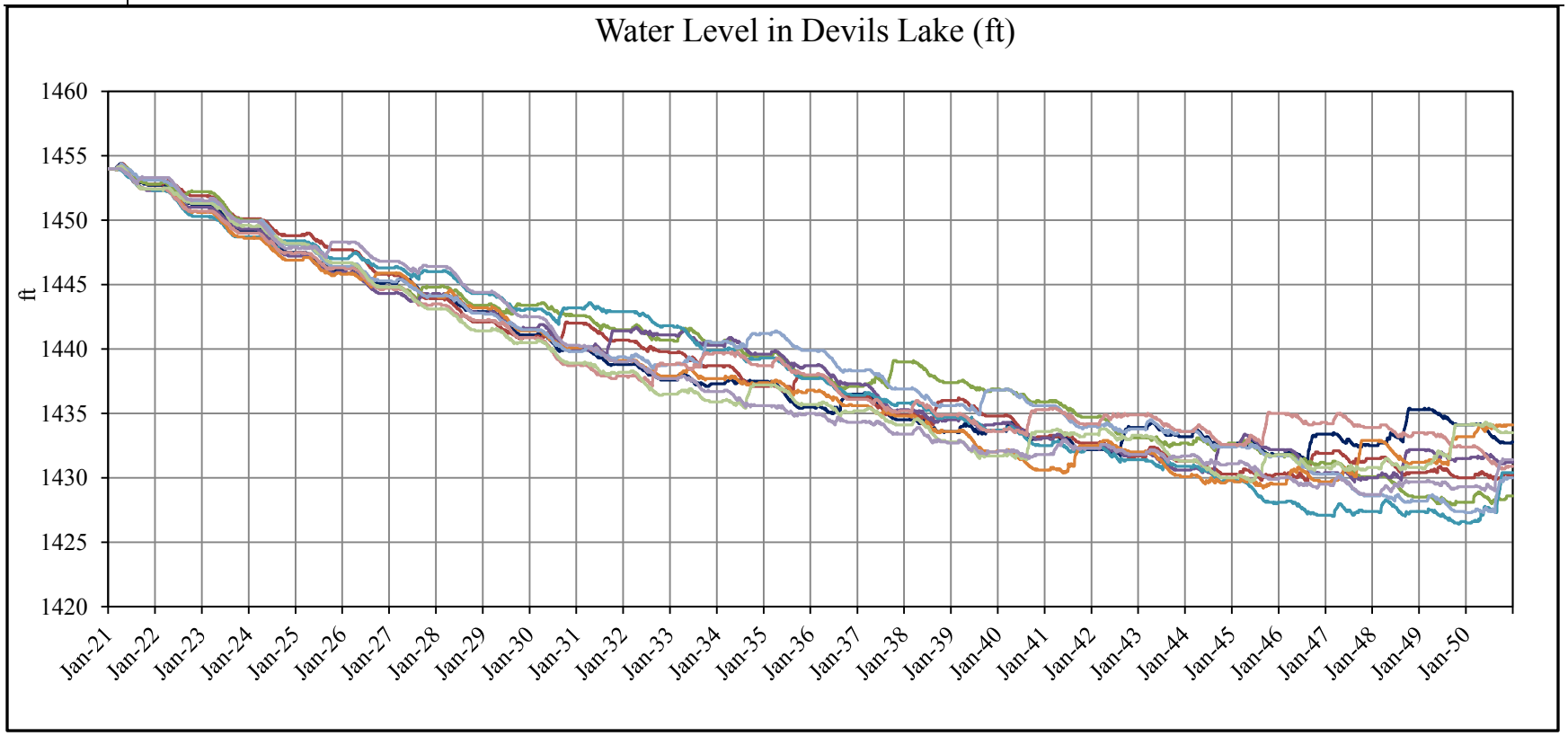

Figure 43: Simulated water level in Case 10: B1_HADCM3_2021-2050

5.6 Sensitivity Analysis

In these simulated lake elevations, evaporation plays a very important role as it is the fundamental dominant factor in reducing the water level. So to analyze the effect of evaporation on the lake water level, a sensitivity analysis is performed using A1B_CSMK3. In the previous simulations average yearly evaporation can be approximated as 30.9 inches. Another simulation is performed using a reduced yearly evaporation of 27 inches out of the lake. The result shows that nearly 4 ft of water level difference can be observed due to the changed evaporation pattern. Results in changed simulated water levels and shift in mean water level due to reduced yearly evaporation are illustrated in Figure 44, Figure 45 and Figure 46.

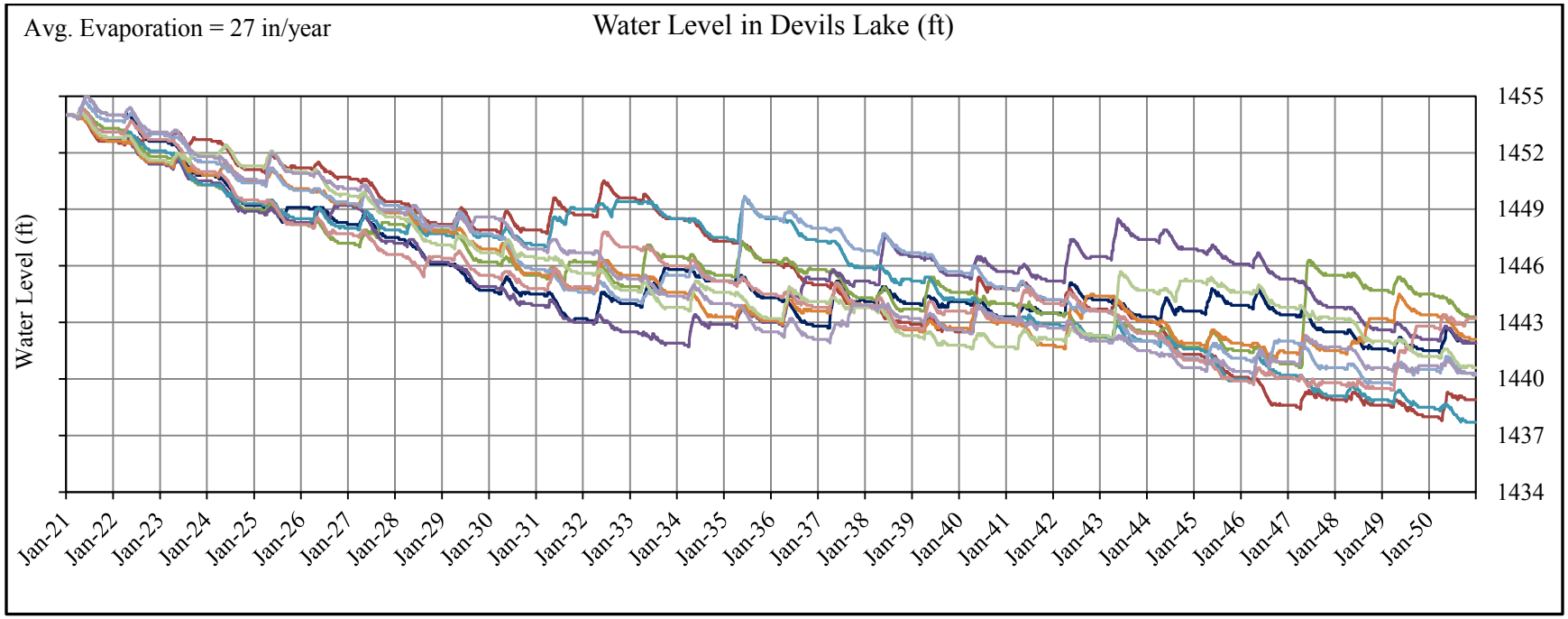

Figure 44: Experimental simulation of water level considering average lake evaporation of 27 in/year

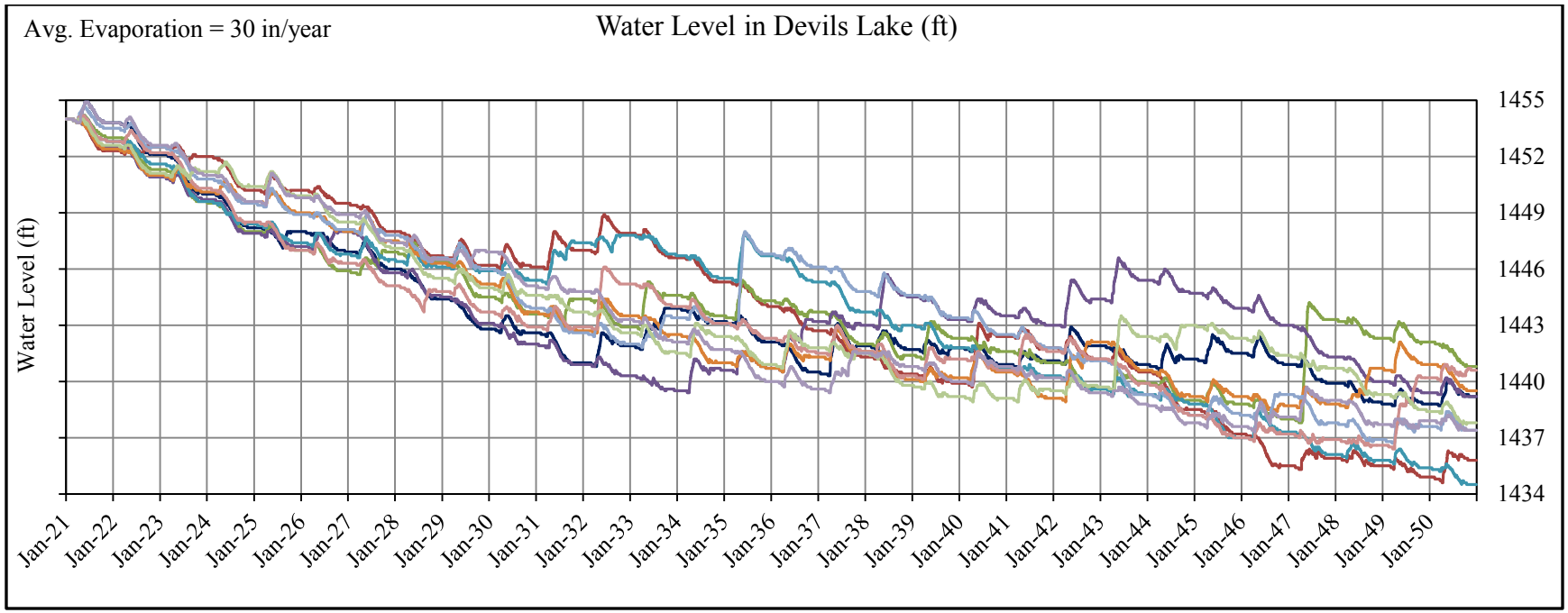

Figure 45: Experimental simulation of water level considering average lake evaporation of 30 in/year

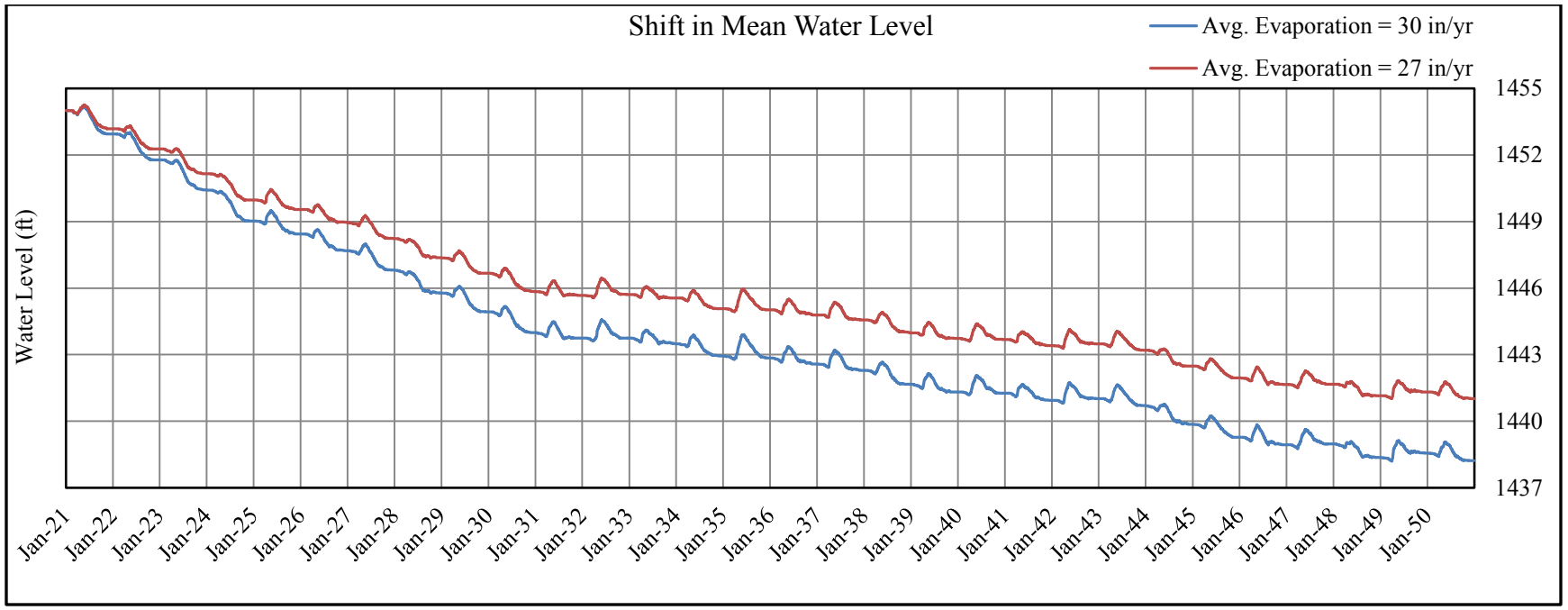

Figure 46: Shift in mean water level due to change in average lake evaporation by 3 in/year

CHAPTER 6

FREQUENCY ANALYSIS OF LAKE-LEVELS

The frequency analysis of the lake stage series were performed by Woodbury and Padmanabhan (1989), Vecchia (2002), and Lim (2004). The design of civil infrastructures, such as highways and dikes, has been highly dependent on the outcomes of reliable flood frequency analysis. The observed flood peak series are used as the primary data. In the US, a method outlined in Bulletin 17-B (US Interagency Advisory Committee on Water Data, IACWD, 1982) is associated with the Log Pearson type 3 distribution. The conventional Bulletin 17-B flood frequency analysis method was developed for the riverine conditions; hence, it is not appropriate for lake-level frequency analysis without proper modifications. The Bulletin 17-B generalized skew map developed for the method does not apply to lake levels. In general, lake levels are not independent events, and they do not have the natural zero value as what river levels or discharges possess. Hence, lake levels typically do not exhibit the extreme variability and skewness as found in flood flows.

6.1 Specific Lake Conditions

The probabilistic approach is a method to interpret the simulated traces of the future lake-levels under multiple GCMs, scenarios, and reshuffles. However, there are several considerations that have to be examined before adopting a particular method for frequency analysis. These factors are specific to the Devils Lake:

1) The lake has no surface-water outlet for at least the most recent history although there is a natural outlet at Tolna Coulee with a spill-level at 1458 ft amsl. Lake-levels of closed-basin lakes are characterized by high serial persistence (Steven, 1995; Niehus *et al*. 1999). Hence, for a terminal lake of this nature, there is substantial serial dependence of lake-levels in successive years.
2) The topography of the lake shore has significant impacts on the lake-level versus storage relationship, meaning a linear extrapolation between the lake-level and storage is not warranted.
3) The lake has several pumping schemes that will eventually have some impacts on the lake-level when they are operated continuously. However, this is not considered significant in the frequency analysis of the current lake-level.

6.2 Probability Distribution Functions (PDFs)

The frequency analysis has been done using four Probability Distribution Functions (PDFs).

a) Normal distribution or Gaussian distribution,
b) Pearson type 3 or Gamma distribution,
c) Lognormal distribution and
d) Log Pearson type 3 (LP3) distribution.

To estimate the probability or return period of a flood event it is necessary to determine several statistical parameters. A series of historical stages or volume constitutes the population of random variables belonging to a PDF with a set of parameters. The parameters define the moments as they are related and can be calculated.

The most important moments that need to be known are mean, variance and skewness. Bedient and Huber (Bedient *et al*, 2002) described the equations of frequency distribution very elaborately. If the number of independent samples of a random variable (stage/volume) is *n*, an estimate of mean is:

$$\hat{\mu} = \bar{x} = \frac{1}{n}\sum_{i=1}^{n} x_i \tag{20}$$

The unbiased variance $\hat{\sigma}^2$ can be calculated as:

$$\hat{\sigma}^2 \equiv S^2 = \frac{1}{n-1}\sum_{i=1}^{n}(x_i - \bar{x})^2 \tag{21}$$

where, the divisor *n-1* eliminates the bias. The variance of the mean of the variables is:

$$Var(\bar{x}) \equiv {S_{\bar{x}}}^2 = \frac{{S_x}^2}{n} \tag{22}$$

To compute the approximate unbiased skewness, the following equation is used.

$$C_s \equiv \hat{g} = \frac{n}{(n-1)(n-2)} \times \frac{\sum(x_i - \bar{x})^3}{{S_x}^3} \tag{23}$$

Error and bias in the skewness is inversely proportional to the number of observations. However, a generalized estimate of the coefficient of skewness, C_w is used by the "Bulletin 17B Method".

$$C_w = WC_s + (1 - W)C_m \tag{24}$$

where,

W = weighting factor,

C_s = Coefficient of skewness computed using the sample data and

C_m = a regional skewness, which can be calculated from a map provided by the Interagency Advisory Committee on Water Data (IACWD), 1982 (Appendix H.1)

The weighting factor, W is used to minimize the variance of C_w and can be calculated as:

$$W = \frac{V(C_m)}{V(C_s)+V(C_m)} \tag{25}$$

$V(C_m)$ = 0.302 (IACWD, 1982). By substituting W into the previous equation, C_w can be written as:

$$C_w = \frac{V(C_m)C_s+V(C_s)C_m}{V(C_m)+V(C_s)} \tag{26}$$

The Monte Carlo experiments by Wallis *et al* (1974) provides the following formula to estimate the variance of station skew, $V(C_s)$.

$$V(C_s) = 10^{A-B\log_{10}(n/10)} \tag{27}$$

where,

$$A = -0.33 + 0.88|C_s| \quad if \quad |C_s| \leq 0.90 \quad or \tag{28}$$

$$A = -0.52 + 0.30|C_s| \quad if \quad |C_s| \geq 0.90, \tag{29}$$

$$B = 0.94 - 0.26|C_s| \quad if \quad |C_s| \leq 1.50 \quad or \tag{30}$$

$$B = 0.55 \quad if \quad |C_s| \geq 1.50 \tag{31}$$

Here,

$|C_s|$ = the absolute value of the station skew and

n = the record length in years

6.2.1 Normal/Gaussian Distribution

The PDF for the normal distribution is given by

$$f(x) = \frac{1}{\sqrt{2\pi}\sigma} e^{-(\frac{1}{2})[(x-\mu)/\sigma]^2}, \quad -\infty \leq x \leq \infty \tag{32}$$

The distribution is dependent on mean, μ and variance, σ^2 and the skewness is zero. The cumulative differential function, CDF is computed after a change in the variable to:

$$Z \equiv (x - \mu)/\sigma \tag{33}$$

Here, *z* is known as the standard normal variate. The CDF can then be computed as

$$\int_{-\infty}^{z} \frac{1}{\sqrt{2\pi}} e^{-\mu^2/2}\, d\mu \tag{34}$$

A table of *F(z)* vs. *z* is used to estimate the value of one variable using the given variable. The return period, *T* can be calculated using the following equation

$$F(z) = 1 - \frac{1}{T} \tag{35}$$

6.2.2 Lognormal Distribution

The distribution has a positive skewness, which is a function of the coefficient of variation. The skewness is given by

$$g = 3CV + CV^3 \tag{36}$$

The moment of the untransformed variables can be found by the following relationships

$$CV_x^2 \equiv \frac{\sigma_x^2}{\mu_x^2} = e^{\sigma_y^2} - 1 \quad and \tag{37}$$

$$\mu_x = e^{\mu_y + \sigma_y^2/2} \tag{38}$$

where, $y = \ln x$

The equations can be solved for μ_y and σ_y^2. Here, one thing should be noted that the log of means is not the mean of the logs

$$\mu_y = \log x_m \tag{39}$$

where,

x_m = the median of x

Another useful relationship for the lognormal distribution is given by

$$\mu_x = x_m(1 + CV_x^2) \tag{40}$$

6.2.3 Pearson type 3 (Gamma) Distribution

This distribution is extensively used in hydrology because of its shape and well known mathematical properties. The distribution has a positive skewness. The frequency factors *k* are a function of skewness and return period and can be obtained from a table (Appendix H.2). The governing equation is

$$Q_T = \bar{Q} + K(C_s, T).S_Q \tag{41}$$

It is not necessary to calculate the skewness of the sample data. Instead the skewness of the two parameter gamma is used:

$$g = 2CV \quad or \tag{42}$$

$$C_s = 2S_x\sqrt{x} = 2CV \tag{43}$$

The skewness is then used in the table (Appendix H.2)

6.2.4 Log Pearson type 3 Distribution

When the gamma distribution is applied to the logs of the random variables, it is called the Log Pearson type 3 or LP3 distribution. This method is widely used as this has been recommended for application to flood flows by the USIACWD, 1982 in the committee's Bulletin 17B method. The methodology is exactly same except the logarithm of the variable instead of random variables is used in the analysis.

6.3 Frequency Analysis: HEC-SSP

The flood frequency of the lake is done both in stage and volume basis. All the methods (Normal, Lognormal, Pearson type 3 and Log Pearson type 3) discussed in the previous articles have been used to estimate the probability of flooding. As stage of the lake can be more sensitive in estimating the flood frequency and return periods of probable flood events, a volume-based frequency analysis has also been done. To perform the calculations of probability distribution and curve fitting, a software from the US Army Corps of Engineers called HEC-SSP has been used. The peak stage and volume of both observed (1901-2011) and simulated (30 years) series are input into HEC-SSP. The model is able to estimate the probability distribution and calculate the return periods for all the above mentioned methods.

6.3.1 Frequency Analysis of Observed Lake-Stages

The process of distribution fitting is performed on the observed annual peak lake stage series from 1901-2010. Table 28 shows the probabilities and return period estimates based on the frequency analysis of the observed lake-level series. Figure 47 and Figure 48 shows the Gaussian/Normal and Lognormal frequency distribution fits for the historical series. The present level is estimated as a 1 in 140-year event. There are some discrepancies between the results obtained by the Normal and Lognormal distributions with that obtained by the Pearson type 3 and Log Pearson type 3 distributions. The plots are included in Appendix H.3.

6.3.2 Frequency Analysis of Simulated Lake-Stages

Multiple probabilistic distributions are also fitted to a batch of preliminary generated traces. The main objective is to make inferences about the flood quantiles of

the future conditions, compare it with the current lake conditions and derive the conditional probabilities given that the current level is known. The current exceedingly high water level makes the use of conditional frequency analysis much more necessary in decision making. The distribution plots are included in Appendix H.4.

Table 28: Probabilities and return periods of current lake-level using different PDFs

Distribution Type	Probability (%)	Return Period (Year)
Normal	0.706	142
Pearson type 3	2.00	50
Log Normal	0.735	136
Log Pearson type 3	2.05	49

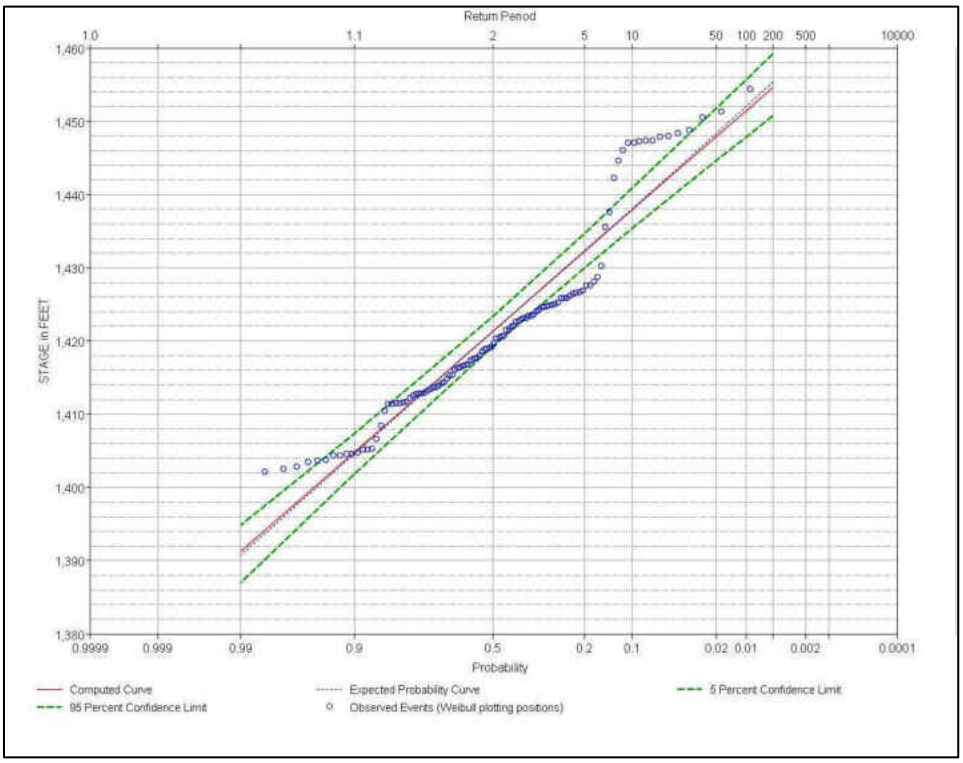

Figure 47: Observed lake-levels fitted using normal distribution

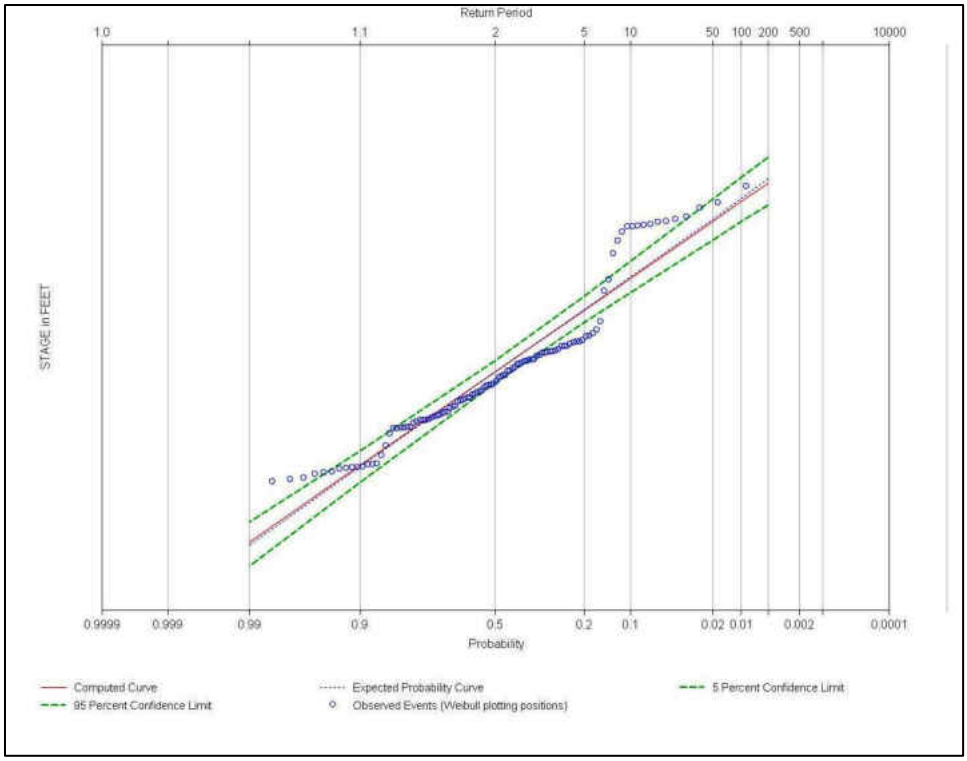

Figure 48: Observed lake-levels fitted using log-normal distribution

6.3.3 Frequency Analysis using Lake-Volumes

Understanding the fact that stage-based frequency analysis can be more sensitive than volume-based frequency analysis, a different approach is undertaken to estimate the probabilities using peak lake volume series. Based on the known stage-volume relationship, an equation is derived, which is shown in Figure 49.

$$y = -0.0001423\ \text{X}\ x\text{^}6 + \ 1.2126\ \text{X}\ x\text{^}5 - 4305.7545\ \text{X}\ x\text{^}4 + 8152745.2381\ \text{X}\ x\text{^}3 - 8681920367.8408\ \text{X}\ x\text{^}2 + 4930173873316.99\ \text{X}\ x - 1166364096660680 \quad (44)$$

The equation is used to convert the simulated lake stages to volumes. As it is a 6 degree polynomial equation, it is very important to use most of the significant numbers after decimal point to obtain a representative value of volume.

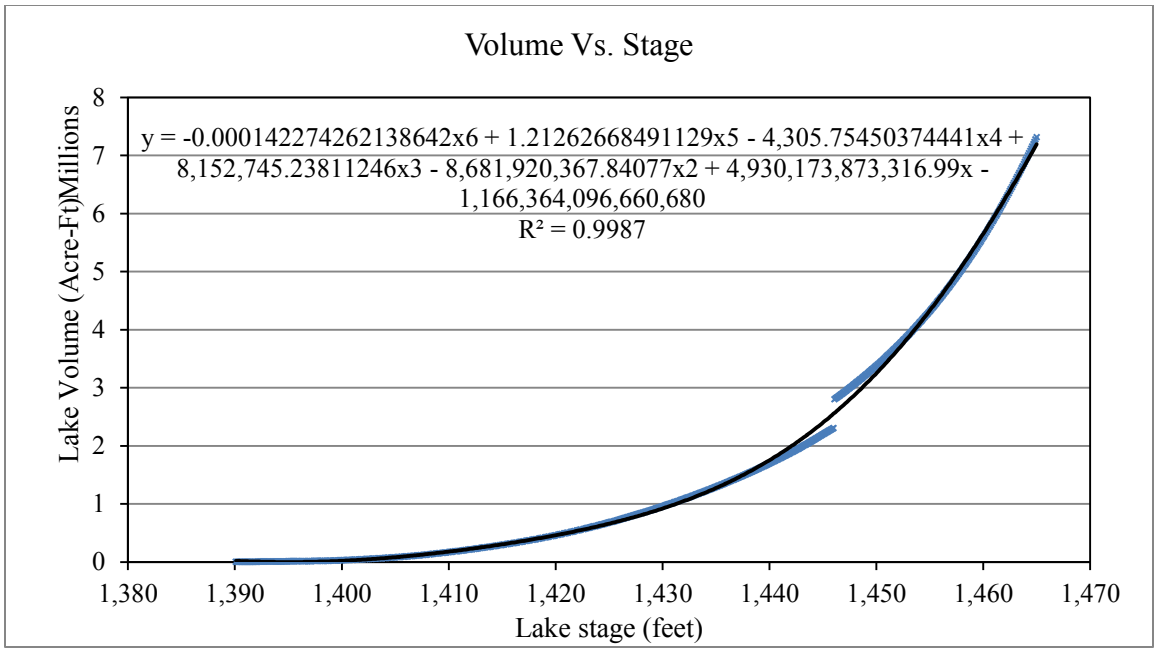

Figure 49: Trend line and equation of the stage-volume function

6.3.4 Frequency Analysis of Observed Lake-Volumes

The converted volumes of the observed lake stages from 1901-2011 has been used in the frequency analysis. The current water level of 1454 ft is the highest in the last 100 years and Table 29 shows the probability and return period of the current lake-volumes based on observed events. Figure 50 and Figure 51 show the general frequency distribution fits for the historical series using Lognormal and Pearson type 3 distributions as they have the better fits. Plots of the fit using other distributions are shown in Appendix H.5. The present level is estimated as a 1 in 300 year event. But discrepancies are observed between the results obtained by LP3, Normal and other two methods.

Table 29: Probabilities and return periods of current lake-volume using different PDFs

Distribution Type	Probability (%)	Return Period (Year)
Normal	0.0046442	21532
Pearson type 3	0.315286	317
Log Normal	0.278361	359
Log Pearson type 3	1.098607	91

6.3.5 Frequency Analysis of Simulated Lake-Volumes

Analogous to the frequency analysis of simulated lake stages, the peak volume series have been used to obtain the probability and return periods of the equivalent volume of 1456 ft, 1458 ft and 1460 ft. These probability values are later used to obtain the conditional probabilities of extreme flood events. Plots of the distribution fits using the four methods can be seen in Appendix H.6.

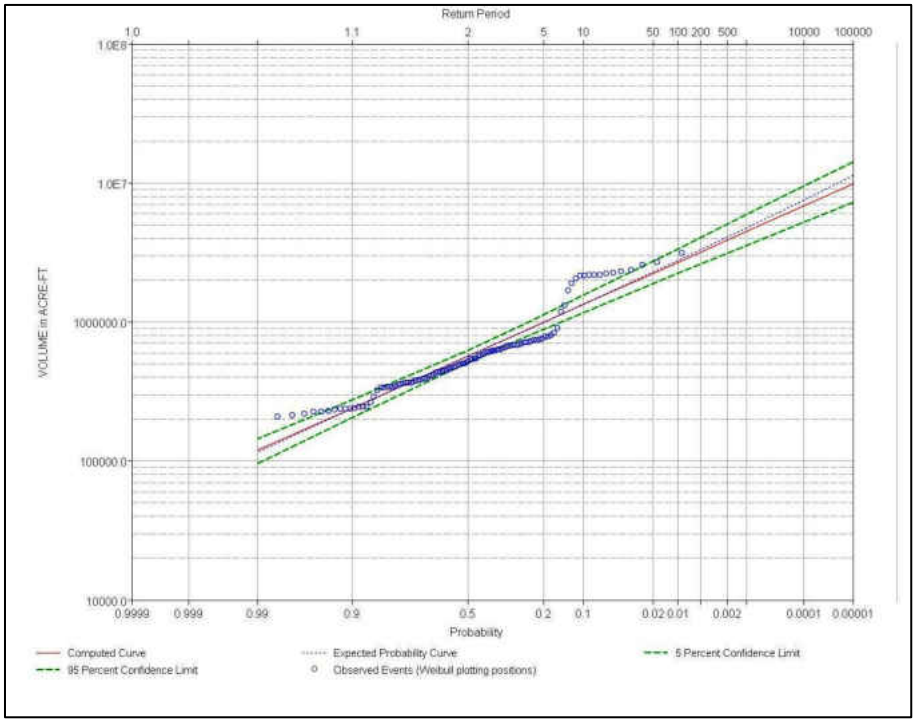

Figure 50: Observed lake-volumes fitted using Lognormal probability distribution

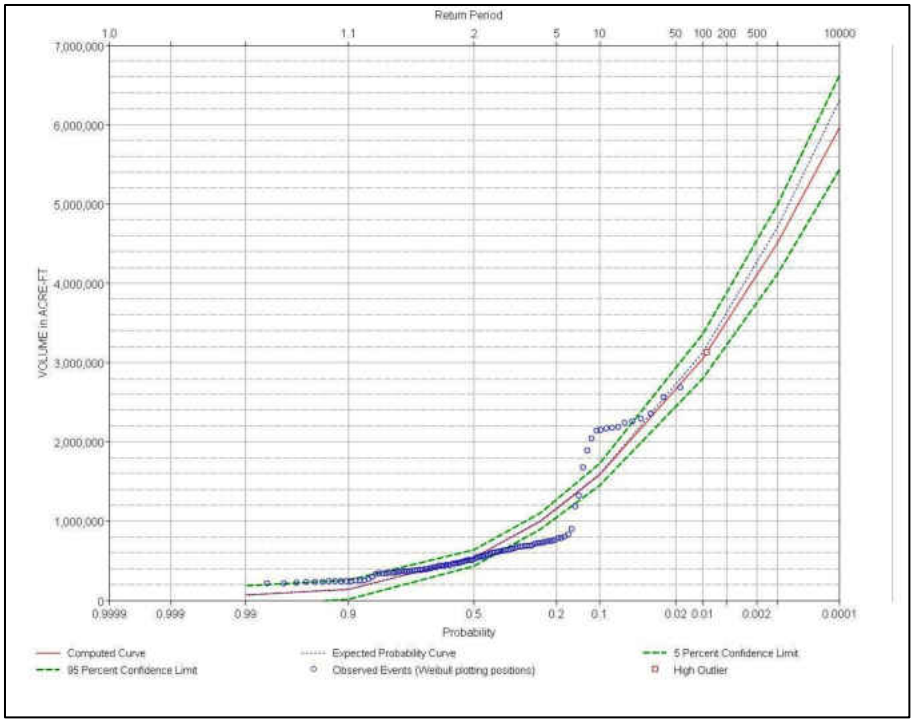

Figure 51: Observed lake-volumes fitted using Pearson type 3 probability distribution

6.3.6 Conditional Frequency Analysis

Because lake levels of closed-basin lakes are characterized by high serial persistence, two frequency analysis methods (unconditional and conditional) should be assessed. Unconditional frequency analysis estimates the frequencies of extreme lake-levels for a long time period. Since the simulation period is a relatively short time period (30 years), the starting conditions at the beginning of the simulation period have significant effect on the analysis. It is also important to note that assessments for flood-mitigation options usually consider relatively short projected time periods, in the order of 30 to 50 years. Thus conditional frequency analysis usually is more appropriate than unconditional frequency analysis. Although Vecchia (Vecchia, 2002) used a Markov model with no factoring of climate change in simulating the future lake-level series for Devils Lake, conditional probabilities were also used in the interpretation of the

simulated series. Kubik (Kubik, 1990) presented the needs of including conditional probabilities to predict the change of lake-levels in transition from one season to another. The probability of an event A given that B occurs is given by

$$P(A/B) = \frac{P(A \cap B)}{P(B)} \tag{45}$$

which leads to

$$P(A \cap B) = P(B) \times P(A/B) \tag{46}$$

The occurrence of the current high lake-level z_o can be construed as an event called B. Its probability of occurrence is defined by the probability density function of the current observed annual instantaneous maximum water level in year i. If the probability distribution of the current annual instantaneous maximum lake-levels Z_i (i = 1, 2,……) is $f(z)$, then

$$P(Z_i > z_0) = \int_{z_0}^{\infty} f(z)dz = P(A) \tag{47}$$

Because multiple climatic change conditions were considered, it is assumed that the simulated future lake-level series can be used to derive the probability density function of the annual instantaneous maximum water level in year k, given some initial condition $Z_k = z_o$. Let function g denoted by $g(z,k|z_0,0)$ be the probability density function of annual instantaneous maximum lake-levels Z_k (i = 1, 2, ...) if the most recent annual maximum is known. Then the conditional exceedance probability for some level z_k^* in a future year k is given by

$$P(Z_k > z_k^* | z_0,0) = \int_{z_k^*}^{\infty} g(z,k|z_0,0)dz = P(A/B) \tag{48}$$

By using equation 47 and 48, the exceedance probability of a future level z_k^* can be estimated given that the current level is z_o.

6.3.7 Conditional Probabilities of Lake-Stages

The current high level (at 1454 ft) can be considered as an event in the *f (z)* domain and various z_k^* values of 1456, 1458, and 1460 are selected. The results of the analysis is shown in Table 30, which represent the conditional probabilities given that z_o =1454. Table 31 shows the final derivatives of the probabilities.

Table 30: Probability of synthetic lake-level series, P(A/B) in %

	Elevation in ft (given z_o =1454)		
Distribution Type	1456	1458	1460
Normal	1.11	0.44	0.17
Log Normal	1.12	0.45	0.18

Table 31: Conditional probability (of synthetic lake-level series, P(A and B), in %

	Elevation in ft (given z_o =1454)		
Distribution Type	1456	1458	1460
Normal	0.0078	0.0031	0.0012
Log Normal	0.0083	0.0033	0.0013
Mean	0.0081	0.0032	0.0013

6.3.8 Conditional Probabilities of Lake-Volumes

Given the current elevation at 1454 ft, the conditional probabilities of extreme volumes have been calculated. The result of the analysis is summarized in Table 32. Table 33 shows the conditional probability of extreme flood events at water levels 1456, 1458 and 1460 ft.

Table 32: Probability of synthetic lake-volume series, P(A/B) in %

Distribution Type	Elevation in ft (given z_o =1454)		
	1456	1458	1460
Normal	0.4023	0.0978	0.0184
Pearson type 3	1.59	0.6850	0.3184
Log Normal	1.40	0.6753	0.3049
Log Pearson type 3	2.33	1.3578	0.7498

Table 33: Conditional probability of synthetic lake-volume series, P(A and B), in %

Distribution Type	Elevation in ft (given z_o =1454)		
	1456	1458	1460
Normal	0.002	0.0005	0.00009
Pearson type 3	0.005	0.0022	0.001
Log Normal	0.004	0.0019	0.00085
Log Pearson type 3	0.026	0.0149	0.00824

CHAPTER 7

DISCUSSION

In this section the difficulties and obstacles are discussed and success and limitations are illustrated.

7.1 Discussion on Steps Followed to Obtain the Future Lake-Level Traces

The project includes several tasks and steps in obtaining the expected outcome, which include modeling the watershed in HEC-HMS, calibrating the model, modeling the Devils Lake in HEC-ResSim, calibrating it with observed water levels, defining the future climate data format in ASCII, importing it into HEC-DSSVue and performing the final simulation.

The first phase of the research was to model the Devils Lake basin using HEC software and investigate the feasibility of using weather samples from downscaled GCMs to predict the future growth of the lake. After this target was achieved, the appropriate format was defined to import the weather samples to make it readily available for future simulation, which can be termed as the second phase. In the third phase, peak yearly values of the simulated traces were obtained and converted into volumes using the stage-storage relationship. Subsequently, the candidate probability distribution functions were implemented and probable return periods of extreme flood events were evaluated to aid in the decisive process of the flood-mitigation plans for the study region.

7.2 Discussion on Basin Delineation

In defining the sub-basins and sub-areas, available DEMs from USGS are used. Considering the fact that the profile of the study area is relatively flat, the resolution of elevation data has profound impact on the appropriate delineation of contributing areas. Hence, the use of latest LIDAR data can be a significant improvement and should be considered at the first place in pursuing further research.

7.3 Discussion on Data, Modeling and Calibration

The watershed model is created in HEC-HMS version 3.4. For calibration purposes stream flow data from all the sub-basins are required to estimate the runoff accurately. Availability of data is one of the main obstacles in achieving the research goal. Gage station at Cando has been chosen for reliable stream flow data, which is within the Mauvais basin. The model is successful in generating the runoff with high flow quantities during the snow-melt period as expected.

The model is calibrated with observed stream flow values in Cando for 2003 through 2010. As explained in the section of calibration, two watershed models are calibrated: one with climate data obtained from ground gage station (HMS-Model A) and the other with data from observations of TMPA by NASA's satellite (HMS-Model B). It is assumed that the Langdon gage climate data is representative for the whole sub-basin area of 3810 square miles approximately, which may not be true in all cases. Availability of continuous daily climate data for 2003 through 2010 is considered the main drawback in this case. The missing data are collected from other nearby sources and is correlated with this station. On the other hand, data from TMPA by NASA's satellite are spatially

distributed throughout the whole basin. There are 48 grid cells that cover the whole area. The quality of data is good in terms of monthly and yearly cumulative, but does not perform well enough in terms of daily values or specific storm events. Here one thing should be noted that big storm events play a key role in modeling the increment of water levels. Most of the small precipitation events are usually lost in the soil and surrounding environment as continuous loss and eventually a very small portion of the runoff reaches the lake, which does not play a big role in increasing the water level. On the other hand big storm events generate considerable amount of runoff even after the losses and cause the water level to increase rapidly in the lake.

After coupling the watershed model with the reservoir model it is possible to generate the water levels with good accuracy and seasonal trend. The ground data-based model is more consistent with observed water levels where the satellite-data-based model is not as good as expected in years 2007 and 2010, which is proven due to the reasons of improper distribution of the magnitude of precipitation. Especially in satellite data, unusually high amount of rainfall is observed in the magnitude of more than 4.4 inches in a day on May 22 and more than 2.75 inches in July 26. The magnitudes of these events are not that high according to the ground gage stations. Due to those high precipitation events in 2007, the calculated runoff was unexpectedly high in that year, which affected the later part of the calibration. Again the satellite data-based model is not accurate enough in year 2010 as it misses some big storm events and does not generate enough runoff to increase the water level. Over all ground data performs better in simulating the water level and provides better calibration results.

One of the main challenges of the task is to model the snow-melt as this is the main factor that triggers the huge flow of water into the lake as soon as the snow begins to melt during spring. The melt rate coefficient, C_m varies from 0.04 to 0.08. While calibrating with ground gage data $C_m = 0.06$ shows better results and with satellite data $C_m = 0.05$ provides a better calibration fit.

The HEC-ResSim model does not account for the precipitation over the lake, which is a significant amount of water that goes directly into the lake with minimal losses. So to model the precipitation over the lake an extra sub-basin is created to portray the lake area. The runoff generated from that sub-basin represents the precipitation to the lake.

7.4 Discussion on Lake Evaporation Model

Being a terminal lake, evaporation is the main source of outflow from the lake. There are not enough gage stations that measure the evaporation on the Devils Lake area. Again, evaporation from ground and evaporation from lake is not the same. The challenge is to develop such a model that can not only simulate the yearly loss but can also provide the necessary seasonal variation with evaporation values in a daily basis. The reason behind simulating the evaporation values in a daily basis is to estimate the continuous daily fluctuation of water level in the lake. Another challenge in achieving the goal is to create such a model, which is only temperature dependent as the weather data from downscaled GCMs provides only the ensembles of precipitation and temperature. It is known that temperature is the key contributing factor in the variation of evaporative losses. But parameters like solar radiation, wind speed, relative humidity etc. are also

very important in estimating the evaporation of a particular area. As projected data for these variables are not available, the model is developed to be only temperature dependent. For other variables, historical observed data has been used from gage station at Crary, ND. Substantial accuracy is obtained while comparing the calculated values with the available penman values from Crary Station. Then the model is arranged to simulate the future estimates by keying in the future temperature values.

7.5 Discussion on HEC-DSSVue

HEC-DSSVue has played the key role in the simulation process by offering an excellent platform to import, store and export data from HEC-HMS, HEC-ResSim, spread sheets of evaporation values, ASCII files of the future weather ensembles and HEC-SSP. The main obstacle has been to import the ASCII files of the future weather ensembles in an appropriate format. It is a very important step because without proper formatting, the data cannot be used for future simulation. There are numerous data files that need to be imported. Manual formatting can be extremely time consuming and can jeopardize the objective of continuous simulation for multiple scenarios. So the success in the automation process is a significant achievement in obtaining the final goal. The simulated values of evaporation loss are also imported and stored in HEC-DSSVue that can be keyed into the HEC-ResSim model for the prediction of future water levels. After importing all the required data in HEC-DSSVue, the continuous simulation is performed in HEC-HMS and HEC-ResSim to obtain the simulated traces of water levels for future years. The simulation indicates a gradual downward trend in future years.

7.6 Discussion on Previous Studies and Comparison with Research Outcomes

Several studies have also been carried out to predict the future growth of the Devils Lake. Out of them the most recent and updated study has been published by USGS in 2011 (Vecchia, 2011). The results of that research have been discussed in the Chapter of "Previous Studies". In that study, a previously developed (Vecchia, 2008) stochastic simulation model is used with minor modifications. The model is not a real-time hydro-dynamic model and simulates the lake condition in a monthly time step. The region is divided into several inter-connected lake boxes that uses the randomly generated future monthly sequences of precipitation, evaporation and inflow data. Numerous traces are generated using the model and several of them are reported. The traces show general upward trend at the beginning of simulation and gradually follows a downward trend after 2015. Some of the traces reported in this thesis also shows an upward trend in the first year and inclines downwards after that.

A USGS report (Vecchia, 2002) published in 2002 investigated the change in precipitation trend from 1950 to 1999. It is found that the average half yearly precipitation from January to June decreases slightly from 8.44 inches (1950-79) to 8.04 inches (1980-99), whereas from July to December it significantly increased from 9.25 inches (1950-79) to 11.11 inches (1980-99), as shown in Figure 52. This increasing trend in precipitation explains the continued increase in lake-levels during the 90's. Similar investigation is carried out to find any change in trend in the simulated precipitation values in the model. It is found that there is almost no change in trend in mean precipitation estimates from January to June (Figure 53, Figure 54 and Figure 55) for each of the three scenarios (A1B, A2 and B1). From July to December the mean values

show a downward trend (Figure 56, Figure 57 and Figure 58) from values observed in 1980-1999 (Figure 52). Mean yearly evaporation from 1950-1979 and 1980-1999 is 29.6 inches and 30.9 inches per year respectively. In the simulated evaporation traces, the yearly mean values are found to be 30.2 inches, 30.5 inches and 30.3 inches per year for A1B, A2 and B1 scenarios respectively. These findings provide a more elaborate explanation of the continued downward trend of the predicted lake levels in future years.

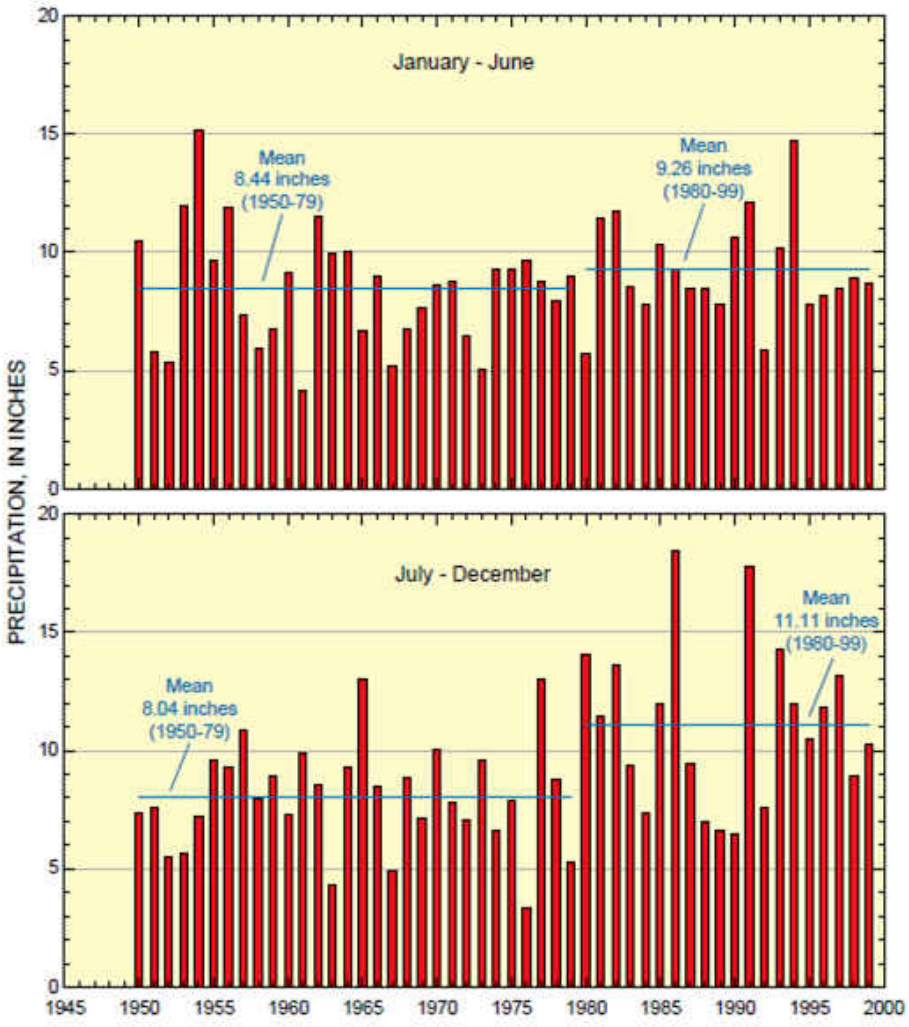

Figure 52: Historic record of precipitation in Devils Lake, 1950-1999 (Source: USGS)

The frequency analysis of the simulated traces is executed using HEC-SSP, which is another excellent tool developed by the Army Corps of Engineers. Candidate probabilistic distributions evaluated by goodness-of-fit include Gaussian/Normal, Log-normal, Gamma/Pearson type 3, and Log-Pearson type 3 distributions.

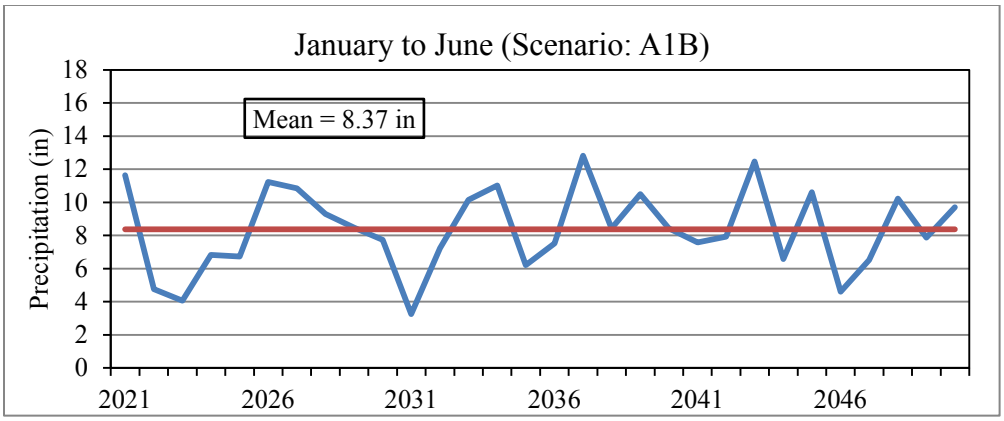

Figure 53: Mean precipitation (in) - January to June (Scenario: A1B)

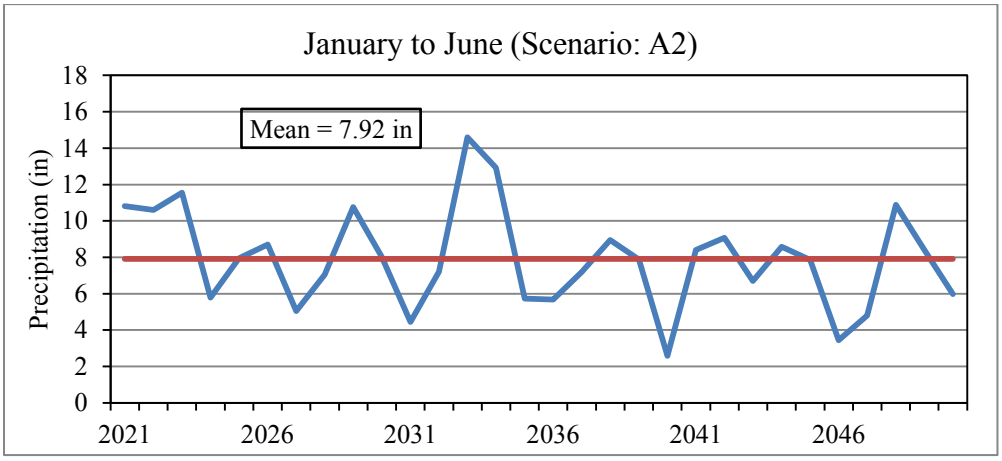

Figure 54: Mean precipitation (in) - January to June (Scenario: A2)

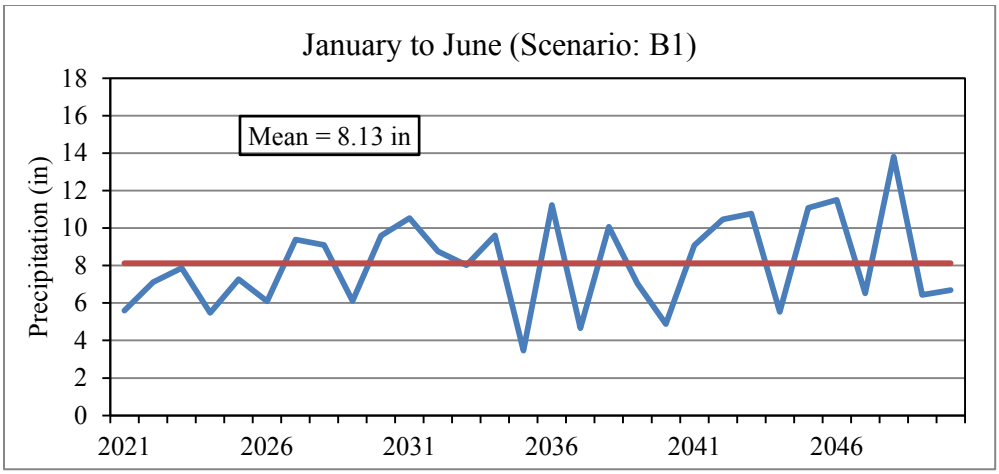

Figure 55: Mean precipitation (in) - January to June (Scenario: B1)

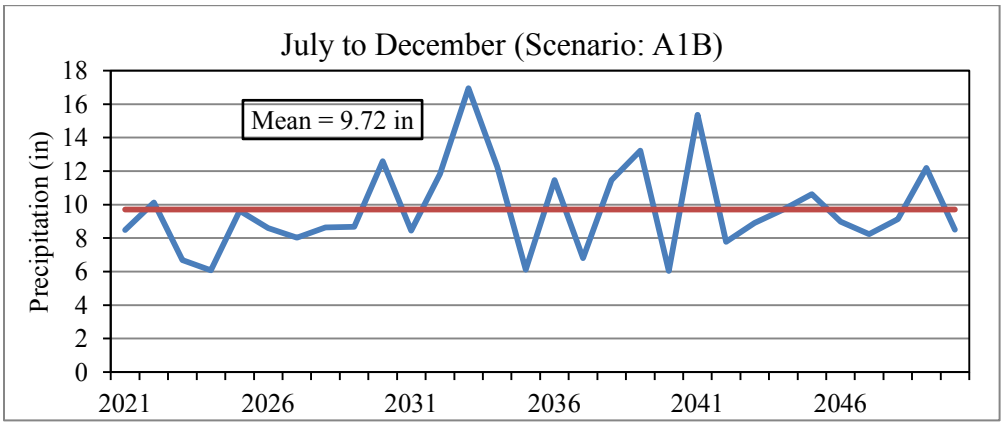

Figure 56: Mean precipitation (in) - July to December (Scenario: A1B)

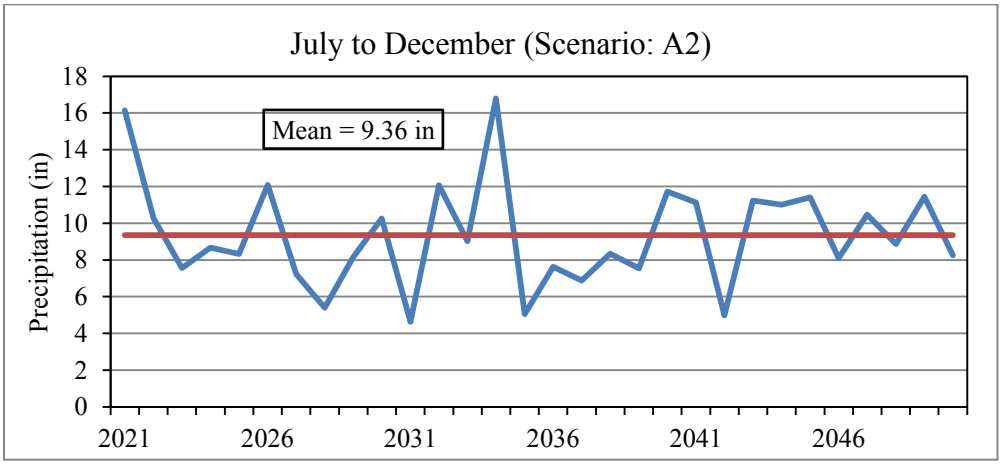

Figure 57: Mean precipitation (in) - July to December (Scenario: A2)

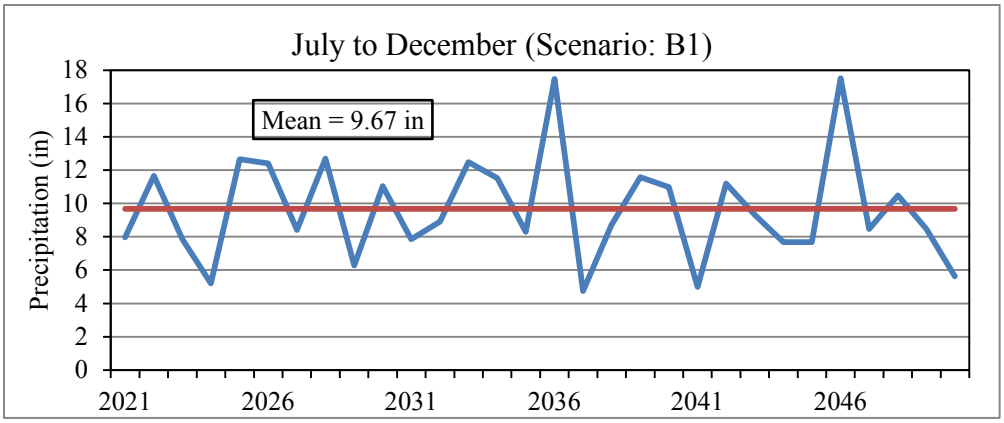

Figure 58: Mean precipitation (in) - July to December (Scenario: B1)

Being a terminal lake, there is substantial serial dependence between lake levels in successive years. As the lake levels are not independent events, they do not have the natural zero value as what river levels or discharges possess. As a result, lake levels typically do not exhibit the extreme variability and skewness, which can be found in flood flows. This lead to the fact that the use of log transforms of lake levels may not be necessary or beneficial. Moreover, the lake level is expected to be more sensitive to the frequency analysis. To overcome that, a volume-based approach has also been completed. The observed relationship between the stage and storage has been used to develop an equation, which is used to convert the yearly peak traces of stage values to representative volume estimates. Then a frequency analysis using all candidate probability distribution functions has been done and compared with stage-based probabilities. The expected lake-level frequencies are computed considering conditional probabilities associated with the starting level, which happens to be the highest in the recorded history.

The research project is successful in using the weather ensembles from downscaled GCMs to simulate the lake levels for multiyear time period. Variation in calibration outputs was observed by using ground gage and NASA TMPA observations.

Distribution of precipitation estimates in terms of magnitude has profound impacts on the proper estimation of surface runoff to the lake. It is found that the TMPA observations are not analogous to nearby ground gage stations in several occasions that affect the calibration to a significant extent. Proper adjustments are made to account for these discrepancies and the parameters from the best calibration fit are selected for the future simulation.

CHAPTER 8

CONCLUSION

The simulation shows a declining trend in the future growth of the Devils Lake. The three different scenarios analyzed for the GCM and Hydro-climatic model simulation provide different ranges of maximum, mean and minimum water levels for the next 30 years. Average maximum water levels for scenario A1B, A2 and B1 are 1455 ft, 1454 ft and 1454 ft respectively. Average mean water levels for these scenarios are 1443 ft, 1438 ft and 1438 ft respectively. And the average minimum water levels are 1434 ft, 1425 ft and 1426 ft correspondingly. Lake evaporation plays a key role in modeling the fluctuation of water level as the Devils Lake does not have any other major outlet. Annual average lake evaporation is approximately 30 inches, which is the main form of water loss from the lake. The Doorenbos and Pruitt model is calibrated to generate the daily time series of future evaporation. It is found that some discrepancies in representing the distribution and magnitude of precipitation events affected the model in few years and are the major obstacles in achieving a better calibration. These discrepancies may also have led to obtain slightly biased calibration parameters, which can affect the output of future simulation. A sensitivity test is performed where it is found that more than 4 ft of mean water level deviation is possible if annual lake evaporation is changed by 3 to 4 inches per year (Figure 46). Finally it is learnt that accurate estimation of evaporation pattern along with proper distribution of temperature and precipitation are extremely important factors in simulating the future water level of the Devils Lake.

The frequency analysis gives a good foresight about extreme flood events in future years. Currently the water level is approximately 1454 ft above mean sea level, which is the highest in the recorded history. After applying the four probability distribution functions in the simulated yearly peak traces of lake levels, it is concluded that the Gaussian/Normal distribution and Gamma/Pearson type 3 distribution have the best fits with the simulated lake-level series. The frequency analysis shows that the current water level is a one in 140 year event. As the lake-level/volume increase is a dependent function, conditional probability is determined to obtain the probabilities of three selected scenarios of 1456 ft, 1458 ft and 1460 ft. It is found that the unconditional mean probabilities of these water levels are 1.12, 0.44 and 0.189 percent respectively, whereas the conditional mean probabilities are 0.008, 0.003 and .001 respectively. For comparison the stages are converted to volume estimates using stage-storage functions and frequency analysis is done for both conditional and unconditional cases. In this case the Gaussian/Normal and LP3 distributions do not provide a better fit. Instead the Gamma/Pearson type 3 and Lognormal distributions give a better match and the mean probabilities for 1456 ft, 1458 ft and 1460 ft are 0.004, 0.002 and 0.0009 percent for conditional case and 1.5, 0.68 and 0.31 percent for unconditional case respectively.

Based on the weather samples from the downscaled GCMs, the simulated traces and corresponding frequency analysis predict a gradually downward trend indicating a reduced expectation of flooding of the lake within the next 30 years. However, considering the variable nature of the climate, more traces can certainly be supportive to randomize the hydrologic responses to various projected conditions of future climate.

APPENDICES

Appendix A

Area Calculation from Geo-pdf Maps

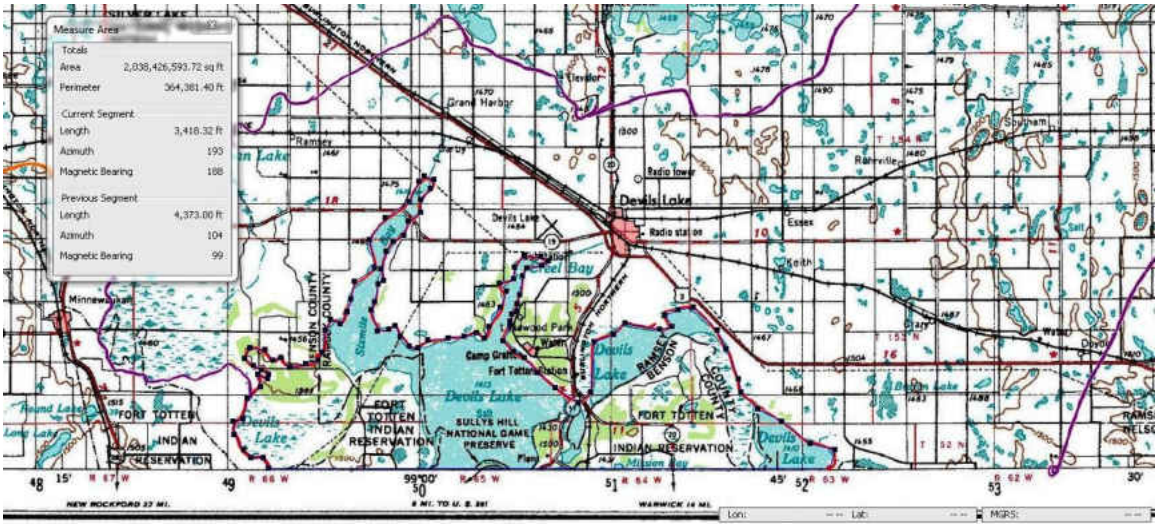

Figure 59: Area calculation of Devils Lake (North) using geo-pdf maps

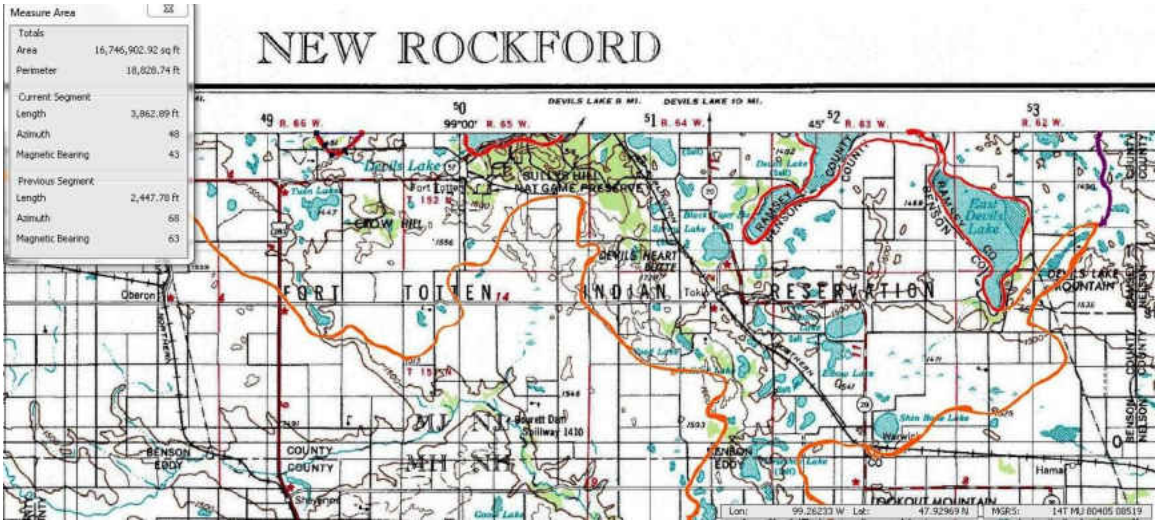

Figure 60: Area calculation of Devils Lake (South 1) using geo-pdf maps

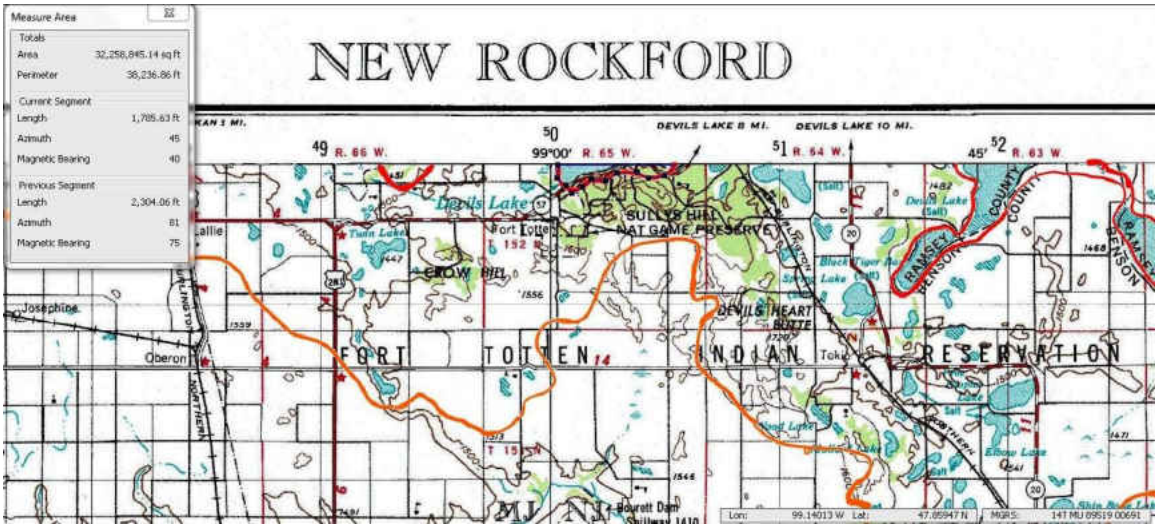

Figure 61: Area calculation of Devils Lake (South 2) using geo-pdf maps

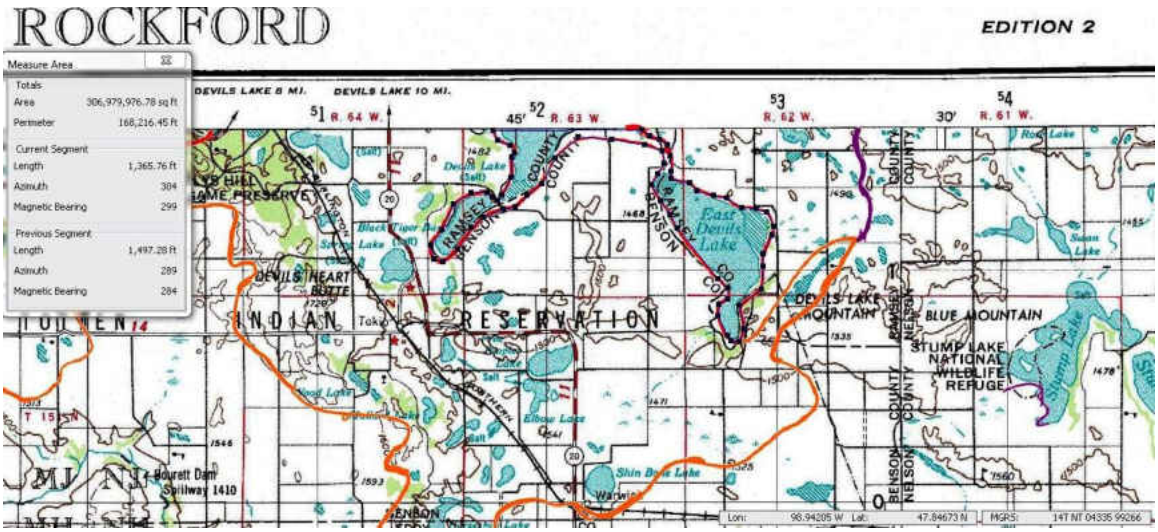

Figure 62: Area calculation of Devils Lake (South 3) using geo-pdf maps

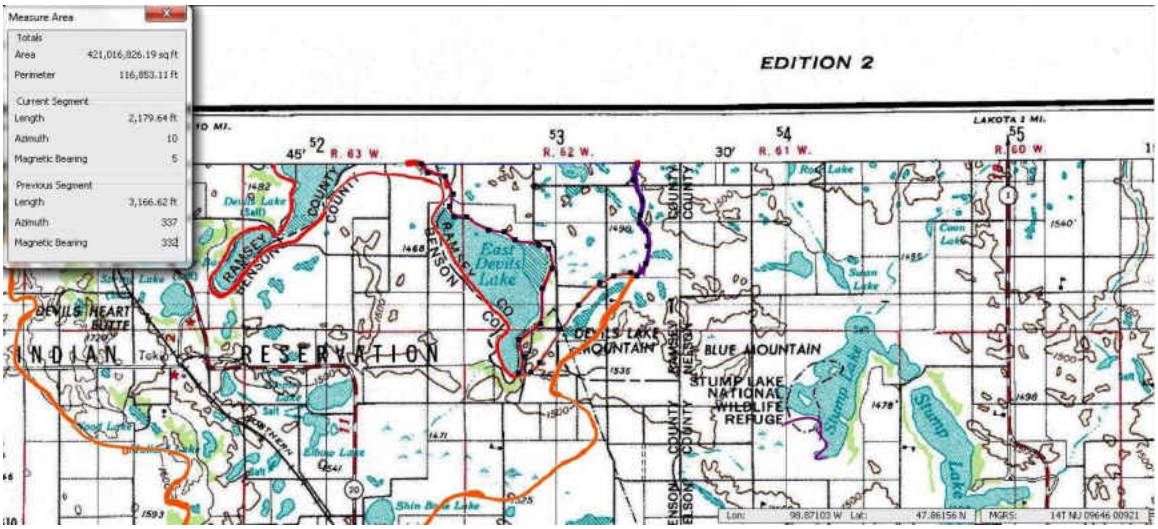

Figure 63: Area calculation of Devils Lake North Slope (Down) using geo-pdf maps

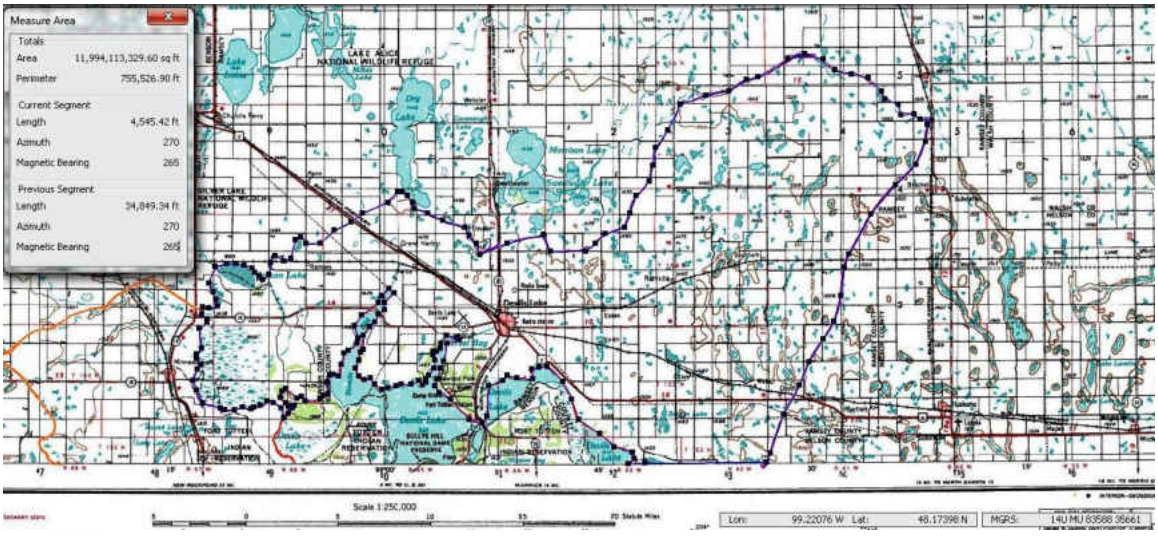

Figure 64: Area calculation of Devils Lake North Slope (Up) using geo-pdf maps

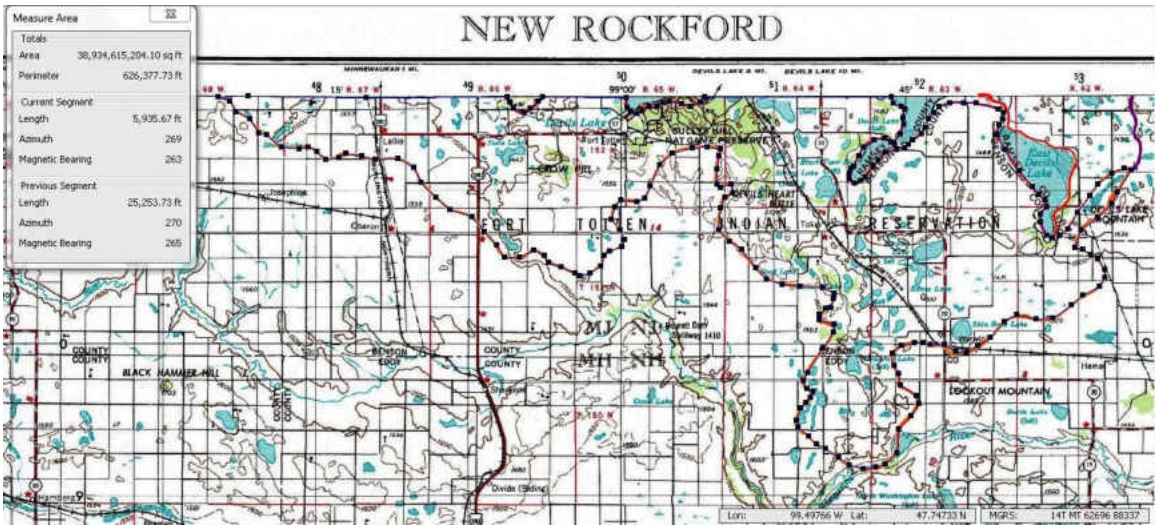

Figure 65: Area calculation of Devils Lake South Slope (Down) using geo-pdf maps

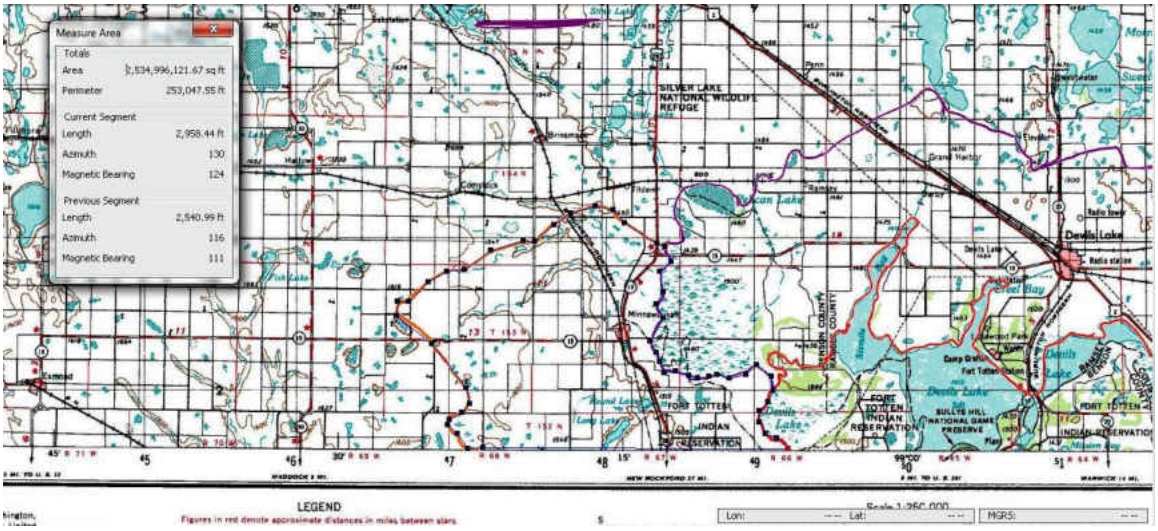

Figure 66: Area calculation of Devils Lake South Slope (Up) using geo-pdf maps

Appendix B

Unique IDs of Sub-Areas in the Basin Model of HEC-HMS

B.1 Naming of the Sub-Areas of the Basin Model in HEC-HMS

M:	Mauvais	i.e:	10_M-8: means 10^{th} sub-area and 8^{th} in Mauvais coulee.
C:	Calio	i.e:	25_C-5: means 25^{th} sub-area and 5^{th} in Calio coulee.
W:	Starkweather	i.e:	35_W-6: means 35^{th} sub-area and 6^{th} in S.Weather coulee.
E:	Edmore	i.e:	50_E-5: means 50^{th} sub-area and 5^{th} in Edmore coulee.
L:	Little Coulee	i.e:	70_L-10: means 70^{th} sub-area and 10^{th} in Edmore coulee.
S:	Stump Lake	i.e:	85_S-12: means 85^{th} sub-area and 12^{th} in Stump Lake.

B.2 Numbers to Identify Sub-Areas, Reaches and Junctions

Sub-Areas

1-20: Mauvais

21-29: Calio

30-45: Starkweather

46-60: Edmore

61-73: Little Coulee

74-95: Stump Lake

Reaches

1-14: Mauvais

15-19: Calio

20-29: Starkweather

30-36: Edmore

37-44: Little Coulee

45-56: Stump Lake

Junctions

1-15: Mauvais

16-20: Calio

21-30: Starkweather

31-37: Edmore

38-45: Little Coulee

46-57: Stump Lake

Appendix C

Calibration Steps

In this section the total calibration process is explained in a step by step manner. The steps can be summarized as follows:

1) Loss Calibration for summer storm events in Mauvais Coulee using HMS-Model A.
2) Applying the calibration parameters obtained from HMS-Model A in HMS-Model B.
3) Snow-melt calibration of Mauvais Coulee.
4) Sensitivity analysis of loss parameters, e.g., initial loss and continuous loss.
5) Multiple year (2001-2010) calibration of the Mauvais Coulee using both HMS Model A and B.
6) Combined approach to calibrate the watershed (HMS) and reservoir (ResSim) model simultaneously, e.g., HMS-Model A + ResSim and HMS-Model B + ResSim.

With two different sources of climate data, it is obvious that the same calibration parameters do not perform similarly in HMS-Model A and B. The result is rational as the HMS-Model A approximates the same precipitation and temperature throughout the basin where the climate data from TMPA by NASA's Satellite provide spatial distribution of precipitation and temperature all over the basin.

Step 1 gives a good idea about the loss factors but as the parameters are used in Step 2, substantial deviations are observed. Difference in the distribution of precipitation seems to be affecting the determination of loss parameters to a significant extent. The result necessitates the calibration of loss parameters in HMS-Model A and B to be done separately. Through step 3 the rate of snow melt is calibrated and the parameters perform similar for both HMS-Model A and B. Step 4 provides a very good understanding of the effect of initial loss and continuous loss in the models. The calibrated loss and snowmelt parameters are used to generate the daily inflow volumes to the lake for years 2003-2010 to allow simulating the lake in ResSim and calibrating the evaporation using observed lake levels. But after calibrating evaporation within the allowable range (Multiplier Coefficient: 0.6 – 0.8), both models show unacceptable deviations. So a multiple year calibration approach is undertaken in step 5 to reduce the mismatch. But still the results are not satisfactory enough to move forward to simulate the future growth of the lake. The reason could be the approximation of the whole basin being similar to Mauvais sub-basin. To overcome this obstacle a combined approach is undertaken in step 6 where both the HMS and ResSim models are calibrated simultaneously. At first the HMS-Model A and the ResSim model are coupled together and calibrated for loss (in HMS), seepage (in ResSim) and evaporation (in ResSim) parameters. Then similar approach is followed for the HMS-Model B and the ResSim model and acceptable outcomes are observed. Details on these steps are explained in the following sub-sections.

C.1 Step 1: Loss Calibration of Mauvais Coulee using HMS-Model A

For observed storm events data from various sources are analyzed. These sources include gage stations of State Water Commission (SWC) and National Climatic Data

Center (NCDC). Precipitation gage stations (Figure 14), which are primarily selected for summer storm calibration, are listed in Table 34.

After analyzing all the stations, Minnewaukan is selected for observed precipitation as it has data for longer time. Snow-melt calibration parameters do not affect the model during the summer storm events. The runoff generation is more dependent on initial and constant loss parameters. To set the initial snow-melt parameters, widely used values are selected as described in section 4.2.

Table 34: Description of gage locations for storm-based loss calibration

County/ Station Name	Source	COOP/ Site ID	Latitude	Longitude	Status
Benson	SWC	4223	48.27	-99.64	Active (Apr-Sep)
Benson	SWC	47	48.30	-99.30	Active (Apr-Sep)
Benson	SWC	50	48.33	-99.30	Active (Apr-Sep)
Towner	SWC	848	48.39	-99.07	Active (Apr-Sep)
Leeds	NCDC	325078	48.17	-99.26	Active (Sep 1935-May 07)
Maddock	NCDC	325434	47.58	-99.31	Active (Jan 1915-Nov 2004)
Minnewaukan	NCDC	325848	48.04	99.15	Active (Apr 1897-Dec 10)

Typically, the PX temperature is one to two degrees above freezing and the base temperature is 0^0C (32^0F) or close to it. These values are set to 34^0 F and 32^0 F respectively. The rain rate Limit is set to 1 inch/day and 0.06 in/^{0}F-day is selected as wet melt-rate. Rainfall events starting from 6th June, 2001 to 15th July, 2001 is considered and observed precipitation records and stream flow data are obtained from NCDC and USGS respectively. Then a series of model run is performed to get an idea of the

appropriate initial and constant loss parameters for the Devils Lake area. The precipitation distributions at Minnewaukan and runoff observation at Cando are plotted in Figure 67.

Here the total observed outflow is 0.22 inch and the for the first calibration trial, the initial and constant losses are taken as 0.07 inch and 0.039 inch per hour respectively. In Table 35 the results of trial runs are illustrated. Relatively better results are found with Initial Loss of 0.075 in and Constant Loss of 0.09 in/hr. Plots of the trials can be found in Appendix D.1.

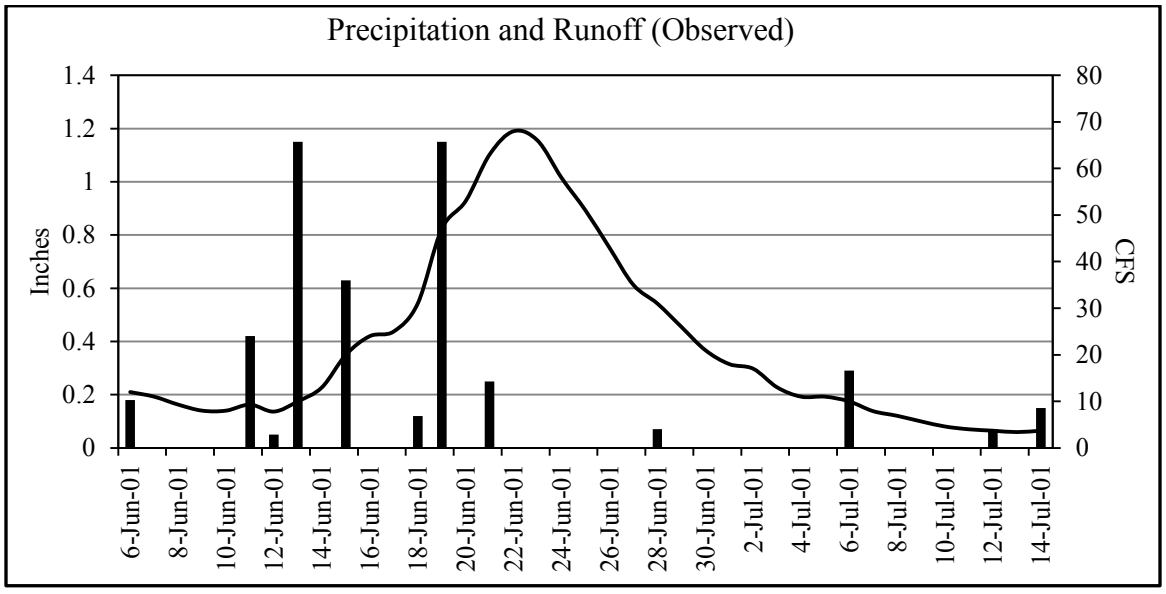

Figure 67: Precipitation at Minnewaukan and Runoff at Cando (Observed)

In these trials it is possible to get a very good idea about how the model responds with varying loss parameters but still some more tuning is required as the peak outflows are not represented accurately. One of the probable reasons can be the use of precipitation data from Minnewaukan. For better calibration a precipitation observation station closer to the stream flow gage station is required. So a new gage in Towner County (Figure 14) is selected, which is very close to our stream gage station as seen in

Table 36 and is expected to explain the runoff pattern more accurately. Calibration trials are repeated and a better fit is observed (Appendix D.2) in terms of total outflow and peak outflow. In these trials, the total observed outflow is same as before, which is 0.22 inches. Results are summarized in Table 37 and Figure 68, both in tabular and graphical format.

Table 35: Trial results of loss calibration of Mauvais coulee

Trial No.	1	2	3	4	5	6	7	8	9
Initial Loss (inch)	0.07	0.1	0.15	0.15	0.15	0.15	0.15	0.15	0.075
Const. Loss (in/hr)	0.039	0.039	0.039	0.045	0.06	0.1	0.075	0.09	0.09
Total Outflow (in)	0.64	0.62	0.58	0.54	0.44	0.17	0.34	0.24	0.26

Note: Duration: Jun 6 to Jul 15, 2001; Precipitation gage: Towner; Stream flow gage: Cando; Outflow observed: 0.22 inch

Table 36: Description of gage location at Cando (stream flow) and Towner (precipitation)

Gage Station	Stream flow	Precipitation
Location	Mauvais Coulee near Cando, ND	Towner County
Station Number	USGS St. 05056100	SWC St. 848
Latitude	48:26:53 N	48:23:32.28 N
Longitude	99:06:08 W	99:04:7.72 W

Table 37: Trial results of loss calibration of Mauvais coulee

Trial No.	**1**	**2**	**3**	**4**	**5**	**6**	**7**
Initial Loss (inch)	0.07	0.15	0.2	0.175	0.2	0.25	0.28
Constant Loss (in/hr)	0.045	0.075	0.075	0.09	0.095	0.095	0.105
Total Outflow (Inch)	0.79	0.52	0.5	0.41	0.37	0.35	0.28
Trial No.	**8**	**9**	**10**	**11**	**12**	**13**	**14**
Initial Loss (inch)	0.29	0.29	0.275	0.25	0.24	0.24	0.24
Constant Loss (in/hr)	0.125	0.12	0.12	0.12	0.105	0.113	0.114
Total Outflow (Inch)	0.15	0.18	0.18	0.19	0.29	0.24	0.23
Trial No.	**15**	**16**	**17**	**18**	**19**	**20**	**21**
Initial Loss (inch)	0.245	0.248	0.252	0.255	0.252	0.255	0.235
Constant Loss (in/hr)	0.1139	0.1138	0.1139	0.1139	0.1142	0.1138	0.115
Total Outflow (Inch)	0.23	0.23	0.23	0.23	0.23	0.23	0.22

Note: Duration: Jun 6 to Jul 15, 2001; Precipitation gage: Towner; Stream flow gage: Cando; Outflow observed: 0.22 inch

In Figure 68, it can be observed that using trial 21 parameters, the total outflow matches perfectly and the peak simulated outflow is 67.1 cfs, which differs 1.32 percent from the observed peak outflow.

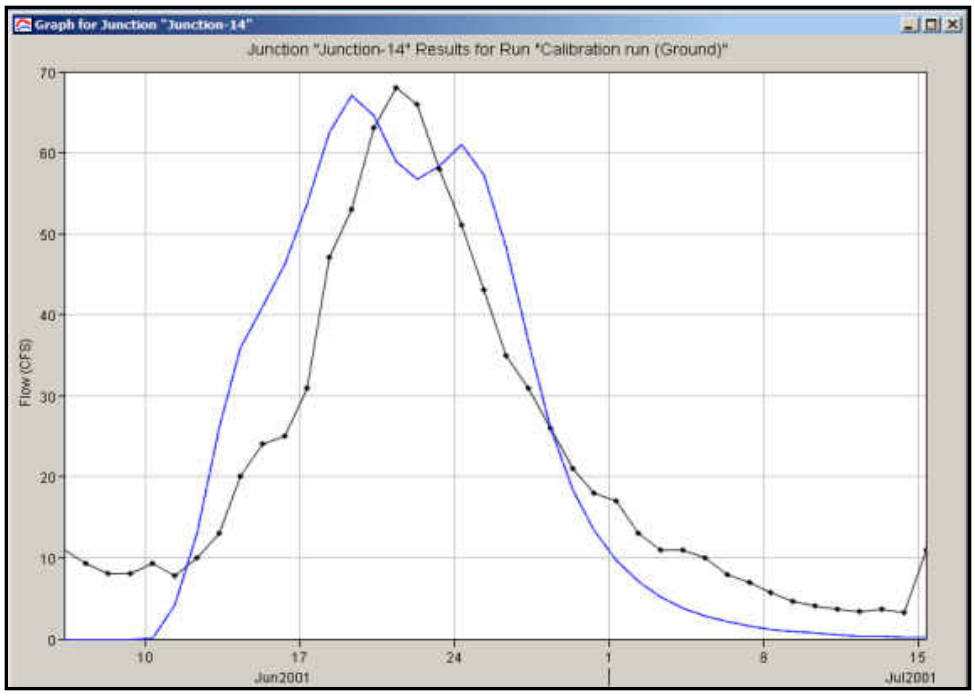

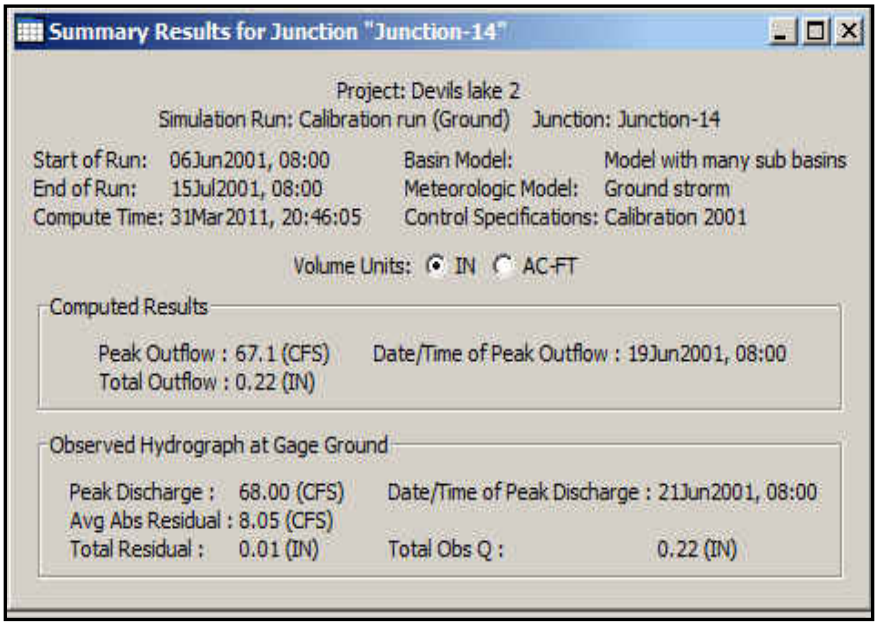

Figure 68: Runoff plot and summary results of Trial 21 in calibrating the loss parameters of the Mauvais coulee

Note: Duration: Jun 6 to Jul 15, 2001; Precipitation gage: Towner; Stream flow gage: Cando; Outflow observed: 0.22 inch

C.2 Step 2: Application of the Calibrated Parameters in HMS-Model B

The parameters obtained from HMS-Model A are very satisfactory but it is also required to check the performance of HMS-Model B with these parameters. The runoff graph and summary results of the simulation using HMS-Model B with previously calibrated loss parameters are shown in Figure 69. The results are found to be unacceptable and the simulated outflow shows significant variation from observed values. It is found that the rainfall events distributed in smaller magnitudes among the sub-basins are getting lost due to the loss parameters. Moreover the cumulative rainfall (TRMM) amount is also significantly lower (6.27 inch in Towner vs. 4.06 inch in TRMM data) than actual observations in Towner station. In Figure 70, the daily distribution of precipitation is shown.

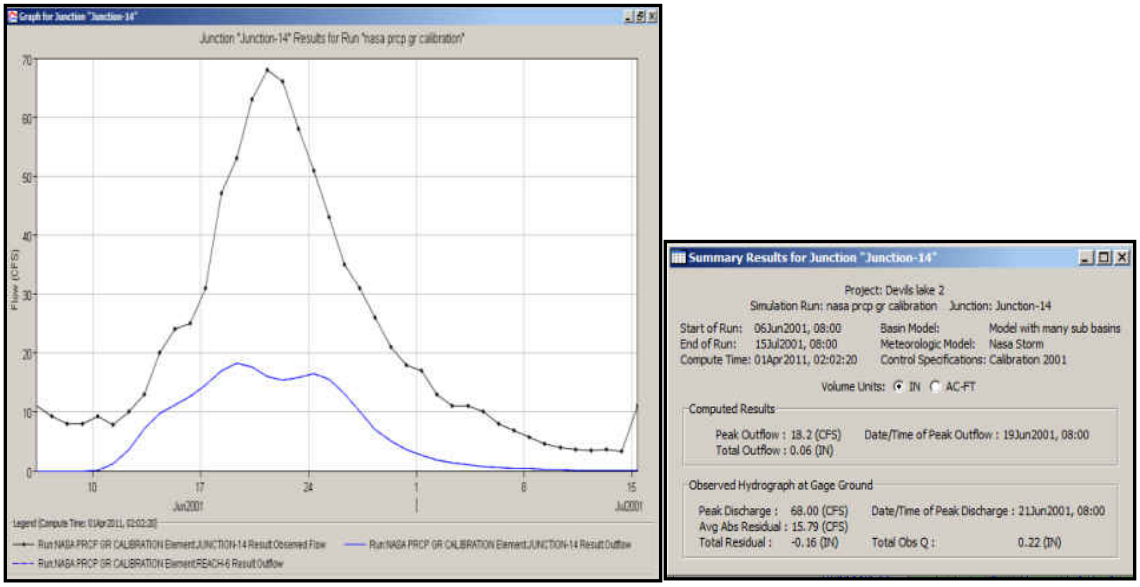

Figure 69: Runoff plot and summary results of HMS-Model B using calibration parameters obtained from HMS-Model A

Note: Duration: Jun 6 to Jul 15, 2001; Precipitation gage: Towner; Stream flow gage: Cando; Outflow observed: 0.22 inch.

It is evident from Figure 70 that several high precipitation events are not recorded in the observations from TMPA by NASA's satellite and total precipitation is 4.06 inches where ground gage at Towner records 6.27 inches of precipitation during the calibration period (6th June, 2001 to 15th July, 2001). Consecutive days of higher precipitation events will surely create greater runoff rather than same amount of total precipitation distributed in smaller magnitudes. Here total precipitation recorded by NASA Satellite is much lower (35%) than observed in Towner gage station. Moreover the high precipitation events are distributed rather than concentrated in the first part of the calibration time period as observed in Towner gage data. The results necessitate the calibration of loss parameters in HMS-Model A and B to be done separately, which is achieved in step 5.

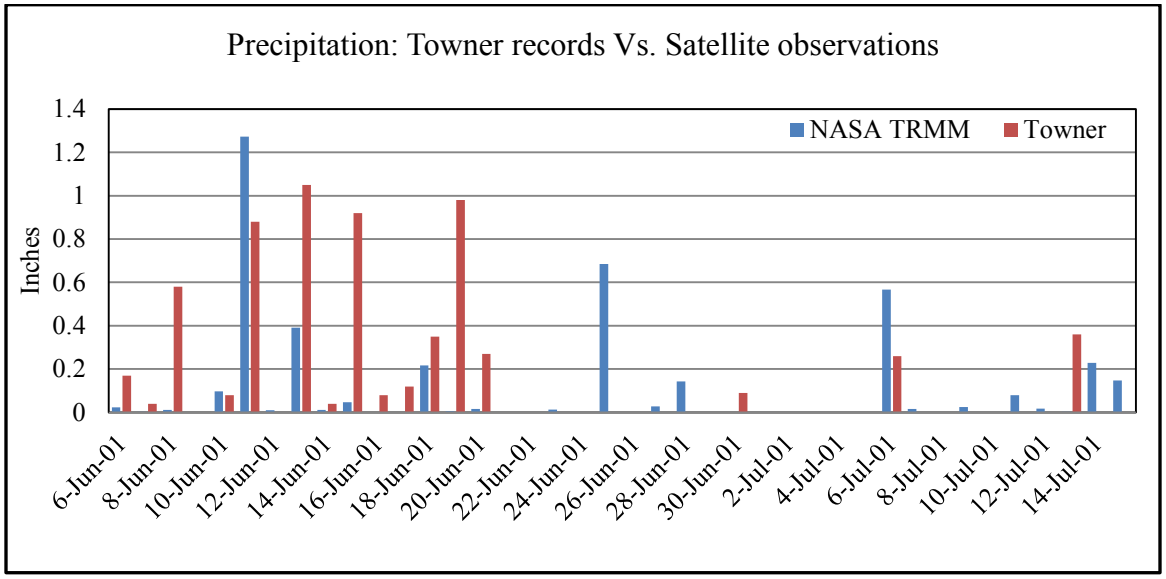

Figure 70: Comparison between precipitation observations in Towner station and NASA satellite (Jun 6, 2001 to Jul 15, 2001)

C.3 Step 3: Snow-Melt Calibration

The snow-melt calibration is performed using the HMS-Model B with the selected time periods from 15th March , 2001 to 10th June 2001 (first 4 trials) and 1st February, 2001 to 10th June 2001 (rest of the trials). Here the observed outflow is 5.45 inches. Several test simulations are run to calibrate the model and to find the appropriate snow-melt parameters. The approach fails to generate required amount of runoff as the simulated outflow is too low than the observed outflow (5.45 in). The loss parameters are too high for the type of distribution of precipitation recorded by the NASA Satellites. Results of the trial runs are summarized in Table 38. Plots of the Calibration runs can be found in Appendix E.

After completing these significant number of runs it is concluded that the Initial Loss (0.235 in) and Constant Loss (0.115 in/hr) are too high for the model. And it is also found that there is less reliability in the temperature data obtained from NASA satellite during that time period. So it is required to go one step back and recalibrate the HMS-Model B to find appropriate initial and constant loss and then calibrate the snow-melt parameters. The trial results with the new simulation period from 17th May, 2004 to 19th June 2004 are listed in Table 39, where the observed outflow is 2.09 inches.

Table 38: Initial trial results of the snow-melt calibration

Trial No.	PX Temp F	Base Temp F	Wet Melt-rate, In/Deg F-Day	Rain Rate Limit In/Day	ATI Melt-rate Coefficient	ATI Melt-rate Function Cm	Cold Limit, In/Day	ATI Cold-rate Coefficient	Water Capacity (%)	Outflow CFS
1	33	32	0.004	0.01	0.98	0.04	0.0039	0.9	5	0.07
2	33	32	0.08	0.01	0.98	0.04	0.0039	0.9	5	0.07
3	33	32	0.08	0.01	0.98	0.08	0.0039	0.9	5	0.07
4	33	32	0.08	0.01	0.98	0.08	0.8	0.9	5	0
5	32	33	0.08	0.01	0.98	0.08	0.8	0.9	5	0.16
6	28	35	0.08	0.01	0.98	0.08	0.8	0.9	5	0.22
7	25	38	0.08	0.01	0.98	0.08	0.8	0.9	5	0.12
8	31	33	0.08	0.01	0.98	0.08	0.8	0.9	5	0.16
9	30	33	0.08	0.01	0.98	0.08	0.8	0.9	5	0.16
10	31	34	0.08	0.01	0.98	0.08	0.8	0.9	5	0.55
11	32	34	0.08	0.01	0.98	0.08	0.8	0.9	5	0.55
12	34	32	0.08	0.01	0.98	0.08	0.8	0.9	5	0.55
13	35	32	0.08	0.01	0.98	0.08	0.8	0.9	5	0.22
14	34	32	0.04	0.01	0.98	0.08	0.8	0.9	5	0.55
15	34	32	0.08	0.01	0.5	0.08	0.8	0.9	5	0.29
16	34	32	0.08	0.01	1.2	0.08	0.8	0.9	5	0.28
17	34	32	0.08	0.01	0.98	0.04	0.8	0.9	5	0.13
18	34	32	0.08	0.01	0.98	0.5	0.8	0.9	5	0.5
19	34	32	0.08	0.01	0.98	0.15	0.8	0.9	5	0.55

Note: Duration: Feb 1 to Jun 10, 2001; Precipitation gage: NASA TMPA; Stream flow gage: Cando; Outflow observed: 5.45 inch

Table 39: Trial results of loss calibration of Mauvais Coulee

Trial No.	1	2	3	4	5	6	7	8
Initial Loss, in	0.235	0.1	0.07	0.03	0.04	0.04	0.04	0.03
Constant Loss, in/hr	0.115	0.05	0.04	0.01	0.01	0.02	0.015	0.015
Runoff, in	0.17	0.71	1.01	2.47	2.47	1.7	2.04	2.04

Note: Duration: May 17 to Jun 19, 2004; Precipitation gage: Towner; Stream flow gage: Cando; Outflow observed: 2.09 inch

The constant loss is found to be 0.015 in/hr, which is on the extreme higher side and using these parameters, the ResSim simulation does not succeed in simulating appropriate water levels as observed. These findings lead us to conclude that event based

calibration is only good to have a rough idea on the parameters and recalibration is required for multiple year simulation. To perform the calibration for multiple years it is necessary to analyze the sensitivity of the loss parameters on the models, which is carried out in step 4.

C.4 Step 4: Sensitivity of Loss Parameters

While testing the sensitivity of Initial loss on the model it is found that the peak outflow does not change at all with varying initial losses. Total outflow changes with varying Initial loss but the amount is negligible. So it can be concluded that the model is not very sensitive to initial loss. Then the constant loss is checked to verify its effect on the model. It is found that both peak outflow and total outflow are significantly sensitive to Constant Loss and relationship is found linear. Figure 71 and Figure 72 illustrate the effects. These findings lead to set the initial loss at 0.1 inches and calibrate the model by varying constant loss for multiple years.

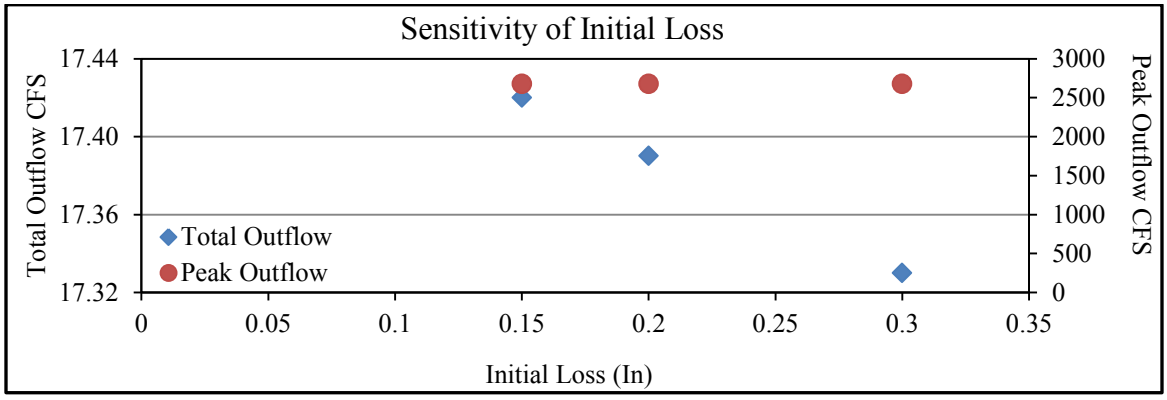

Figure 71: Sensitivity of initial loss on the model.

Note: The constant loss is kept constant at 0.053 in/hr and effect of changing initial loss is plotted.

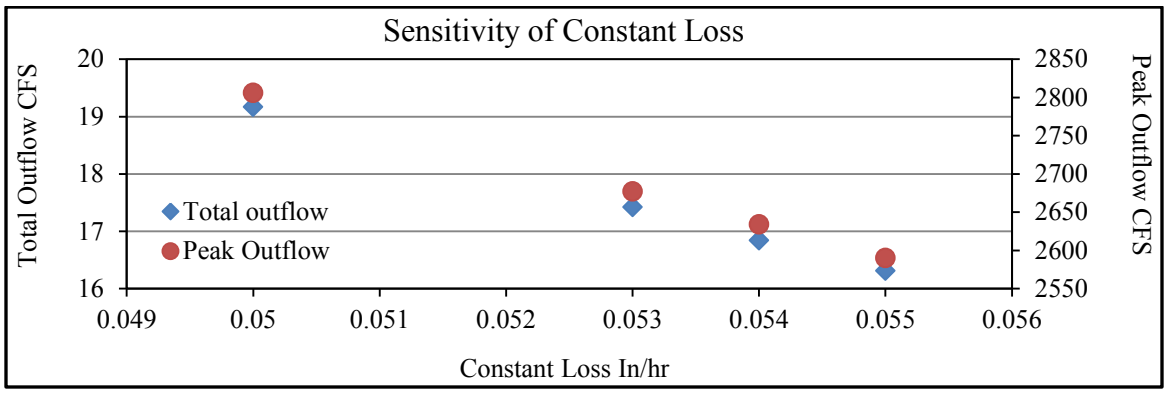

Figure 72: Sensitivity of constant loss on the model.

Note: The initial loss is kept constant at 0.15 in and effect of changing constant loss is plotted.

C.5 Step 5: Calibration of Mauvais Basin for Multiple Years

For multiple years, the ground observation gage for precipitation is changed to Langdon Experimental Farm due to gaps in continuous data in Towner gage station. The simulation period is set from 2003 to 2010 and initial loss is kept constant at 0.1 in. After performing several trial runs the constant loss is found to be 0.0979 in/hr for HMS-Model A as shown in Figure 73. Same approach is followed for HMS-Model B and the constant loss is found to be 0.0955 in/hr as summarized in Figure 74, which is very close to the value obtained for HMS-Model A. In both cases the total outflow from Mauvais basin is modeled accurately, which is 13.89 inches. However, success of the models are limited in simulating the peak outflow from the basin, but that is considered acceptable because generating the water level in HEC-ResSim is primarily dependent on the volume of water.

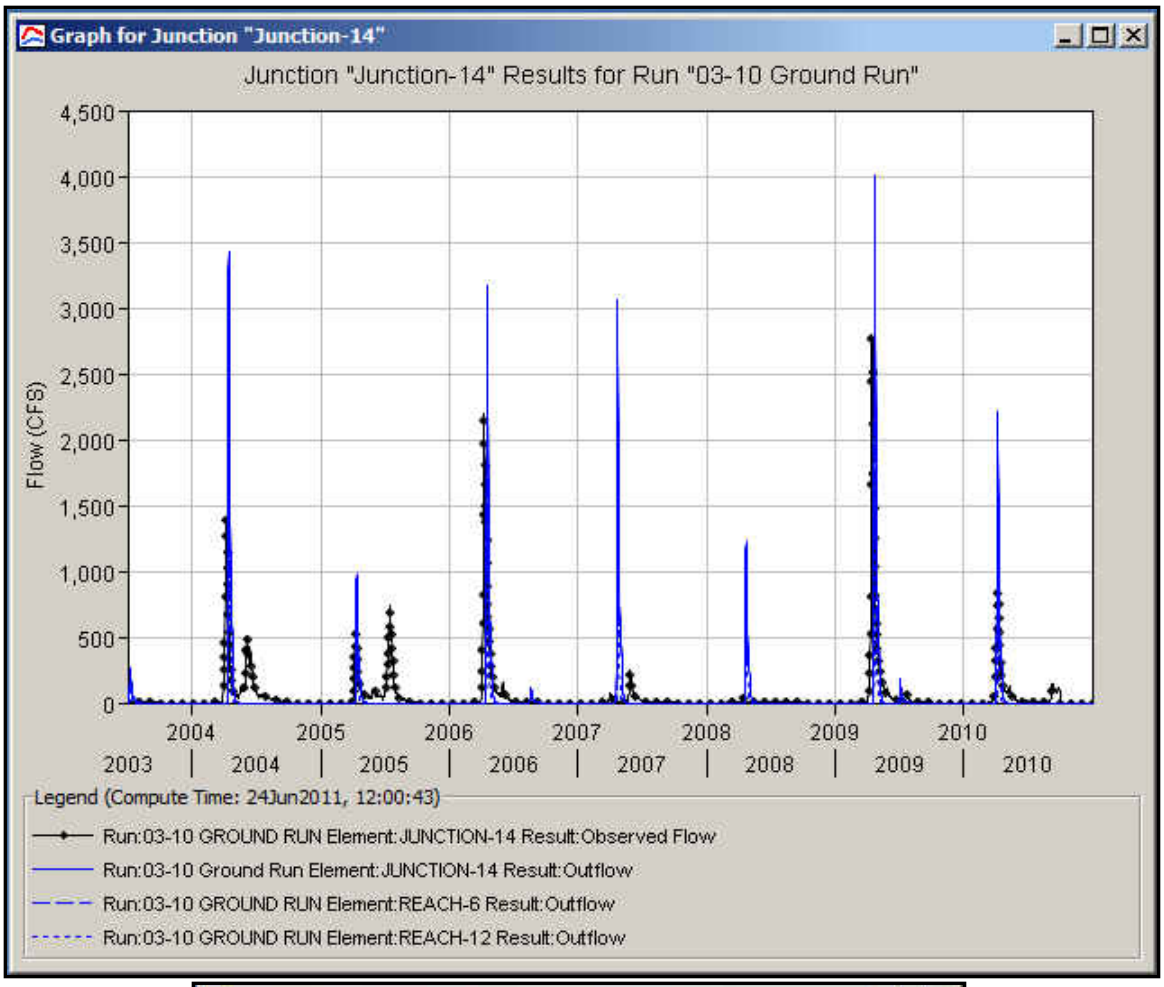

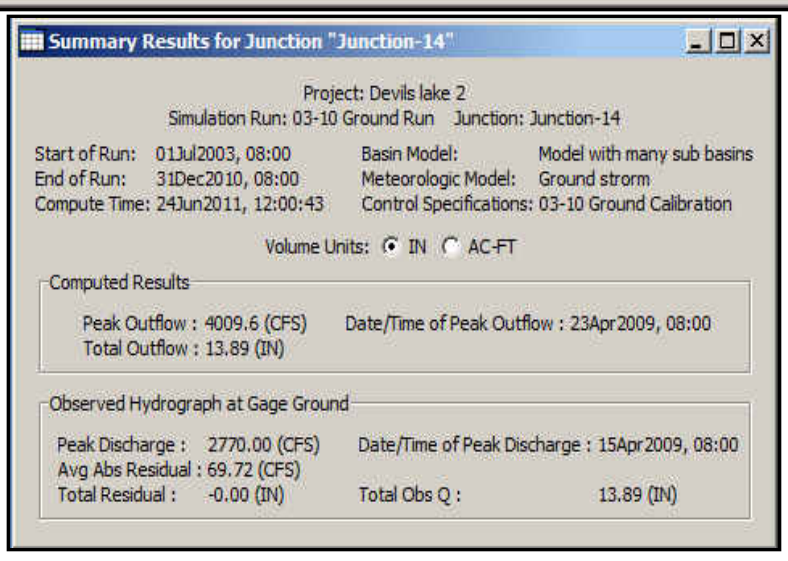

Figure 73: Runoff plot and summary results for multiple year calibration using HMS-Model A

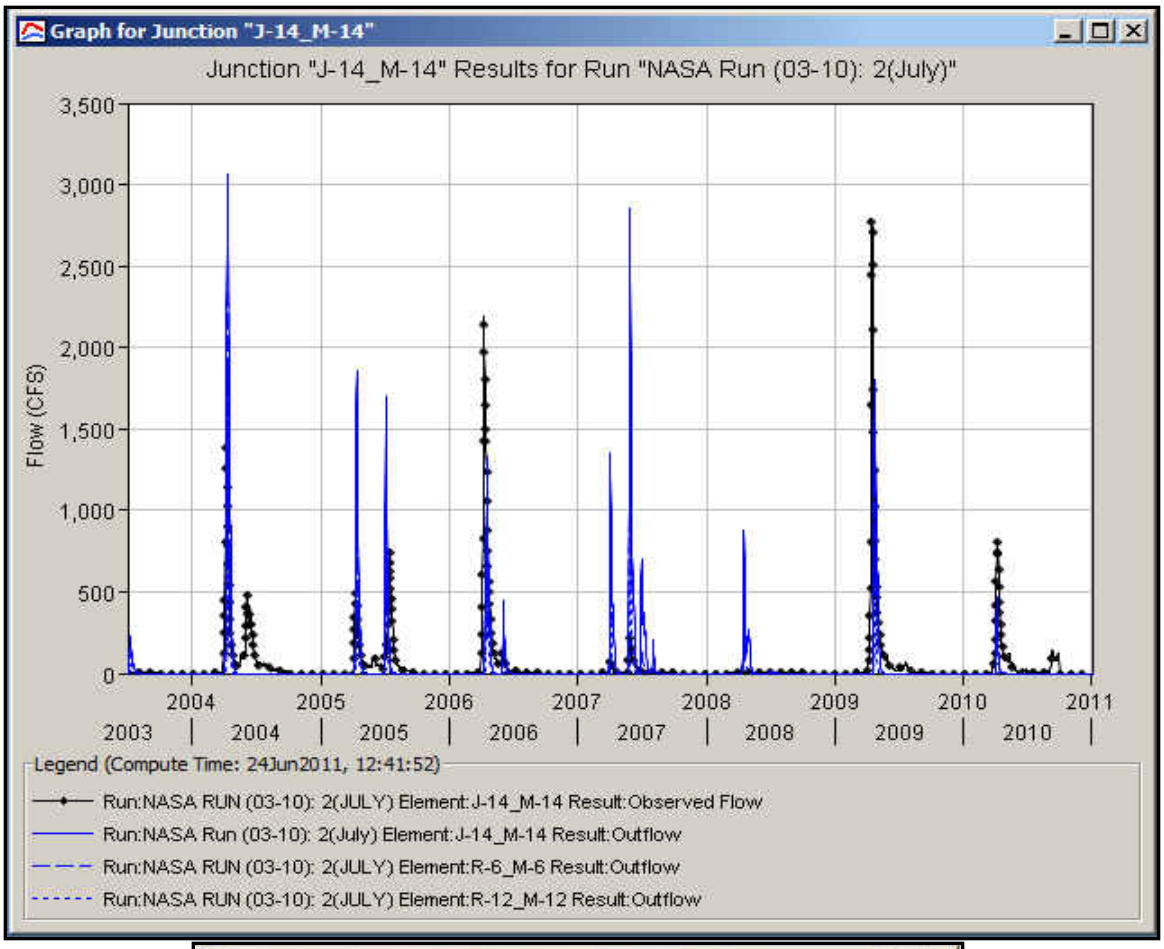

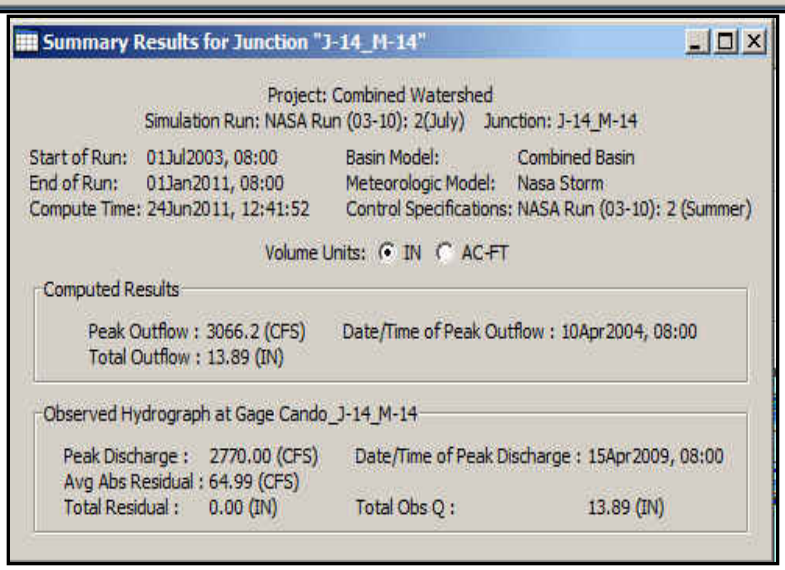

Figure 74: Runoff plot and summary results for multiple year calibration using HMS-Model B

C.6 Step 6: Combined Approach in Calibration

The calibrated model is coupled with HEC-ResSim, and simulations are performed to obtain daily water levels from 2003 to 2010. The ResSim model considers the physical properties of the lake and evaporation out of the lake. Considering the fact that seepage through the lake is very low, evaporation is the major source of outflow from the water body. To obtain a proper fit with observed water level in Devils Lake, calibration of the evaporation is required. Time series values of pan evaporation are obtained from Crary gage station from North Dakota Agricultural Weather Network (NDAWN). Pan coefficients ranging from 0.6 to 0.8 are analyzed to calibrate the ResSim model with observed water levels. At this stage a combined approach is followed where both the HEC-HMS and HEC-ResSim models are calibrated simultaneously. With varying loss parameters, the runoff is generated from both HMS-Model A and B and used in the HEC-ResSim model separately to simulate the water level. This approach has provided very good results and 0.085 in/hr is found to be most appropriate to be used as constant loss for both models. Seepage has been varied from 0 cfs to 50 cfs and its effect on the calibration is found very low on the models. Plots of the calibration trials can be seen in Appendix F.

Appendix D

Calibration Plots of Loss Calibration of Mauvais Coulee

D.1 Calibration using Precipitation Gage at Minnewaukan

Duration: Jun 6 to Jul 15, 2001

Precipitation gage: Minnewaukan

Stream flow gage: Cando

Outflow observed: 0.22 inch

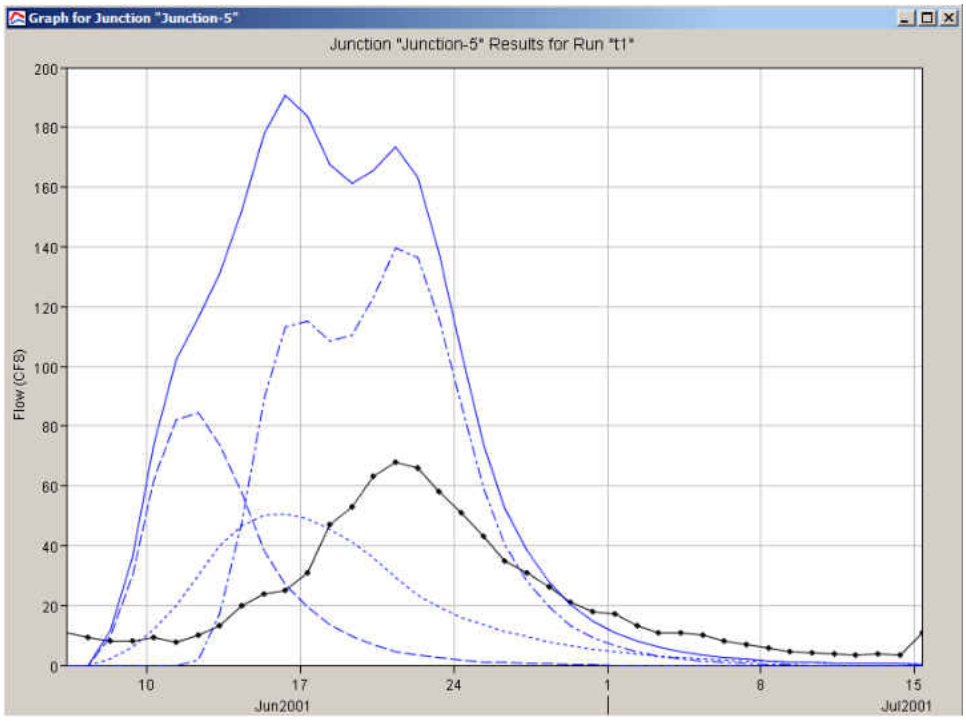

Figure 75: Calibration plot of Trial 1 (Loss calibration: storm-based)

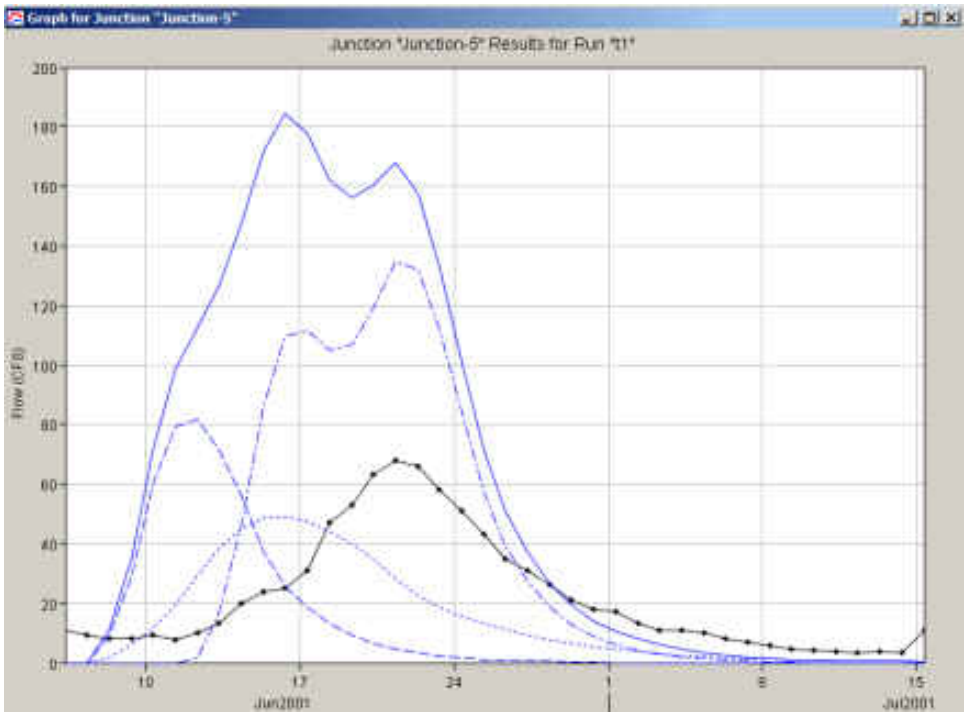

Figure 76: Calibration plot of Trial 2 (Loss calibration: storm-based)

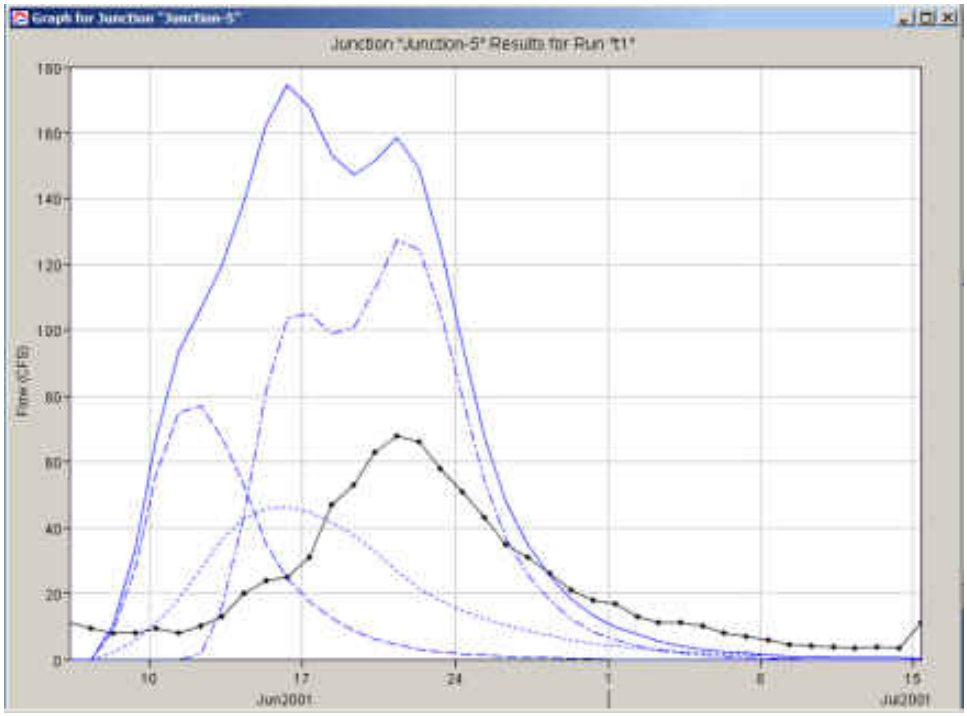

Figure 77: Calibration plot of Trial 3 (Loss calibration: storm-based)

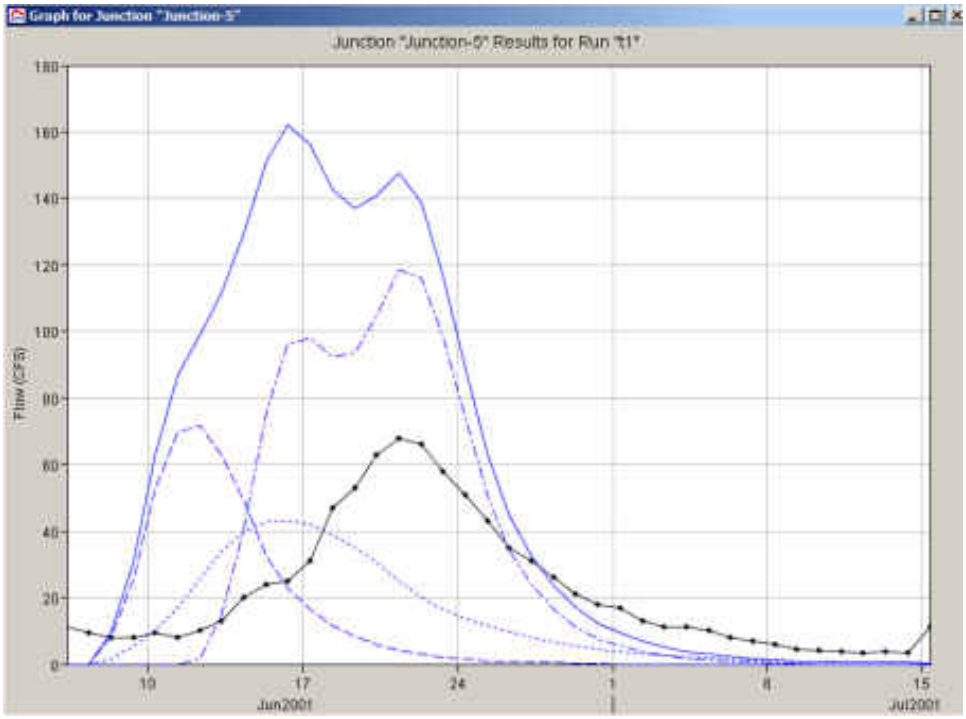

Figure 78: Calibration plot of Trial 4 (Loss calibration: storm-based)

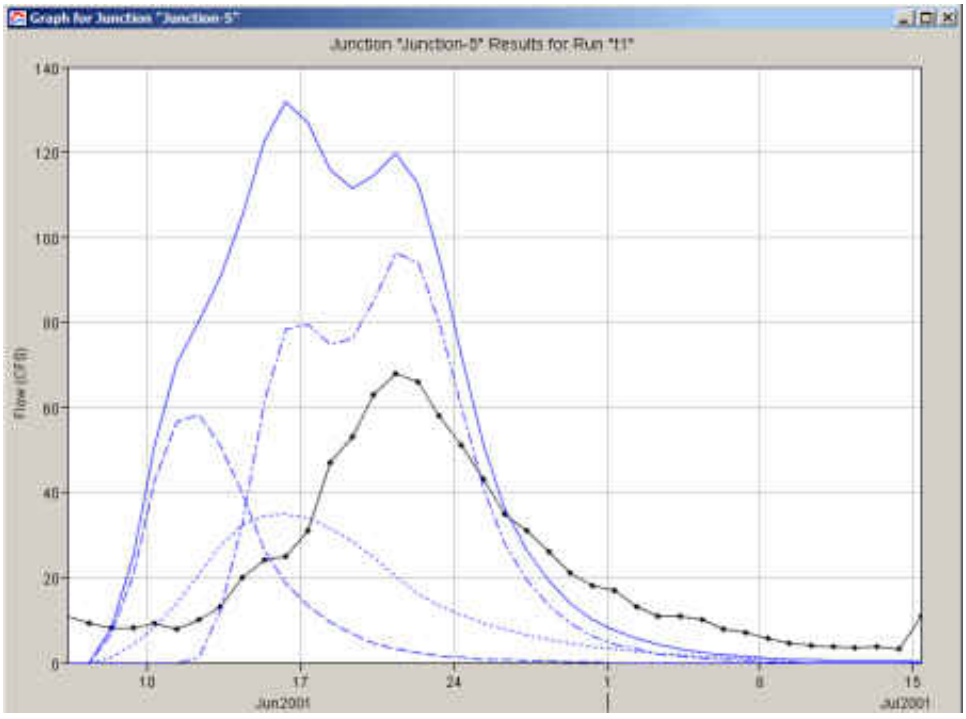

Figure 79: Calibration plot of Trial 5 (Loss calibration: storm-based)

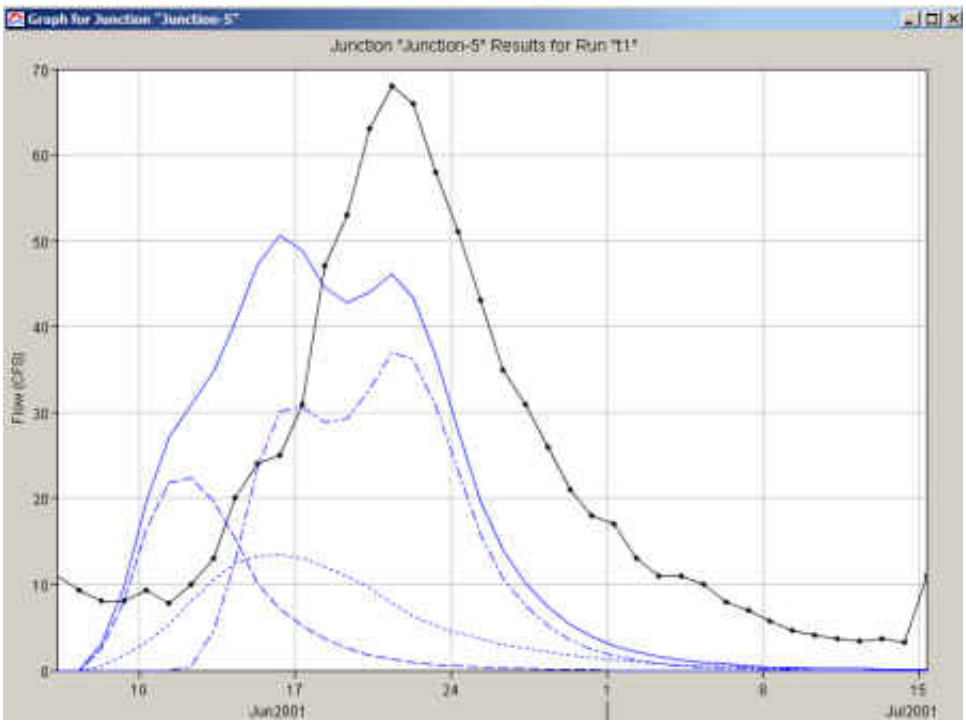

Figure 80: Calibration plot of Trial 6 (Loss calibration: storm-based)

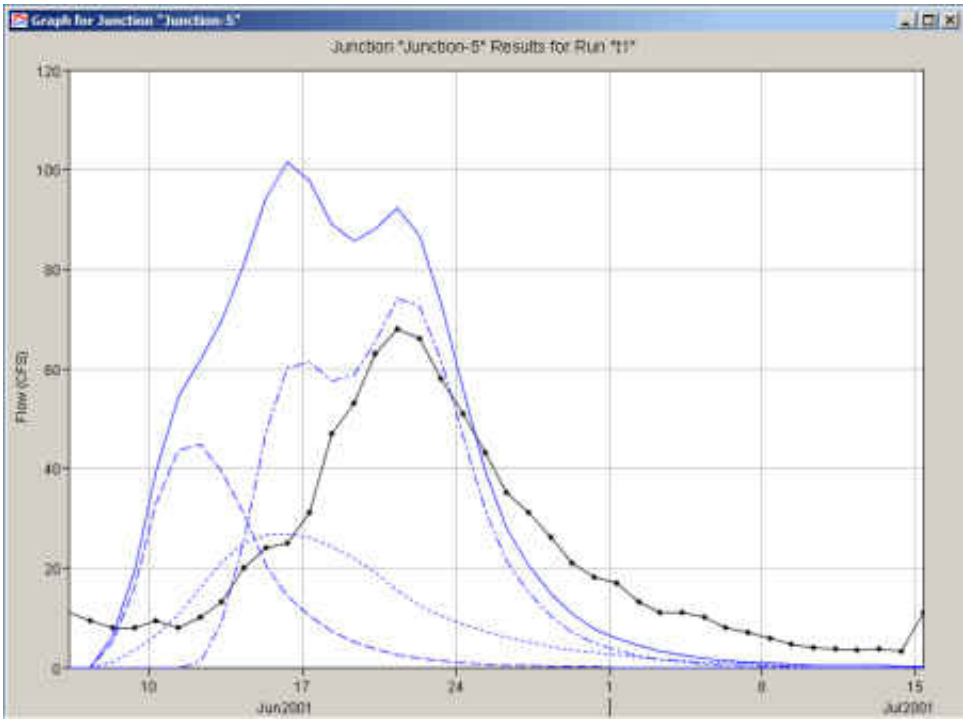

Figure 81: Calibration plot of Trial 7 (Loss calibration: storm-based)

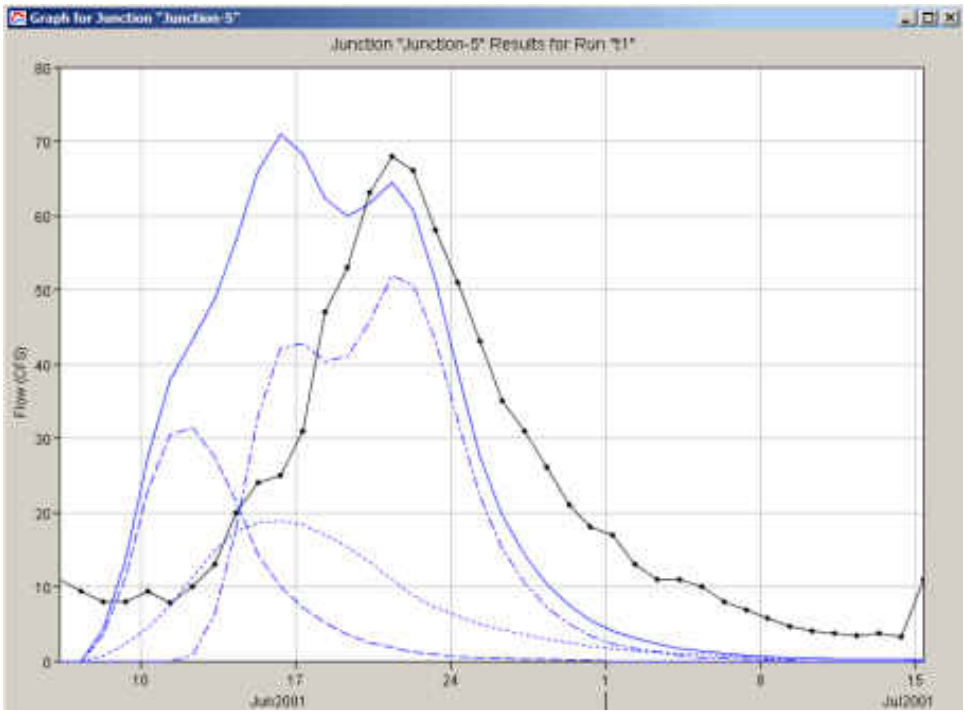

Figure 82: Calibration plot of Trial 8 (Loss calibration: storm-based)

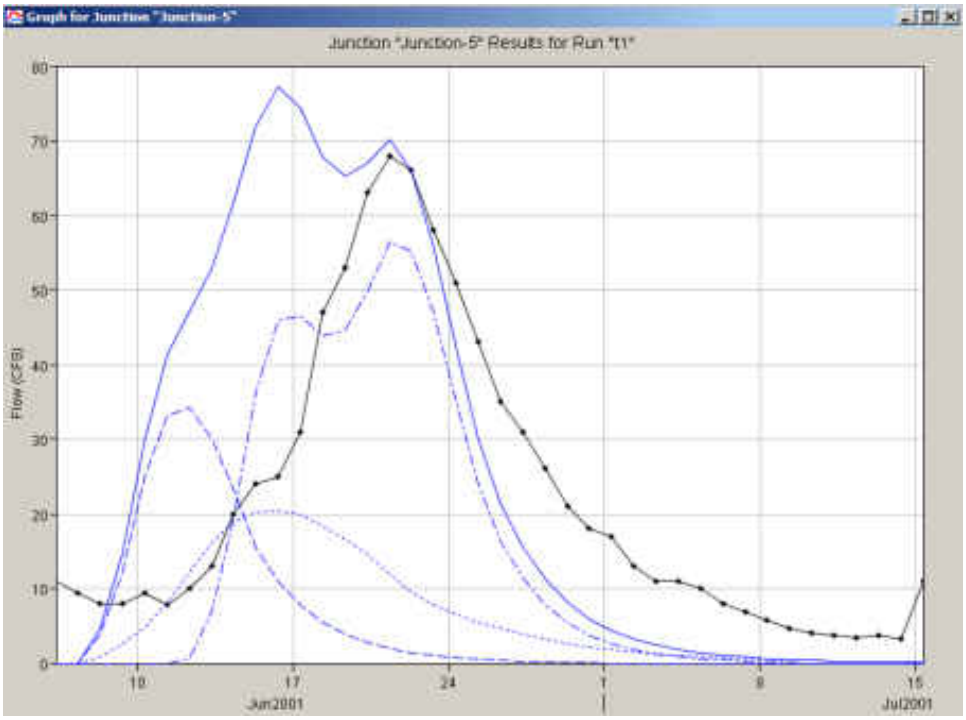

Figure 83: Calibration plot of Trial 9 (Loss calibration: storm-based)

D.2 Calibration using Precipitation Gage at Towner

Duration: Jun 6 to Jul 15, 2001

Precipitation gage: Towner

Stream flow gage: Cando

Outflow observed: 0.22 inch

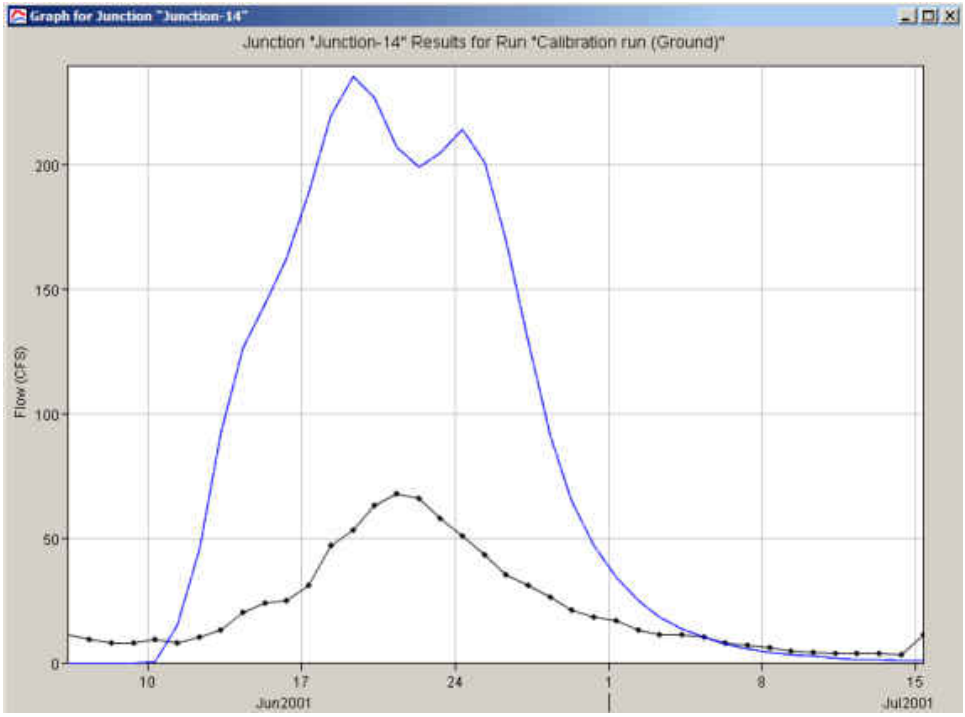

Figure 84: Loss calibration of Mauvais coulee (Precipitation: Towner) - Trial 1

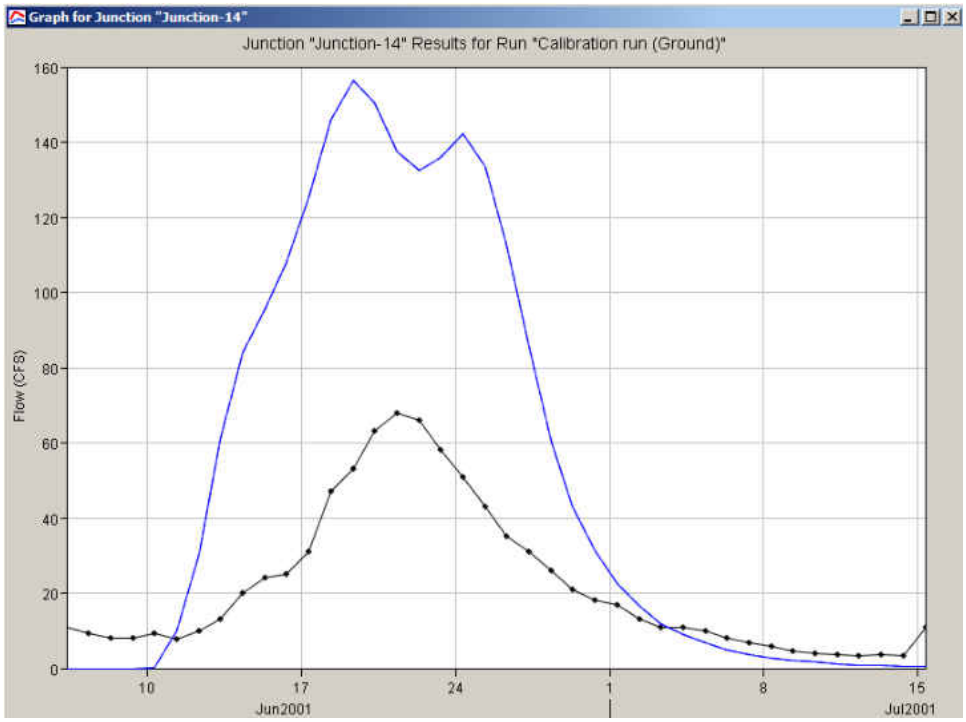

Figure 85: Loss calibration of Mauvais coulee (Precipitation: Towner) - Trial 2

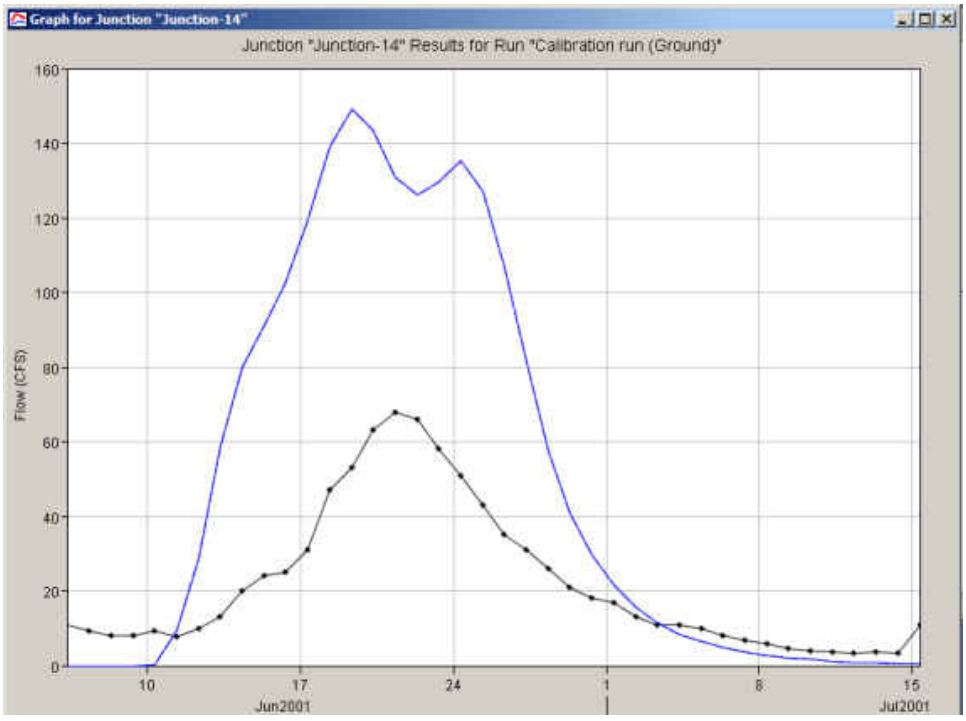

Figure 86: Loss calibration of Mauvais coulee (Precipitation: Towner) - Trial 3

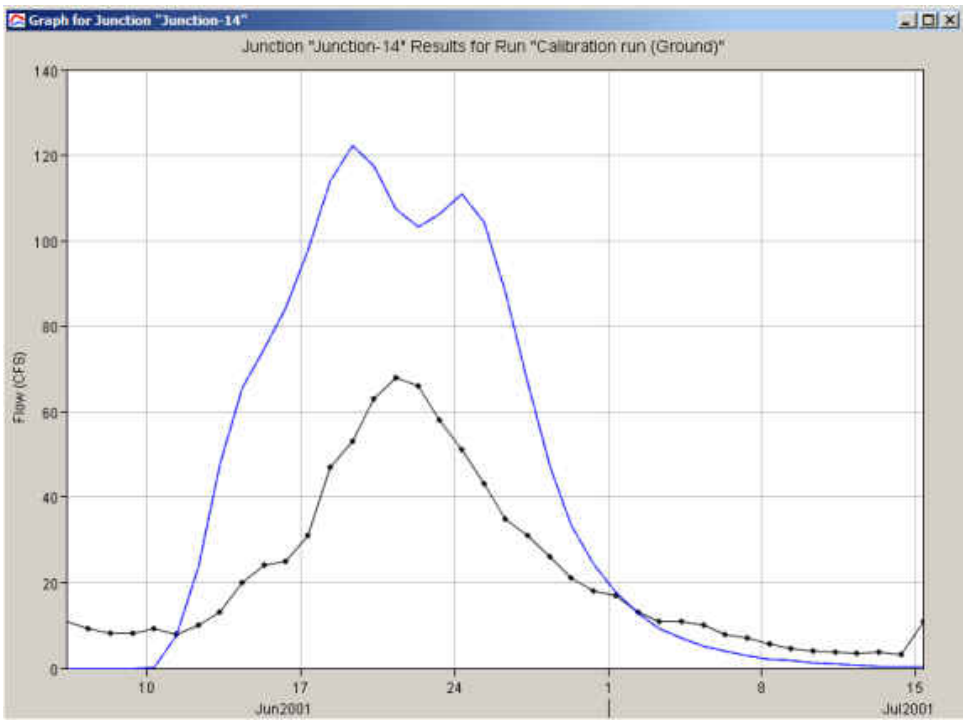

Figure 87: Loss calibration of Mauvais coulee (Precipitation: Towner) - Trial 4

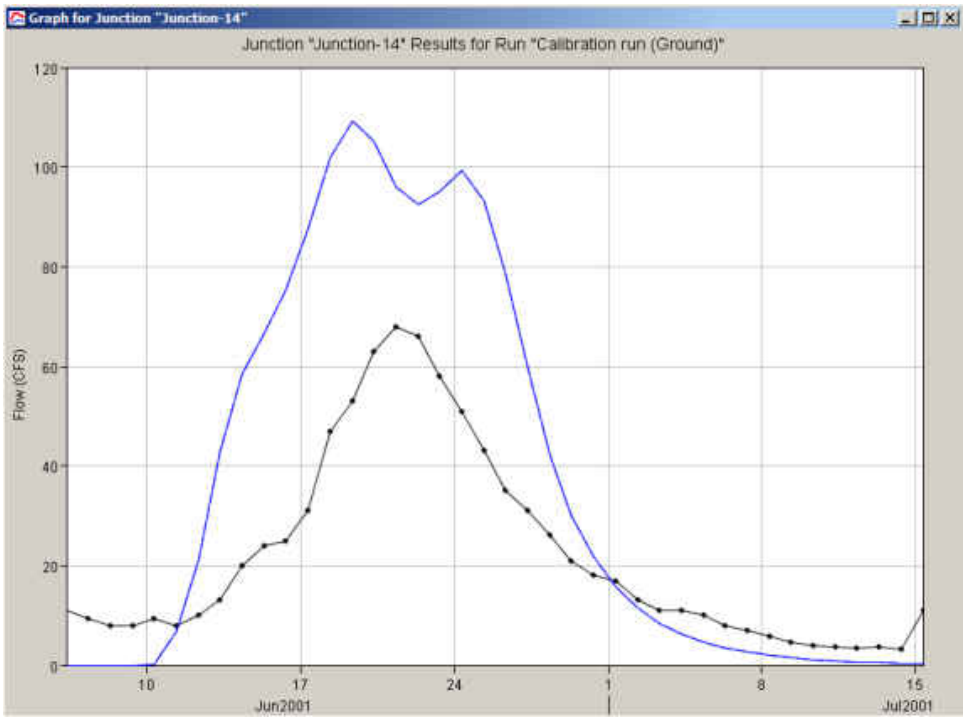

Figure 88: Loss calibration of Mauvais coulee (Precipitation: Towner) - Trial 5

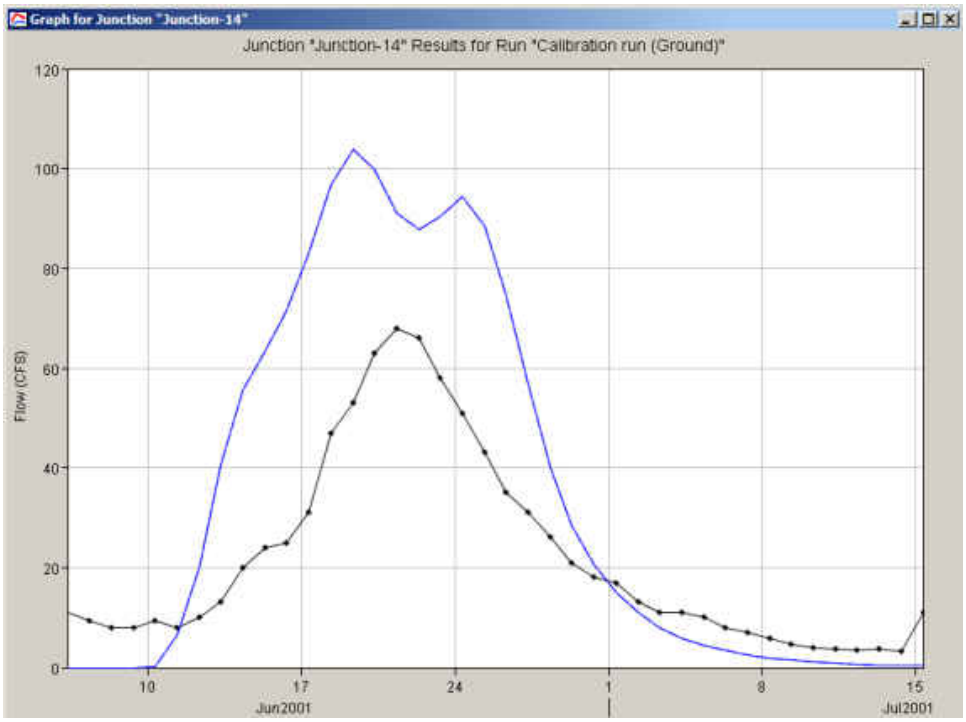

Figure 89: Loss calibration of Mauvais coulee (Precipitation: Towner) - Trial 6

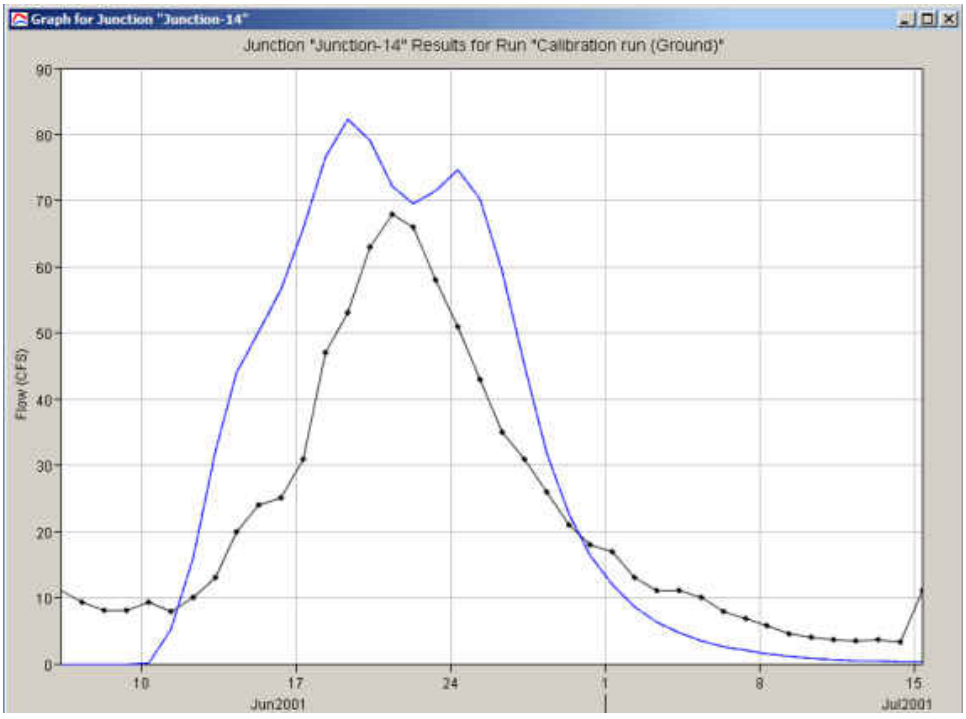

Figure 90: Loss calibration of Mauvais coulee (Precipitation: Towner) - Trial 7

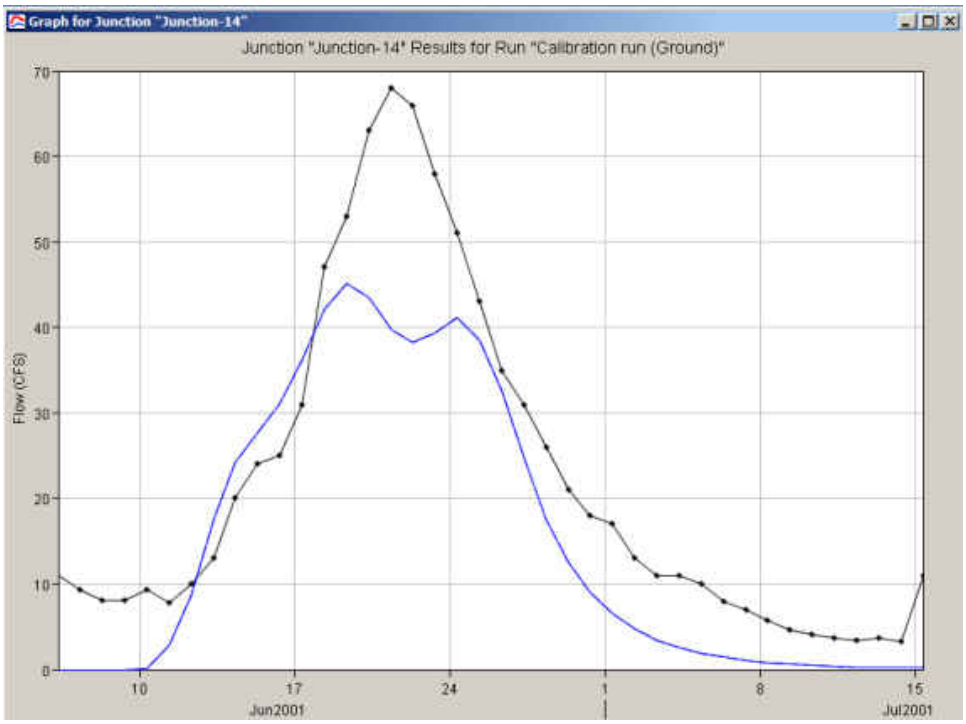

Figure 91: Loss calibration of Mauvais coulee (Precipitation: Towner) - Trial 8

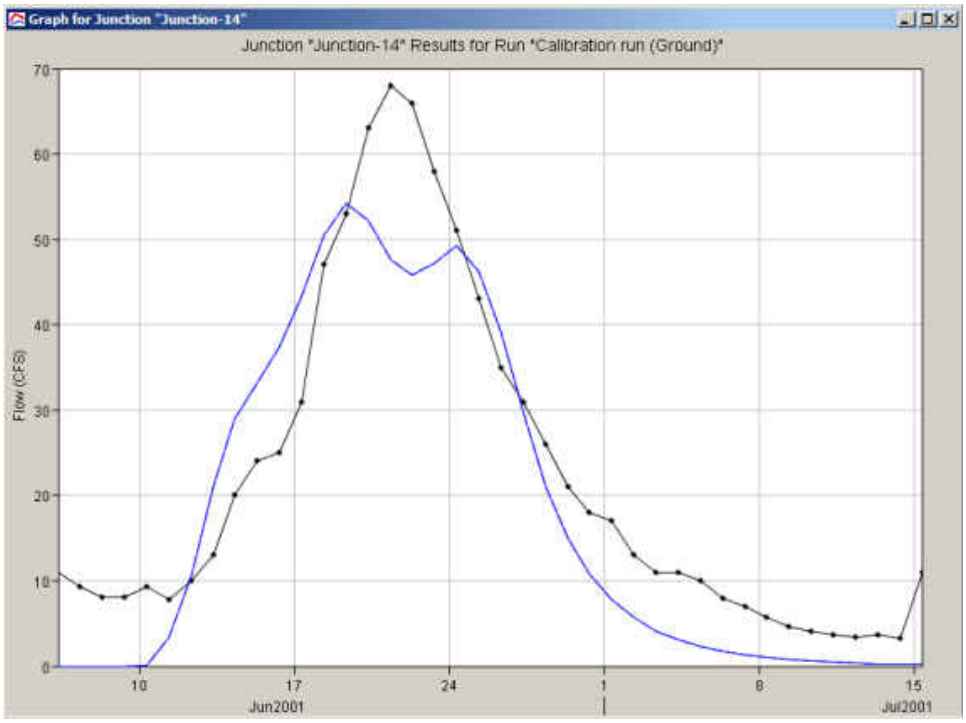

Figure 92: Loss calibration of Mauvais coulee (Precipitation: Towner) - Trial 9

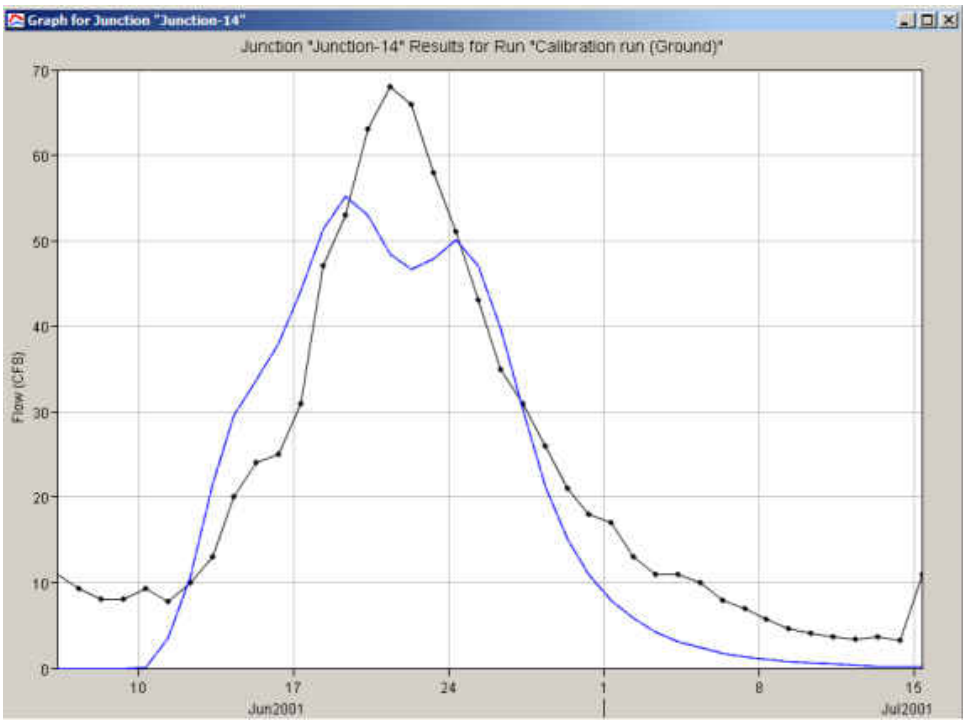

Figure 93: Loss calibration of Mauvais coulee (Precipitation: Towner) - Trial 10

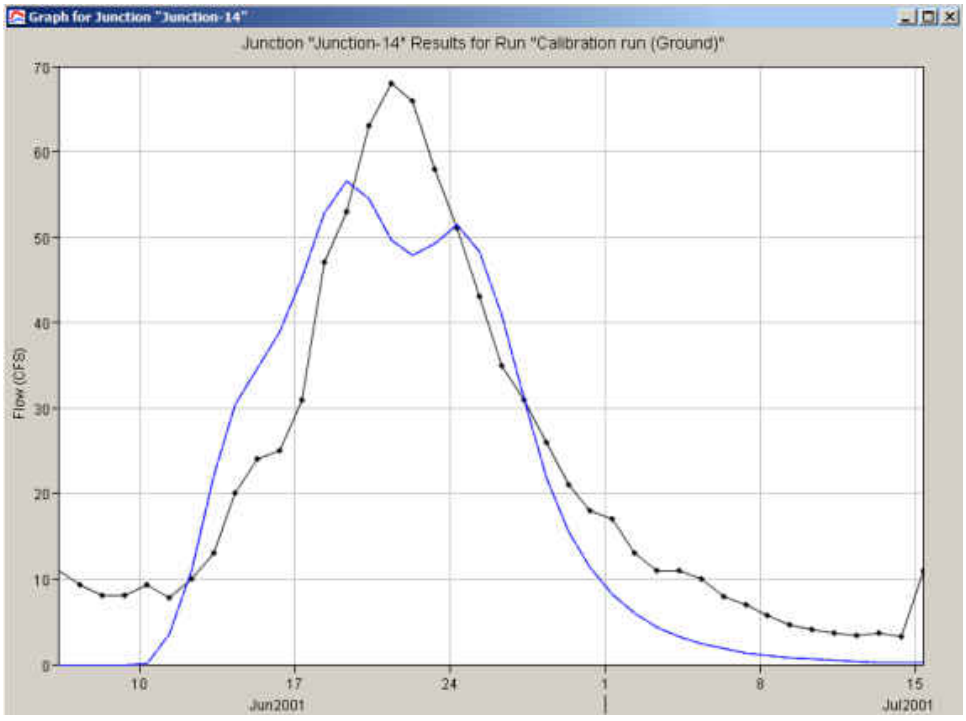

Figure 94: Loss calibration of Mauvais coulee (Precipitation: Towner) - Trial 11

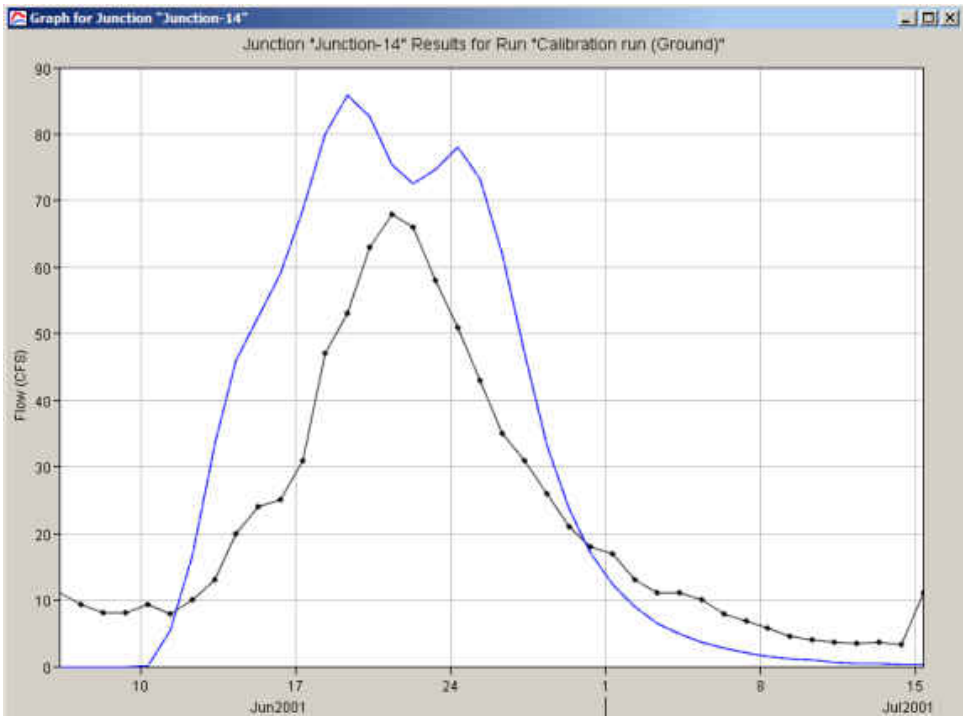

Figure 95: Loss calibration of Mauvais coulee (Precipitation: Towner) - Trial 12

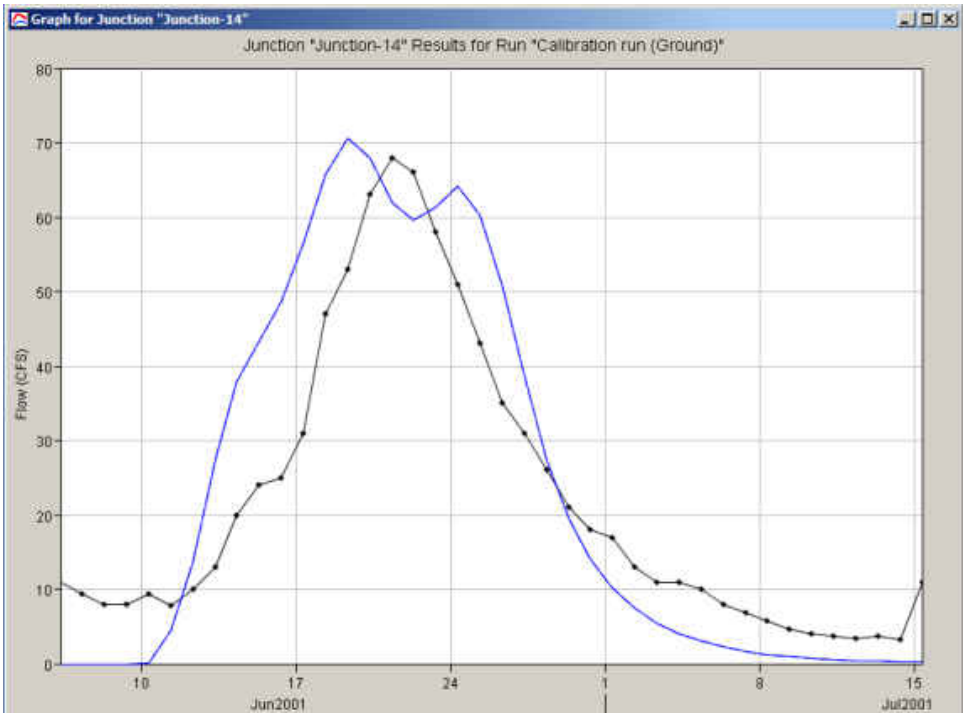

Figure 96: Loss calibration of Mauvais coulee (Precipitation: Towner) - Trial 13

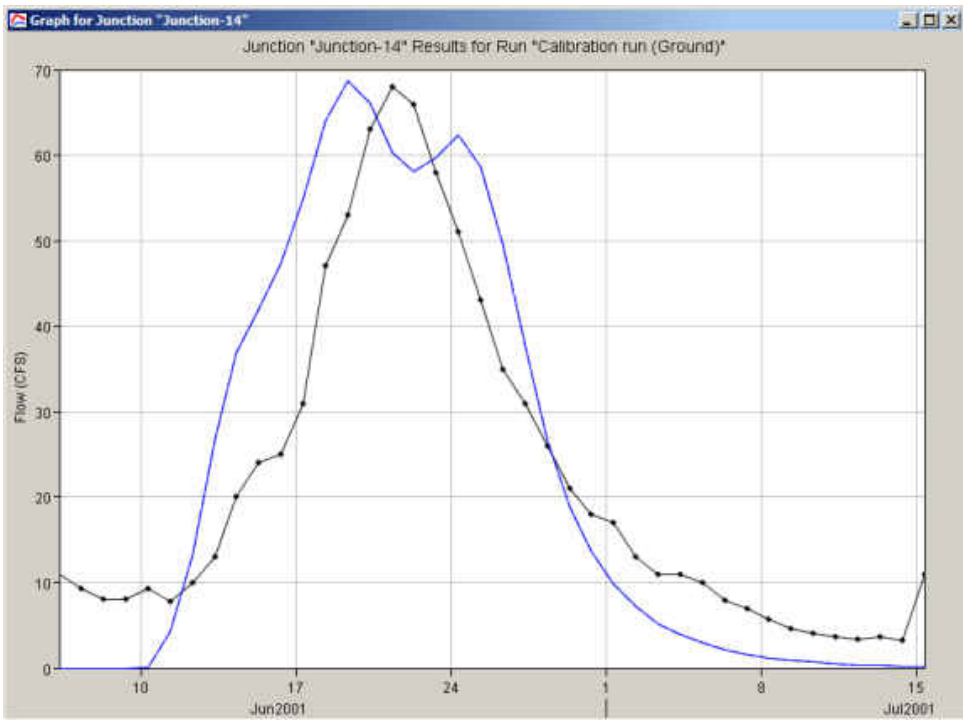

Figure 97: Loss calibration of Mauvais coulee (Precipitation: Towner) - Trial 14

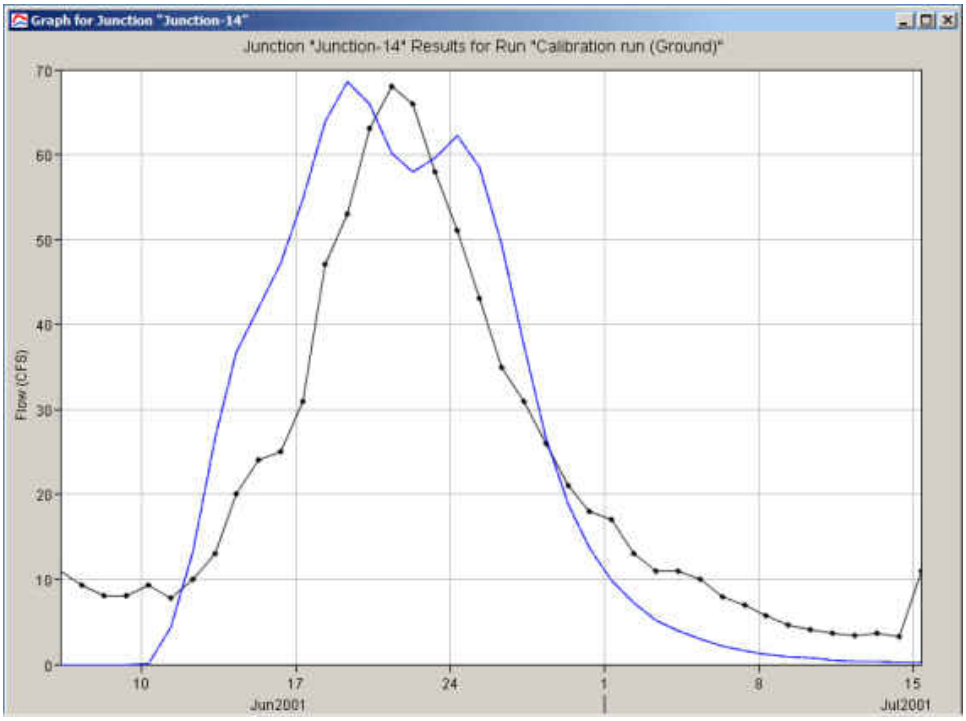

Figure 98: Loss calibration of Mauvais coulee (Precipitation: Towner) - Trial 15

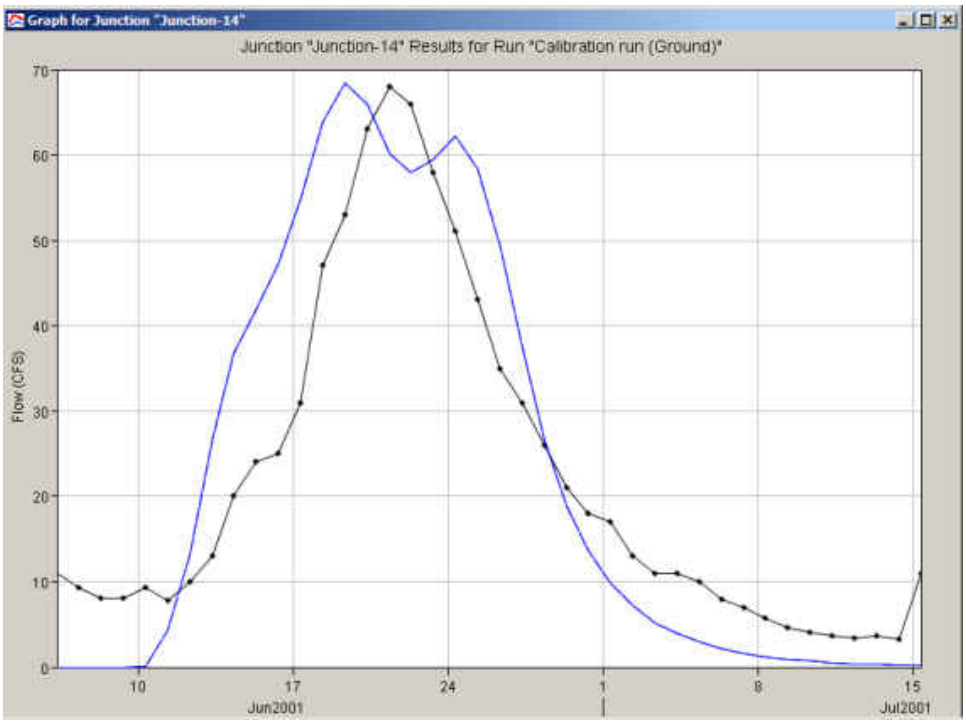

Figure 99: Loss calibration of Mauvais coulee (Precipitation: Towner) - Trial 16

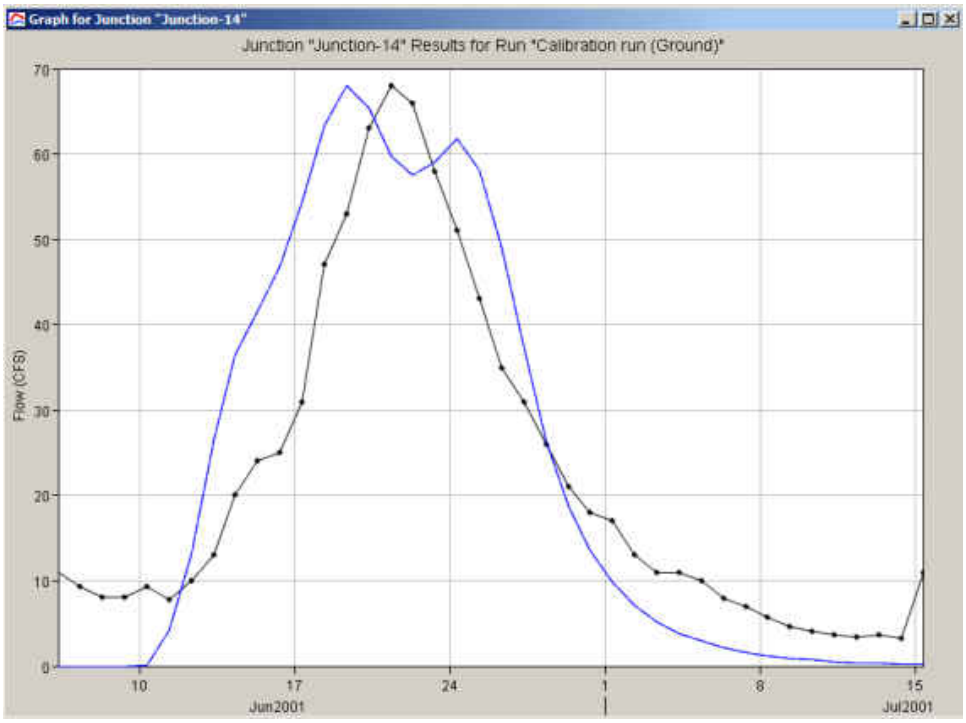

Figure 100: Loss calibration of Mauvais coulee (Precipitation: Towner) - Trial 17

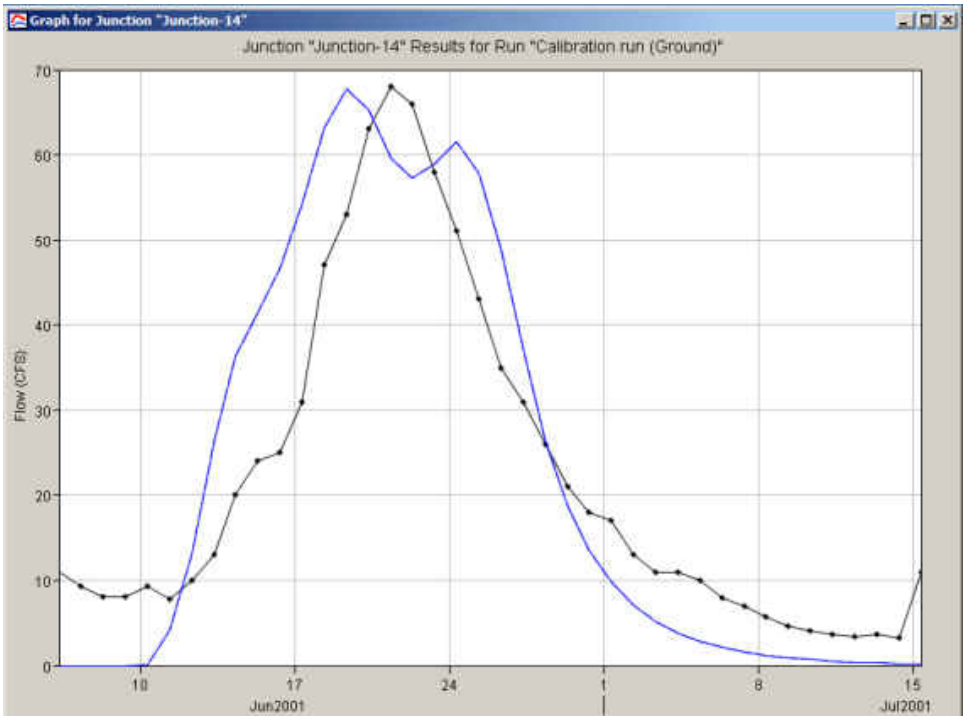

Figure 101: Loss calibration of Mauvais coulee (Precipitation: Towner) - Trial 18

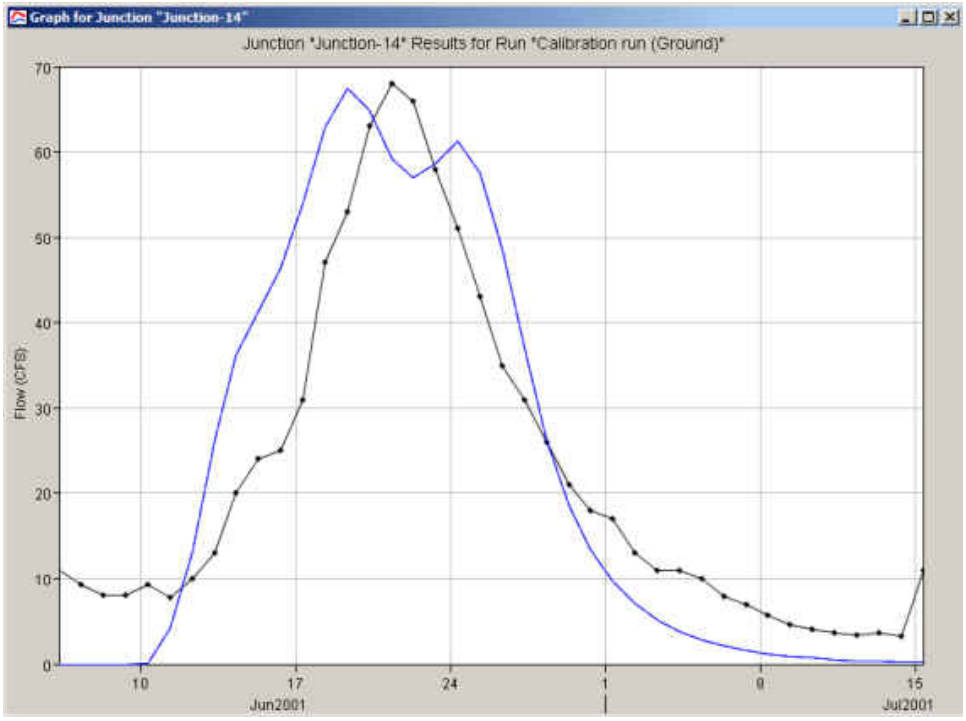

Figure 102: Loss calibration of Mauvais coulee (Precipitation: Towner) - Trial 19

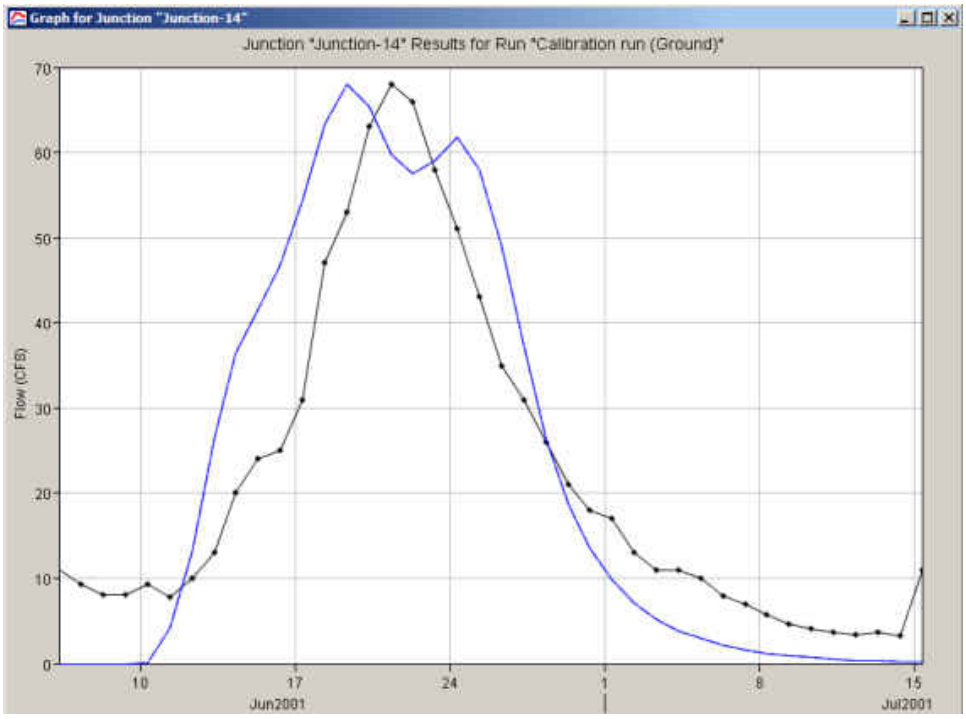

Figure 103: Loss calibration of Mauvais coulee (Precipitation: Towner) - Trial 20

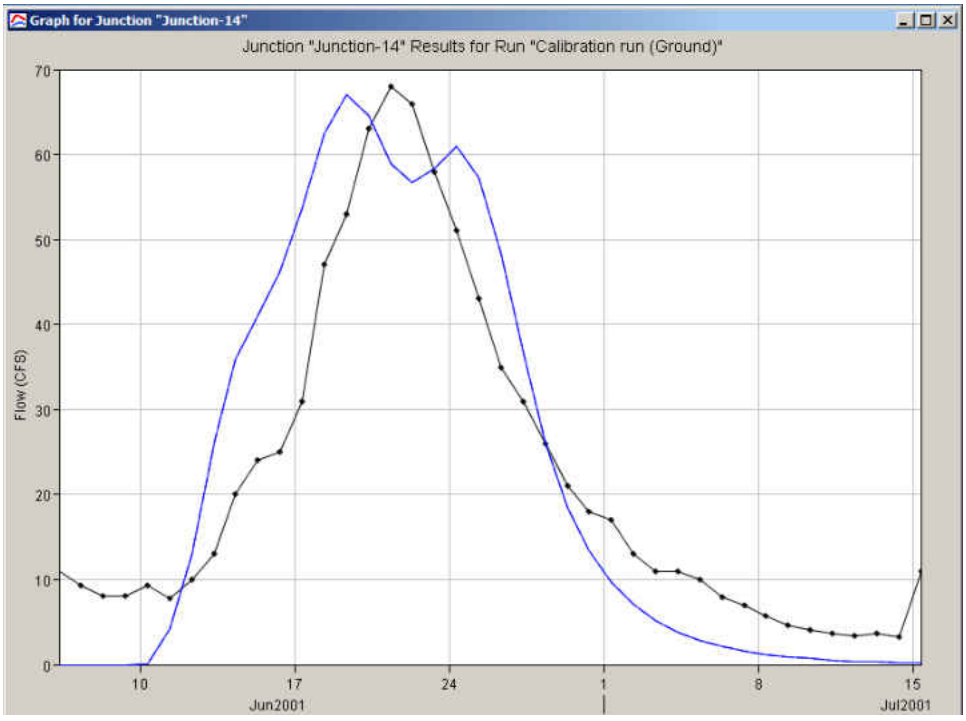

Figure 104: Loss calibration of Mauvais coulee (Precipitation: Towner) - Trial 21

Appendix E

Calibration Plots of Snow-Melt Calibration of Mauvais Coulee

Duration: 15th March to 10th June, 2001 and 1st February to 10th June

Precipitation gage: NASA TMPA

Stream flow gage: Cando

Outflow observed: 5.45 inch

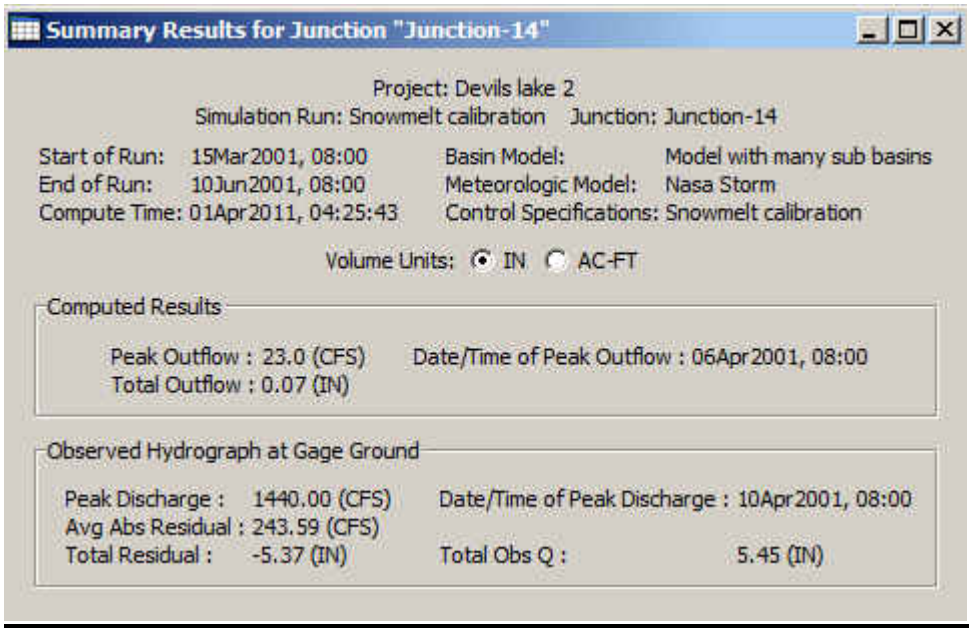

Figure 105: Snowmelt calibration of Mauvais coulee - Trial 1

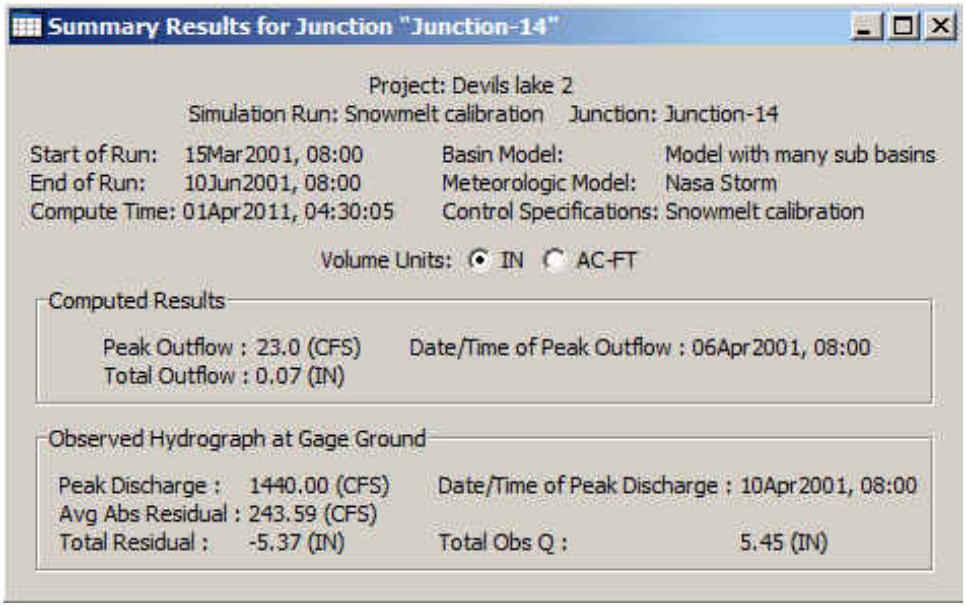

Figure 106: Snowmelt calibration of Mauvais coulee - Trial 2

Figure 107: Snowmelt calibration of Mauvais coulee - Trial 3

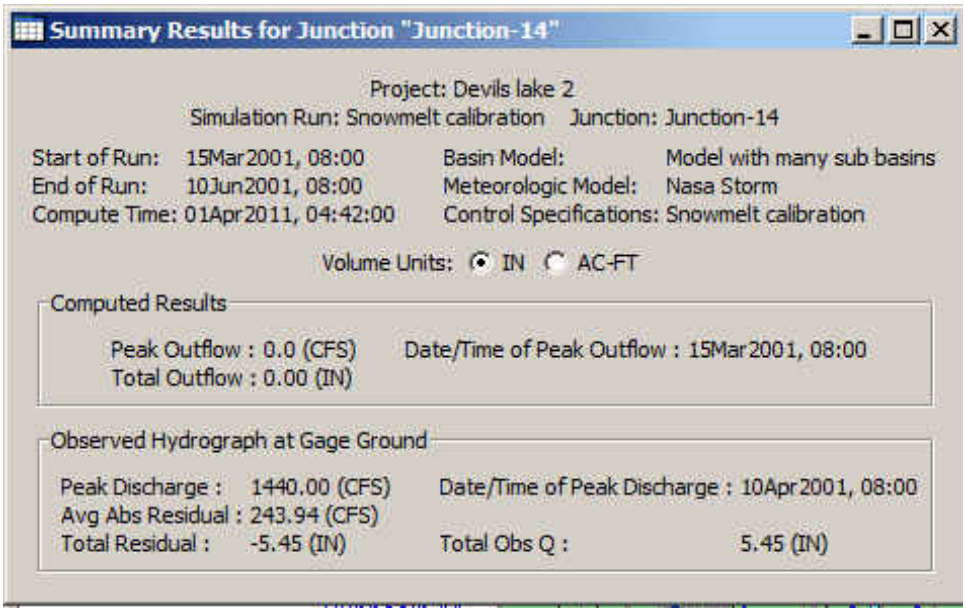

Figure 108: Snowmelt calibration of Mauvais coulee - Trial 4

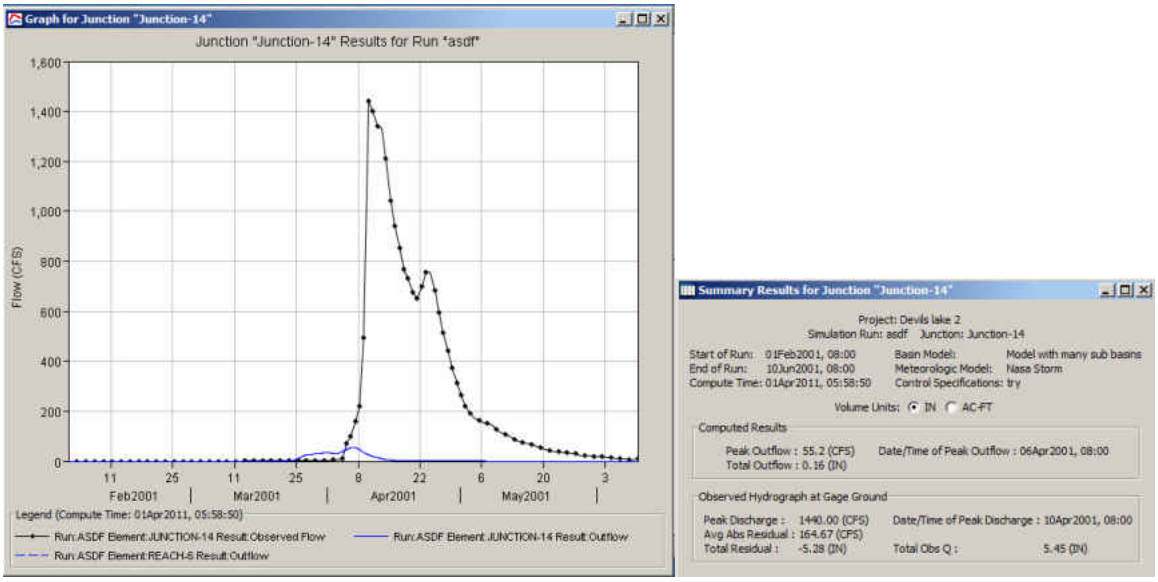

Figure 109: Snowmelt calibration of Mauvais coulee - Trial 5

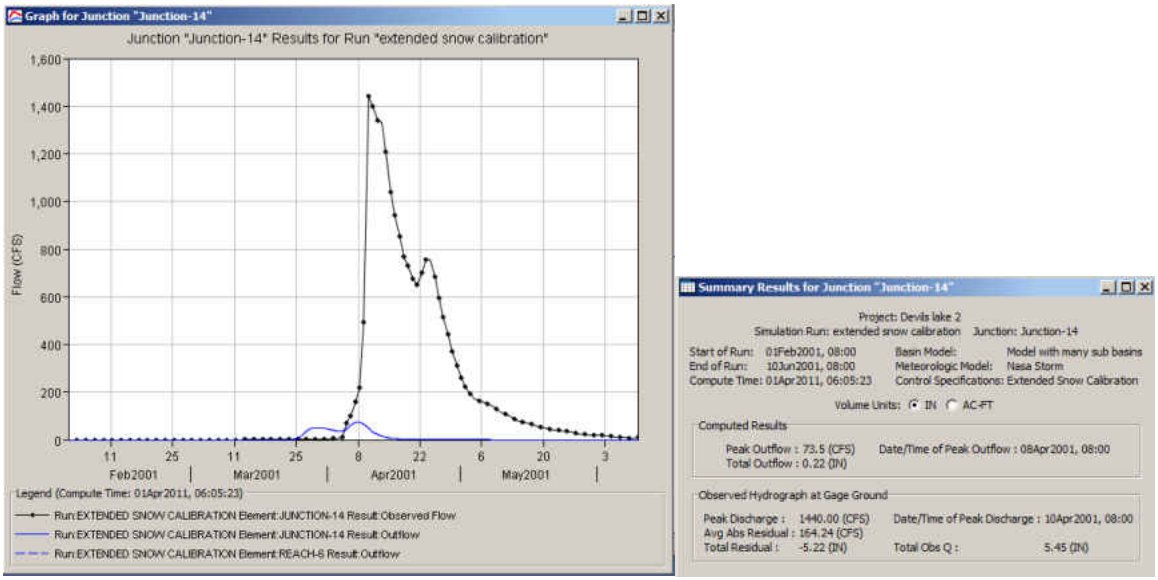

Figure 110: Snowmelt calibration of Mauvais coulee - Trial 6

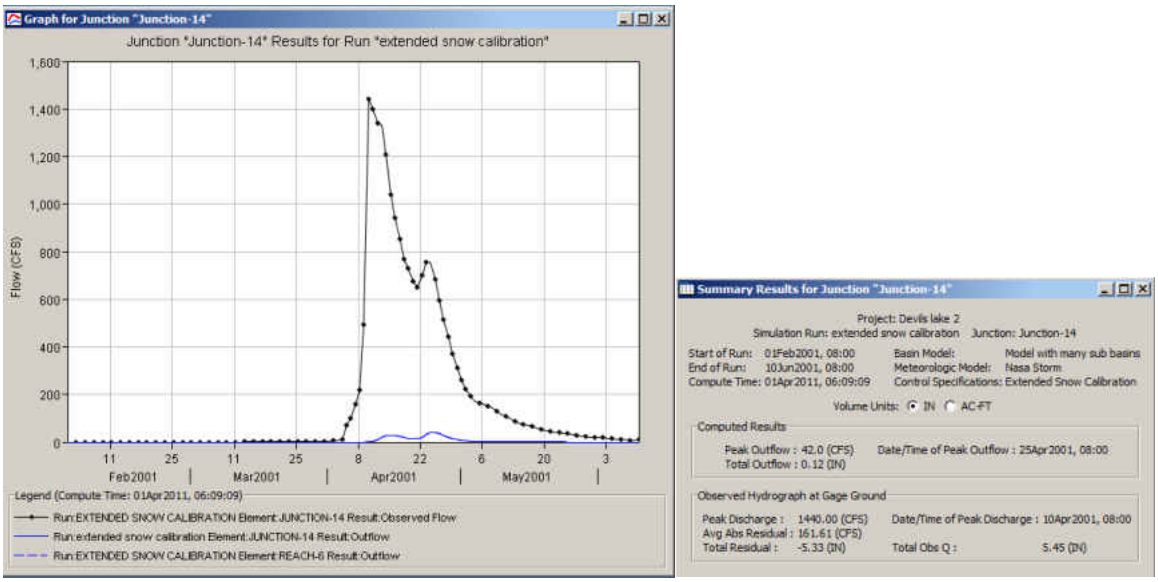

Figure 111: Snowmelt calibration of Mauvais coulee – Trial 7

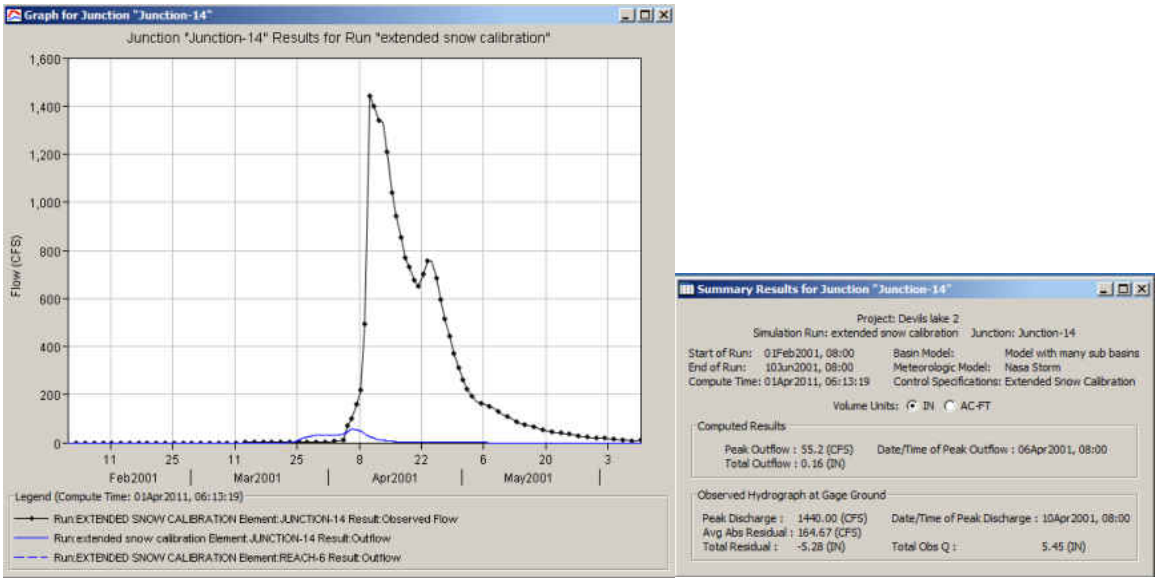

Figure 112: Snowmelt calibration of Mauvais coulee – Trial 8

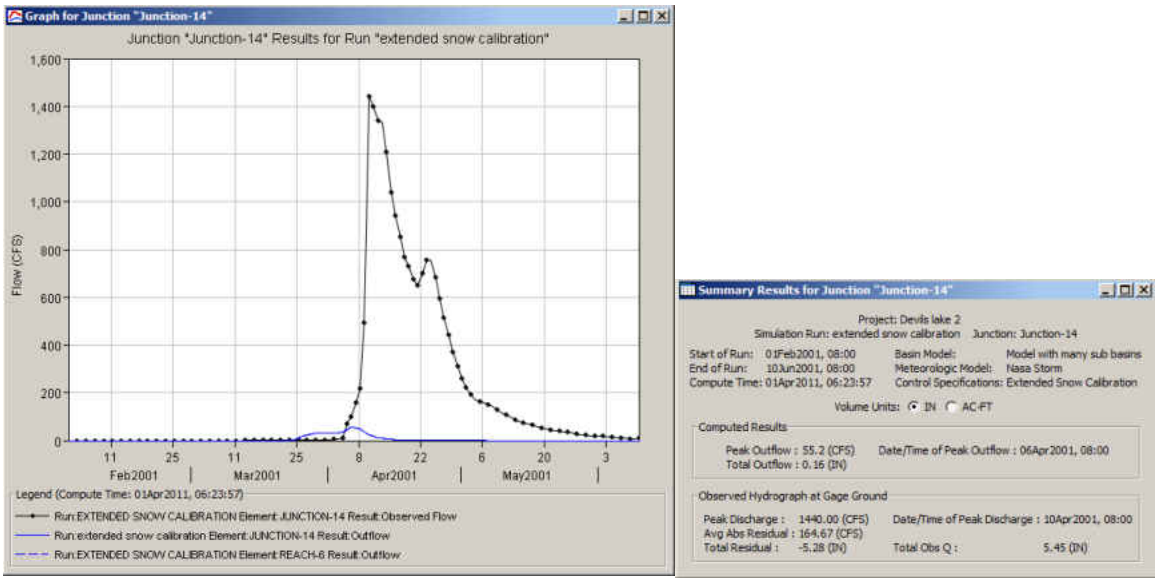

Figure 113: Snowmelt calibration of Mauvais coulee – Trial 9

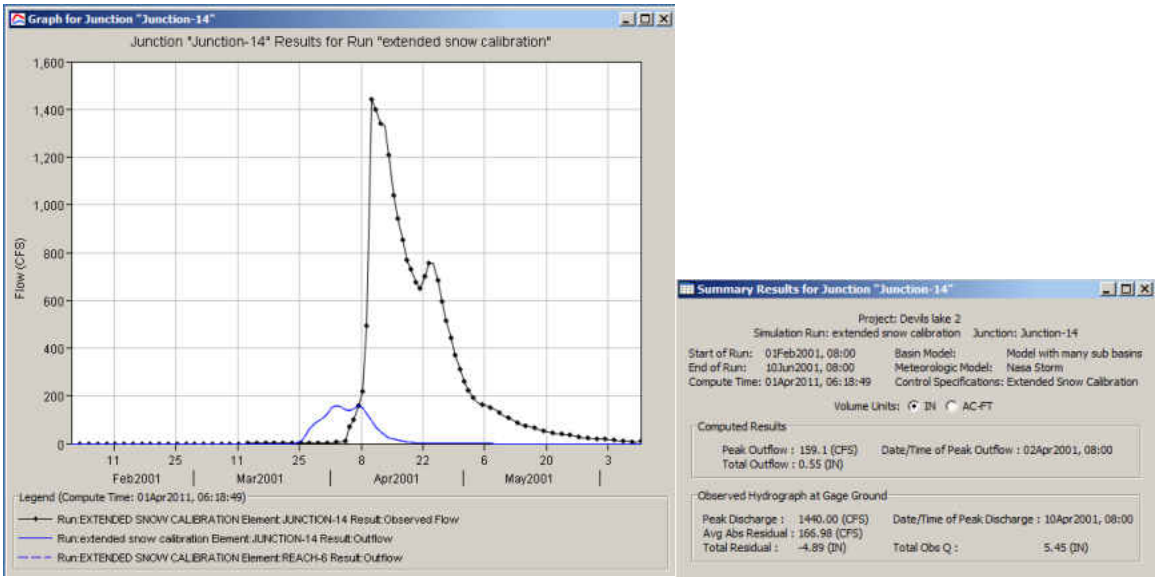

Figure 114: Snowmelt calibration of Mauvais coulee – Trial 10

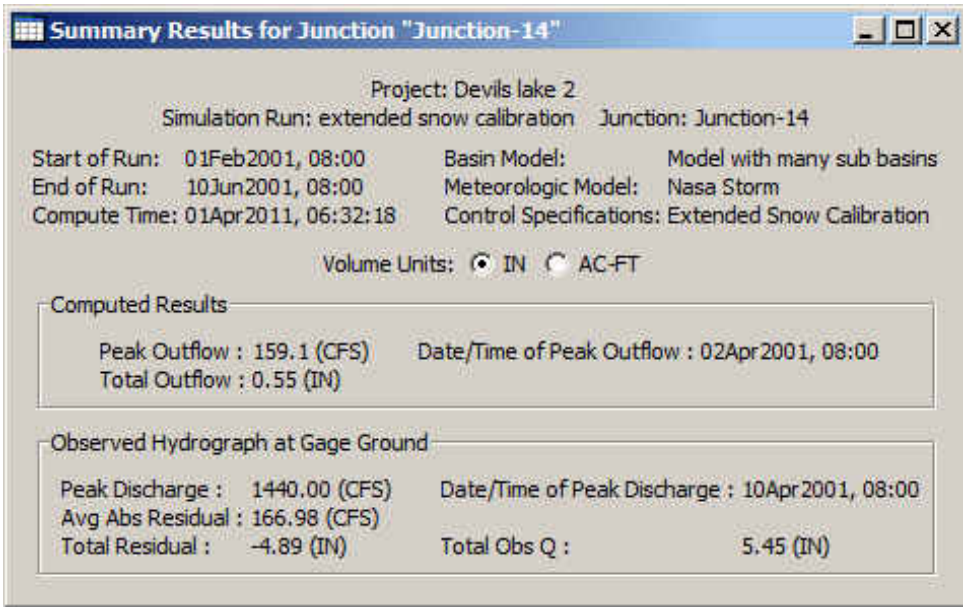

Figure 115: Snowmelt calibration of Mauvais coulee – Trial 11

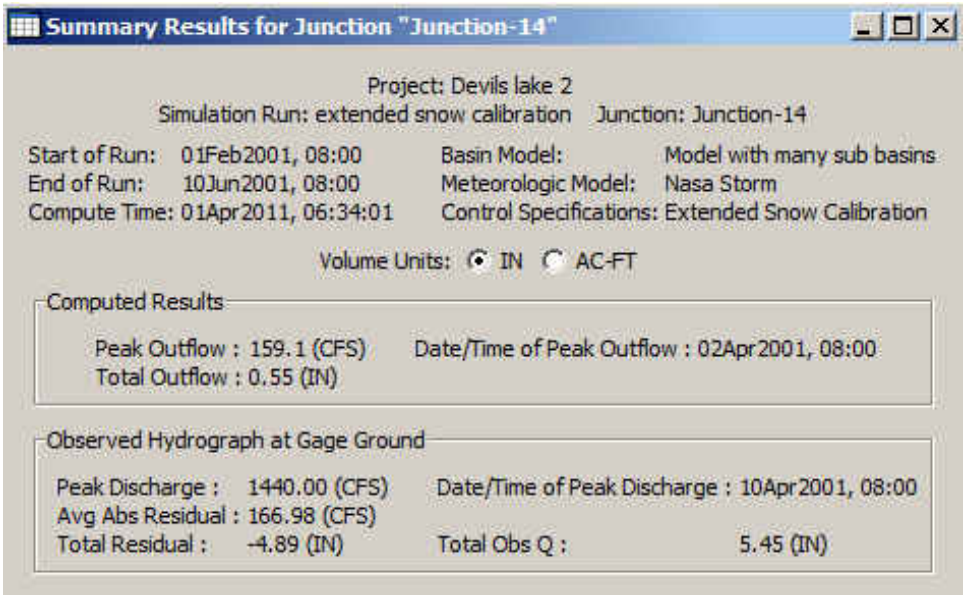

Figure 116: Snowmelt calibration of Mauvais coulee – Trial 12

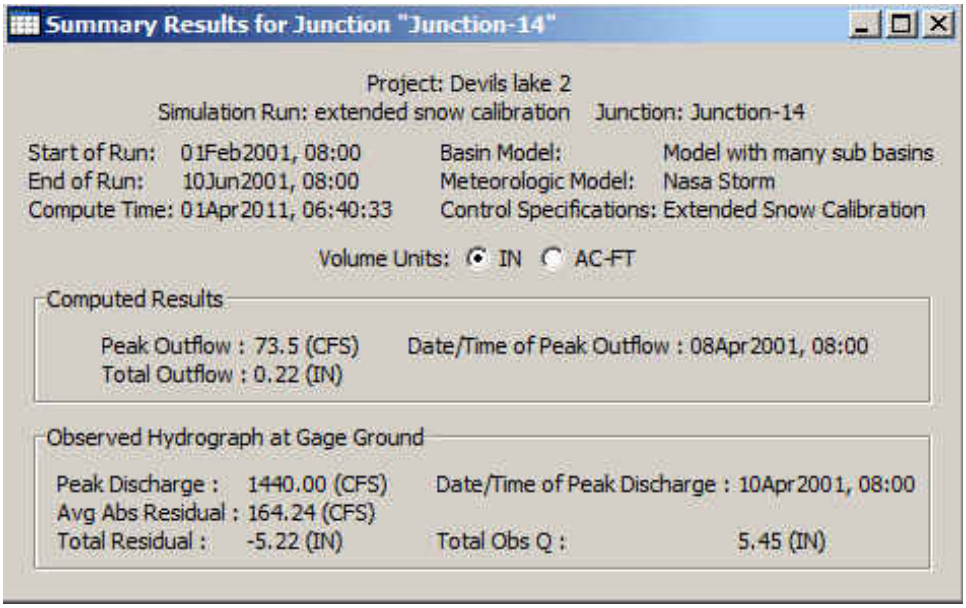

Figure 117: Snowmelt calibration of Mauvais coulee – Trial 13

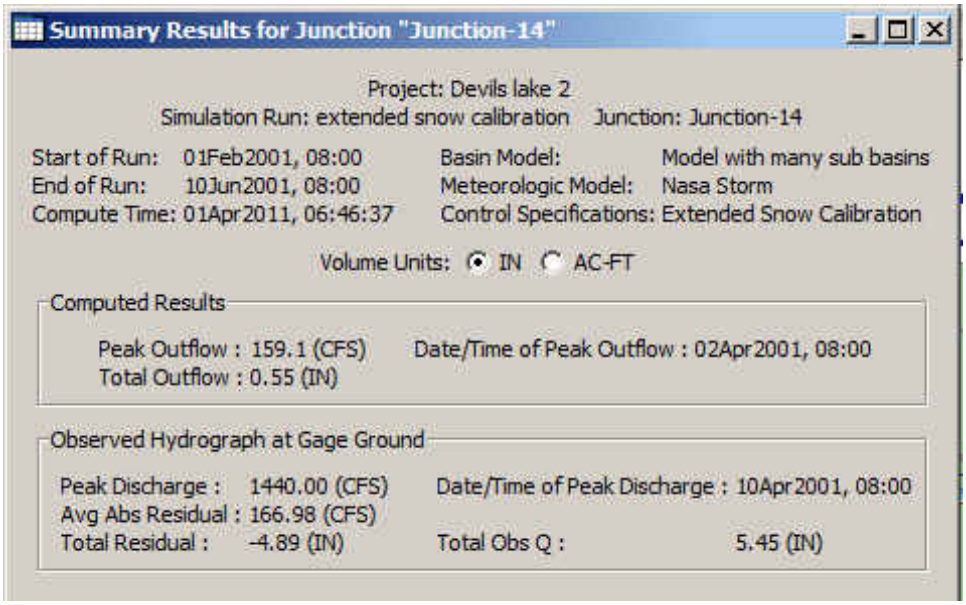

Figure 118: Snowmelt calibration of Mauvais coulee – Trial 14

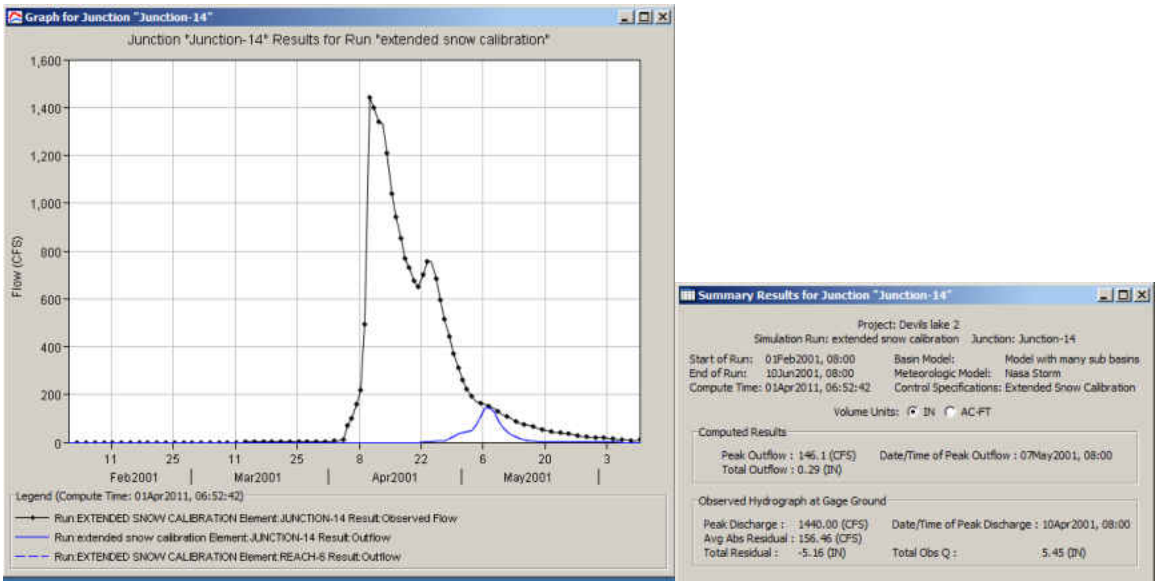

Figure 119: Snowmelt calibration of Mauvais coulee – Trial 15

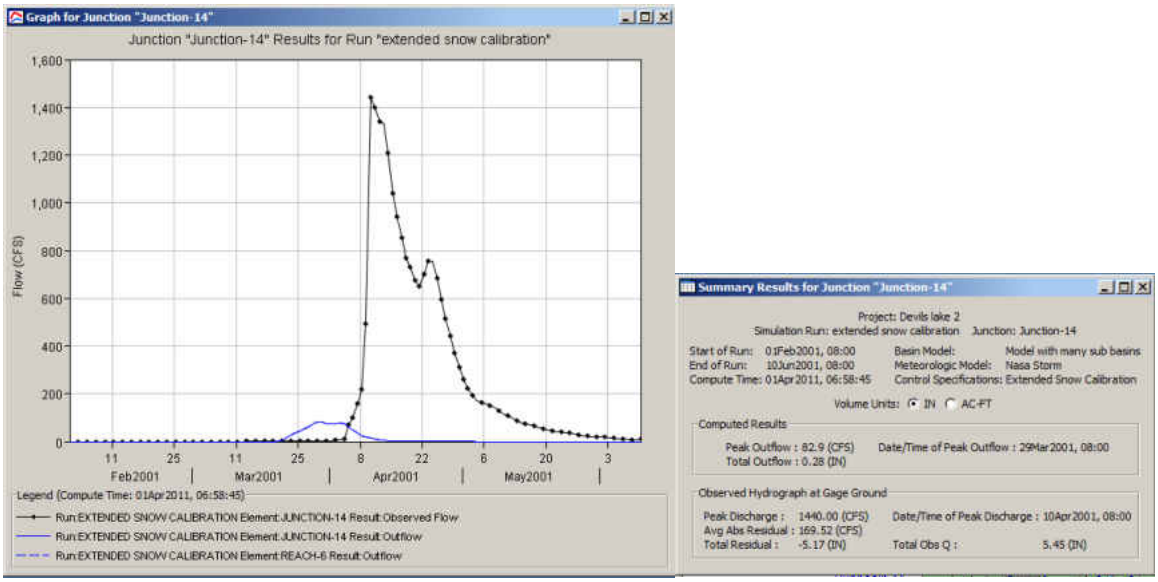

Figure 120: Snowmelt calibration of Mauvais coulee – Trial 16

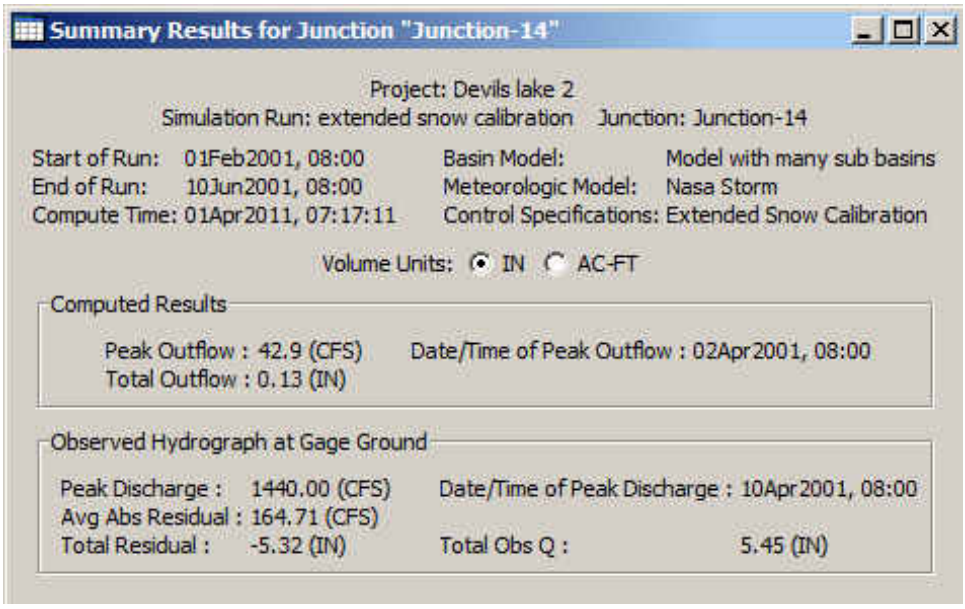

Figure 121: Snowmelt calibration of Mauvais coulee – Trial 17

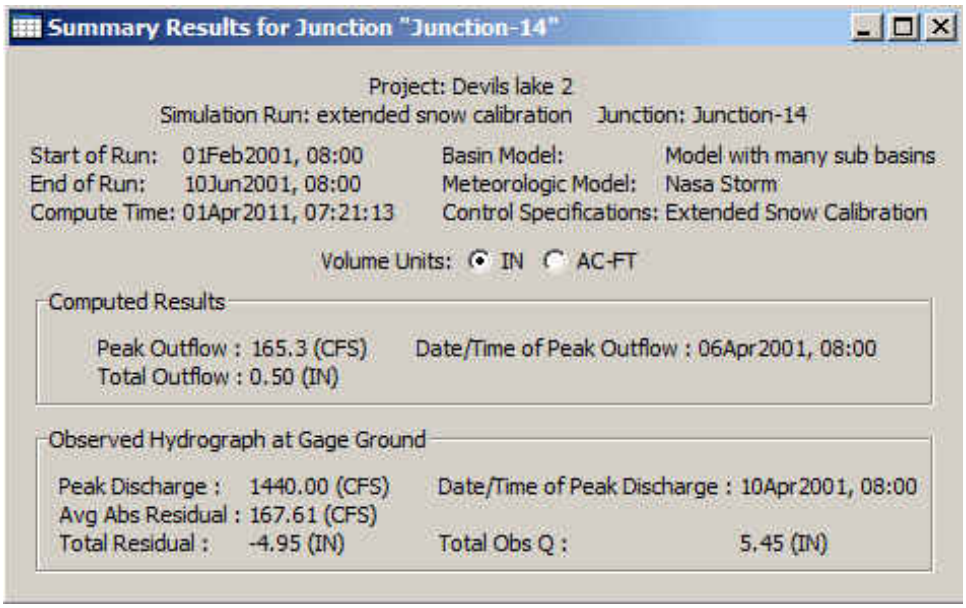

Figure 122: Snowmelt calibration of Mauvais coulee – Trial 18

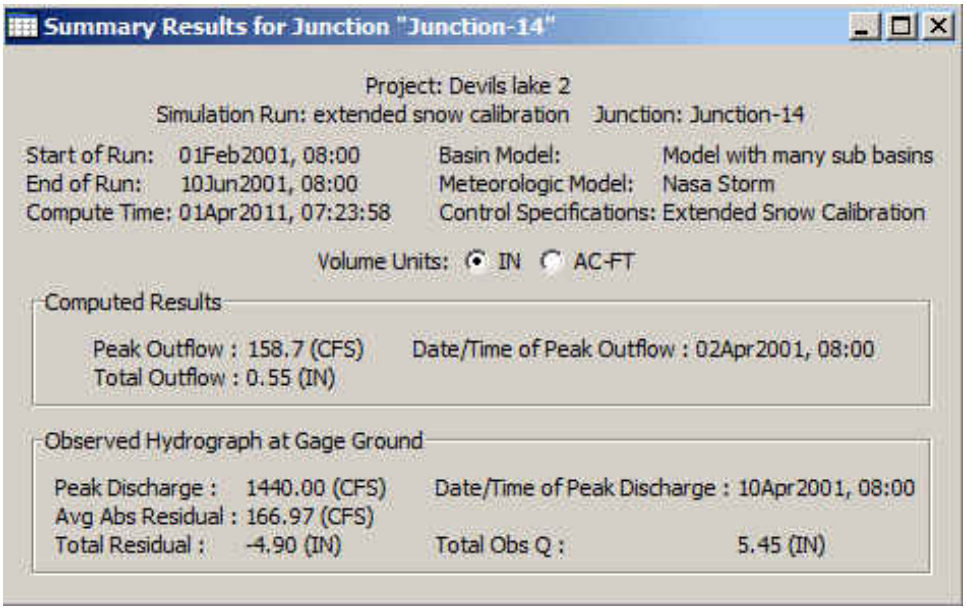

Figure 123: Snowmelt calibration of Mauvais coulee – Trial 19

Appendix F

Plots of the Combined Approach in Calibration

F.1 Calibration Plots of HMS-Model A Coupled with ResSim Model

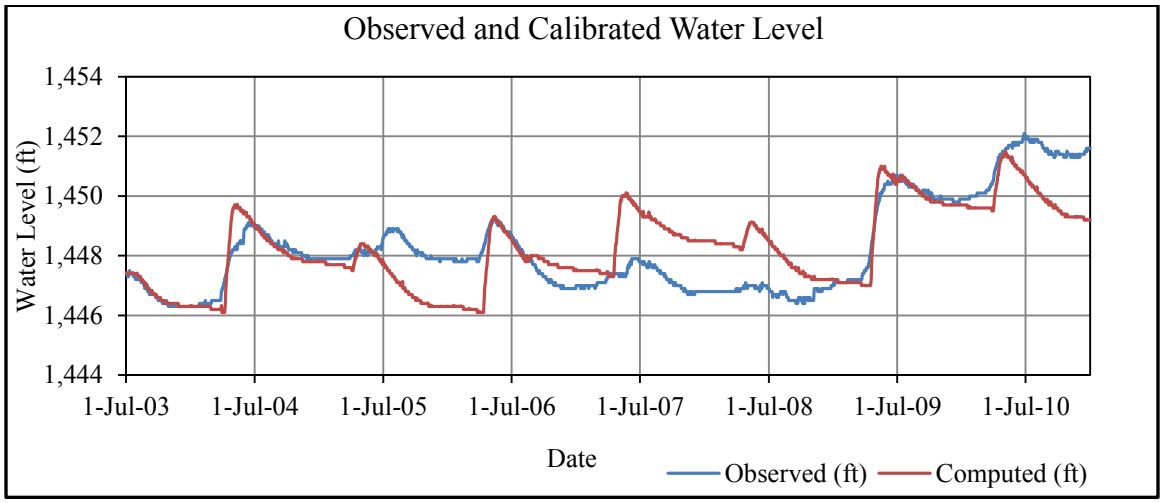

Figure 124: Calibration of HMS-Model A + ResSim (Combined approach) - Initial loss: 0.0 in; Constant loss: 0.085 in/hr; Seepage: 0 cfs

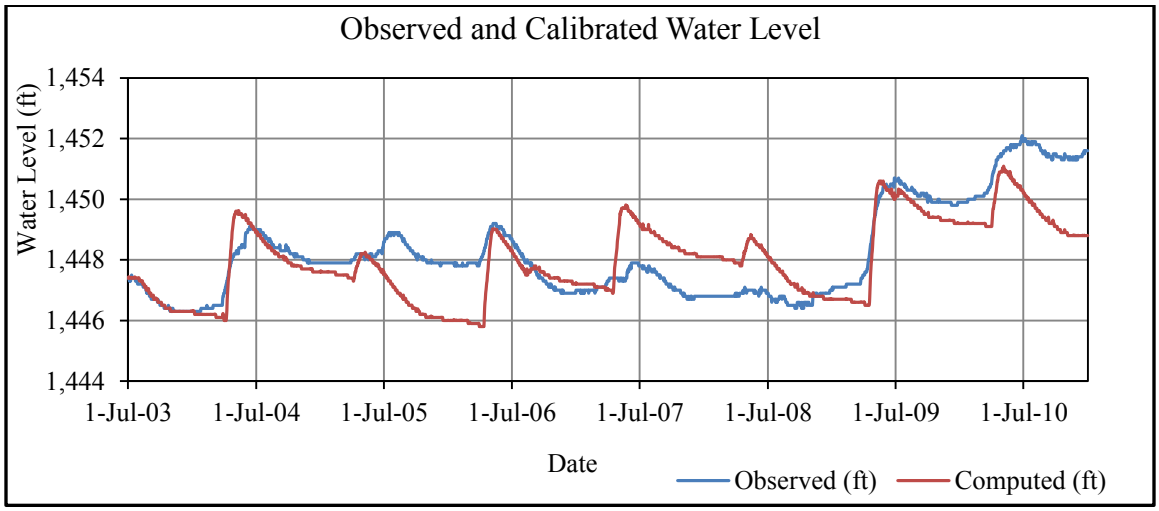

Figure 125: Calibration of HMS-Model A + ResSim (Combined approach) - Initial loss: 0.1 in; Constant loss: 0.085 in/hr; Seepage: 20 cfs

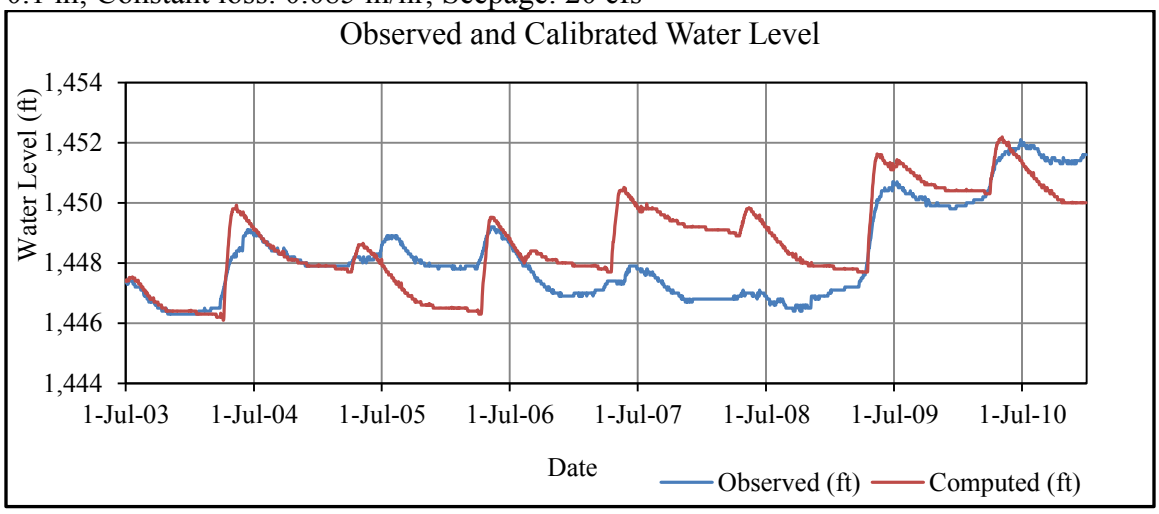

Figure 126: Calibration of HMS-Model A + ResSim (Combined approach) - Initial loss: 0.1 in; Constant loss: 0.085 in/hr; Seepage: 0 cfs

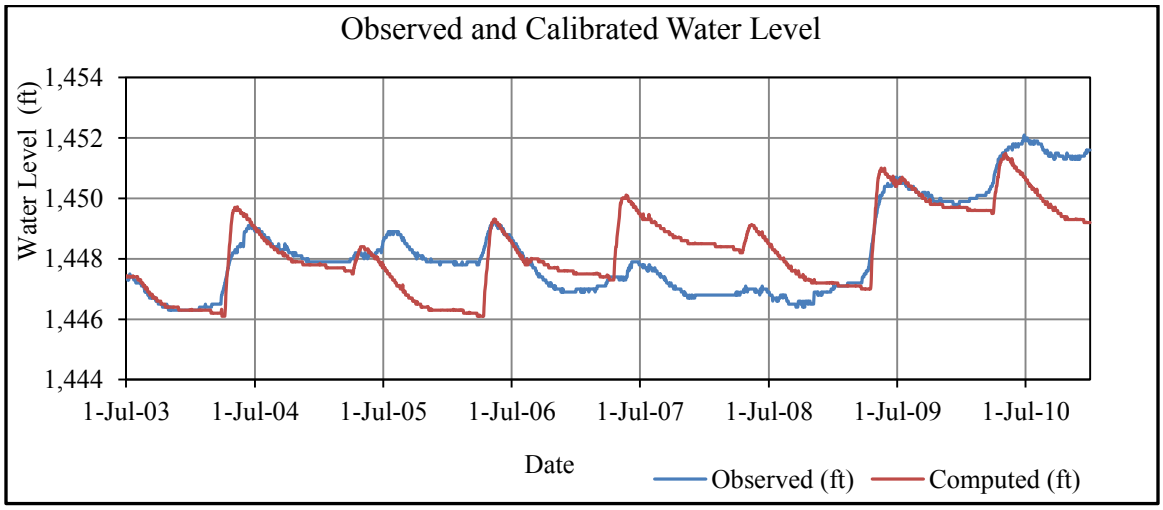

Figure 127: Calibration of HMS-Model A + ResSim (Combined approach) - Initial loss: 0.1 in; Constant loss: 0.085 in/hr; Seepage: 10 cfs

F.2 Calibration Plots of HMS-Model B Coupled with ResSim Model

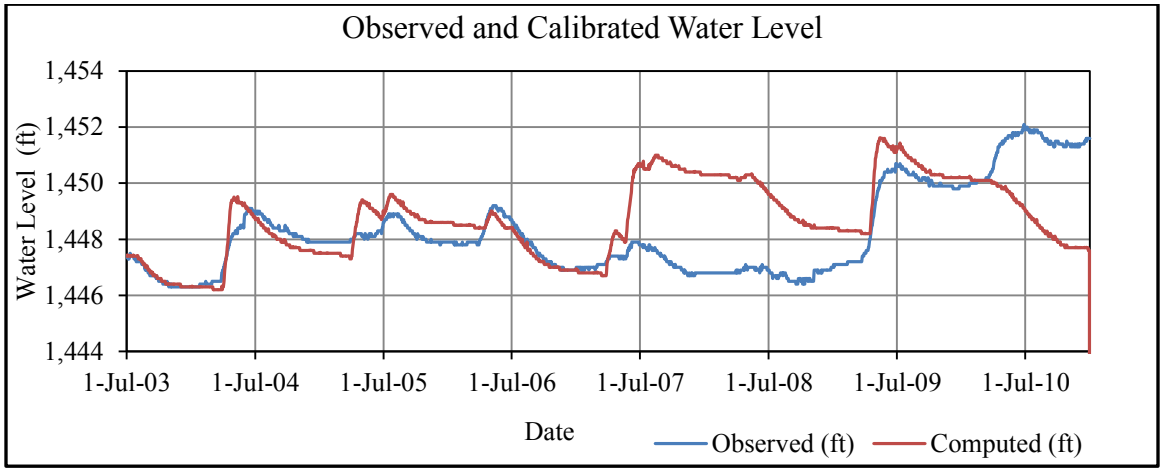

Figure 128: Calibration of HMS-Model B + ResSim (Combined approach) - Initial loss: 0.0 in; Constant loss: 0.085 in/hr; Seepage: 0 cfs

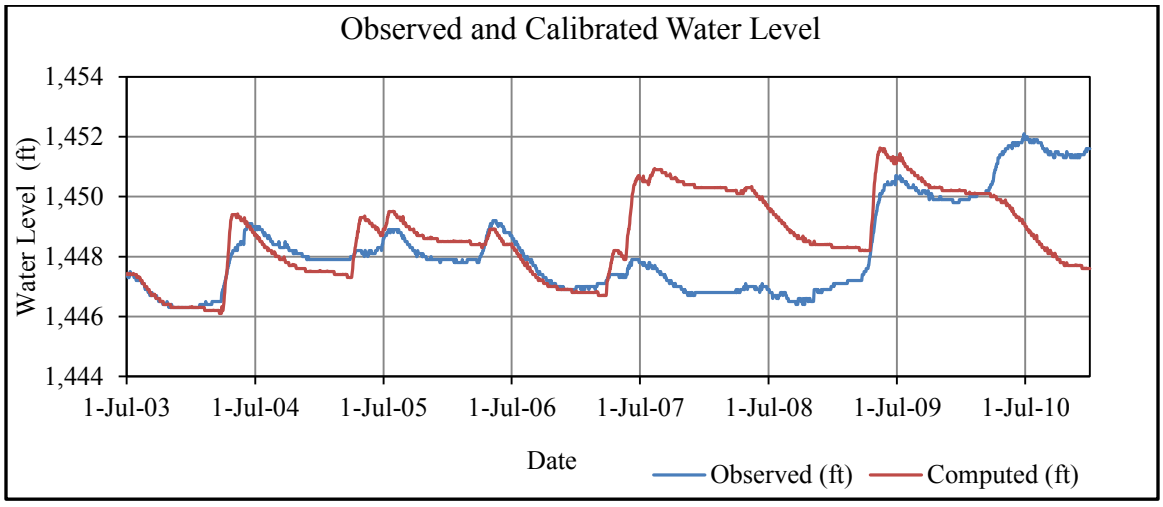

Figure 129: Calibration of HMS-Model B + ResSim (Combined approach) - Initial loss: 0.1 in; Constant loss: 0.085 in/hr; Seepage: 0 cfs

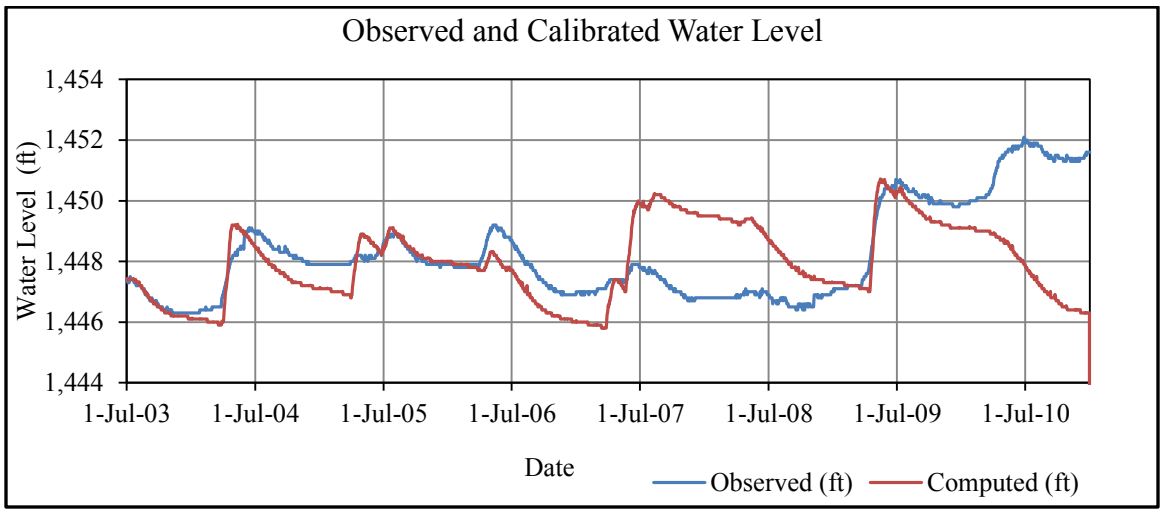

Figure 130: Calibration of HMS-Model B + ResSim (Combined approach) - Initial loss: 0.1 in; Constant loss: 0.085 in/hr; Seepage: 50 cfs

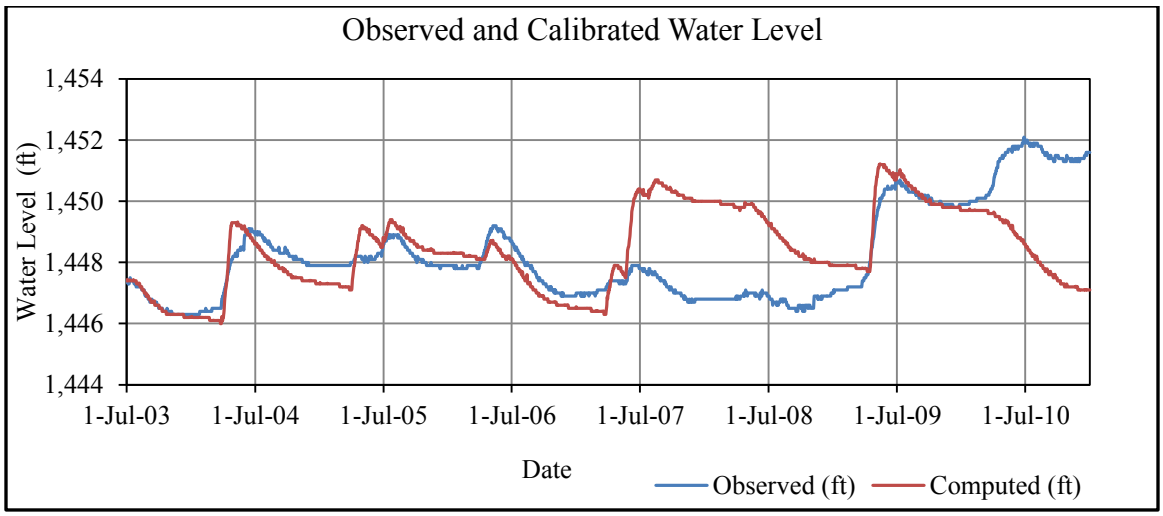

Figure 131: Calibration of HMS-Model B + ResSim (Combined approach) - Initial loss: 0.1 in; Constant loss: 0.085 in/hr; Seepage: 20 cfs

Appendix G

HEC-DSSVue

G.1 File Format in HEC-DSSVue

To import simulated synthetic precipitation and temperature series DSSVue was used, which can import properly oriented ASCII files.

Data Format:

1. The first paragraph must be :

DSET,COOPID,WBNID,CD,ELEM,UN,YEARMO,DAHR, DAY01,DAHR,
DAY02,DAHR, DAY03,DAHR, DAY04,DAHR, DAY05,DAHR, DAY06,DAHR,
DAY07,DAHR, DAY08,DAHR, DAY09,DAHR, DAY10,DAHR, DAY11,DAHR,
DAY12,DAHR, DAY13,DAHR, DAY14,DAHR, DAY15,DAHR, DAY16,DAHR,
DAY17,DAHR, DAY18,DAHR, DAY19,DAHR, DAY20,DAHR, DAY21,DAHR,
DAY22,DAHR, DAY23,DAHR, DAY24,DAHR, DAY25,DAHR, DAY26,DAHR,
DAY27,DAHR, DAY28,DAHR, DAY29,DAHR, DAY30,DAHR, DAY31

2. 2nd paragraph is:

----,------,-----,--,----,--,------,----,------,----,------,----,------,----,------,----,------,----,------
,----,------,----,------,----,------,----,------,----,------,----,------,----,------,----,------,----,------
,----,------,----,------,----,------,----,------,----,------,----,------,----,------,----,------,----,------
,----,------,----,------,----,------,----,------,----,------,----,------,----,------

3. From the third paragraph data input should be started.

3200,324958,99999,03,PRCP,HI,200912,0108, 00017,0208, 00021,0308, 00002,0408, 00000,0508, 00000,0608, 00000,0708, 00000,0808, 00000,0908, 00000,1008, 00000,1108, 00000,1208, 00000,1308, 00000,1408, 00000,1508, 00000,1608, 00000,1708, 00000,1808, 00000,1908, 00000,2008,

4. After the first and second paragraph there should be an “ENTER”.

5. After each month/year there should be one “ENTER”. At the end of dataset there should be one “ENTER”.

6. The dataset is “COMMA” (,) delimited. So there should be “COMMA” (,) after each entry.

7. 2nd paragraph is no. of allotted characters for the particular category denoted by “HIPHEN” (-).

8. Characters allotted are:

Green	: 4,6,5,2 respectively
Yellow	: 4
Grey	: 2
Magenta	: 6 (First 4 for year and rest of the two for month no.)
Cyan	: 4 and 6 respectively.

9. The Fifth category is “Element” where the type will be indicated, i.e. “PRCP” for precipitation and “TOBS” for temperature.

10. Unit of precipitation and temperature is ‘Inch’ and ‘Degree Fahrenheit’ respectively.

11. Among the six character spaces in ELEM category the first one is for sign. Put "SPACE" as the first character for positive sign and HIPHEN (-) for negative sign. Among the rest of five spaces:

    For PRCP: the first three are for values before decimal point and the last two are for values after decimal point.

    For TOBS: It can take only whole numbers (No Decimal values)

12. In the first four and sixth category (Green and Grey labeled) any data or text can be given as input. There is specific character limit as stated in bullet 9. Value entered as 'COOPID' can be seen after extraction of data.

    For missing data, the sign of the data value is set to "-", the data value is set to "99999"

G.2 Individual Cell Number, ID, Latitude and Longitude

Table 40: Table of all cell numbers, ID, latitude and longitude

CELL NO.	COOPID	LONGITUDE	LATITUDE
1	1A2030	-98.25	47.75
2	1B2030	-98.25	48.00
3	1C2030	-98.25	48.25
4	1D2030	-98.25	48.50
5	1E2030	-98.25	48.75
6	1F2030	-98.25	49.00
7	1G2030	-98.25	49.25
8	2A2030	-98.50	47.75
9	2B2030	-98.50	48.00
10	2C2030	-98.50	48.25
11	2D2030	-98.50	48.50
12	2E2030	-98.50	48.75
13	2F2030	-98.50	49.00
14	2G2030	-98.50	49.25
15	3A2030	-98.75	47.75
16	3B2030	-98.75	48.00
17	3C2030	-98.75	48.25
18	3D2030	-98.75	48.50
19	3E2030	-98.75	48.75
20	3F2030	-98.75	49.00
21	3G2030	-98.75	49.25
22	4A2030	-99.00	47.75

CELL NO.	COOPID	LONGITUDE	LATITUDE
23	4B2030	-99.00	48.00
24	4C2030	-99.00	48.25
25	4D2030	-99.00	48.50
26	4E2030	-99.00	48.75
27	4F2030	-99.00	49.00
28	4G2030	-99.00	49.25
29	5A2030	-99.25	47.75
30	5B2030	-99.25	48.00
31	5C2030	-99.25	48.25
32	5D2030	-99.25	48.50
33	5E2030	-99.25	48.75
34	5F2030	-99.25	49.00
35	5G2030	-99.25	49.25
36	6A2030	-99.50	47.75
37	6B2030	-99.50	48.00
38	6C2030	-99.50	48.25
39	6D2030	-99.50	48.50
40	6E2030	-99.50	48.75
41	6F2030	-99.50	49.00
42	6G2030	-99.50	49.25
43	7A2030	-99.75	47.75
44	7B2030	-99.75	48.00
45	7C2030	-99.75	48.25
46	7D2030	-99.75	48.50
47	7E2030	-99.75	48.75
48	7F2030	-99.75	49.00
49	7G2030	-99.75	49.25

In the ASCII file the name of the COOPID is shown for all the cells according to the grid. So for each simulation period there would be 49 files for each element (i.e. precipitation & temperature). In each file the COOPID would be according to the format shown above. Here COOPID means the Cell No. in the grid pattern. The ASCII file name can be the COOPID too. All the 49 files with different COOPID can be in a folder, which can be renamed by the simulation period.

Example Folder name: Temp_2030, Prcp_2050

Example File name: 1B2030, 7E203

Appendix H

Frequency Analysis

H.1 General Skew Coefficient in USA

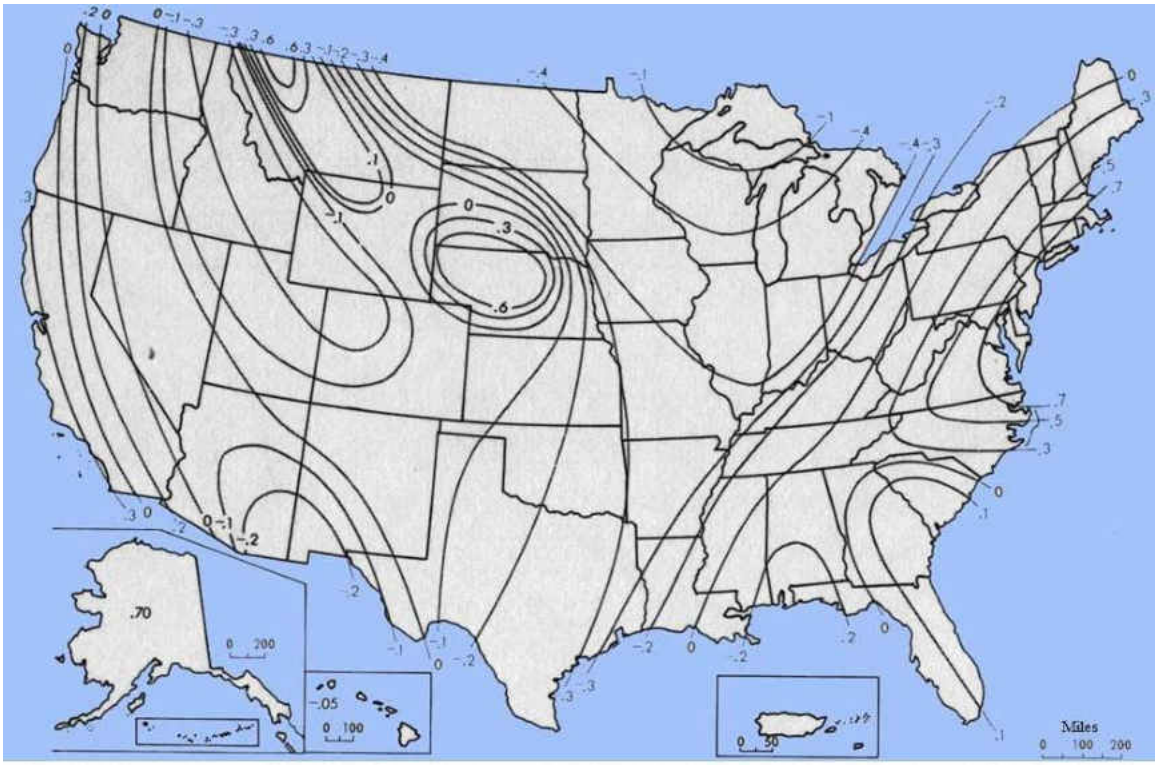

Figure 132: Map of general skew coefficient in USA (Source: IACWD, 1982)

H.2 Table of Frequency Factor, k

Table 41: Frequency factor *k* for gamma and LP3 distributions (Haan, 1977, Table 7.7)

	Recurrence Interval In Years							
	1.0101	2	5	10	25	50	100	200
SKEW COEFF.	% Chance (≥) = 1-F							
Cs	99	50	20	10	4	2	1	0.5
3	-0.667	-0.396	0.42	1.18	2.278	3.152	4.051	4.97
2.9	-0.69	-0.39	0.44	1.195	2.277	3.134	4.013	4.904
2.8	-0.714	-0.384	0.46	1.21	2.275	3.114	3.973	4.847
2.7	-0.74	-0.376	0.479	1.224	2.272	3.093	3.932	4.783
2.6	-0.769	-0.368	0.499	1.238	2.267	3.071	3.889	4.718
2.5	-0.799	-0.36	0.518	1.25	2.262	3.048	3.845	4.652
2.4	-0.832	-0.351	0.537	1.262	2.256	3.023	3.8	4.584
2.3	-0.867	-0.341	0.555	1.274	2.248	2.997	3.753	4.515
2.2	-0.905	-0.33	0.574	1.284	2.24	2.97	3.705	4.444
2.1	-0.946	-0.319	0.592	1.294	2.23	2.942	3.656	4.372
2	-0.99	-0.307	0.609	1.302	2.219	2.912	3.605	4.298
1.9	-1.037	-0.294	0.627	1.31	2.207	2.881	3.553	4.223
1.8	-1.087	-0.282	0.643	1.318	2.193	2.848	3.499	4.147
1.7	-1.14	-0.268	0.66	1.324	2.179	2.815	3.444	4.069
1.6	-1.197	-0.254	0.675	1.329	2.163	2.78	3.388	3.99

1.5	-1.256	-0.24	0.69	1.333	2.146	2.743	3.33	3.91
1.4	-1.318	-0.225	0.705	1.337	2.128	2.706	3.271	3.828
1.3	-1.383	-0.21	0.719	1.339	2.108	2.666	3.211	3.745
1.2	-1.449	-0.195	0.732	1.34	2.087	2.626	3.149	3.661
1.1	-1.518	-0.18	0.745	1.341	2.066	2.585	3.087	3.575
1	-1.588	-0.164	0.758	1.34	2.043	2.542	3.022	3.489
0.9	-1.66	-0.148	0.769	1.339	2.018	2.498	2.957	3.401
0.8	-1.733	-0.132	0.78	1.336	1.993	2.453	2.891	3.312
0.7	-1.806	-0.116	0.79	1.333	1.967	2.407	2.824	3.223
0.6	-1.88	-0.099	0.8	1.328	1.939	2.359	2.755	3.132
0.5	-1.955	-0.083	0.808	1.323	1.91	2.311	2.686	3.041
0.4	-2.029	-0.066	0.816	1.317	1.88	2.261	2.615	2.949
0.3	-2.104	-0.05	0.824	1.309	1.849	2.211	2.544	2.856
0.2	-2.178	-0.033	0.83	1.301	1.818	2.159	2.472	2.763
0.1	-2.252	-0.017	0.836	1.292	1.785	2.107	2.4	2.67
0	-2.326	0	0.842	1.282	1.751	2.054	2.326	2.576
-0.1	-2.4	0.017	0.846	1.27	1.716	2	2.252	2.482
-0.2	-2.472	0.033	0.85	1.258	1.68	1.945	2.178	2.388
-0.3	-2.544	0.05	0.853	1.245	1.643	1.89	2.104	2.294
-0.4	-2.615	0.066	0.855	1.231	1.606	1.834	2.029	2.201
-0.5	-2.686	0.083	0.856	1.216	1.567	1.777	1.955	2.108
-0.6	-2.755	0.099	0.857	1.2	1.528	1.72	1.88	2.016
-0.7	-2.824	0.116	0.857	1.183	1.488	1.663	1.806	1.926

-0.8	-2.891	0.132	0.856	1.166	1.448	1.606	1.733	1.837
-0.9	-2.957	0.148	0.854	1.147	1.407	1.549	1.66	1.749
-1	-3.022	0.164	0.852	1.128	1.366	1.492	1.588	1.664
-1.1	-3.087	0.18	0.848	1.107	1.324	1.435	1.518	1.581
-1.2	-3.149	0.195	0.844	1.086	1.282	1.379	1.449	1.501
-1.3	-3.211	0.21	0.838	1.064	1.24	1.324	1.383	1.424
-1.4	-3.271	0.225	0.832	1.041	1.198	1.27	1.318	1.351
-1.5	-3.33	0.24	0.825	1.018	1.157	1.217	1.256	1.282
-1.6	-3.88	0.254	0.817	0.994	1.116	1.166	1.197	1.216
-1.7	-3.444	0.268	0.808	0.97	1.075	1.116	1.14	1.155
-1.8	-3.499	0.282	0.799	0.945	1.035	1.069	1.087	1.097
-1.9	-3.553	0.294	0.788	0.92	0.996	1.023	1.037	1.044
-2	-3.605	0.307	0.777	0.895	0.959	0.98	0.99	0.995
-2.1	-3.656	0.319	0.765	0.869	0.923	0.939	0.946	0.949
-2.2	-3.705	0.33	0.752	0.844	0.888	0.9	0.905	0.907
-2.3	-3.753	0.341	0.739	0.819	0.855	0.864	0.867	0.869
-2.4	-3.8	0.351	0.725	0.795	0.823	0.83	0.832	0.833
-2.5	-3.845	0.36	0.711	0.711	0.793	0.798	0.799	0.8
-2.6	-3.899	0.368	0.696	0.747	0.764	0.768	0.769	0.769
-2.7	-3.932	0.376	0.681	0.724	0.738	0.74	0.74	0.741
-2.8	-3.973	0.384	0.666	0.702	0.712	0.714	0.714	0.714
-2.9	-4.013	0.39	0.651	0.681	0.683	0.689	0.69	0.69
-3	-4.051	0.396	0.636	0.66	0.666	0.666	0.667	0.667

H.3 Observed Lake-Levels Fitted using Different PDFs

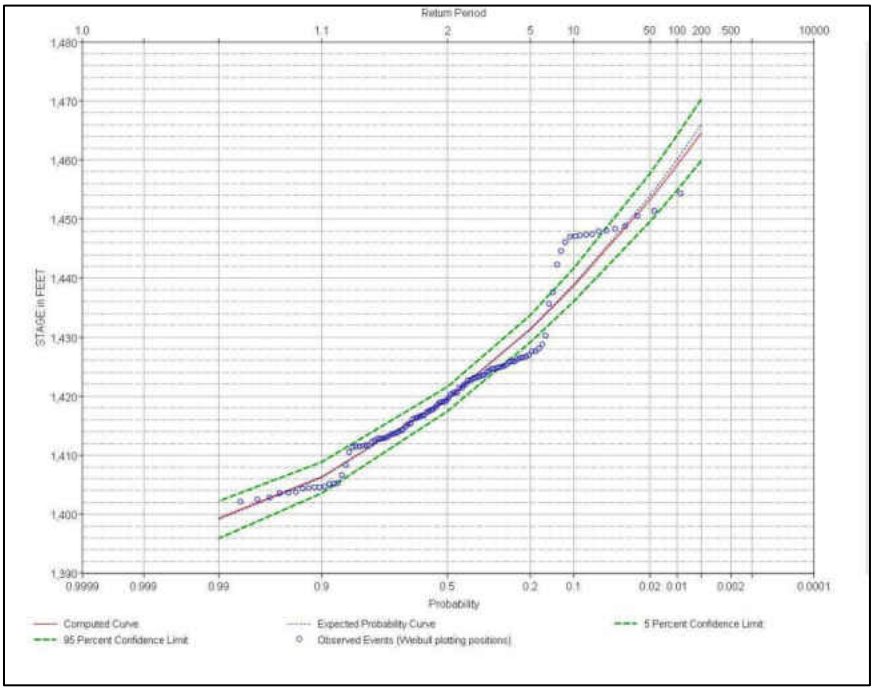

Figure 133: Observed lake-levels fitted using Pearson type 3 distribution

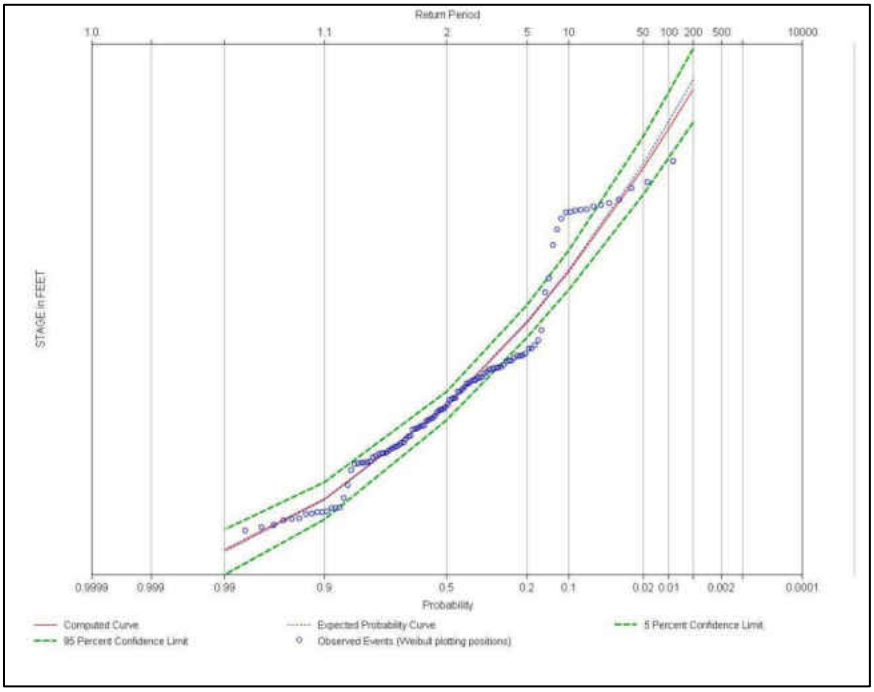

Figure 134: Observed lake-levels fitted using Log Pearson type 3 distribution

H.4 Simulated Lake-Levels Fitted using Different PDFs

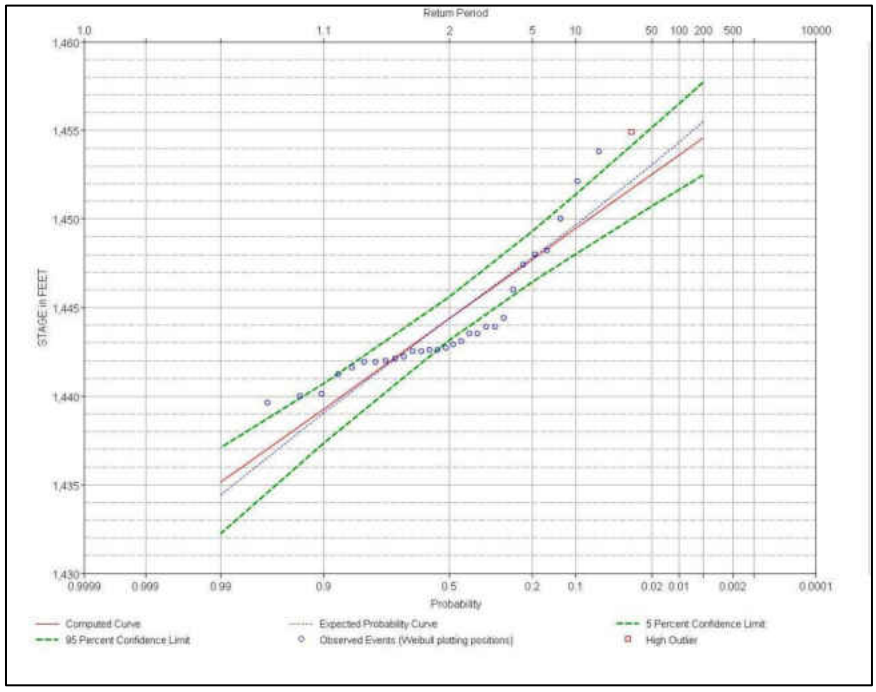

Figure 135: Simulated lake-levels fitted using Normal distribution

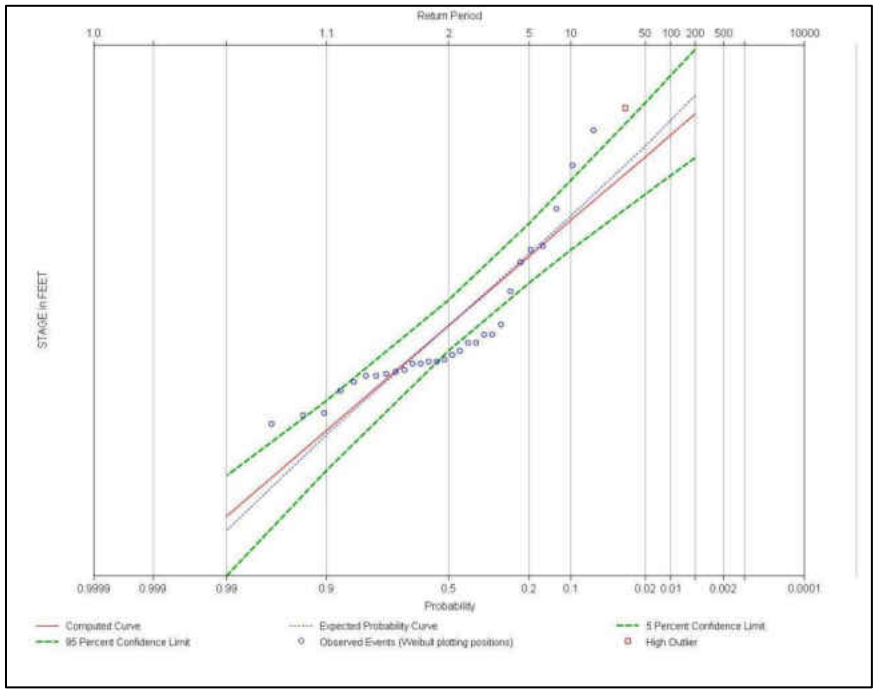

Figure 136: Simulated lake-levels fitted using Log-Normal distribution

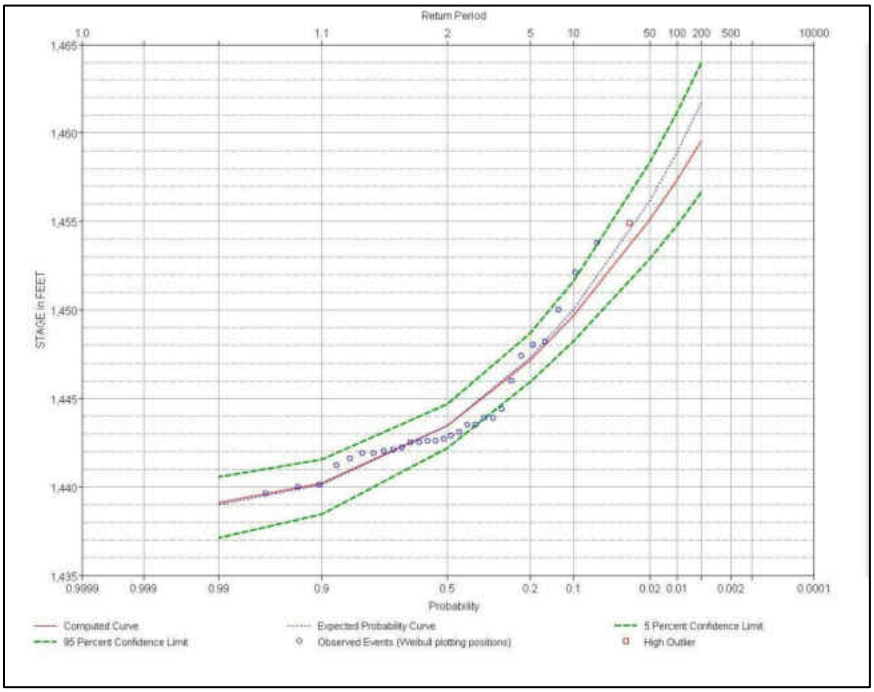

Figure 137: Simulated lake-levels fitted using Pearson type 3 distribution

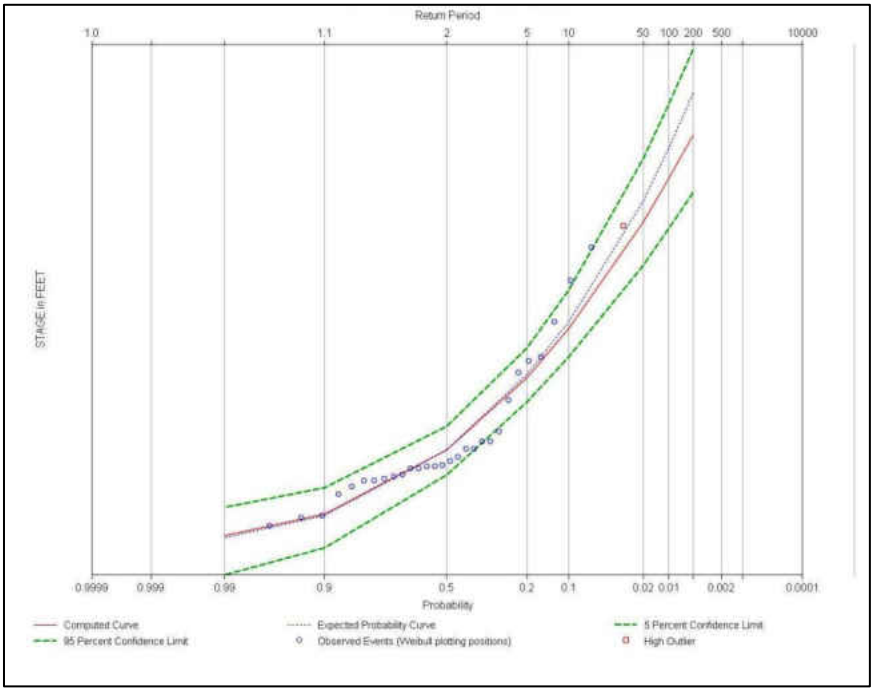

Figure 138: Simulated lake-levels fitted using LP type 3 distribution

H.5 Observed Lake-Volumes Fitted using Different PDFs

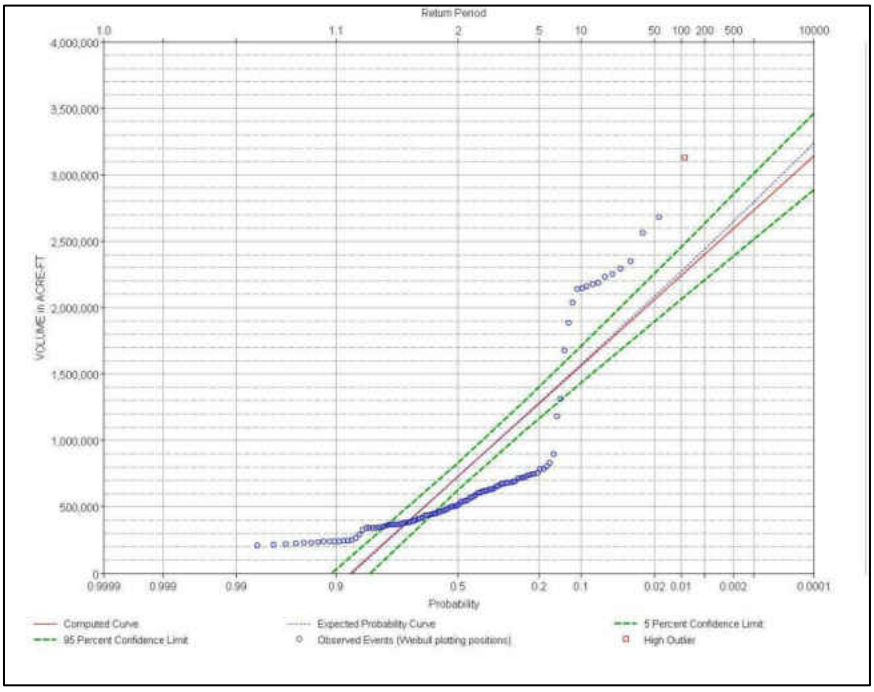

Figure 139: Observed lake-volumes fitted using Normal distribution

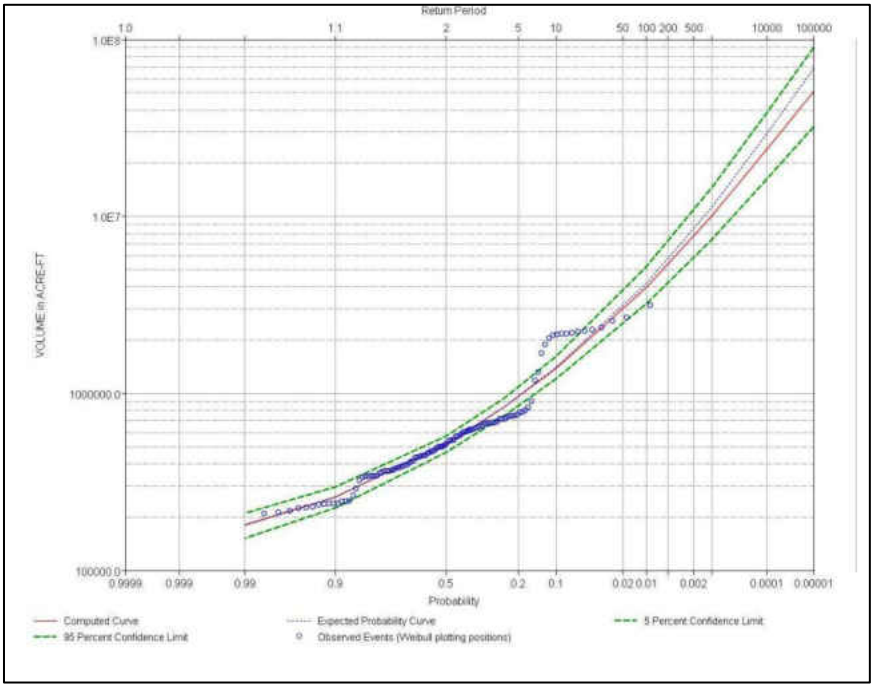

Figure 140: Observed lake-volumes fitted using LP type 3 distribution

H.6 Simulated Lake-Volumes Fitted using Different PDFs

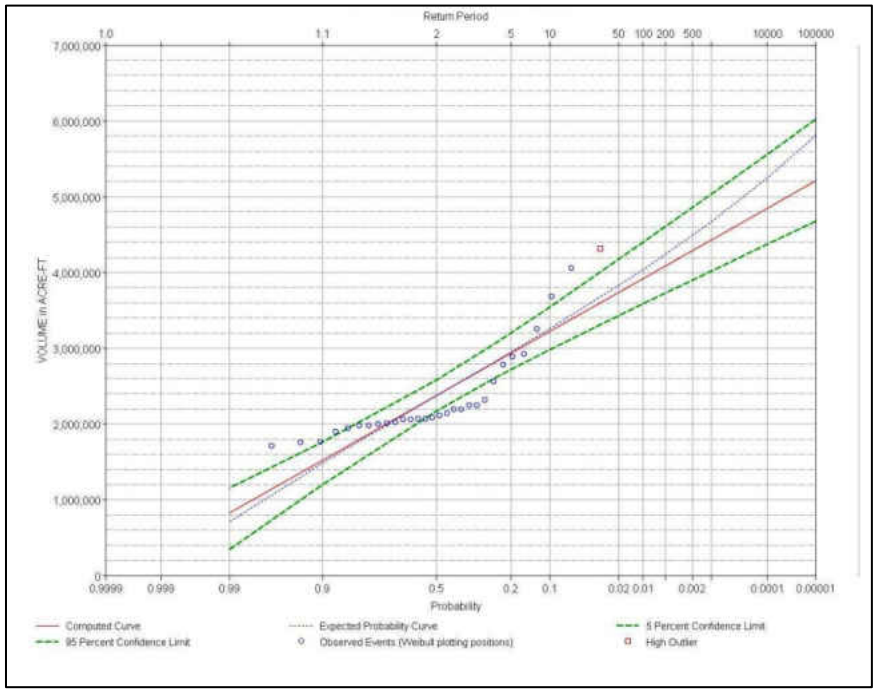

Figure 141: Simulated lake-volumes fitted using Normal distribution

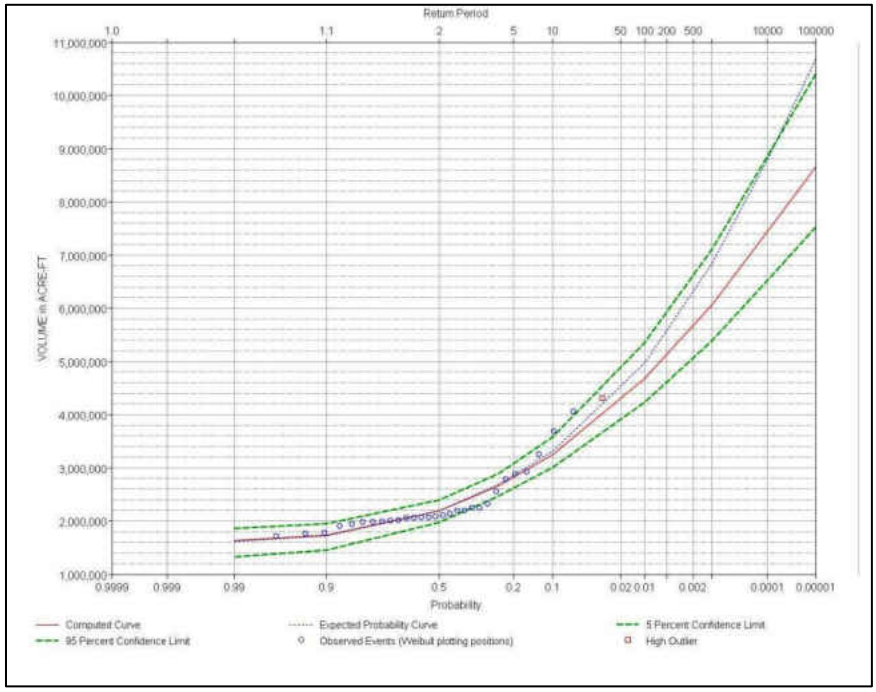

Figure 142: Simulated lake-volumes fitted using Pearson type 3 distribution

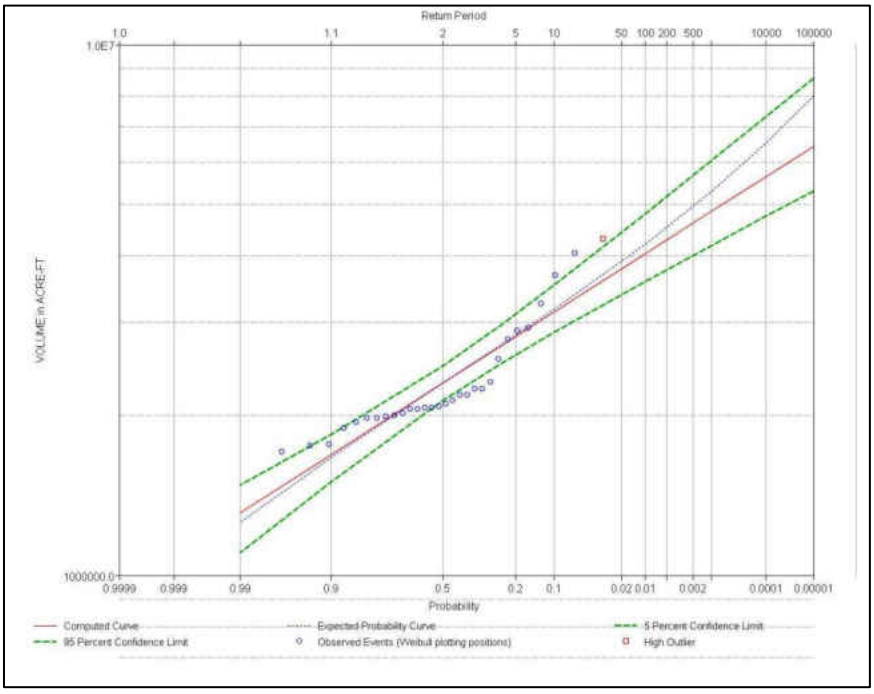

Figure 143: Simulated lake-volumes fitted using Log-Normal distribution

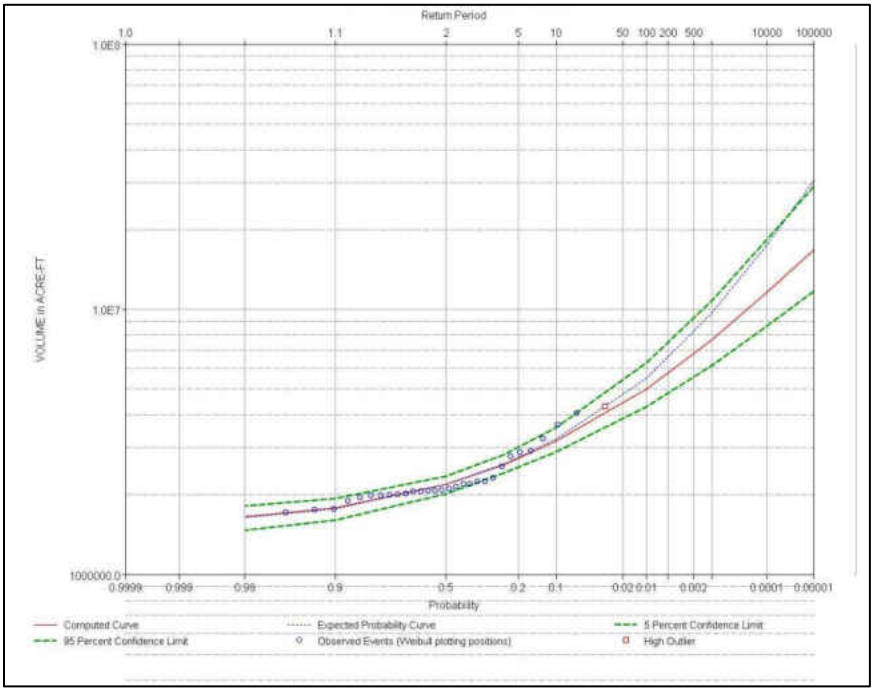

Figure 144: Simulated lake-volumes fitted using LP type 3 distribution

REFERENCES

Abtew, W. (1996). Evapotranspiration measurement and modeling for three wetland systems in South Florida. *Water Resources Bulletin, 32*, 465-473.

Bedient, P. B., & Huber, W. C. (2002). Frequency Analysis. In *Hydrology and Floodplain Analysis* (pp. 182-207).

Bluemle, J. P. (1991). *Radiocarbon dating of beaches and outlets of Devils Lake.* North Dakota Geological Survey.

Doorenbos, J., & Pruitt, W. O. (1977). Crop Water Requirements. *Irrigation and Drainage Paper, 24*, 144.

Hargreaves, G. H. (1975). Moisture Availability and Crop Production. *Transactions of the ASAE, 18*, 980-984.

Hargreaves, G. H., & Samni, Z. A. (1982). Estimation of potential evapotranspiration. *Journal of Irrigation and Drainage Division, Proceedings of the ASCE, 108*, 223-230.

Hassell, J. (2010). *Devils Lake Hydrologic Model and Prediction.* University of North Dakota, Department of Civil Engineering.

Hoerling, M., Eischeid, J., Easterling, D., Peterson, T., & Webb, R. (2010). *Understanding and Explaining Hydro-Climate Variations at Devils Lake.* National Oceanic and Atmospheric Administration (NOAA).

Hydrologic Engineering Center. (April 2007). *HEC-ResSim, Reservoir System Simulation, Quick Start Guide, Version 3.0.* Davis, CA: US Army Corps of Engineers.

Hydrologic Engineering Center. (July 2009). *HEC-DSSVue, HEC Data Storage System, Visual Utility Engine, User's Manual, Version 2.0.* Davis, CA: US Army Corps of Engineers.

Hydrologic Engineering Center. (March 2000). *Hydrologic Modeling System, HEC-HMS, Technical Reference Manual.* Davis, CA: US Army Corps of Engineers.

Hydrologic Engineering Center. (October 2010). *HEC-SSP, Statistical Software Package, User's Manual, Version 2.0.* Davis, CA: US Army Corps of Engineers.

IACWD. (1982). Guidelines for Determining Flood Flow Frequency. USGS.

Jensen, M. E., & Haise, H. R. (1963). Estimation of evapotranspiration from solar radiation. *Proceedings of the American Society of Civil Engineers*, *89*, pp. 15-41.

Kilsby, C. G., Ewen, J., Sloan, W. T., & Fallows, C. S. (1999). The UP Modeling System for Large Scale Hydrology: Simulation of the Arkansas Red River Basin. *Hydrology and Earth System Sciences*, 137-149.

Kirilenko, A. (2010). Climate change impact on agriculture: Devils Lake basin. *2010 International Congress on Environmental Modelling and Software.* Ottawa: International Environmental Modelling and Software Society (iEMSs).

Kubik, H. (1990). Annual extreme lake elevations by total probability theorem. Hydrologic Engineering Center, US Army Corps of Engineers, Davis, CA.

Lim, Y. H. (2004). Trend Analysis of Devils Lake Levels and the Related Environmental Parameters. *Water and Environment Specialty Conference. WE-149*, pp. 1-9. Montreal: Canadian Society for Civil Engineering.

Lim, Y. H., Hassell, J., & Teng, W. (2010). Modeling Hydrologic Regime of a Terminal Lake Basin with GCM Down-scaled Scenarios. *2010 International Congress on Environmental Modelling and Software.* Ottawa: International Environmental Modelling and Software Society (iEMSs).

Linsley, R. K., Kohler, M. A., & Paulhus, J. L. (1982). *Hydrology for Engineers*.

Makkink, G. F. (1957). Testing the Penman formula by means of lysimeters. *Journal of the Institution of Water Engineers, 11*, 277-288.

McGuinness, J. L., & Bordne, E. F. (1972). A Comparison of Lysimeter-derived Potential Evapotranspiration with Computed Values. *Technical Bulletin 1452, Agricultural Research Service, US Department of Agriculture*, 71.

Murphy, E. C., Fritz, A. K., & Fleming, R. F. (1997). *The Jerusalem and Tolna outlets in the Devils Lake Basin, North Dakota.* North Dakota Geological Survey Report of Investigation No. 100.

NCDC. (2010, November). *NOAA Satellite and Information Service*. Retrieved November 2010, from National Climatic Data Center: http://www.ncdc.noaa.gov/oa/mpp/digitalfiles.html#DIG

NDAWN. (2010, November). *Daily Data Table*. Retrieved November 2010, from North Dakota Agricultural Weather Network: http://ndawn.ndsu.nodak.edu/daily-table-form.html

Niehus, C. A., Vecchia, A. V., & Thompson, R. F. (1999). *Lake-level frequency analysis for the Waubay Lakes Chain, northeastern South Dakota.* US Geological Survey.

NOAA. (2010). *The Changing Precipitation Patterns at Devils Lake, ND*. Retrieved 2012, from Prescient Weather Ltd.: Weather Intelligence, Climate Innovation: http://devilslake.prescientweather.com/science

North Dakota Agricultural Weather Network (NDAWN) Center. (n.d.). *Daily Data Table*. Retrieved December 5, 2010, from NDAWN Center Web site: http://ndawn.ndsu.nodak.edu/daily-table-form.html

Northern Prairie Wildlife Research Center. (n.d.). *Climate of North Dakota: Sunshine and Cloudiness*. Retrieved November 25, 2010, from USGS Web site: http://www.npwrc.usgs.gov/resource/habitat/climate/sunshine.htm

Nustad, R. A., Wood, T. M., & Bales, J. D. (2011, U.S Geological Survey Scientific Investigations Report 2011–5035). *Use of a two-dimensional hydrodynamic model to evaluate extreme flooding and transport of dissolved solids through Devils Lake and Stump Lake, North Dakota.* 1: U.S Geological Survey Scientific Investigations Report 2011–5035.

Ohmura, A. (2001). Physical Basis for the Temperature-Based Melt-Index Method. *American Meteorological Society, 40*(4).

Penman, H. L. (1948). Natural evaporation from open water, bare and grass. *Proc. R Soc. Lond. Ser, A 193*, 120–145.

Penman, H. L. (1956). Evaporation: An introductory survey. *Journal of Agricultural Science, 4*, 9–29.

Penman, H. L. (1963). Vegetation and hydrology. *Technical Communication no. 53, Commonwealth Bureau of Soils*.

Priestley, C. H., & Taylor, R. J. (1972). On the Assessment of the Surface Heat Flux and Evaporation using Large-Scale Parameters. *Monthly Weather Review, 100*, 81-92.

Ryan, G. L., & Wiche, G. J. (1988). *Hydrology of the Chain of Lakes Tributary to Devils Lake and Water-Level Simulations of Devils Lake, Northeastern North Dakota.* U.S. Geological Survey Water-Resources Investigations Report 88–4020.

Scharffenberg, W., Ely, P., Daly, S., Fleming, M., & Pak, J. (2010). Hydrologic Modeling System (HEC-HMS): Physically-based Simulation Components. *2nd Joint Federal Interagency Conference.* Las Vegas.

Shahad, H. (2012). Development of a Temperature-based Model to Simulate Evaporative Losses over Water Bodies in Cold Regions. *World Environmental and Water Resources Congress, EWRI.* Albuquerque, New Mexico: ASCE-EWRI.

Steven, G. B. (1995). Conditional Frequency Analysis of Autocorrelated Lake Levels. *Journal of Water Resources Planning and Management, 121(2)*, 158-170.

Turc, L. (1961). Estimation of Irrigation Water Requirements, Potential Evapotranspiration: A Simple Climatic Formula Evolved up to Date. *Annals of Agronomy, 12*, 13-49.

U.S. Army Corps of Engineers. (2010). *Report of the Federal Interagency Devils Lake Working Group.*

USGS. (2010, November). *United States Geological Survey*. Retrieved November 2010, from National Water Information System: Web Interface: http://nwis.waterdata.usgs.gov/nd/nwis/nwisman/?site_no=05056500&agency_cd=USGS

Valiantzas, J. D. (2006). Simplified version of the Penman evaporation equation using routine weather data. *Journal of Hydrology, 331*, 690-702.

Vecchia. (2008). *Climate Simulation and Flood Risk Analysis for 2008-40 for Devils Lake, North Dakota.* U.S. Geological Survey Scientific Investigations Report 2008–5011.

Vecchia, A. V. (2002). *Simulation of a proposed emergency outlet from Devils Lake, North Dakota.* U.S. Geological Survey Water-Resources Investigations Report 02–4042.

Vecchia, A. V. (2011). *Simulation of the Effects of Devils Lake Outlet Alternatives on Future Lake Levels and Downstream Water Quality in the Sheyenne River and Red River of the North.* U.S. Geological Survey Scientific Investigations Report 2011–5050.

Vuyovich, C. M., & Daly, S. F. (2010). Temperature Index Snow Model.

Vuyovich, C. M., & Daly, S. F. (n.d.). *Temperature Index Snow Model.* ERDC-CRREL.

Wallis, J. R., Matalas, N., & R, S. J. (1974). Just a Moment! *Water Resources Research, 10*(2), 211-219.

Wiche, G. J. (1994). *Hydrology of the Devils Lake area, North Dakota.* North Dakota State Water Commission Water Resources Investigation 22.

Wiche, G. J., & Vecchia, A. V. (1996). *Lake-Level Frequency Analysis for Devils Lake, North Dakota.* U.S. Geological Survey Water-Supply Paper 2469.

Wiche, G. J., Vecchia, A. V., Osborne, L., & Wood, C. M. (2000). *Climatology, Hydrology, and Simulation of an Emergency Outlet, Devils Lake Basin, North Dakota.* U.S. Geological Survey Water-Resources Investigations Report 00–4174.

Woodbury, L. H., & Padmanabhan, G. (1989). Estimating terminal lake level frequencies. *Journal of Water Resources Planning & Management, 115*, 321-337.

Xu, C.-Y., & Singh, V. P. (2000). Evaluation and generalization of radiation-based methods for calculating evaporation. *Hydrological Processes, 14*, 339-349.

Zhang, X. (2010). The Fate of Devils Lake: An Interwoven Aftermath of Agriculture and Climate Change. *2010 International Congress on Environmental Modelling and Software.* Ottawa: International Environmental Modelling and Software Society (iEMSs).